The Mechanism and Mitigation of Fire-induced Spalling of Concrete with Recycled Tyre Fibres

Yifan Li

Doctor of Philosophy

Supervisors:

Prof. Kypros Pilakoutas

Dr. Shan-Shan Huang

The University of Sheffield

April 2023

ACKNOWLEDGEMENT

First and foremost, I would like to express my deepest gratitude to my supervisors, Prof. Kypros Pilakoutas and Dr. Shan-Shan Huang, for their inspiration, guidance, patience, and moral support throughout my PhD journey. I consider myself incredibly fortunate to have had the opportunity to learn from and work with them.

I am profoundly grateful to my parents, who have showered me with their unconditional love and support in pursuing my PhD. Without their encouragement and faith in me, I would have missed out on this invaluable experience.

I would also like to extend my appreciation to all the technicians, colleagues, and collaborators who have contributed to my research. Especially for Alessandro Tengattini, Stefano Dal Pont, Kieran Nash, Samuel Gibson, Ian Ross, Paul Bentley, Paul Blackbourn, Mehmet Senturk… Their professionalism, expertise, and camaraderie have played an indispensable role in the success of my work.

Lastly, I wish to thank all my friends, and particularly my wife, Siyu Qiu, for their companionship and unwavering support during the most challenging moments of my PhD journey. Their presence has been a source of strength and motivation, and I am truly grateful for their love and friendship.

Together, all of you have made this journey possible and immensely rewarding. Thank you.

ABSTRACT

In extreme conditions involving rapid heating and high temperatures, concrete can spall explosively. High-strength concrete (HSC) has a higher propensity for fire spalling compared to normal-strength concrete (NSC) due to its denser microstructure. To mitigate spalling, small amounts of micro-polymer fibres, such as polypropylene (PP) fibres, can be used to increase the permeability of concrete. This research aims to improve the sustainability of this mitigation method by investigating the potential of substituting manufactured PP fibres with Recycled Polymer Tyre Microfibres (RPTM) and Recycled Steel Tyre Microfibre (RSTM).

To examine the effects of fibres and other factors on fire spalling propensity, fire spalling tests were conducted on concrete specimens using a radiant panel heating system. The mechanisms of polymer fibres in fire spalling were investigated using Neutron and X-ray tomographies, which provided experimental evidence for the moisture migration process and changes in the porous structure of heated concrete.

The test results confirm the effectiveness of RPTM and RSTM in mitigating fire spalling supported by explanations of the underlying mechanisms. This research highlights the potential of utilising sustainable fibres, such as RPTM and RSTM, to mitigate fire spalling in concrete structures. Consequently, it contributes to the advancement of more environmentally friendly solutions for fire-resistant construction.

TABLE OF CONTENTS

1 Literature review

Fire-induced spalling is one of the most complex and poorly understood phenomena affecting concrete structures. It can be defined as the process of explosive ejection or gradual peeling off of concrete pieces from the fire-exposed surface of concrete elements. The damage caused by fire-induced spalling has detrimental effects on concrete structures, as it reduces the effective cross-sectional area of structural elements and exposes the steel reinforcement directly to fire, resulting in a decrease in load carrying capacity. Previous accidents have demonstrated the destructive nature of explosive fire spalling [1], [2], [3], [4], which has the potential to cause significant economic losses and interruption in the service of critical infrastructures.

1.1 FIRE SPALLING TYPES AND CLASSIFICATION

Depending on the location of fire spalling, it can be categorised into the following types:

- Aggregate spalling

Aggregate spalling typically occurs within 10 mm from the heated surface of the concrete during the initial stages of fire. Numerous aggregates burst off, leaving coin-sized craters on the surface due to thermal shock. As aggregate spalling neither removes significant material nor exposes the underlying reinforcement, it primarily causes aesthetic concerns. Two examples of aggregate spalling are illustrated in Figure 1. Figure 1(a) is adapted from the study by Mindeguia et al [5]; notably, the aggregate spalling occurred on the lateral surface subjected to heating rather than the exposed surface. Figure 1(b) is derived from the author's fire spalling test, demonstrating aggregate spalling on the fire-exposed surface.

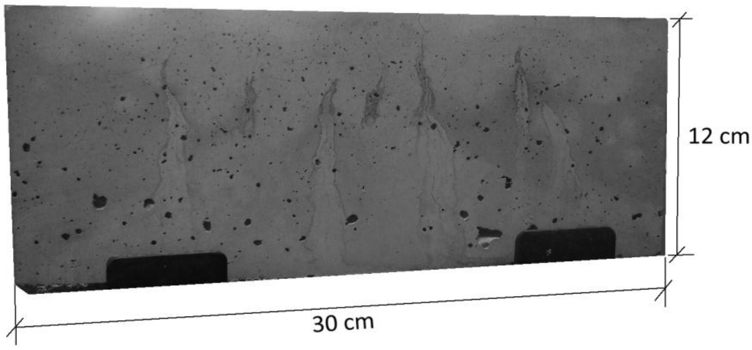

(a) (b)

Figure 1 (a) Aggregate spalling observed by Mindeguia et al [5] *(b) Aggregate spalling observed in the author's test.*

•Corner spalling

Corner spalling typically occurs in beams or columns with reinforcement when concrete elements are heated non-uniformly. It is attributed to thermal-induced cracks at the interface between heated concrete and reinforcement [6]. The initial curvature and inherent corrosion-induced fractures by the reinforcement are also considered contributing factors to corner spalling [6], [7]. Corner spalling poses greater challenges compared to aggregate spalling as it worsens the loss of load capacity of structural elements, potentially resulting in the global failure of the entire structure. Figure 2(a) shows an example of corner spalling that observed in prior tests while Figure 2(b) shows the fracture mechanism proposed by Arman et al. [6].

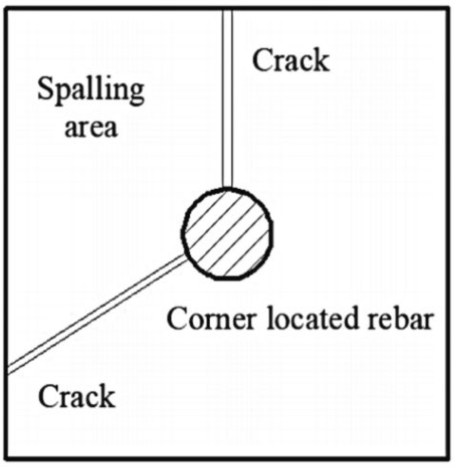

(a) (b)

Figure 2 (a) Example of corner spalling of a reinforced concrete column [8] *(b) Proposed mechanism of corner spalling caused by inherent corrosion-induced fracture of reinforcement* [6].

• Surface spalling

Surface spalling is a considerably more commonly seen phenomenon in a structural fire. It initiates at the heated concrete surface and progresses as heating continues. This phenomenon can inflict significant damage on structural elements. Surface spalling can occur in the early stages of a fire (within 5 minutes), presenting a challenge for engineers designing fire-resistant concrete structures [9]. Figure 3 shows a typical specimen experienced surface spalling during heating from the author's test.

Figure 3 Surface spalling of a concrete specimen.

When fire spalling occurs, it can occur either violently or non-violently. Hence, another method of grouping can be based on the energy level involved in spalling.

• Sloughing-off spalling

Sloughing-off spalling is the gradual peeling off of concrete layers from the concrete surface. Typically, this type of spalling is associated with cracks induced by the chemical dehydration of calcium silicate hydrate at high temperatures, rather than rapid heating rates. The process is progressive as long as the heat condition persists. Sloughing-off spalling typically occurs in the latter stages of a fire as calcium hydroxide begins to dissociate at 550°C, and concrete could undergo shrinkage thereafter [10].

• Explosive spalling

Explosive spalling represents a highly violent form of spalling characterized by the bursting of concrete pieces accompanied by a loud blasting sound. The ejection of concrete parts results from the release of pore pressure buildup and mechanical potential energy at high temperatures. The start time of explosive spalling can be as early as 7 min [11], [12] at a temperature of 200°C [13]. Explosive spalling inflicts significant damage on concrete, observations have noted parts of slabs being ejected up to 12 meters from the test building, with the spalling area reaching nearly 1 m^2 [7].

Unlike the previous fire spalling types that occurs during the heating process, there is another type of spalling known as post-fire spalling.

- Post-fire spalling (post-cooling spalling)

Post-fire spalling is a distinct type of fire spalling that occurs when the fire is being extinguished, after the fire has been extinguished, or even during the cooling of the concrete. It is caused by the chemical rehydration process affecting the calcareous materials within the concrete, as the remaining moisture in the concrete diffuses to the dried surface. The expansion of calcareous materials leads to cracks and diminishes the strength of the concrete [14], [15], resulting in spalling.

According to site damage assessments conducted by Albrektsson et al. [2], fire-induced spalling is classified into five classes, as illustrated in Table 1.

Table 1: Damage classification of fire spalling [2]

Class	Characterization	Description
1	Cosmetic damage, surface	Soot deposits and discoloration of surface.
2	Technical damage, surface	Damage on surface treatments and coating. Limited extent of concrete spalling and corrosion of exposed reinforcement.
3	Structural damage, surface	Concrete cracking or spalling. Some deformation of metal surfaces or moderate corrosion. This type of damage can be repaired but still might leave minor damages.
4	Structural damage, cross-section	Major concrete cracking or spalling in the web of I-beams and deformed flanges. The large structural deformation can reduce the load-bearing capacity.
5	Structural damage to members and components	Concrete constructions have extensive spalling and expose the reinforcement. Severe damage in structural members, with local failures in the materials and large deformations.

Jansson [16] compiled images from past fire spalling incidents to provide a clearer illustration of the five distinct damage levels, as shown in Figure 4.

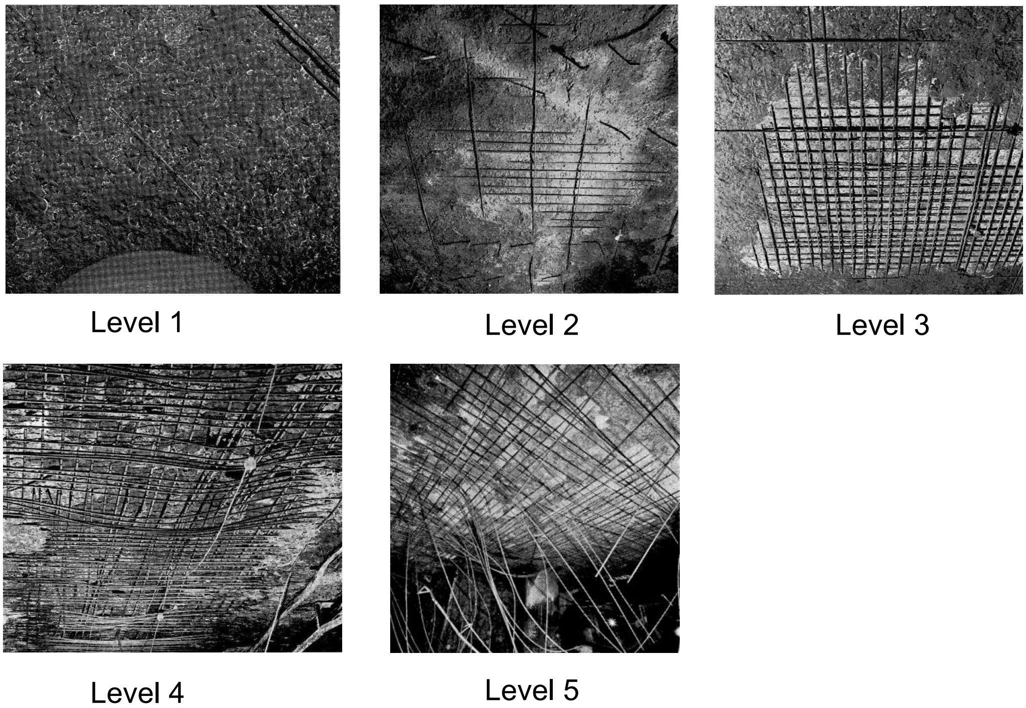

Figure 4 *Classification of spalling based on damage level* [16].

Based on the fire spalling mechanism, fire spalling can also be classified as thermo-hydral spalling, thermo-chemical spalling, thermo-mechanical spalling, or combinations thereof. These mechanisms are interconnected, making it challenging to differentiate one mechanism solely from others. Further details on fire spalling mechanisms in the literature will be introduced in subsequent sections.

In summary, the various types of fire-induced spalling exhibit overlapping characteristics (e.g., surface spalling can result in both progressive and explosive spalling). The real difference is the consequences that each type of spalling can cause. In Eurocode, fire safety design adopts a performance-based approach, where the duration a structure can withstand fire is the primary determinant in design considerations. The characteristics of early occurrence and significant impact render explosive spalling particularly hazardous in fire incidents. This paper specifically focuses on explosive surface spalling, as it represents one of the most complex, dangerous, and prevalent types of fire spalling.

1.2 FIRE SPALLING MECHANISMS

The mechanism of fire spalling is considered complex and involves thermo-hydro-chemo-mechanical mechanisms. The interdependency and the large number of influencing factors make the investigation very challenging. From the author’s perspective, despite the sophistication of the fire spalling phenomenon, all the aforementioned mechanisms can be ultimately attributed to the mechanical degradation of heated concrete. However, a comprehensive understanding of the fire spalling mechanism remains necessary. Concrete is a highly versatile material, with various properties that are heavily dependent on local materials and environmental conditions. For the standardization of engineering practice, a universal solution must be provided to address the fire spalling problem in concrete under different conditions. This necessitates the identification of key influencing factors and the corresponding mitigation methods for fire spalling. Therefore, a thorough understanding of the fire spalling mechanism becomes an essential step.

1.2.1 Thermo-mechanical mechanism

As mentioned earlier, all fire spalling mechanisms ultimately lead to mechanical degradation. In this section, only the mechanical degradation of concrete directly induced by high temperatures is introduced. Indirect damage to concrete, such as chemical dehydration, will be addressed in later sections.

On a macroscale, the low thermal conductivity and heat capacity of concrete result in a steep temperature gradient forming near the heated surface of the concrete. For a concrete wall subjected to one-sided heating following standard fire conditions, the temperature distribution and induced thermal stress are calculated by Hertz [9], as shown in Figure 5.

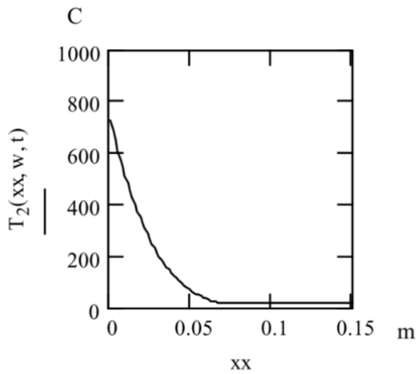

(a)

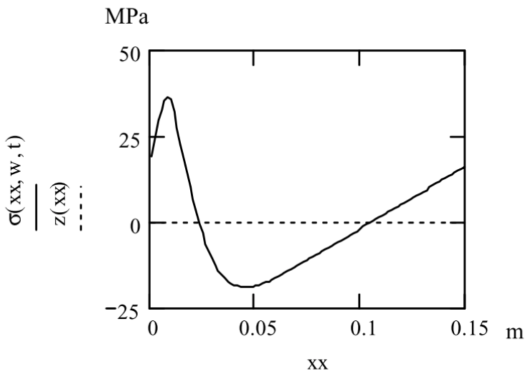

(b)

Figure 5 (a) Temperature distribution, and (b) thermal stresses in a one-sided heating wall [9].

The exposed surface of the concrete wall experiences the highest temperature, resulting in the greatest thermal expansion. However, the inner sections of the concrete remain relatively cold, thereby restraining the thermal expansion of the surface. This impairment of thermal expansion can lead to compression exerted on the exposed surface and tension exerted on the cold inner sections of the concrete wall [17]. Consequently, this leads to the formation of thermal cracks parallel to the isotherm and delamination of the surface, as illustrated in Figure 6.

Figure 6 Thermal induced crack of a dense concrete wall [9].

In practical applications, concrete elements are often restrained or loaded, which can alter the thermal damage mechanism of concrete since thermal expansion may be hindered or suppressed on a macroscale. However, the thermal cracks suppressed due to restraint could potentially lead to (1) increased stored potential energy or (2) additional cracking in the internal structure of concrete [18], thereby increases the risk of fire spalling [11].

On a mesoscale level, the variation in thermal expansion coefficient between different concrete constituents, including the cement matrix and aggregate, could be another significant cause of mechanical degradation [19]. Through restrained ring tests conducted by Ozawa et al. [20], clear thermal cracks can be observed due to differential volume changes of the aggregate within the concrete, as shown in Figure 7.

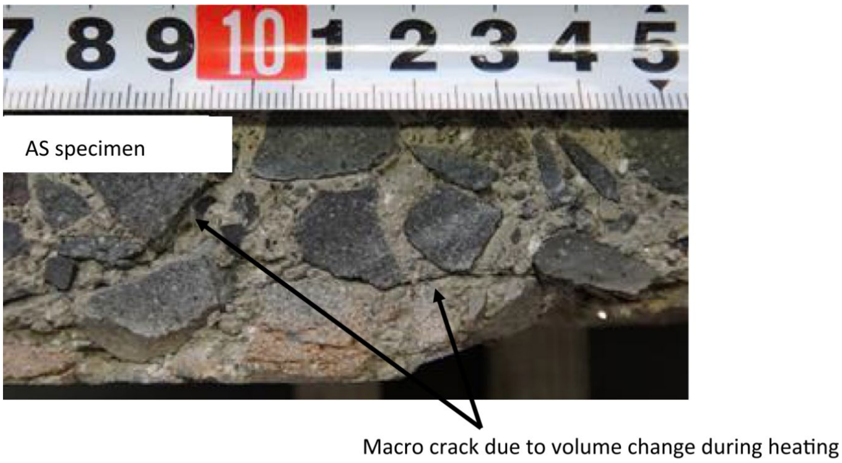

Figure 7 Cracks formed in the interfacial zone of aggregates and cement in concrete specimen after heating [20].

Additionally, investigations into thermal microcracks using scanning electron microscopy (SEM) have been conducted. These investigations reveal the formation of microcracks inside heated concrete at 300°C near a sand particle and a weak porous aggregate, as shown in Figure 8.

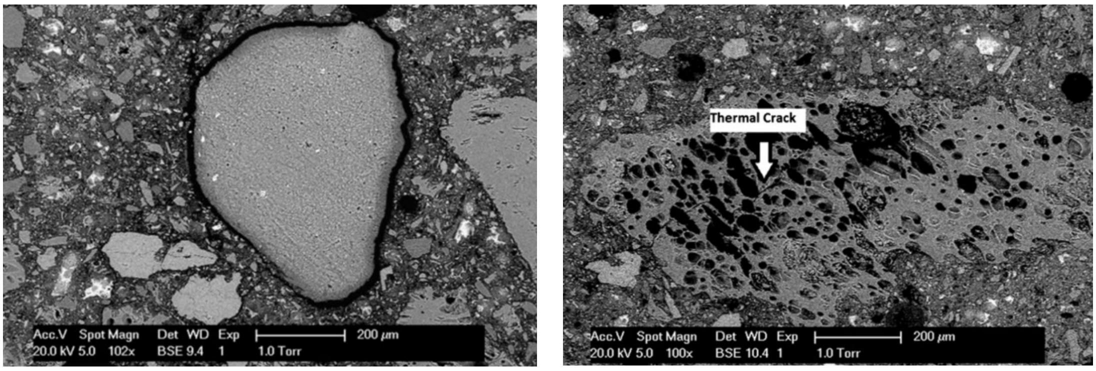

(a) *(b)*

Figure 8 Thermal microcracks of (a) a sand particle and (b) a weak aggregate in heated concrete [18].

1.2.2 Thermo-chemical mechanism

The thermos-chemical spalling mainly consists of two types of spalling, as introduced in Section 1.1: sloughing off spalling and post-fire spalling.

Sloughing off spalling is caused by the loss of bonding between aggregate and cement, particularly involving the breakdown of calcium hydroxide, calcium-silicate-hydrates (C-S-H), and calcareous aggregate. The cement paste involved in the hydration reaction primarily consists of approximately 60% C-S-H gel and about 20% portlandite (Ca(OH)2) [21]. Previous investigations into cement paste at elevated temperatures have revealed differential chemical reactions occurring within various temperature ranges: the loss of bound water resulting from the decomposition of C-S-H and the hydration of carboaluminate typically occurs within the range of approximately 180–300°C; dehydroxylation of portlandite takes place at temperatures ranging from 450 to 500°C; the decarbonation of calcium carbonate occurs at approximately 700°C or higher [15], [22], [23]. These processes, particularly the dehydration of C-S-H, can lead to shrinkage of the cement paste. In addition to the thermal expansion of the aggregate, the loss of bonding between cement and aggregate is pronounced, resulting in significant strength loss for the heated concrete. In the SEM images obtained by Liu and Chen [24], the shrinkage of C-S-H gel can be observed from temperatures of 200°C to 400°C, as shown in Figure 9.

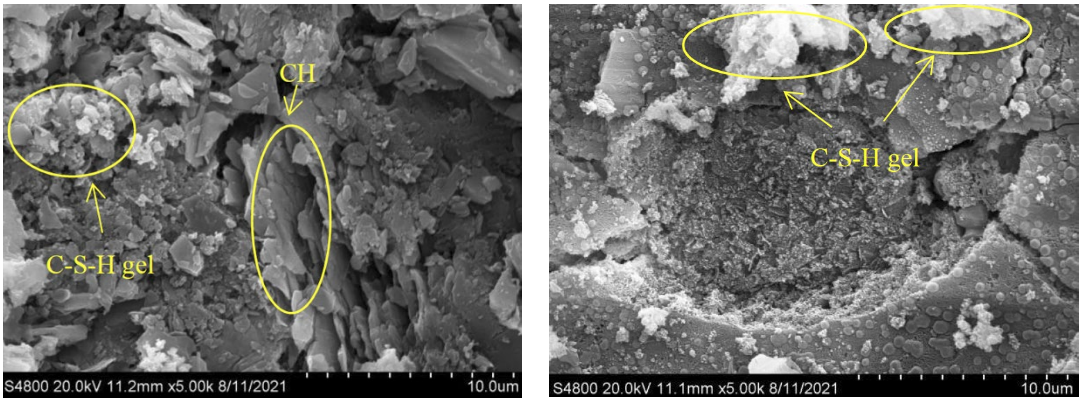

(a) *(b)*

Figure 9 SEM images of the concrete at (a) 200 °C and (b) 400 °C [24].

In the macroscale, the mechanical degradation resulting from chemical reactions at elevated temperatures has been investigated using various techniques. For instance, Kim et al. [25] used X-ray tomography to track the cracks forming in unloaded concrete specimens at very high temperatures (ranging from 600 to 1000°C). During the test, a major crack was observed via X-ray, initiating at 600°C and leading to fire spalling at 900°C. Acoustic emission (AE) tests conducted by Heap et at. [26] revealed that the failure mode of concrete below 300°C is rapid and violent, while above 300°C it is relatively gradual. This observation also supports the belief that thermo-chemical mechanisms are the primary cause of sloughing off spalling, as it occurs at high temperatures. Moreover, although the primary cause of crack formation at high temperatures is believed to be thermo-chemical mechanisms, thermo-mechanical mechanisms are also involved. In fire spalling research, it is exceedingly challenging to exclude or quantify the influence of a single mechanism.

Contrary to sloughing off spalling, which is induced by the shrinkage of concrete composites during dehydration, post-fire spalling occurs due to the expansion of calcium oxide in the cement paste during the rehydration process. This expansion specifically takes place in the heated surface of concrete due to the steep thermal gradient experienced during a fire. Consequently, moisture from the inner wet section of the concrete diffuses and is absorbed by the heated concrete surface [14], [24]. The expansion of the concrete surface induces microcracks, leading to delamination between the surface and the inner layer, ultimately resulting in spalling. To date, there are very few real-case examples or investigations on post-fire spalling in the literature. Luckily, it is widely acknowledged that the reduction in the rigidity of concrete structures after a fire is a common occurrence.

1.2.3 Thermo-hydral mechanism

The thermo-hydral mechanism of fire spalling is a generally recognized and challenging topic to investigate. It includes the phase changing of moisture, hydraulic transformation, pore vapour pressure, and microstructure change, all of which are temperature-dependent. Furthermore, this mechanism must be coupled with thermo-chemo-mechanical mechanisms, as they are interdependent. Hence, the thermos-hydral mechanism is very difficult to describe, verify, and numerically model. In this section, the author attempts to introduce the existing understanding of the thermo-hydraulic mechanism to the best of their ability, recognizing that there is still a significant knowledge gap for a full understanding of this mechanism. This also underscores one of the main objective of this PhD project: to enhance understanding of this mechanism through experimental verifications.

The earliest trackable explanation (by the author's knowledge) of the thermo-hydral mechanism of fire spalling was proposed by G. W. Shorter and T. Z. Harmathy in a previous proceeding in 1961 [27]. They concluded that the presence of moisture is the main cause of explosive spalling during their fire tests. The proposed mechanism was later illustrated in a graph from Gary et al.'s work [28] and redraw by Zeiml el al. [29], as shown in Figure 10.

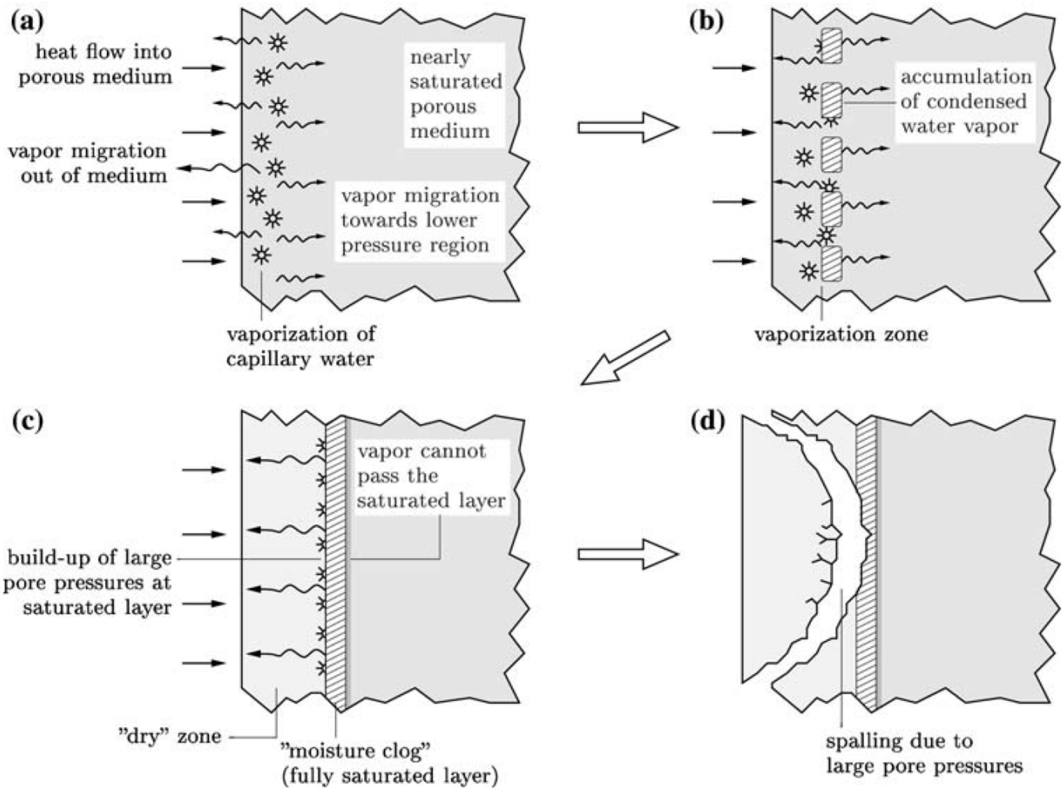

Figure 10 Illustration of fire spalling caused by the thermo-hydral mechanism [29].

Concrete contains both free capillary water and chemically bonded water. In fire conditions, a steep temperature gradient forms, with the exposed concrete surface experiencing the highest temperature. Water in concrete will vaporize once the temperature exceeds its boiling temperature, where the boiling temperature depends on the pore pressure. The vapor can migrate towards both the outer surface and the inner layers through the porous structure of the concrete, where the rate of migration depends on the permeability of concrete. Vapor escaping through the concrete surface is considered drying, while vapor migrating to the inner layers will condense due to the lower temperature within the concrete. Gradually, the concrete pores become filled with condensed moisture until a fully saturated layer, termed 'moisture clog,' is formed. This moisture clog blocks further vapor migration, resulting in pore pressure accumulation near the moisture clog [30]. Under restricted moisture migration conditions near the moisture clog, thermal pressurization develops due to the discrepancy between the thermal expansion of the fluid and the solid skeleton [31]. The combination of pore vapor pressure buildup and differential thermal expansion can lead to significant damage to the concrete microstructure [32]. Hence, the moisture clog is believed to be the critical zone for the occurrence of explosive fire spalling of concrete [33].

A comprehensive understanding of the process by which pore pressure builds up in heated concrete is essential for investigating the fire spalling mechanism. To measure vapor pore pressure, Kalifa et al. [34] utilized a specially designed apparatus to conduct pore pressure, temperature, and mass loss (PTM) tests on heated concrete, as shown in Figure 11. This pore pressure gauge mainly consists of a porous sensing head and a pressure transfer tube filled with silica oil. The porous head is constructed from a sintered metal plate with a uniformly distributed porous system. The flat surface of the head helps reduce transverse cracks, making the entire setup less intrusive. Another advantage of the sensor head is its larger measurement area, which provides mean pressure results over a wider region. The use of silica oil to fill the stainless steel pipe ensures thermal stability, making it a superior pressure transfer medium compared to air or water.

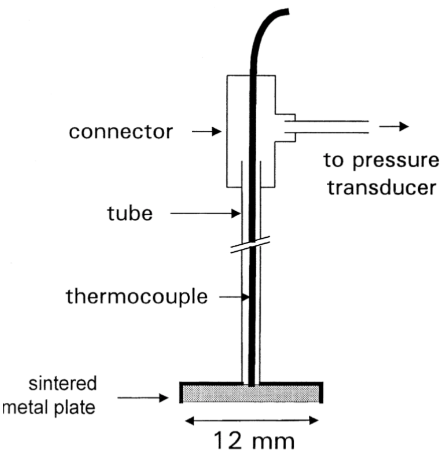

Fig. 3. Pressure–temperature gauge.

(a)

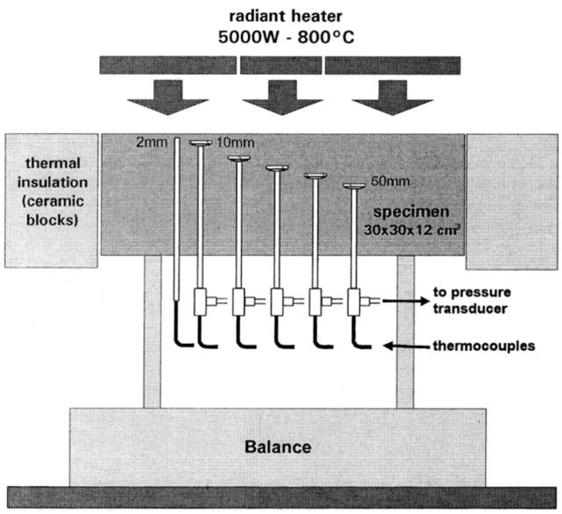

(b)

Figure 11 (a) The pore pressure-temperature gauge (b) the PTM test set-up [34].

The key influencing factors for pore pressure within heated concrete are investigated using the PTM test method. Increased moisture content in concrete has been found to increase the pore vapor pressure of heated concrete [35], [36]. Concrete strength is also found to be related to the maximum pore pressure of heated concrete, but with varied conclusions. Kalifa et al. [34] and Bangi and Horiguchi [37] found that an increase in concrete strength can lead to high pore vapor pressure due to the dense microstructure of high-performance concrete (HPC). However, for ultra-high-performance concrete (UHPC) studied by Choe et al. [36], the maximum vapor pore pressure is much lower, possibly attributed to the brittleness of UHPC and concrete spalling. Moreover, the propensity for fire spalling was found not to be linearly linked to the increase in pore vapor pressure level [36], [38], [39]. Some spalled concrete has maximum pore vapor pressure lower than 0.5 MPa, which is far below the tensile strength of concrete. Hence, Jansson and Boström [39] concluded that pore vapor pressure might only serve as an initiator of explosive fire spalling. To verify this conclusion and quantify the influence of pore pressure on the mechanical strength of concrete at elevated temperatures, Felicetti et al. [40] designed a novel splitting test to determine the relationship between pore vapor pressure and tensile splitting strength. The test results confirmed that spalling cannot be triggered by pore vapor pressure alone, but a low level of pore pressure (about 1 MPa) is enough to induce explosive spalling of concrete with much higher tensile strength. Figure 12 is adopted from the test to illustrate the relationship between tensile strength and pore vapor pressure at various heating rates.

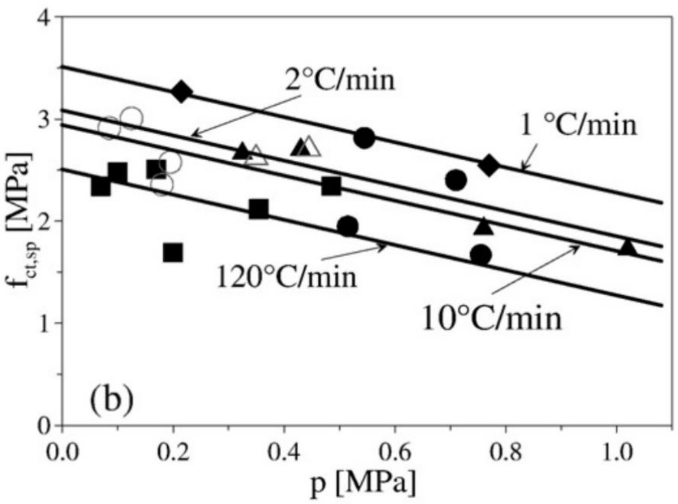

Figure 12 The relationship between the tensile strength and the pore vapour pressure of concrete at various heating rate [40].

Although the pressure gauge adopted in the PTM test is specially designed to minimize its influence on the concrete microstructure, the intrusive nature of the pressure gauge inevitably alters the test results from the authentic condition. From the non-intrusive X-ray and neutron tomography results obtained by Dauti et al. [41] and the authors' work, air voids or interfacial transition zones can form due to the presence of thermocouples with a diameter of only 0.3 mm. For a sintered metal head with a diameter of around 12 mm, the change in concrete microstructure could be significant and has yet to be quantified.

To comprehend the thermo-hydraulic mechanism of fire spalling, investigating the moisture migration process, particularly the presence of moisture clogs within heated concrete, is another essential step.

The existence of moisture clog was observed using a simplified method by splitting a concrete sample during heating [33]. However, to quantify the saturation level and migration process of moisture in concrete, some state-of-the-art non-intrusive test methods offer more advantages compared to conventional methods. Nuclear magnetic resonance (NMR) [42] has been successfully used to observe the moisture profile of concrete, although it is limited by one-directional analysis. X-ray tomography is another popular method capable of detecting density variations in pores [43], thus providing insight into the moisture drying or wetting process [44]. The potential influences from the pore structure changes due to thermo-chemical or thermos-mechanical mechanisms could affect the accuracy of X-ray tomography.

Another advanced imaging method employed in testing facilities is named "NeXT," developed by Tengattini et al. [45] at the University Grenoble Alpes (UGA) and the Institut Laue Langevin (ILL). It aims to produce simultaneous neutron and X-ray topographies, capitalizing on the high complementarity of the two beams. The high attenuation coefficient of hydrogen atoms in water molecules makes the neutron beam ideal for detecting the presence of moisture, while the X-ray beam, sensitive to the density of concrete, can easily detect the porous system of concrete, which has lower density than the surrounding matrix, in X-ray tomography. Dauti et al. [46] conducted neutron tomography using "NeXT" to obtain 3D analysis of moisture inside heated concrete, while Moreira et al. [47] improved the sealing condition of concrete samples. Both studies analyzed moisture migration in heated concrete and revealed the evolution of moisture. Figure 13 shows the drying process of a UHPC specimen obtained from neutron tomography test.

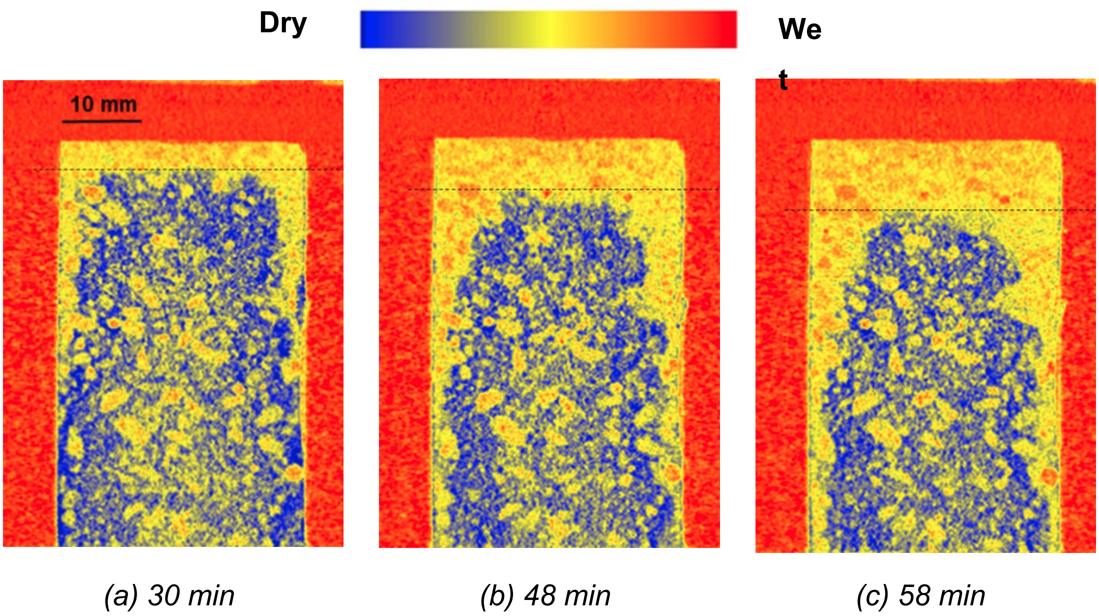

Figure 13 Neutron tomography image showing the drying process of a cross section of concrete specimen at elevated temperatures [46].

1.2.4 Other methods to study the spalling mechanisms

Zeiml et al. [29] utilized a high-speed camera to measure the size and speed of spalled concrete pieces at the moment of fire spalling. Through the computation of thermo-hydral and thermo-mechanical kinetic energy, the authors found that thermo-hydral kinetic energy contributed the most to spalling energy for small, high-speed pieces, whereas thermo-mechanical kinetic energy played a larger role in larger chunks of spalled concrete with slower speed. Ozawa et al. [32] combined the AE test and the PTM test in their study, wherein they discovered a good correlation between AE events (internal cracking), pore pressure levels, and the occurrence of fire spalling. Stelzner et al. [48] employed a non-simultaneous X-ray and NMR technique to investigate the moisture profile of heated concrete. Their study also observed possible moisture accumulation in the concrete.

1.3 THE ROLE OF FIBRES IN FIRE SPALLING

1.3.1 Polypropylene fibres

The incorporation of synthetic fibres, such as polypropylene (PP) fibres, into concrete is a widely acknowledged method for preventing fire-induced spalling [20], [49], [50], [51], [52]. According to the new Eurocode 2 [53], specific spalling assessment must be conducted on concrete with higher risk factors (e.g. high moisture content, high strength, etc), unless PP fibres are included. In comparison to the previous version [54], the new Eurocode highlights various factors related to spalling and reaffirms the effectiveness of PP fibres.

Compare to plain concrete, concrete with PP fibres exhibits very similar compressive strength and modulus of elasticity at both ambient temperature and 200 °C [55]. At ambient temperature, the flexural strength of concrete with PP fibres is higher than that of plain concrete, attributed to the bridging effect of the fibres [56]. However, this enhancement in flexural strength diminishes as temperature increases due to the softening and subsequent melting of the PP fibres [55], [57].

The addition of PP fibres can enhance the high-temperature permeability of concrete by (1) creating thermal microcracks due to different thermal expansion between the fibres and concrete [58] and (2) forming empty channels from melting at approximately 170 °C [59]. The measured permeability of PP fibre concrete and the thermal expansion at elevated temperatures are shown in Figure 14. Interestingly, it can be observed that the main increase in permeability of PP fibre concrete occurs within the temperature range of 100 °C to 150 °C. The melting of fibres, is not as dominant as expected in enhancing the permeability of concrete. The SEM images illustrating the thermal expansion cracks and empty channels left by melted PP fibres in heated concrete are presented in Figure 15.

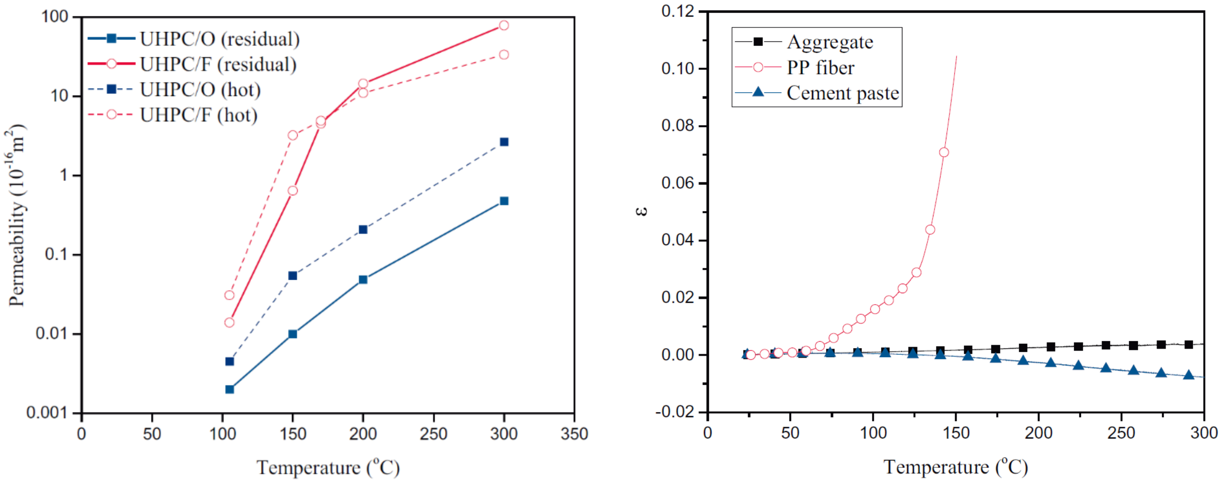

(a) (b)

Figure 14 (a) Permeability of ordinary concrete and PP fibre concrete at elevated temperatures, (b) thermal expansion of PP fibre, cement and aggregate [58].

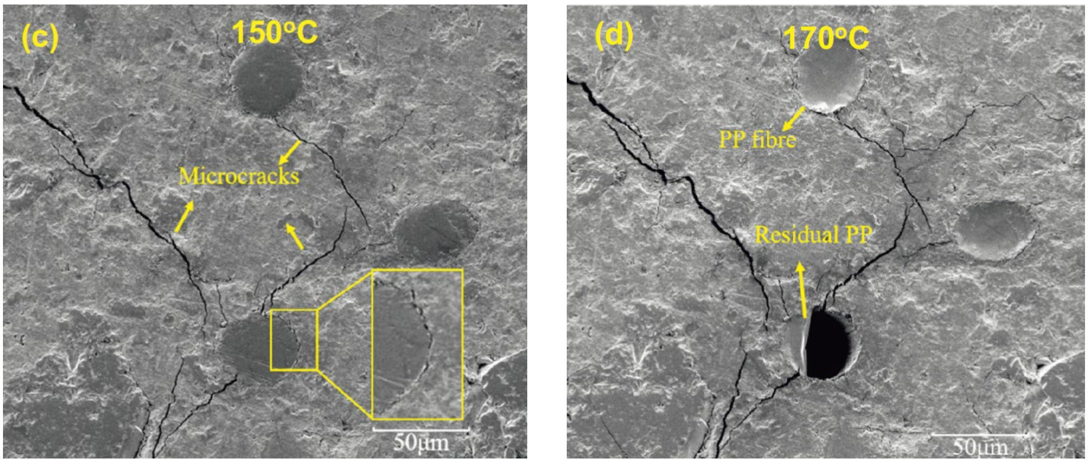

(a) (b)

Figure 15 (a) Microcracks induced by the thermal expansion of PP fibres at 150 °C (b) Empty channel created by the melting PP fibre at 170 °C [58].

To explain the disappearance of the melted fibres, a previous study conducted by Kalifa et al. [49] used water droplets to observe the water absorption of concrete covered by PP films. They confirmed the penetration of melted PP into the cement matrix and the pathways left for liquid water and gas. Based on the SEM observations, as shown in Figure 15, Zhang et al. [58] also confirmed this explanation and deduced that the melted PP might flow into the microcracks created by itself.

As vapour can escape through these empty channels and microcracks, the peak pore pressure within heated concrete with PP fibres can be reduced, thereby leading to the suppression of explosive fire spalling. To verify this theory, Kalifa et al. [49] firstly investigated the role of PP fibres using PTM tests, which concluded that increasing the dosage of PP fibres can decrease the peak pore pressure in heated concrete. Following PTM were then carried out and the pore pressure of concrete was found to be significantly reduced by the inclusion of PP fibres [38], [60]. In Jansson and Boström's study [39], they found that the vapor pressure was higher in PP fiber-added concrete than that of spalled plain concrete, which could be attributed to the occurrence of fire spalling as it can release the vapor. The pore vapour pressure measured by Felicetti et al. [40] indicates that the inclusion of PP fibre is more effective at reducing the peak pore pressure at relatively high heating rate (10 °C/min) instead of slow heating rate (2 °C/min). This could also be due to another influence of PP fibre, as it may suppress early-stage thermal cracks by their crack bridging effect [56], [57] at lower temperatures.

1.3.2 Steel fibres

Steel fibres are commonly added to concrete as an effective approach for improving its performance under both normal and high-temperature conditions [21], [61], [62], [63]. Consequently, Steel Fiber Reinforced Concrete (SFRC) is particularly popular in infrastructures such as tunnels and road pavements [64]. However, the effectiveness of including steel fibres in concrete to prevent fire-induced explosive spalling has not been thoroughly investigated, largely due to the numerous influential variables and the uncertainty of the fire spalling results.

Three main influences of steel fibres in heated concrete can be related to the fire spalling: (1) the decrease in thermal gradient and hence thermal stress of heated concrete due to the higher thermal conductivity of steel fibres [65], as shown in Figure 16; (2) the improvement of thermal-mechanical performance of concrete due to the cracking bridging effect of steel fibres [66]; and (3) similar like PP fibres, the difference in thermal expansion coefficient between concrete and steel fibres can induce microcracks which increase the permeability of concrete [60], as shown in Figure 17.

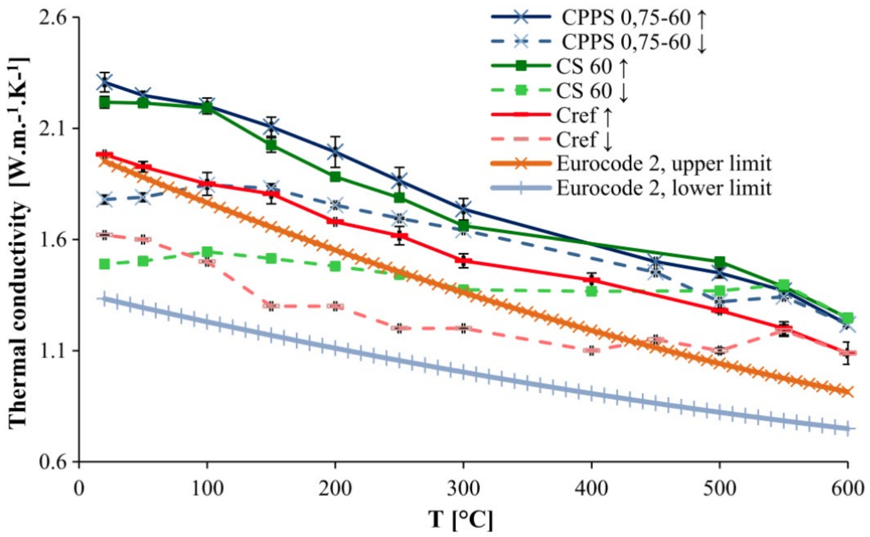

Figure 16 The thermal conductivity of concrete with steel fibres (CS 60) compared with plain concrete (Cref) and Eurocode limit [65]*.*

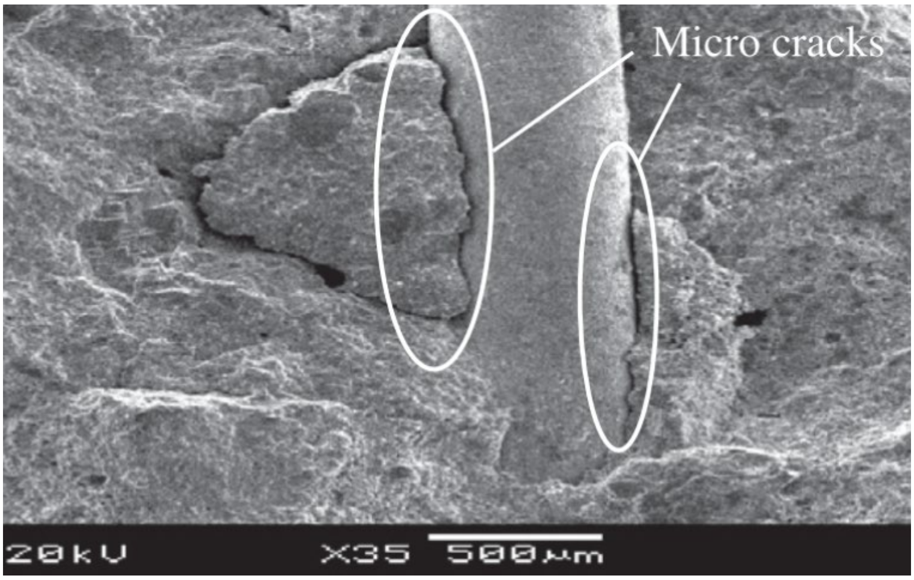

Figure 17 SEM image of the microcracks induced by the presence of steel fibres in concrete at 600 °C [67]*.*

In the fire endurance test conducted by Kodur et al. [64], the addition of steel fibres was found to enhance the fire resistance of high-strength concrete columns. For fire spalling test of SFRC, the presence of steel fibres may have detrimental effect. In the biaxial loading test conducted by Monte et al. [68], none of the PP fibre concrete specimens experienced spalling, but the steel fibre-included concrete specimens did. The peak pore pressure of the spalled specimens was 2 MPa, which is higher than that of PP fibre concrete (0.7 MPa). Similar results were found by Algourdin et al. [65], which showed that concrete specimens with 60 kg/m³ of steel fibres experienced spalling at elevated temperatures. When PP fibres were added to the concrete in the same programme, spalling did not occur. It is speculates that the development of thermal cracks was limited in the samples with steel fibres, which led to greater pore pressure followed by spalling. Algourdin et al. [65] also highlights the sensitivity of spalling behaviour to a range of interconnected properties, including the presence, dosage, and type of fibre in the mix. The performance of steel fibres can deteriorate at high temperatures, resulting in a loss of bond between the fibres and concrete, which may be another cause of excessive spalling [69]. Additionally, it was shown that the effectiveness of a given steel fibre content in spalling control may vary depending on the size of the specimen [70], as this affects the thermal gradient and also the boundary effect on the sample.

Although the addition of steel fibre alone cannot completely prevent spalling, steel fibre cocktails (a mix of steel fibres with other fibres) could bring benefits or, at the very least, have no adverse effect on the mitigation of fire spalling in concrete. In the fire test conducted by Sanchayan and Foster [71], concrete specimens with only steel fibres or only polyvinyl alcohol (PVA) fibres exhibited different levels of fire spalling, but the specimen with a specific fibre cocktail of these two (0.13% steel fibre and 0.007% PVA fibre by volume) surprisingly experienced no spalling. Yermak et al. [51] found that explosive spalling occurred in concrete with 60 kg/m³, but there was no spalling when the specimen were added with 0.75 kg/m³ of PP fibre. Czoboly et al. [69] also found that the fire spalling of steel fibre concrete can be mitigated by adding either cellulose fibre or PP fibre.

Li et al. [59] investigated the permeability of concrete at elevated temperatures, comparing the permeability data obtained from specimens with plain concrete, PP fibre, and steel fibre, respectively. The test results are shown in Figure 18, where UHPC-C represents plain concrete, UHPC-PP represents concrete with PP fibre, and UHPC-S represents concrete with steel fibre. It can be observed that the hot permeability of PP fibre concrete is nearly 15 times that of steel fibre concrete (at 150 °C). This disparity in permeability during early-stage heating might explain the limited effectiveness of steel fibre in controlling spalling. However, this hot permeability of concrete may not be representative of real fire scenarios, as the heating rate in standard fire is much higher than that adopted in the permeability test (less than 1 °C/min). The bonding and crack control mechanisms of steel fibres were not engaged during the test due to the slow heating. Therefore, to better understand the differences between the two fibres, a comparison of the permeability of steel fibre concrete and PP fibre concrete at different heating rates could be investigated in the future.

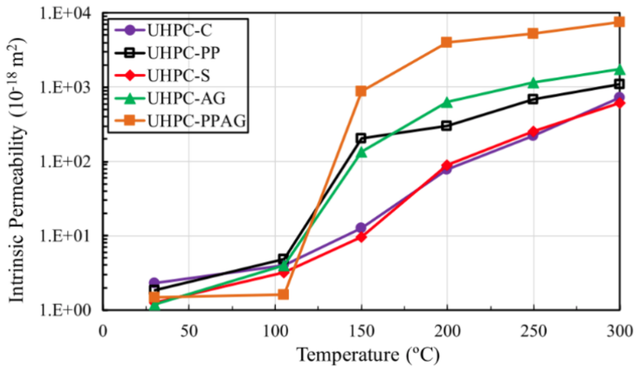

(a)

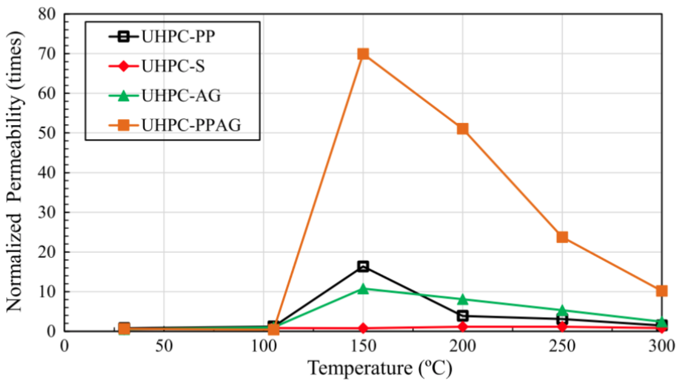

(b)

Figure 18 The (a) permeability and (b) normalized permeability of concrete with different fibres at elevated temperatures [59].

Other than permeability, the porosity of concrete might also explain the role of steel fibres in heated concrete. Yermak, et al. [51] found that the porosity of plain concrete is about 3% higher than that of steel fibres at 80 °C. The increase in porosity from 200 °C to 500 °C, however, is more drastic in steel fibre specimen. For the size and distribution of pores, more large pores were found at higher temperatures for plain concrete and PP fibre concrete. The steel fibre concrete seems good at control the pore size increase from 8 μm and above at high temperatures. The pore size distribution of different concrete specimens at elevated temperatures are shown in Figure 19.

In addition to permeability, the porosity of concrete may also explain the role of steel fibres in heated concrete. Yermak et al. [51] found that the porosity of plain concrete is approximately 3 % higher than that of steel fibre concrete at 80 °C. At temperatures ranging 200 °C to 500 °C, the increase in porosity is more pronounced in steel fibre specimens compared to plain concrete. Regarding the size and distribution of pores, there is increased number of large pores observed at higher temperatures for plain concrete and PP fibre concrete. Conversely, steel fibre concrete appears to effectively control the increase in large pore (8 μm and above) at high temperatures, as shown in Figure 19.

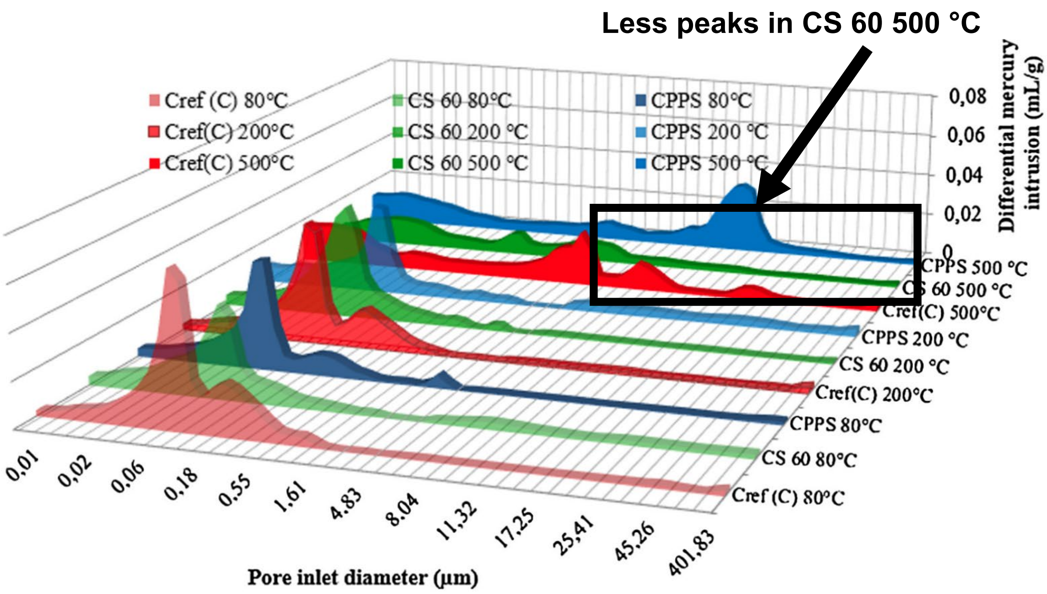

Figure 19 The pore size distribution of concrete with plain concrete (Cref), steel fibre concrete (CS 60) and PP fibre concrete (CPPS) at elevated temperatures [51].

1.3.3 Natural fibres

Ozawa et al. [72] investigated the performance and mechanism of concrete with natural jute fibres and polyvinyl alcohol fibres. The straw-like structure of the jute fibres can reduce the pore vapour pressure and the propensity of fire spalling of concrete. Zhang et al. [73] also examined the influence of jute fibres in heated concrete and found that the thermal shrinkage of the fibres can mitigate fire spalling. This mechanism is opposite to that of PP fibres, which control fire spalling through thermal expansion. Netinger et al. [74] studied hemp fibres and found that the residual concrete strength is increased due to the crack suppression mechanism of the fibres. Unfortunately, the spalling behaviour of the specimens with hemp fibres was not mentioned. Castoldi [75] investigated the mechanical influence of sisal fibres in concrete, noting that microcracks may also form at the interface between fibres and the cement matrix due to the swelling of the fibres when absorbing water.

Currently, there are numerous natural options available for substituting PP fibres in concrete, which offer greater environmental benefits compared to manufactured PP fibres. However, natural fibres may also encounter challenges such as limited production scale and the aging effects of natural products.

1.4 INTRODUCTION OF RECYCLED TYRE FIBRES

The integration of Recycled Steel Tyre Microfibers (RSTM) and Recycled Polymer Tyre Microfibres (RPTM) into concrete represents an innovative approach that has, until now, remained largely unexplored in terms of its impact on spalling resistance. This is partly attributed to the differing properties of RSTM and RPTM compared to virgin steel fibre and PP fibres, as illustrated in Table 2. The appearances of RSTM and RPTM are shown in Figure 20.

Table 2 Properties of various types of fibres

Properties	Density (kg/m^3)	Tensile strength (MPa)	Melting point (°C)	Length (mm)	Diameter (mm)
Virgin Steel Fibre	7800	1225	--	60	0.75
RSTM	7800	2000	--	10 - 40	0.12 - 0.4
Virgin PP Fibre	910	--	160	12	0.032
RPTM	500	--	230 - 250	0.8 - 16	0.008 – 0.06

Note: the length and diameter of all fibre types are the typical values of the fibres adopted in this study, which could vary depending on different specifications in practice.

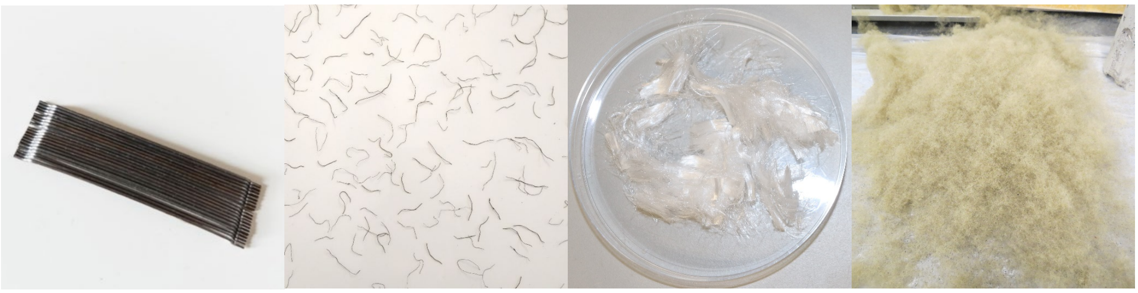

(a) (b) (c) (d)

Figure 20 Picture of (a) Virgin steel fibre (b) RSTM (c) Virgin PP Fibre (d) RPTM

1.4.1 Significance of recycled tyre fibres

RSTM was initially introduced as an ingredient in concrete design mixes to enhance concrete performance while addressing environmental challenges posed by the significant volume of waste tyres worldwide. Annually, approximately 1.5 billion waste tyres are generated, with around 3.5 million tons discarded in the EU alone [76]. The EU prohibited waste tyre disposal in 2006 [77] due to its adverse environmental impact [78]. Consequently, recycling waste tyres became imperative, and the construction sector proposed a suitable application – substituting steel fibres and PP fibres in concrete admixtures. Waste tyres typically contain approximately 12% to 25% steel fibres and 5.5% to 10% polymer fibres, depending on the tyre grade [79]. The typical composition of a tyre is illustrated in Figure 21.

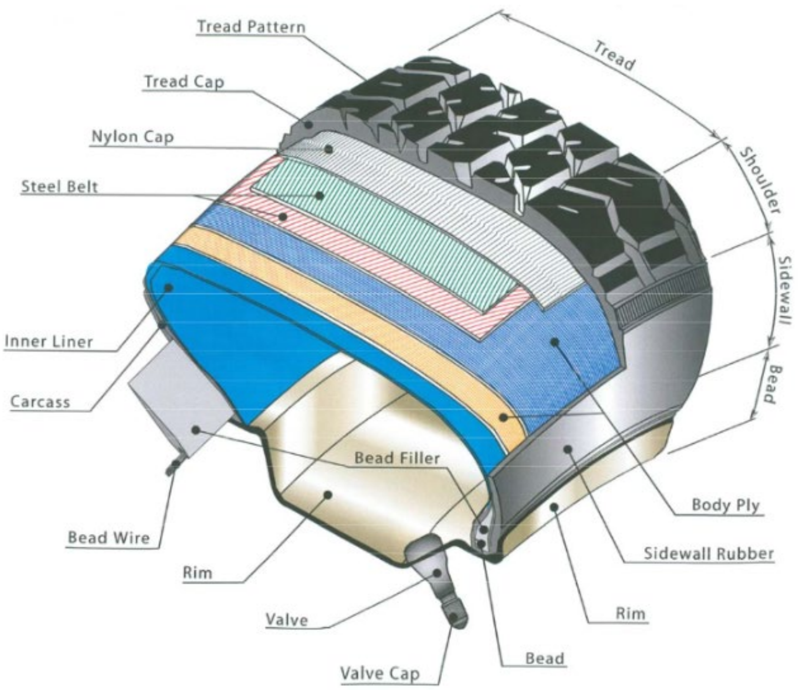

Figure 21 Schematic drawing of the composition of a typical tyre [79].

Raw recycled steel fibres from waste tyres are estimated to cost about 10% of virgin steel fibres [77], while cleaned RSTM can cost about half of the price of virgin steel fibres [80]. The use of recycled steel fibres can effectively resolve the high-cost issue associated with UHPC, as steel fibres constitute the primary expense in UHPC production [81]. Moreover, RSTM has been demonstrated to be at least as effective, if not superior, to virgin steel fibres in enhancing concrete performance under various ambient temperature conditions [82], [83], [84], [85], [86]. Regarding the use of RPTM in concrete, which also costs about half as much as manufactured PP fibres, research has shown its effectiveness in enhancing concrete resistance to shrinkage and chloride penetration [77], as well as improving post-fire concrete properties [87]. However, the compressive strength of RPTM concrete at elevated temperatures was found to decrease as fibre dosage increases [88].

For FRC concrete, a total of 2.6 tons of CO_2 can be produced per ton of steel fibre used [89]. In contrast, the CO_2 emission from RSTM is nearly neglectable compared to virgin steel fibres [80], [90]. According to the life cycle assessment (LCA) conducted by Gigli et al [91], each ton of polymer fibres produced from tyre recycling reduces the total carbon footprint by about 0.38 tons of CO_2 by avoiding cellulose production. Additionally, a total of 1.93 tons of CO_2 can be reduced by avoiding the incineration disposal of these fibres. This aligns with the calculated carbon footprint of fossil PP production by Tähkämö et al [92]., as shown in Figure 22. In broader terms, for the 3.5 million tons of annual waste tyres produced in Europe, approximately 0.4 million tons and 1.37 million tons of CO_2 can be saved by recycling the polymer fibres and steel fibres, respectively.

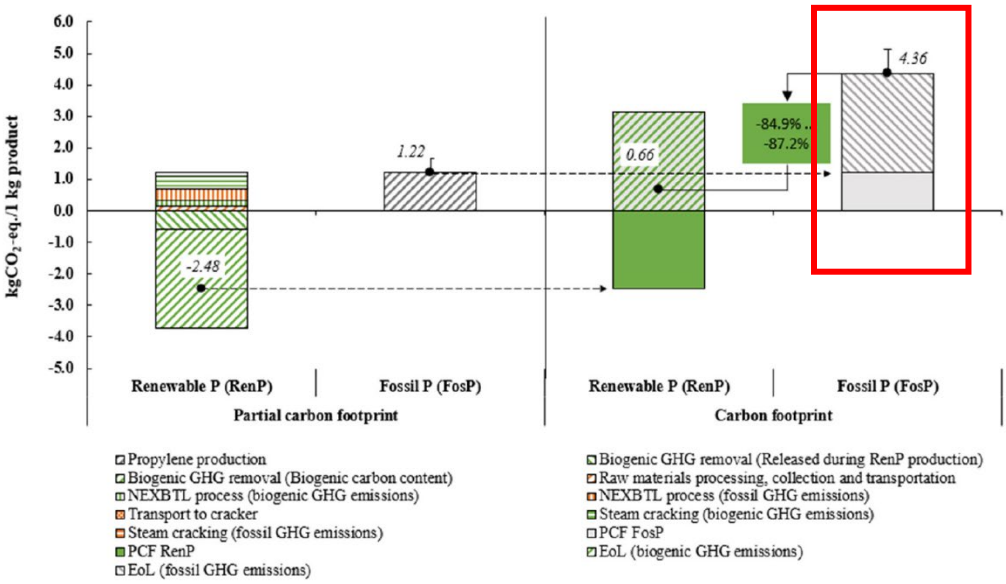

Figure 22 The calculated carbon footprints for fossil polypropylene (highlighted in red) [92].

1.4.2 Fire spalling studies on recycled tyre fibres

To date, there has been limited tests conducted to investigate fire-induced spalling in concrete with RSTM or RPTM. In a preliminary study at the University of Sheffield, Figueiredo et al. [93] conducted fire tests on concrete specimens containing both types of recycled tyre fibres. As shown in Figure 23. they subjected the specimen surfaces to heat from a row of three blowtorches while applying uniaxial compression load to the lateral sides of the specimens. The results indicated that as the dosage of fibres increased, the propensity and severity of fire spalling decreased significantly for both types of fibres. These initial findings suggest the effectiveness of incorporating RSTM and RPTM in concrete to mitigate fire spalling, potentially serving as substitutes for manufactured steel and PP fibres. However, as noted in the study, adopting a more standardized testing regimen, such as using standard fibre curves or larger specimen sizes, could yield more robust conclusions.

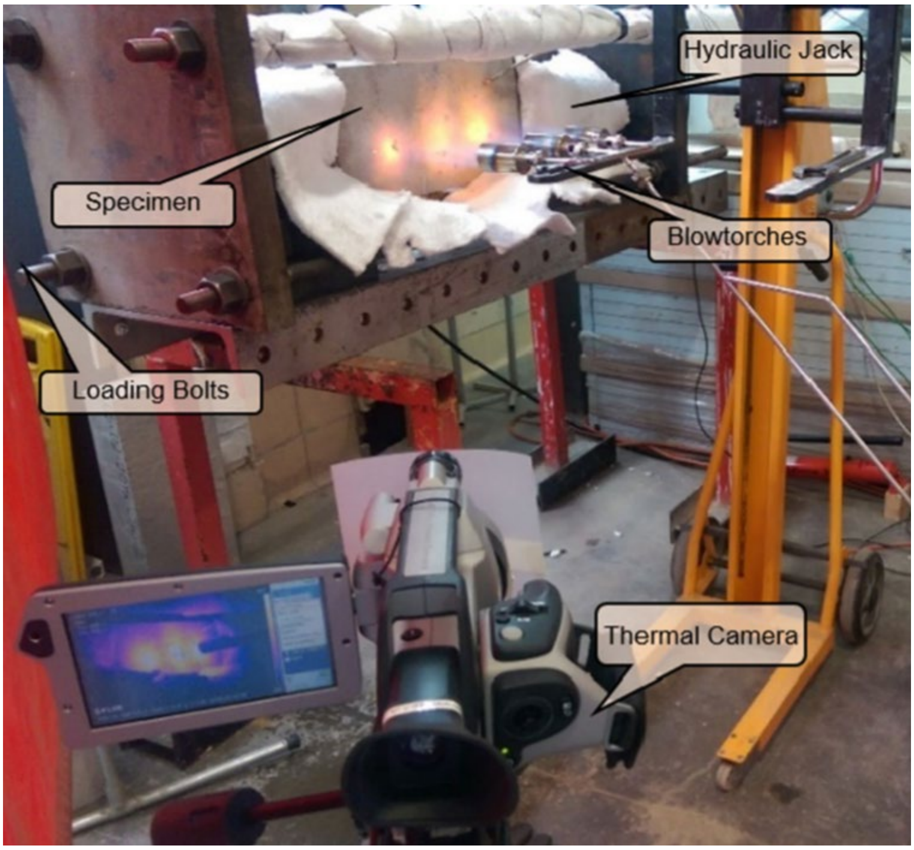

Figure 23 Fire spalling test setup by Figueiredo et al. [93].

Yang et al. [94] similarly discovered that the incorporation of recycled steel fibres can reduce the occurrence of fire spalling in concrete. However, their tests were conducted in a temperature-controlled furnace using small specimen sizes (100 mm cubes), which may diminish the persuasiveness of the conclusions due to the significant size effect in fire spalling test of concrete. Chen et al. [88] investigated concrete with different dosages of RPTM at elevated temperatures. Their results suggested that higher fibre dosages can result in increased porosity of concrete at ambient temperature. However, at 600 °C, the relationship between RPTM dosage and porosity becomes less clear. Additionally, the influence of RPTM on the pore size distribution varies with different fibre dosages, leading to an unclear indication of the role of fibres in heated concrete. The pore size distribution obtained in their study is shown in Figure 24.

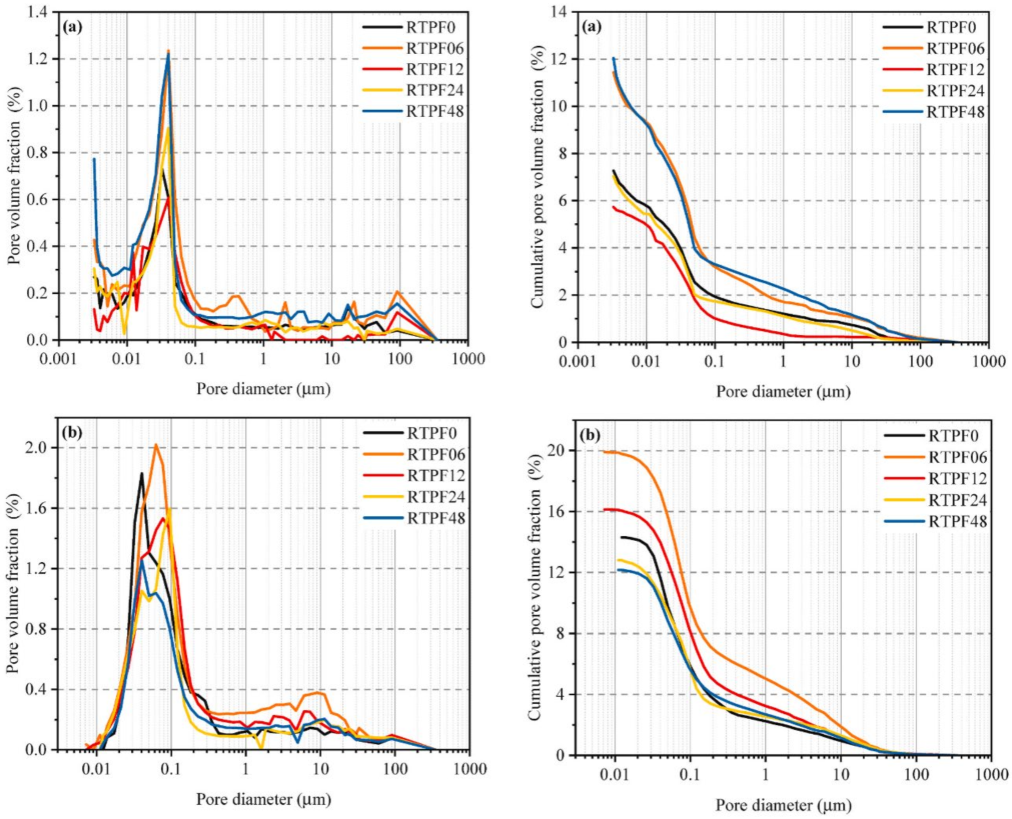

Figure 24, Pore size distribution of concrete with various dosages of recycled polymer fibres at (a) 20 °C and (b) 600 °C. Note: RTPF06 means 0.6 kg/m³ of recycled polymer fibre in concrete [88].

To summarize, while previous results indicate promising resistance to fire-induced spalling for RSTM and RPTM concrete, it is important to note that these tests were conducted under diverse configurations (e.g., blow torch heating, small sample size, unloaded conditions, etc.). To further validate the effectiveness of RPTM and RSTM under various conditions and gain a better understanding of the mechanism of these fibres in controlling fire spalling of concrete, the author conducted a series of investigations in their PhD project, which will be presented in the following chapters.

REFERENCES

[1] RAIB, *Rail Accident Report: Fire on HGV shuttle in the Channel Tunnel 21 August 2006*. Rail Accident Investigation Branch, Department for Transport., 2007. [Online]. Available: www.raib.gov.uk.

[2] J. Albrektsson, M. Flansbjer, J. E. Lindqvist, and R. Jansson, *Assessment of concrete structures after fire*. SP Technical Research Institute of Sweden, 2011.

[3] A. Leitner, 'The fire catastrophe in the Tauern Tunnel: experience and conclusions for the Austrian guidelines', *Tunnelling and Underground Space Technology*, vol. 16, p. 217223, 2001.

[4] R. Jansson and K. Ödeen, 'Fire in Storehouse 6 in the Free Port of Stockholm', in *2nd International RILEM Workshop on Concrete Spalling due to Fire Exposure*, Delft, 2011, pp. 205–210. [Online]. Available: https://www.researchgate.net/publication/281107891

[5] J. C. Mindeguia, H. Carré, P. Pimienta, and C. La Borderie, 'Experimental discussion on the mechanisms behind the fire spalling of concrete', *Fire Mater*, vol. 39, no. 7, pp. 619–635, Nov. 2015, doi: 10.1002/fam.2254.

[6] M. Amran, S. S. Huang, A. M. Onaizi, G. Murali, and H. S. Abdelgader, 'Fire spalling behavior of high-strength concrete: A critical review', *Construction and Building Materials*, vol. 341. Elsevier Ltd, Jul. 25, 2022. doi: 10.1016/j.conbuildmat.2022.127902.

[7] Raymond John Connolly, 'The Spalling of Concrete in Fires', PhD thesis, The University of Aston in Birmingham, Birmingham, 1995.

[8] A. M. B. Martins and J. P. C. Rodrigues, 'Fire behaviour of concrete columns with restrained thermal elongation', *Journal of Structural Fire Engineering*, vol. 2, no. 4, pp. 319–331, Dec. 2011, doi: 10.1260/2040-2317.2.4.319.

[9] K. D. Hertz, 'Limits of spalling of fire-exposed concrete', *Fire Saf J*, vol. 38, no. 2, pp. 103–116, Mar. 2003, doi: 10.1016/S0379-7112(02)00051-6.

[10] B. Georgali and P. E. Tsakiridis, 'Microstructure of fire-damaged concrete. A case study', *Cem Concr Compos*, vol. 27, no. 2, pp. 255–259, Jan. 2005, doi: 10.1016/j.cemconcomp.2004.02.022.

[11] R. Jansson and L. Boström, 'Factors influencing fire spalling of self compacting concrete', *Materials and Structures/Materiaux et Constructions*, vol. 46, no. 10, pp. 1683–1694, Oct. 2013, doi: 10.1617/s11527-012-0007-z.

[12] C. H. M. Zedán, 'Development and Application of a Novel Test Method for Studying the Fire Behaviour of CFRP Prestressed Concrete Structural Elements', 2014.

[13] S. S. Huang, H. Angelakopoulos, K. Pilakoutas, and I. Burgess, 'Reused tyre polymer fibre for fire-spalling mitigation', in *Applications of Structural Fire Engineering 2015*, Prague, Oct. 2015. doi: 10.14311/asfe.2015.056.

[14] E. Klingsch, A. Frangi, and M. Fontana, 'Experimental Analysis of Concrete Strength at High Temperatures and after Cooling', *Acta Polytechnica*, vol. 49, no. 1, 2009, [Online]. Available: http://ctn.cvut.cz/ap/

[15] G. A. Khoury, 'Compressive strength of concrete at high temperatures: a reassessment', *Magazine of Concrete Research*, vol. 44, no. 161, pp. 291–309, 1992.

[16] Robert Jansson, 'Fire Spalling of Concrete：Theoretical and Experimental Studies', PhD thesis, KTH Architecture and the Built Environment, Stockholm, 2013.

[17] Z. Bazant, 'Analysis of Pore Pressure, Thermal Stress and Fracture in Rapidly Heated Concrete', in *International Workshop on Fire Performance of High-Strength Concrete*, Gaithersburg, 1997. [Online]. Available: https://tsapps.nist.gov/publication/get_pdf.cfm?pub_id=916655

[18] Ö. Andiç-Çakir and S. Hizal, 'Influence of elevated temperatures on the mechanical properties and microstructure of self consolidating lightweight aggregate concrete', *Constr Build Mater*, vol. 34, pp. 575–583, Sep. 2012, doi: 10.1016/j.conbuildmat.2012.02.088.

[19] W. H. Johnson and W. H. Parsons, 'Thermal Expansion of Concrete Aggregate Materials', *Part of Journal of Research of the National Bureau of Standards*, vol. 32, Mar. 1944.

[20] M. Ozawa, T. Tanibe, R. Kamata, Y. Uchida, K. Rokugo, and S. S. Parajuli, 'Behavior of ring-restrained high-performance concrete under extreme heating and development of screening test', *Constr Build Mater*, vol. 162, pp. 215–228, Feb. 2018, doi: 10.1016/j.conbuildmat.2017.11.144.

[21] J. Kim, G. P. Lee, and D. Y. Moon, 'Evaluation of mechanical properties of steel-fibre-reinforced concrete exposed to high temperatures by double-punch test', *Constr Build Mater*, vol. 79, pp. 182–191, Mar. 2015, doi: 10.1016/j.conbuildmat.2015.01.042.

[22] W. Sha, E. A. O'neill, and Z. Guo, 'Differential scanning calorimetry study of ordinary Portland cement', 1999.

[23] C. Alonso and L. Fernandez, 'Dehydration and rehydration processes of cement paste exposed to high temperature environments', *J Mater Sci*, vol. 39, no. 9, pp. 3015–3024, May 2004, doi: 10.1023/B:JMSC.0000025827.65956.18.

[24] C. Liu and J. Chen, 'High Temperature Degradation Mechanism of Concrete with Plastering Layer', *Materials*, vol. 15, no. 2, Jan. 2022, doi: 10.3390/ma15020398.

[25] K. Y. Kim, T. S. Yun, and K. P. Park, 'Evaluation of pore structures and cracking in cement paste exposed to elevated temperatures by X-ray computed tomography', *Cem Concr Res*, vol. 50, pp. 34–40, 2013, doi: 10.1016/j.cemconres.2013.03.020.

[26] M. J. Heap *et al.*, 'The influence of thermal-stressing (up to 1000 °c) on the physical, mechanical, and chemical properties of siliceous-aggregate, high-strength concrete', *Constr Build Mater*, vol. 42, pp. 248–265, 2013, doi: 10.1016/j.conbuildmat.2013.01.020.

[27] L. A. Ashton and S. C. C. Bate, 'Discussion on the Fire-Resistance of Prestressed Concrete Beams', in *Proceedings of the Institution of Civil Engineers*, ICE, Oct. 1961, pp. 305–320.

[28] 'Gary R (1998)_Measurement and prediction of pore poressure in saturated cement mortar in elevated pressure'.

[29] M. Zeiml, R. Lackner, and H. A. Mang, 'Experimental insight into spalling behavior of concrete tunnel linings under fire loading', in *Acta Geotechnica*, Springer Verlag, 2008, pp. 295–308. doi: 10.1007/s11440-008-0069-9.

[30] Harmathy T. Z., 'Effect of moisture on the fire endurance of building elements', *ASTM Special Technical Publications no.385*, no. Ottawa, pp. 74–95, 1965, [Online]. Available: https://publications-cnrc.canada.ca/fra/voir/objet/?id=fcaa348d-5a0c-4341-92d4-ab6defae1340

[31] S. Ghabezloo, J. Sulem, and J. Saint-Marc, 'The effect of undrained heating on a fluid-saturated hardened cement paste', *Cem Concr Res*, vol. 39, no. 1, pp. 54–64, Jan. 2009, doi: 10.1016/j.cemconres.2008.09.004.

[32] M. Ozawa, S. Uchida, T. Kamada, and H. Morimoto, 'Study of mechanisms of explosive spalling in high-strength concrete at high temperatures using acoustic emission', *Constr Build Mater*, vol. 37, pp. 621–628, Dec. 2012, doi: 10.1016/j.conbuildmat.2012.06.070.

[33] R. Jansson and L. Boström, 'Fire Spalling-The Moisture Effect', in *1st International Workshop on Concrete Spalling due to Fire Exposure*, Leipzig: MFPA Institute, Sep. 2009, pp. 120–129. [Online]. Available: https://www.researchgate.net/publication/281113999

[34] P. Kalifa, Ë.-D. Menneteau, and D. Quenard, 'Spalling and pore pressure in HPC at high temperatures', *Cem Concr Res*, pp. 1915–1927, 2000.

[35] L. T. Phan, 'Pore pressure and explosive spalling in concrete', *Materials and Structures/Materiaux et Constructions*, vol. 41, no. 10, pp. 1623–1632, Dec. 2008, doi: 10.1617/s11527-008-9353-2.

[36] G. Choe, G. Kim, M. Yoon, E. Hwang, J. Nam, and N. Guncunski, 'Effect of moisture migration and water vapor pressure build-up with the heating rate on concrete spalling type', *Cem Concr Res*, vol. 116, pp. 1–10, Feb. 2019, doi: 10.1016/j.cemconres.2018.10.021.

[37] M. R. Bangi and T. Horiguchi, 'Effect of fibre type and geometry on maximum pore pressures in fibre-reinforced high strength concrete at elevated temperatures', *Cem Concr Res*, vol. 42, no. 2, pp. 459–466, Feb. 2012, doi: 10.1016/j.cemconres.2011.11.014.

[38] J. C. Mindeguia, P. Pimienta, A. Noumowé, and M. Kanema, 'Temperature, pore pressure and mass variation of concrete subjected to high temperature - Experimental and numerical discussion on spalling risk', *Cem Concr Res*, vol. 40, no. 3, pp. 477–487, Mar. 2010, doi: 10.1016/j.cemconres.2009.10.011.

[39] R. Jansson and L. Boström, 'The influence of pressure in the pore system on fire spalling of concrete', *Fire Technol*, vol. 46, no. 1, pp. 217–230, 2010, doi: 10.1007/s10694-009-0093-9.

[40] R. Felicetti, F. Lo Monte, and P. Pimienta, ‘A new test method to study the influence of pore pressure on fracture behaviour of concrete during heating’, *Cem Concr Res*, vol. 94, pp. 13–23, Apr. 2017, doi: 10.1016/j.cemconres.2017.01.002.

[41] D. Dauti, A. Tengattini, S. D. Pont, N. Toropovs, M. Briffaut, and B. Weber, ‘Some Observations on Testing Conditions of High-Temperature Experiments on Concrete: An Insight from Neutron Tomography’, *Transp Porous Media*, vol. 132, no. 2, pp. 299–310, Mar. 2020, doi: 10.1007/s11242-020-01392-2.

[42] G. H. A. Van Der Heijden, H. P. Huinink, L. Pel, and K. Kopinga, ‘One-dimensional scanning of moisture in heated porous building materials with NMR’, *Journal of Magnetic Resonance*, vol. 208, no. 2, pp. 235–242, Feb. 2011, doi: 10.1016/j.jmr.2010.11.010.

[43] J. D. Ríos, J. Mínguez, A. Martínez-De La Concha, M. Á. Vicente, and H. Cifuentes, ‘Microstructural analyses of the addition of PP fibres on the fracture properties of high-strength self-compacting concrete by X-ray computed tomography’, *Constr Build Mater*, vol. 261, Nov. 2020, doi: 10.1016/j.conbuildmat.2020.120499.

[44] B. Powierza, L. Stelzner, T. Oesch, C. Gollwitzer, F. Weise, and G. Bruno, ‘Water Migration in One-Side Heated Concrete: 4D In-Situ CT Monitoring of the Moisture-Clog-Effect’, *J Nondestr Eval*, vol. 38, no. 1, Mar. 2019, doi: 10.1007/s10921-018-0552-7.

[45] A. Tengattini *et al.*, ‘NeXT-Grenoble, the Neutron and X-ray tomograph in Grenoble’, *Nucl Instrum Methods Phys Res A*, vol. 968, Jul. 2020, doi: 10.1016/j.nima.2020.163939.

[46] D. Dauti, A. Tengattini, S. Dal Pont, N. Toropovs, M. Briffaut, and B. Weber, ‘Analysis of moisture migration in concrete at high temperature through in-situ neutron tomography’, *Cem Concr Res*, vol. 111, pp. 41–55, Sep. 2018, doi: 10.1016/j.cemconres.2018.06.010.

[47] M. H. Moreira, S. Dal Pont, A. Tengattini, A. P. Luz, and V. C. Pandolfelli, ‘Experimental proof of moisture clog through neutron tomography in a porous medium under truly one-directional drying’, *Journal of American Ceramic Society*, vol. 105, no. 5, pp. 3534–3543, May 2022.

[48] L. Stelzner, B. Powierza, T. Oesch, R. Dlugosch, and F. Weise, ‘Thermally-induced moisture transport in high-performance concrete studied by X-ray-CT and 1H-NMR’, *Constr Build Mater*, vol. 224, pp. 600–609, Nov. 2019, doi: 10.1016/j.conbuildmat.2019.07.065.

[49] P. Kalifa, G. Chéné, and C. Gallé, ‘High-temperature behaviour of HPC with polypropylene fibres From spalling to microstructure’, *Cem Concr Res*, pp. 1487–1499, 2001.

[50] A. Bilodeau, V. K. R. Kodur, and G. C. Hoff, ‘Optimization of the type and amount of polypropylene fibres for preventing the spalling of lightweight concrete subjected to hydrocarbon fire’, *Cem Concr Compos*, vol. 26, no. 2, pp. 163–174, Feb. 2004, doi: 10.1016/S0958-9465(03)00085-4.

[51] N. Yermak, P. Pliya, A. L. Beaucour, A. Simon, and A. Noumowé, ‘Influence of steel and/or polypropylene fibres on the behaviour of concrete at high temperature: Spalling, transfer and

mechanical properties', *Constr Build Mater*, vol. 132, pp. 240–250, Feb. 2017, doi: 10.1016/j.conbuildmat.2016.11.120.

[52] H. Dang, A. Liang, R. Feng, J. Zhang, X. Yu, and Y. Shao, 'Experimental study on mechanical properties and low-cycle fatigue behaviour of stainless steels subjected to salt spray and dry/wet cycle', *Int J Fatigue*, vol. 165, Dec. 2022, doi: 10.1016/j.ijfatigue.2022.107187.

[53] British Standards Institution, 'BS EN 1992-1-2:2023, Eurocode 2: Design of concrete structures : Part 1-2: Structural fire design', London, 2023.

[54] British Standards Institution., 'BS EN 1992-1-2:2004, Eurocode 2: Design of concrete structures : Part 1-2: General rules — Structural fire design', BSi, London, 2010.

[55] A. Noumowe, 'Mechanical properties and microstructure of high strength concrete containing polypropylene fibres exposed to temperatures up to 200 °c', *Cem Concr Res*, vol. 35, no. 11, pp. 2192–2198, Nov. 2005, doi: 10.1016/j.cemconres.2005.03.007.

[56] A. Bentur, S. Mindessf, and G. Vondran4, 'Bonding in polypropylene fibre reinforced concretes', *The International Journal of Cement Composites and Lightweight Concrete*, vol. 11, pp. 153–158, 1989.

[57] S. P. Yap, Y. Goh, W. X. Goh, K. H. Mo, M. Y. J. Liu, and H. A. Ibrahim, 'Relationship between microstructure and performance of polypropylene fibre reinforced cement composites subjected to elevated temperature', *European Journal of Environmental and Civil Engineering*, vol. 26, no. 5, pp. 1792–1806, 2022, doi: 10.1080/19648189.2020.1734489.

[58] D. Zhang, A. Dasari, and K. H. Tan, 'On the mechanism of prevention of explosive spalling in ultra-high performance concrete with polymer fibers', *Cem Concr Res*, vol. 113, pp. 169–177, Nov. 2018, doi: 10.1016/j.cemconres.2018.08.012.

[59] Y. Li, K. H. Tan, and E. H. Yang, 'Influence of aggregate size and inclusion of polypropylene and steel fibers on the hot permeability of ultra-high performance concrete (UHPC) at elevated temperature', *Constr Build Mater*, vol. 169, pp. 629–637, Apr. 2018, doi: 10.1016/j.conbuildmat.2018.01.105.

[60] Y. Ding, C. Zhang, M. Cao, Y. Zhang, and C. Azevedo, 'Influence of different fibers on the change of pore pressure of self-consolidating concrete exposed to fire', *Constr Build Mater*, vol. 113, pp. 456–469, Jun. 2016, doi: 10.1016/j.conbuildmat.2016.03.070.

[61] A. Lau and M. Anson, 'Effect of high temperatures on high performance steel fibre reinforced concrete', *Cem Concr Res*, vol. 36, no. 9, pp. 1698–1707, Sep. 2006, doi: 10.1016/j.cemconres.2006.03.024.

[62] R. Serrano, A. Cobo, M. I. Prieto, and M. de las N. González, 'Analysis of fire resistance of concrete with polypropylene or steel fibers', *Constr Build Mater*, vol. 122, pp. 302–309, Sep. 2016, doi: 10.1016/j.conbuildmat.2016.06.055.

[63] M. Tayebi and M. Nematzadeh, 'Effect of Hot-Compacted waste nylon fine aggregate on compressive Stress-Strain behavior of steel Fiber-Reinforced concrete after exposure to fire:

Experiments and optimization', *Constr Build Mater*, vol. 284, May 2021, doi: 10.1016/j.conbuildmat.2021.122742.

[64] V. K. R. Kodur, ; Fu, P. Cheng, T.-C. Wang, and M. A. Sultan, 'Effect of Strength and Fiber Reinforcement on Fire Resistance of High-Strength Concrete Columns', *JOURNAL OF STRUCTURAL ENGINEERING*, vol. 129(2), pp. 253–259, Feb. 2003, doi: 10.1061/ASCE0733-94452003129:2253.

[65] N. Algourdin, P. Pliya, A. L. Beaucour, A. Simon, and A. Noumowé, 'Influence of polypropylene and steel fibres on thermal spalling and physical-mechanical properties of concrete under different heating rates', *Constr Build Mater*, vol. 259, Oct. 2020, doi: 10.1016/j.conbuildmat.2020.119690.

[66] S. L. Suhaendi and T. Horiguchi, 'Effect of short fibers on residual permeability and mechanical properties of hybrid fibre reinforced high strength concrete after heat exposition', *Cem Concr Res*, vol. 36, no. 9, pp. 1672–1678, Sep. 2006, doi: 10.1016/j.cemconres.2006.05.006.

[67] Y. Ding, C. Azevedo, J. B. Aguiar, and S. Jalali, 'Study on residual behaviour and flexural toughness of fibre cocktail reinforced self compacting high performance concrete after exposure to high temperature', *Constr Build Mater*, vol. 26, no. 1, pp. 21–31, Jan. 2012, doi: 10.1016/j.conbuildmat.2011.04.058.

[68] F. Lo Monte, R. Felicetti, and C. Rossino, 'Fire spalling sensitivity of high-performance concrete in heated slabs under biaxial compressive loading', *Materials and Structures/Materiaux et Constructions*, vol. 52, no. 1, Jan. 2019, doi: 10.1617/s11527-019-1318-0.

[69] O. Czoboly, É. Lublóy, V. Hlavička, G. L. Balázs, O. Kéri, and I. M. Szilágyi, 'Fibers and fiber cocktails to improve fire resistance of concrete', *J Therm Anal Calorim*, vol. 128, no. 3, pp. 1453–1461, Jun. 2017, doi: 10.1007/s10973-016-6038-x.

[70] Y. S. Heo, C. G. Han, and K. M. Kim, 'Combined fiber technique for spalling protection of concrete column, slab and beam in fire', *Materials and Structures/Materiaux et Constructions*, vol. 48, no. 10, pp. 3377–3390, Oct. 2015, doi: 10.1617/s11527-014-0406-4.

[71] S. Sanchayan and S. J. Foster, 'High temperature behaviour of hybrid steel–PVA fibre reinforced reactive powder concrete', *Materials and Structures/Materiaux et Constructions*, vol. 49, no. 3, pp. 769–782, Mar. 2016, doi: 10.1617/s11527-015-0537-2.

[72] M. Ozawa and H. Morimoto, 'Effects of various fibres on high-temperature spalling in high-performance concrete', *Constr Build Mater*, vol. 71, pp. 83–92, Nov. 2014, doi: 10.1016/j.conbuildmat.2014.07.068.

[73] D. Zhang, K. H. Tan, A. Dasari, and Y. Weng, 'Effect of natural fibers on thermal spalling resistance of ultra-high performance concrete', *Cem Concr Compos*, vol. 109, May 2020, doi: 10.1016/j.cemconcomp.2020.103512.

[74] I. Netinger Grubeša, B. Marković, A. Gojević, and J. Brdarić, ‘Effect of hemp fibers on fire resistance of concrete’, *Constr Build Mater*, vol. 184, pp. 473–484, Sep. 2018, doi: 10.1016/j.conbuildmat.2018.07.014.

[75] R. de S. Castoldi, L. M. S. de Souza, and F. de Andrade Silva, ‘Comparative study on the mechanical behavior and durability of polypropylene and sisal fiber reinforced concretes’, *Constr Build Mater*, vol. 211, pp. 617–628, Jun. 2019, doi: 10.1016/j.conbuildmat.2019.03.282.

[76] Fazilet Cinaralp and Jean-Pierre Taverne, ‘End of life tyres: A valuable resource with growing potential’, ETRMA. Accessed: Feb. 08, 2023. [Online]. Available: https://www.etrma.org/wp-content/uploads/2019/09/2010_etrma_elt_management_brochure_final.pdf

[77] M. Serdar, A. Baričević, S. Lakušić, and D. Bjegović, ‘Special purpose concrete products from waste tyre recyclates’, *Journal of the Croatian Association of Civil Engineers*, vol. 65, no. Građevinar, pp. 793–801, 2013.

[78] B. S. Thomas and R. C. Gupta, ‘A comprehensive review on the applications of waste tire rubber in cement concrete’, *Renewable and Sustainable Energy Reviews*, vol. 54. Elsevier Ltd, pp. 1323–1333, Feb. 01, 2016. doi: 10.1016/j.rser.2015.10.092.

[79] Anne and E. Russ, ‘The Composition of a Tyre: Typical Components Creating markets for recycled resources’, May 2006. Accessed: Apr. 06, 2024. [Online]. Available: https://docplayer.net/20736072-The-composition-of-a-tyre-typical-components.html

[80] Zero Waste Works, ‘Recycled Steel Tyre Microfibres’. Accessed: Mar. 18, 2024. [Online]. Available: https://www.zerowasteworks.co.uk/recycled-steel-microfibres

[81] K. M. Liew and A. Akbar, ‘The recent progress of recycled steel fiber reinforced concrete’, *Construction and Building Materials*, vol. 232. Elsevier Ltd, Jan. 30, 2020. doi: 10.1016/j.conbuildmat.2019.117232.

[82] E. Gholami, H. Afshin, M. Charkhtab Basim, and M. Sharghi, ‘Ultra-high performance recycled steel fiber reinforced concrete segments under the thrust force of TBM jacks and their environmental potentialities’, *Structures*, vol. 47, pp. 2465–2484, Jan. 2023, doi: 10.1016/j.istruc.2022.12.051.

[83] X. Qin and S. Kaewunruen, ‘Environment-friendly recycled steel fibre reinforced concrete’, *Construction and Building Materials*, vol. 327. Elsevier Ltd, Apr. 11, 2022. doi: 10.1016/j.conbuildmat.2022.126967.

[84] M. H. Abd-Elrahman, I. S. Agwa, Y. Elsakhawy, and M. S. Rizk, ‘Effect of utilising ferrosilicon and recycled steel fibres on ultra-high-strength concrete containing recycled granite’, *Case Studies in Construction Materials*, vol. 18, Jul. 2023, doi: 10.1016/j.cscm.2023.e01903.

[85] F. Soltanzadeh, A. Edalat-Behbahani, and E. N. B. Pereira, ‘Bond behavior of recycled tyre steel fiber reinforced concrete and basalt fiber-reinforced polymer bars under static and

fatigue loading conditions', *Journal of Building Engineering*, p. 106291, Mar. 2023, doi: 10.1016/j.jobe.2023.106291.

[86] H. Zhong, E. W. Poon, K. Chen, and M. Zhang, 'Engineering properties of crumb rubber alkali-activated mortar reinforced with recycled steel fibres', *J Clean Prod*, vol. 238, Nov. 2019, doi: 10.1016/j.jclepro.2019.117950.

[87] M. Jelcic Rukavina, A. Baricevic, M. Serdar, and M. Grubor, 'Study on the post-fire properties of concrete with recycled tyre polymer fibres', *Cem Concr Compos*, vol. 123, Oct. 2021, doi: 10.1016/j.cemconcomp.2021.104184.

[88] M. Chen, Z. Sun, W. Tu, X. Yan, and M. Zhang, 'Behaviour of recycled tyre polymer fibre reinforced concrete at elevated temperatures', *Cem Concr Compos*, vol. 124, Nov. 2021, doi: 10.1016/j.cemconcomp.2021.104257.

[89] A. M. Matos, S. Nunes, C. Costa, and J. L. Barroso-Aguiar, 'Spent equilibrium catalyst as internal curing agent in UHPFRC', *Cem Concr Compos*, vol. 104, Nov. 2019, doi: 10.1016/j.cemconcomp.2019.103362.

[90] H. Abdolpour *et al.*, 'Performance and life cycle of ultra-high performance concrete mixes containing oil refinery waste catalyst and steel fibre recovered from scrap tyre', *Journal of Building Engineering*, vol. 79, Nov. 2023, doi: 10.1016/j.jobe.2023.107890.

[91] S. Gigli, D. Landi, and M. Germani, 'Cost-benefit analysis of a circular economy project: a study on a recycling system for end-of-life tyres', *J Clean Prod*, vol. 229, pp. 680–694, Aug. 2019, doi: 10.1016/j.jclepro.2019.03.223.

[92] L. Tähkämö, A. Ojanperä, J. Kemppi, and I. Deviatkin, 'Life cycle assessment of renewable liquid hydrocarbons, propylene, and polypropylene derived from bio-based waste and residues: Evaluation of climate change impacts and abiotic resource depletion potential', *J Clean Prod*, vol. 379, Dec. 2022, doi: 10.1016/j.jclepro.2022.134645.

[93] F. P. Figueiredo, S. S. Huang, H. Angelakopoulos, K. Pilakoutas, and I. Burgess, 'Effects of Recycled Steel and Polymer Fibres on Explosive Fire Spalling of Concrete', *Fire Technol*, vol. 55, no. 5, pp. 1495–1516, Sep. 2019, doi: 10.1007/s10694-019-00817-9.

[94] J. Yang, G. F. Peng, G. S. Shui, and G. Zhang, 'Mechanical properties and anti-spalling behavior of ultra-high performance concrete with recycled and industrial steel fibers', *Materials*, vol. 12, no. 5, Mar. 2019, doi: 10.3390/ma12050783.

2 Structure of the papers

Given the significant potential benefits of using recycled tyre fibres and the initial efficacy of these fibres in mitigating the fire spalling of concrete, the first objective of this project is to:

- Establish a more comprehensive and validated understanding of the effectiveness of RSTM and RPTM in controlling fire spalling of concrete.

Considering (1) the limited comprehension of the mechanisms of fire spalling of concrete; (2) the ambiguous role of steel and polypropylene fibres in heated concrete; (3) the differential properties between virgin fibre and recycled tyre fibre; as well as (4) the deficiencies of the existing investigation methods, the second objective of this project is to:

- Utilize advanced imaging techniques to examine the behaviour of concrete with RPTM at elevated temperatures, thereby revealing the mechanisms and the function of RPTM in fire spalling of concrete.

2.1 RESEARCH PROGRESS AND RELATIONSHIP OF THE PAPERS

The sequence of papers is presented following the research process of the author's PhD career. The experiments progressed from testing the influence of few parameters to multiple parameters, and the level of investigation ranged from a global scale to a micro scale. The focus of the research shifted from practical applications to fundamental mechanism studies.

As introduced in Section 1.4.2, preliminary tests conducted at the University of Sheffield had shown the effectiveness of recycled tyre fibres, but the test configurations can be further improved. The first step of the project aims to establish relatively more standardized test conditions for the fire spalling test of concrete, and to better examine the potential of RPTM to substitute PP fibres. Although the main components of the newly designed test setup have been assembled at the University of Sheffield, several manoeuvres are still required to fulfil its purpose, including temperature calibration and load calibration. The whole test system awaits an authentic test to exclude uncertainties.

The first paper is then introduced. The fire spalling tests initially verified the reliability of the newly developed test rig, as the occurrence of fire spalling results are repeatable for plain concrete, and no spalling occurred for concrete included with 2 kg/m^3 of RPTM. Other than confirming the effectiveness of RPTM in controlling fire spalling in the test condition, the surface moisture content of concrete is also identified as a more specific influencing factor for fire spalling compared to global moisture content.

The second paper included studies of the influence of several novel concrete materials at elevated temperatures. The use of stainless steel rebar can significantly increase the service time and reduce the maintenance cost of concrete structures. Similar to stainless steel, as introduced in Section 1.4.1, the use of RSTM can also reduce the cost and carbon footprint of concrete by substituting virgin steel fibres. The combination of these two materials could bring huge benefits, but there is very limited knowledge on the fire performance in concrete. Hence, fire spalling tests were conducted, and the results showed significant improvement of fire spalling resistance for steel fibre concrete. The use of stainless steel rebar, on the other hand, is not as effective as steel fibres in fire spalling control. However, the combination of a shallow cover depth and the use of austenitic stainless steel rebar was found to be able to mitigate fire spalling without the inclusion of steel fibres. This finding may suggest another significant benefit brought by the use of stainless steel rebar. Since corrosion-induced spalling and fire-induced spalling are both avoided in concrete with stainless steel rebar at shallow cover depth, the reduction of the concrete cover is possible in future concrete design. This shallower cover depth may further reduce the cost and carbon footprint of concrete structures compared to traditional carbon steel rebar concrete.

The third paper presents a comparative study examining the effectiveness of RPTM and PP fibres in mitigating fire spalling under extreme conditions, such as high moisture content and reduced fibre dosage. In addition, the investment methods were more versatile than the previous tests. To better understand the role of polymer fibres in heated concrete, the vapour pore pressure, void ratio, permeability, and SEM study of the fibres were conducted. To boost the vast application of RSTM, the fibre integration method was changed from the previous tests, from machine dispersion (slower process but better fibre distribution) to manual dispersion (faster but unknown effect on fibre distribution). The idea is to rely on the grinding of the aggregates during the concrete mixing process to disperse the tangled RPTM. The test results demonstrate that the virgin PP fibres were found to be the most effective type of fibre to control spalling, while the use of RPTM with the manual dispersion method is less effective. The magnitude of vapour pore pressure was found not directly linked to the propensity of fire spalling of concrete. The mechanism of PP fibres could be different from RPTM in controlling fibre spalling, due to different concrete properties at ambient and high temperatures.

The fourth paper aims to better understand the role of RPTM on the fire spalling of concrete. This is a mechanism study which mainly focus on the thermos-hydro-mechanical behaviour of the heated concrete. Three related hypotheses were proposed based on the moisture clog theory and the corresponding experimental verification was designed. Through advanced in-situ X-ray and neutron tomographies, the moisture distribution and porous structure of concrete at elevated temperatures are revealed. The alteration of pores due to the presence of the thermocouple is also investigated. The hypotheses explaining the mechanism of fire spalling and the role of fibres were examined but not fully verified. The test results can confirm the presence of moisture clogs and the accelerating effect of RPTM on moisture migration.

The fourth paper aims to better understand the role of RPTM on the fire spalling of concrete. This is a mechanism study which mainly focuses on the thermos-hydro-mechanical behaviour of heated concrete. Three related hypotheses were proposed based on the moisture clog theory, and the corresponding experimental verification was designed. Through advanced in-situ X-ray and neutron tomographies, the moisture distribution and porous structure of concrete at elevated temperatures are revealed. The alteration of pores due to the presence of the thermocouple is also investigated. The hypotheses explaining the mechanism of fire spalling and the role of fibres were examined but not fully verified. The test results confirm the presence of moisture clogs and the accelerating effect of RPTM on moisture migration.

2.2 HIGHLIGHTS OF THE PAPERS

Paper I:

Mitigation of Fire-Induced Spalling of Concrete using Recycled Polymer Tyre Microfibres

Fire spalling tests were conducted on C60 high-strength concretes with and without RPTM at various surface moisture content. Based on the findings and the specified test conditions, the following conclusions were drawn:

- The addition of RTPF at a dosage of 2kg/m^3 could be sufficient to mitigate fire-induced spalling in concrete.
- The severity (volume) of spalling is more influenced by the surface moisture content than by the average moisture content.

Paper II:

Fire Spalling Behaviour of Stainless Steel Reinforced Concrete with Recycled Steel Tyre Microfibres

The fire spalling behaviour of concrete specimens was studied with different specimen configurations, including concrete element type, stainless steel rebar type, cover depth, and various types of steel fibres. The following conclusions can be drawn:

- The use of virgin steel fibre and RSTM at 30 kg/m^3 effectively mitigated fire-induced explosive spalling for the specific test configuration. The mitigation mechanism of steel fibres appears to involve faster leaking of heated vapour, as no vapour leaks were observed from the side of steel FRC concrete compared with plain concrete.
- The virgin steel fibre might be more effective at controlling aggregate spalling.
- For the designed specimen sizes, the propensity and severity of spalling were found to be higher in larger specimens than in smaller specimens.
- The use of duplex steel rebar was found to delay concrete spalling compared to austenitic steel rebar. This effect was independent of the shape and size of the specimen in our test.
- The typical configuration of austenitic rebar and 15 mm cover depth specimen did not exhibit any signs of explosive spalling without the addition of fibres. This could be due to the amplified internal cracking of the concrete caused by the differential thermal expansion between the rebar and concrete.

Paper III:
Study on the fire spalling behaviour of recycled polymer tyre microfibre and virgin polypropylene fibre reinforced concrete

Fire spalling tests were conducted to study the difference between PP fibres and RPTM concrete at various dosages and high moisture content. Several side tests were also conducted to study the properties of concrete at elevated temperatures. The following conclusions can be drawn:

- Virgin PP fibres are the most effective method for mitigating fire spalling in concrete. The melting of PP fibres increases the permeability of the concrete and facilitates moisture movement, reducing the risk of spalling.

- The inclusion of RPTM is relatively less effective in mitigating fire spalling compared to PP fibres but still offers some benefits. RPTM primarily act to control thermal stress in the concrete, as opposed to increasing permeability like PP fibres.

- Pore pressure levels in concrete at elevated temperatures are not the main cause of fire spalling. The plain concrete specimen experienced the most intense explosive spalling, despite having relatively low pore pressure.

- The manual integration process of RPTM in concrete casting may not bring the most idealized fibre distribution condition in the tested specimen.

Paper IV:
Fire Spalling Mechanisms and effect of Recycled Polymer Tyre Microfibres in Concrete at Elevated Temperatures through Neutron and X-Ray Tomographies

Combined neutron and X-ray tomographies were performed on concrete with RPTM at elevated temperatures. This in-situ, non-intrusive imaging technique reveals the evolution of 3D moisture profiles and porous structures within heated concrete. The main conclusions are:

- The formation of moisture clog and its location were investigated through neutron tomography results. The inclusion of RPTM facilitates moisture migration and leads to a lower temperature at the drying front compared with plain concrete. The X-ray results indicate that the inclusion of RPTM can increase both the intrinsic porosity and thermal porosity of concrete via fibre addition and thermal expansion. All test specimens provide some evidence to support the moisture clog theory.

- The presence of thermocouples can alter the intrinsic porous structure and the moisture migration process in heated concrete, even when the diameter of the thermocouple is minimised.
- The observed wetting phase in the drying volume ratios analysis of heated concrete provides indirect evidence to indicate the transportation of moisture from gel pores and capillaries to macropores.
- No obvious crack opening was observed near the drying front in the X-ray tomography results, as the sphericity of the pores remained constant after heating. This may be due to the low heating intensity or the relatively low resolution of the X-ray tomography.

2.3 CONTRIBUTION OF AUTHORS

Paper I:

Yifan Li: Conceptualization, Methodology, Investigation, Formal analysis, Writing - Original Draft, Project administration. **Shan-Shan Huang:** Conceptualization, Methodology, Resources, Writing - Review & Editing, Supervision, Project administration, Funding acquisition. **Kypros Pilakoutas:** Conceptualization, Writing - Review & Editing, Supervision. **Harris Angelakopoulos:** Resources, Writing - Review & Editing. **Ian Burgess:** Writing - Review & Editing.

The concrete specimens had already been cast by the time the author began their PhD, and the test rig had also been assembled. The author's main contributions included calibrating and preparing the fire spalling test rig, designing the test concept, preparing the concrete specimens (remoisturizing), conducting all the tests, analysing the data, and drafting the original manuscript.

Paper II:

Yifan Li: Methodology, Validation, Investigation, Formal analysis, Writing - Original Draft, Project administration. **Katherine A. Cashell:** Conceptualization, Methodology, Resources, Writing - Review & Editing, Funding acquisition. **Harris Angelakopoulos:** Resources, Methodology, Writing - Review & Editing. **Shan-Shan Huang:** Conceptualization, Methodology, Resources, Writing - Review & Editing, Supervision, Project administration, Funding acquisition.

The test specimens were cast by Katherine A. Cashell, while the author's contributions involved project administration, updating the test rig (including implementing a better loading system with a stiffened loading frame and two hydraulic jacks, and improving the heat isolation plan), conducting all the tests, analysing the data, and drafting the first version of the manuscript.

Paper III:

Yifan Li: Conceptualization, Methodology, Validation, Formal analysis, Investigation, Resources, Writing - Original Draft, Project administration. **Kypros Pilakoutas:** Methodology, Writing - Review & Editing, Supervision. **Shan-Shan Huang:** Conceptualization, Methodology, Resources, Writing - Review & Editing, Supervision, Project administration, Funding acquisition.

With the guidance of two supervisors, the author fully designed, developed, conducted, analyzed, and firstly drafted this paper.

Paper IV:

Yifan Li: Conceptualization, Methodology, Software, Investigation, Formal analysis, Writing - Original Draft, Project administration. **Stefano Dal Pont:** Methodology, Resources, Writing - Review & Editing**. Alessandro Tengattini:** Methodology, Software, Resources, Data Curation, Writing - Review & Editing. **Kypros Pilakoutas:** Writing - Review & Editing, Supervision**. Shan-Shan Huang:** Conceptualization, Methodology, Resources, Writing - Review & Editing, Supervision, Project administration, Funding acquisition.

The test equipment was prepared by Stefano Dal Pont (specimen heating chamber) and Alessandro Tengattini (tomographies). The main contributions of the author include: project administration, all specimen preparation, most test investigations, full data analysis, first draft writing.

2.4 FUTURE WORKS

Although fire spalling tests have examined four types of fibres in this thesis, their effectiveness still lacks comprehensive understanding for full potential and practical application. Virgin PP fibre, known for outstanding performance in preventing fire spalling, was not pushed to its limits in our tests. We used half of the recommended dosage of 1 kg/m^3 by the Eurocode in high strength concrete of 60 MPa with a relatively high moisture content of 5.4% on the concrete surface. Despite this, the PP fibre concrete specimens still survived the fire test, indicating the need to further push the limits in future studies. It is recommended to use hydrocarbon fire curves or higher concrete grades for future spalling tests.

For virgin steel fibres and RSTM, the results initially demonstrated their effectiveness in relatively low-strength concrete. However, UHPC, which typically includes steel fibres to enhance ductility, was found to be very vulnerable in fire conditions. Therefore, future research should include more fire spalling tests using UHPC with RSTM and virgin steel fibres.

While RPTM performed well in aged concrete in this study, its performance was less than ideal for fresh concrete with high moisture content. Thus, a sensitivity analysis of RPTM dosages, moisture content, and fire spalling propensity of heated concrete is recommended. Additionally, the current automatic RPTM integration process using machines is slow, and manual dispersion of fibres, although faster, does not provide sufficient functionality in fire spalling mitigation. Thus, future work should focus on improving the fibre integration process for practical use in vast concrete productions.

For the mechanism investigations, it was observed that the influence of stainless steel rebars and the concrete cover depth affected the fire spalling behaviour of concrete. Although speculations explaining the mechanisms were proposed based on observations and spalling results, there is lack of direct evidence. Therefore, future research should focus on investigating the mechanisms of steel fibres, stainless steel rebars, and cover depths to provide more conclusive evidence. Instruments such as thermocouples, strain sensors, and pressure gauges could offer further insights into the basic mechanisms.

The thermal expansion coefficient of the RPTM fibre, as well as investigation of the melting process of RPTM can bring crucial information for its performance in heated concrete. If possible, obtaining a true profile of the porous structures of RPTM concrete can be very helpful for understanding its mechanism. This profile needs analysis from the microscale

(SEM analysis), mesoscale (MIP intrusions), and macroscale (hot gas/water permeabilities) at elevated temperatures. Since the melting point of the RPTM is not constant, this work can be very challenging.

Moreover, exploring the thermal expansion coefficient of RPTM fibres and investigating the melting process of RPTM can provide crucial information for understanding its performance in heated concrete. Obtaining an accurate profile of the porous structures of RPTM concrete would also be beneficial. This profile might requires analysis at elevated temperatures and in various scales, including microscale (SEM analysis), mesoscale (MIP intrusions), and macroscale (gas/water permeabilities). However, this task may be challenging due to the variable properties of RPTM.

Finally, as discussed in Paper IV, advancements in X-ray and neutron tomography technology could potentially provide a final solution to the mechanism study of fire spalling. If the resolution and speed of tomography improve sufficiently to track changes in heated concrete in real-time, it would enable direct observation of processes such as microcrack formation, moisture clogging, fibre melting, and vapour migration in high resolution. This advancement could lead to greater confidence in concluding on the fire spalling mechanism and predicting the behaviour of concrete in practical applications.

3 Paper I

Mitigation of Fire-Induced Spalling of Concrete using Recycled Tyre Polymer Fibre

Yifan Li[1,*], Shan-Shan Huang[1], Kypros Pilakoutas[1], Harris Angelakopoulos[2] & Ian Burgess[1]
[1] Department of Civil & Structural Engineering, The University of Sheffield, Sheffield, UK
[2] Twincon Ltd, Sheffield, UK
* Corresponding author (yli101@sheffield.ac.uk)

ABSTRACT

Under extreme circumstances, such as rapid heating or high temperatures, concrete can spall explosively. The propensity of fire spalling is higher for High-Strength Concrete (HSC) than normal concrete, mainly due to its low permeability. Effective spalling mitigation measures include the use of small quantities of micro-polymer fibres, such as polypropylene (PP) fibres. To improve the sustainability of this mitigation method, this paper presents a study on a novel substitution of manufactured PP fibres with Recycled Polymer Tyre Microfibres (RPTM) that require only a fraction of the energy needed to make equivalent manufactured fibres. To examine the effects of RPTM on fire spalling propensity, experiments were conducted on self-compacting HSC specimens. A new radiant panel heating system was developed to replicate the standard fire curve. The test results demonstrate the effectiveness of RPTM in the mitigation of fire-induced spalling. The severity of fire spalling is shown to be related to the surface moisture content rather than overall moisture content.

KEYWORDS: fire, spalling, concrete, recycled fibre

3.1 INTRODUCTION

Fire-induced spalling is one of the most complex and poorly understood phenomena affecting concrete structures. It is defined in CIRIA Technical Note [1] as: "*the breaking-off of layers of pieces of concrete from the surface of a structural element when it is exposed to the high and rapidly rising temperatures experienced in building fires*". It is generally accepted that the fire spalling of concrete is caused by a combination of mechanisms, which includes thermal expansion, change in mechanical properties, chemical degradation, hydraulic phase change and moisture transport [2-5]. Concrete contains free capillary water and chemically bonded water due to hydration. In fire conditions, the heating causes dehydration and the evaporation of water. As water is confined inside the pore system, pore pressure is built-up. Once the pore pressure generates stresses which exceed the critical tensile stress of concrete, cracking and spalling occur. The pore pressure may act as a trigger for explosive spalling [2]. The actual occurrence of explosive spalling may also depend on the thermal-mechanical behaviour of concrete. Due to the low thermal conductivity of concrete, rapid heating, in particular, will generate a highly non-uniform temperature distribution within a cross-section. This can induce high compressive stresses close to the heated surface due to restrained thermal-expansion. The differential stresses between the hotter outer layer and the cooler concrete core lead to local fractures, which may cause the spalling-off of the whole section [4].

The damage caused by fire spalling has detrimental effects on structures, as it reduces the effective cross-sectional area of structural elements, causing reduced load capacity. The loss of concrete also leads to the direct fire exposure of steel reinforcement, which can significantly decrease its mechanical properties. Based on the damage level observed on structural elements, the severity of fire-induced spalling was classified by Jansson & Ödeen [6], from Level 1 of slight spalling of the concrete surface to Level 5 of bottom reinforcement falling off.

Conventionally, the characteristics of non-combustibility and low thermal conductivity make concrete an inherently good fire-resistant material. However, the development of modern HSC with a much denser pore system amplifies the risk of fire spalling [7, 8]. Spalling of concrete has been observed in tunnel fires, such as the Channel Tunnel fire 2008 [9], the Mont Blanc Tunnel fire 2001 [10], and building fires such as the HengZhou Building fire 2003 [11] and the Kings Dock Car Park Fire 2017 [12].

Four measures are provided to mitigate spalling of concrete in Clause 6.2 of Eurocode 2-1-2 [13]. One of these measures is to include more than 2kg/m^3 of monofilament PP fibres in the concrete mix. The addition of PP fibres into high-strength concrete has been demonstrated experimentally to increase its fire resistance [14-18]. Common PP fibres have a typical melting point of around 160℃, while at around 200℃ their complete melting and diffusion creates pathways through the concrete pore system, which increase permeability. This enables the release of pore pressure build-up, facilitating the migration of the moisture clog, and hence mitigating the propensity to spalling [19] [20].

Sustainability is one of the global grand challenges [21, 22] with existential consequences if it is not addressed effectively. More than 3.5 million tonnes of waste tyres are dumped in Europe every year, but the disposal of the tyres is challenging, because they are non-biodegradable and highly durable. Recycling end-of-life tyres, which comprise 80% rubber 15% steel and 5% polymers, is of interest to both the construction and waste management industries [23].

In contrast to manufactured PP fibres, RPTM is more environment-friendly, as it requires only a small amount of energy for its production. Since RPTM has a melting point similar to PP fibres, it also has the potential to mitigate fire spalling. However, unlike manufactured fibres which are of certain length and diameter, recycled fibres have distributions of lengths and diameters, are agglomerated and contaminated with rubber [24]. To utilise RPTM in concrete, they need to be cleaned, separated and then effectively integrated into the concrete. Therefore, a prototype of RPTM cleaning and integration system has been adopted which allows the cleaned and separated fibres to be uniformly dispersed into concrete during the mixing stage.

This paper presents the results of fire spalling tests on HSC specimens with and without RPTM, in order to investigate the effect of RPTM on fire spalling mitigation. A new radiant panel heating system was used for fire spalling tests. As moisture content significantly affects the occurrence of fire spalling, the moisture content distribution through the specimen's depth, as well as its evolution over time, were measured and are presented in this paper.

3.2 EXPERIMENTAL DETAILS & METHODOLOGY

3.2.1 Fire spalling test setup

The fire spalling tests were carried out using the radiant panel heating system built at the University of Sheffield. The system comprises a transformer, a Eurotherm temperature controller, a heating element radiant panel, a loading frame and a NI data acquisition system, as shown in Figure 1. This setup can develop 100kW/m^2 of heat flux on the concrete surface, 1700kN of compression and can simulate the first 30min of the ISO834 standard fire.

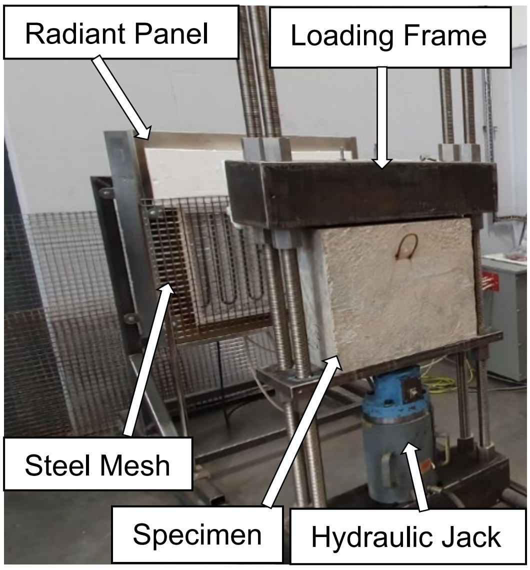

Figure 1 Experimental setup of the fire spalling testing system.

3.2.2 Fibre processing

Contaminated RPTM (Figure 2a) are firstly cleaned to remove rubber particles and dirt, and a sample of clean fibres is shown in Figure 2b. The fibre length of clean RPTM ranges from 2mm to 6mm and the fibre diameter ranges from 11μm to 23μm. The clean fibres are separated using a vibrating wire arrangement before being blown into the mixer. This enables a homogeneous dispersion, and once mixed in the concrete the fibres can barely be seen.

Figure 2 (a) Raw RPTM; (b) Dispersed clean RPTM.

3.2.3 Concrete mix design

The mix design for self-compacting high-strength concrete, C50/60, are shown in Table 1.

Table 1 Concrete mix design.

Materials Type	Source	Quantity
CEM I	Cemex - South Ferriby	440 (kg/m^3)
0/2 mm	Humberside Aggs-North Cave	250 (kg/m^3)
4/10 mm	Cemex - Doveholes	970 (kg/m^3)
Fine Limestone	Cemex - Doveholes	620 (kg/m^3)
Admix 1	Cemex WRA-CP105	2930 (ml/m^3)
Admix 2	Cemex Superplasticiser - CSP313	5280 (ml/m^3)
W/C	Free water/Cement Ratio	0.35
RPTM Mix	Recycled Tyre Polymer Fibre	2 (kg/m^3)

Ready-mix concrete was used. Six concrete specimens were cast in 500mm × 500mm × 250mm moulds, three specimens were plain concrete and the other three contained 2kg/m^3 of RPTM. Thermocouples were placed in one specimen at depths 1mm, 5mm, 10mm, 20mm, and 50mm from the heated surface, to measure the temperature distribution through the depth of the specimen. Cubes and cylinders were also cast for measurement of compressive strength and moisture content.

3.2.4 Moisture content monitoring

As fire spalling occurs near the surface of concrete, its spalling propensity is expected to be more dependent on the heated surface moisture content than the average moisture content overall. A convenient method to determine moisture content is to extract a core from a specimen, dry it, and determine the relative weight loss. However, the coring process requires cooling water to protect the cutting saw, and this may affect the moisture content of the sampled core. To solve this problem, cylinders of 200mm in height and 100mm in diameter were cast from the same batch and cured under the same conditions as the test specimen. Before curing, all cylinders were cut at 5mm, 10mm, and 15mm from the top surface, and reassembled to maintain the length of the moisture path, as shown in Figure 3a. The circumferential surface of each slice was sealed individually using aluminium tape, and the joints between adjacent layers were sealed using water-proof plastic tape, as shown in Figure 3b. This arrangement allowed for a unidirectional moisture transport condition, for the main test specimens.

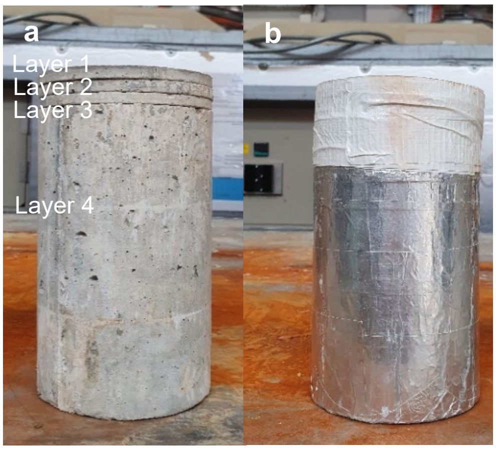

Figure 3 (a) Cylinder cut into slices at heights 5mm, 10mm and 15mm; (b) Sliced cylinder wrapped with aluminium foil and plastic tapes.

After the curing stage, one cylinder from each mix was oven dried at 105℃ until its weight was stabilised. The initial concrete moisture content (by mass) can be calculated by subtracting the dried weight from the total weight of wet cylinders. The moisture content of all slices gives the moisture distribution across the depth of the concrete specimen.

To investigate the effect of surface moisture content on the severity of fire spalling, the specimens and control cylinders are divided into three groups, as shown in Table 2.

Table 2 Drying condition of two groups.

Groups	Specimen		Time of drying
Series 1	P1	F1	1 Day
Series 2	P2	F2	15 Days
Series 3	P3	F3	35 Days

Note: P = plain concrete; F = specimens with 2kg/m^3 of RPTM

3.2.5 Test Calibration

The concrete specimens were heated by the radiant panel following the ISO 834 standard fire curve [25]. A plate thermometer was placed close to the centre of the heated surface of a specimen to calibrate the radiant panel system. Through the calibration process, the heating outputs of the radiant panel over the testing period were tuned for the plate thermometer measurements (approximately representing the adiabatic surface temperature of the concrete specimen [26]) to match the ISO 834 standard fire curve. The temperature calibration data is shown in Figure 4. The “Concrete surface” curve is the temperature-time relationship measured by the plate thermometer.

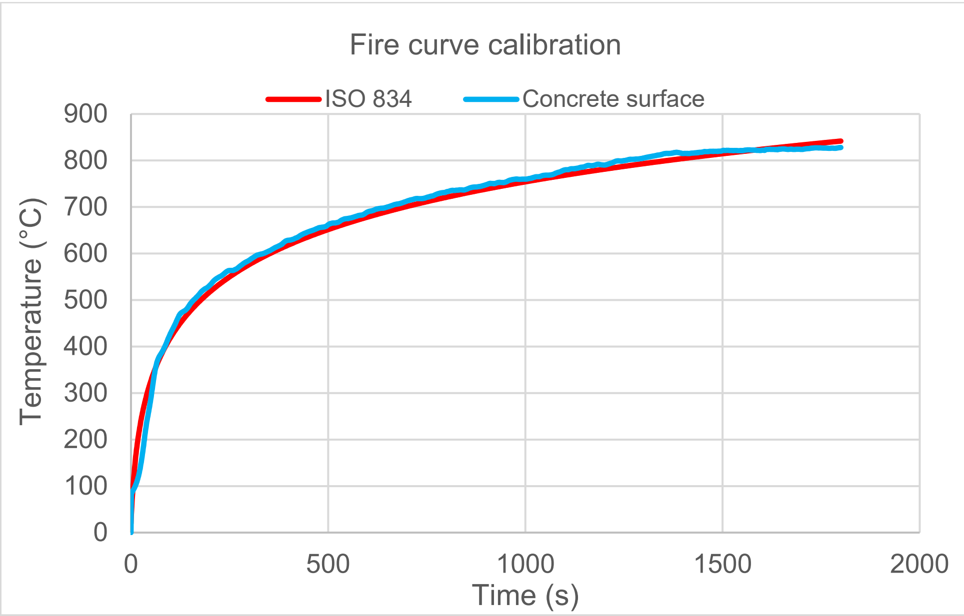

Figure 4 Temperature calibration curve of the radian panel.

3.2.6 Test procedure

Before testing, all specimens were aged for 18 months. The average compressive strength of concrete cubes was around 49 MPa. The distance between the concrete specimen and the radiation panel was fixed at 100mm. Two steel meshes were used, as shown in Figure 5, to protect the heating elements from being damaged by concrete debris generated during the explosive spalling. Two cameras were used to record the test. One camera faced the heated concrete surface to monitor spalling and the other faced the back of the concrete specimen to monitor the appearance of surface water. Fire blankets were used for isolating the loading frame from the heat. The load imposed by a hydraulic jack underneath the concrete were distributed by a steel plates to create a relatively uniform load distribution. 10MPa, which is

20% of the compressive strength of the concrete, was applied on the specimen during the test.

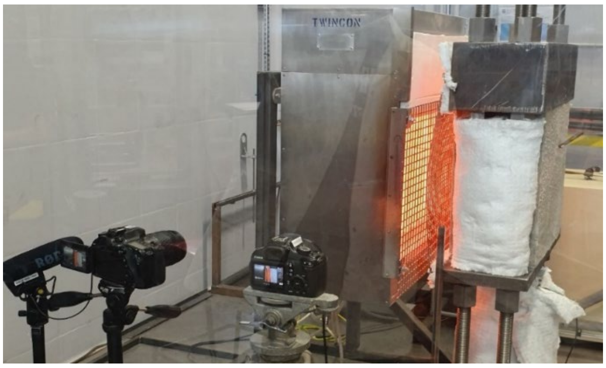

Figure 5 Fire spalling test in procedure.

After each spalling test, the profile of spalled specimens was examined using a laser scanning system. This comprises a laser head, a supporting frame and a two-dimensional stepper motor. The laser scanner determines the spalling depth across the concrete surface. The point data were collected and processed using MATLAB code to output the maximum spalling depth, spalling volume and the 3-D spalling profile.

3.3 RESULTS AND DISCUSSIONS

3.3.1 Moisture Content

The specimens were moisturised to increase the surface moisture content, and thus test the effectiveness of the RPTM in fire spalling mitigation in a relatively severe situation. The measured moisture content distributions in the specimens on the testing dates are shown in Figure 6.

The moisture content of the top layer of the cylinder is the largest (7.3%) on Day 1, decreasing from the surface towards the inner part of the cylinder. From Day 1, the specimens were exposed to the lab environment, and the surface moisture content decreased over time since then. After Day 20, Layer 4 (from depth 15mm to 200mm) had the highest moisture content and stabilised at about 5.9% until Day 35.

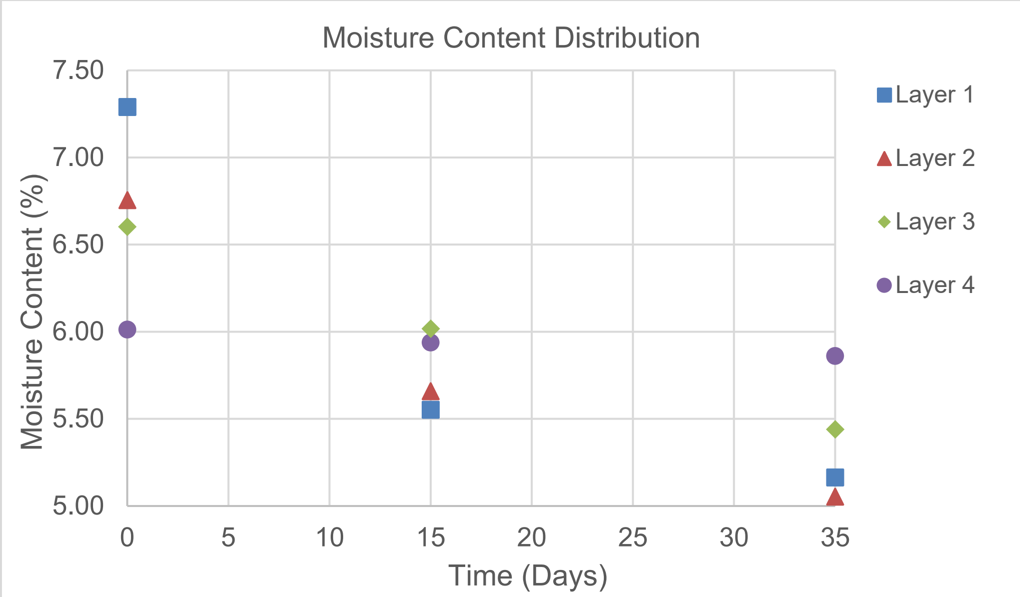

Figure 6 Moisture content distribution.

3.3.2 Temperature

Specimen F1 was instrumented with five thermocouples at different depths, as described in section 3.2.2. The temperature distribution of one specimen during the fire spalling test is shown in Figure 7, where “F1” is the specimen name and “x mm” indicates the location of the thermocouple, as its distance from the heated surface.

In the temperature range between 100℃ and 200℃, several plateaux can be seen in curves “F1 1mm”, “F1 10mm”, and “F1 50mm”. The plateau is believed to be caused by the latent heat needed for the vaporization of water. After 270℃, assuming in perfectly sealed pores containing moisture, the water saturation pressure is expected to exceed 5MPa. Such pressure level is higher than the tensile strength of HSC with compressive strength of 50Mpa to 80Mpa [28, 29]. Hence, cracks are expected to develop in the pore system, which releases the moisture and reduce the vapour pressure. Therefore, no temperature plateau is expected beyond this point as the concrete pores are not strong enough to support the vaporization of water at this temperature.

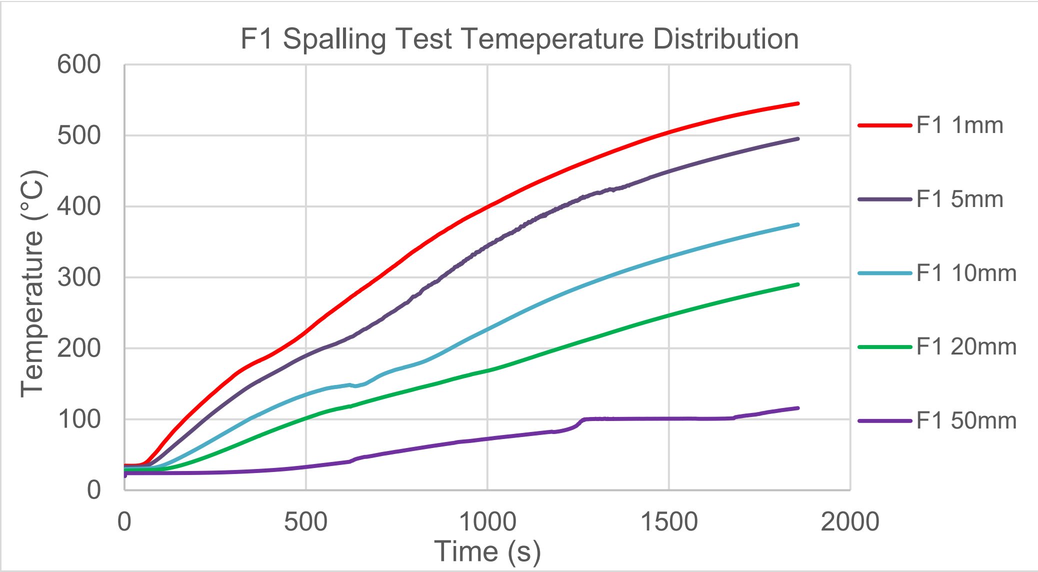

Figure 7 The temperature distribution of RPTM specimens at depths of 1, 5, 10, 20 and 50mm from the heated surface.

3.3.3 Spalling

The spalling events for all test series were recorded using in-situ cameras. Several phenomena were observed during the fire spalling tests:

1. Series 2 & 3 specimens tended to spall into smaller pieces of concrete, with a crisp sound like a bullet shot. Series 1 specimens spalled much more violently, with large concrete pieces exploding with a loud blast sound. The spalling sound was the loudest for specimen P1.
2. Water leaking, a common phenomenon in fire spalling tests, was observed from some of the unheated surfaces of the specimens.
3. For specimens with RPTM, a significant amount of vapour release was seen from the heated surface and the sides of the specimen, due to the increased permeability caused by the melting of the RPTM.

Figure 8 illustrates the conditions of all the specimens from Test Series 1, 2 and 3. All plain concrete specimens experienced fire-induced spalling. The spalling damage was generally more severe for Test Series 1, as shown in Table 3. Maximum spalling occurred in P1 with a volume loss of 3.65 L, followed by P2 (2.04 L) and P3 (1.43 L).

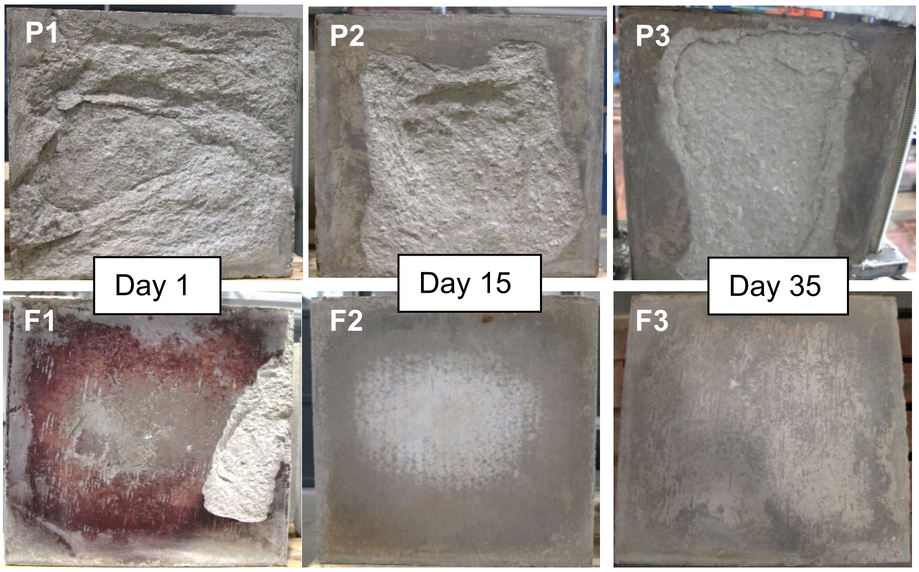

Figure 8 Specimens at 1, 15 and 35 days of drying.

For RPTM concrete, only the specimen tested 1 day after drying spalled. “F1” lost a layer of concrete at its edge rather than the heated centre, which appeared to be due to surface delamination, possibly due to weakness caused during concrete casting.

Since both “F2” and “F3” exhibited no spalling, it can be concluded that the RPTM fibres were effective in mitigating fire-induced spalling at $2kg/m^3$ when the average moisture content was below 6%.

The average moisture content, which is widely believed to be a dominating factor influencing the spalling behaviour of concrete, did not appear to be the decisive factor in this experiment. The average moisture content of all specimens was around 6%, but Series 1 specimens had much higher surface moisture after 1 day of drying. This implies that the volume of fire spalling is more closely related to the moisture content of the surface layer of concrete, rather than the average moisture content of the whole specimen.

Due to the limited number of tests, there are no clear indications of the factors affecting maximum spalling depth. Moreover, the complexity of concrete’s properties and spalling mechanisms appear to be the main reason for the variation in spalling time and the extent of spalling in each experiment. The details of spalling events are shown in Table 3 below.

Table 3 List of all specimens and corresponding spalling details.

Specimens	RPTM dosage (kg/m^3)	1st Spalling Time	Number of Spalling	Concrete Loss (Litre)	Maximum Spalling Depth (mm)	Surface moisture content (%)
P1	0	10:08	5	3.65	36	6.9
P2	0	09:20	6	2.04	45	5.7
P3	0	07:07	5	1.43	24	5.2
F1	2	--	0	--	--	6.9
F2	2	--	0	--	--	5.7
F3	2	--	0	--	--	5.2

3.4 CONCLUSIONS

This paper presents results from experiments that were carried out to demonstrate the effectiveness of RPTM in mitigating fire-induced spalling, as an environmentally friendly alternative to PP fibres.

The following initial conclusions can be made based on the behaviour of the tested specimens subject to the testing condition:

- The addition of RPTM at a dosage of $2kg/m^3$ could be sufficient to mitigate fire-induced spalling in concrete.

- The severity (volume) of spalling is more influenced by the surface moisture content than by the average moisture content.

Future research will focus on the determination of the optimum dosage of RPTM and will examine parametrically different fire and loading conditions. Numerical analysis will be undertaken in the development of a better understanding of the spalling mechanism.

REFERENCES

[1] H. L. Malhotra, "CIRIA Technical Note 118," *Spalling of Concrete in Fires,* 1984.

[2] Z. P. Baiant, "B. IO Analysis of Pore Pressure, Thermal Stress and Fracture in Rapidly Heated Concrete," 1997.

[3] D. Gawin, C. Alonso, C. Andrade, C. E. Majorana, and F. Pesavento, "Effect of damage on permeability and hygro-thermal behaviour of HPCs at elevated temperatures: Part 1. Experimental results," *Computers and Concrete,* vol. 2, no. 3, pp. 189-202, 2005.

[4] Y. Fu and L. Li, "Study on mechanism of thermal spalling in concrete exposed to elevated temperatures," *Materials and structures,* vol. 44, no. 1, pp. 361-376, 2011.

[5] G. Choe, G. Kim, M. Yoon, E. Hwang, J. Nam, and N. Guncunski, "Effect of moisture migration and water vapor pressure build-up with the heating rate on concrete spalling type," *Cement and Concrete Research,* vol. 116, pp. 1-10, 2019.

[6] R. Jansson and K. Ödeen, "Fire in storehouse 6 in the free port of stockholm," 2011: RILEM Publications SARL, pp. 205-210.

[7] V. K. R. Kodur, "Spalling in high strength concrete exposed to fire: concerns, causes, critical parameters and cures," in *Advanced Technology in Structural Engineering*, 2000, pp. 1-9.

[8] H. Mostafaei, "State-of-the-Art on Fire Resistance of Concrete Structure Structure-Fire Model Validation," 2014.

[9] I. Rickard, C. Maluk, F. Robert, L. Bisby, S. Deeny, and C. Tessier, "Development of a Novel Small-Scale Test method to Investigate Heat-Induced Spalling of Concrete Tunnel Linings," 2015 2015, pp. 195-205.

[10] R. M. Faure and M. Karray, "Investigation of the concrete lining after the mont blanc tunnel fire," *Structural engineering international,* vol. 17, no. 2, pp. 123-132, 2007.

[11] Y. Li, X. Lu, H. Guan, M. Ying, and W. Yan, "A case study on a fire-induced collapse accident of a reinforced concrete frame-supported masonry structure," *Fire technology,* vol. 52, no. 3, pp. 707-729, 2016.

[12] M. F. R. Service, "Kings Dock Car Park Fire Protection Report," April 2018.

[13] *Eurocode 2: Design of concrete structures - Part 1-2: General rules - Structural fire design*, B. Standard, 2004.

[14] P. Kalifa, G. Chene, and C. Galle, "High-temperature behaviour of HPC with polypropylene fibres: From spalling to microstructure," *Cement and concrete research,* vol. 31, no. 10, pp. 1487-1499, 2001.

[15] M. R. Bangi and T. Horiguchi, "Effect of fibre type and geometry on maximum pore pressures in fibre-reinforced high strength concrete at elevated temperatures," *Cement and Concrete Research,* vol. 42, no. 2, pp. 459-466, 2012.

[16] Y. Ding, C. Zhang, M. Cao, Y. Zhang, and C. Azevedo, "Influence of different fibers on the change of pore pressure of self-consolidating concrete exposed to fire," *Construction and Building Materials,* vol. 113, pp. 456-469, 2016.

[17] A. Bilodeau, V. K. R. Kodur, and G. C. Hoff, "Optimization of the type and amount of polypropylene fibres for preventing the spalling of lightweight concrete subjected to hydrocarbon fire," *Cement and Concrete Composites,* vol. 26, no. 2, pp. 163-174, 2004.

[18] Y. Li, K. H. Tan, and E.-H. Yang, "Influence of aggregate size and inclusion of polypropylene and steel fibers on the hot permeability of ultra-high performance concrete (UHPC) at elevated temperature," *Construction and Building Materials,* vol. 169, pp. 629-637, 2018.

[19] G. A. Khoury, "Polypropylene fibres in heated concrete. Part 2: Pressure relief mechanisms and modelling criteria," *Magazine of concrete research,* vol. 60, no. 3, pp. 189-204, 2008.

[20] P. Kalifa, F.-D. Menneteau, and D. Quenard, "Spalling and pore pressure in HPC at high temperatures," *Cement and concrete research,* vol. 30, no. 12, pp. 1915-1927, 2000.

[21] (2013). *Construction 2025, Industrial Strategy:government and industry in partnership*.

[22] E. J. Yan and B. Liu. "Construction and projects in China: overview." (accessed 01/August, 2019).

[23] M. Serdar, A. Baričević, M. Jelčić Rukavina, M. Pezer, D. Bjegović, and N. Štirmer, "Shrinkage behaviour of fibre reinforced concrete with recycled tyre polymer fibres," *International Journal of Polymer Science,* vol. 2015, 2015.

[24] S.-S. Huang, H. Angelakopoulos, K. Pilakoutas, and I. Burgess, "Reused tyre polymer fibre for fire-spalling mitigation," *Applications of Structural Fire Engineering,* 2016.

[25] *Fire Resistance Test, Part 1: General Requirements*, B. S. Publication, 2012.

[26] U. Wickström, R. Jansson, and H. Tuovinen, "Validation fire tests on using the adiabatic surface temperature for predicting heat transfer," ed, 2009.

[27] E. T. Box. "*Water - Saturation Pressure* [online]." https://www.engineeringtoolbox.com/water-vapor-saturation-pressure-d_599.html (accessed 29/July, 2019).

[28] M. B. Dwaikat and V. K. R. Kodur, "Hydrothermal model for predicting fire-induced spalling in concrete structural systems," *Fire safety journal,* vol. 44, no. 3, pp. 425-434, 2009.

[29] M. F. M. Zain, H. B. Mahmud, A. Ilham, and M. Faizal, "Prediction of splitting tensile strength of high-performance concrete," *Cement and Concrete Research,* vol. 32, no. 8, pp. 1251-1258, 2002.

4 Paper II

Fire Spalling Behaviour of Stainless Steel Reinforced Concrete with Recycled Steel Tyre Microfibres

Yifan Li[1*], Katherine A. Cashell[2], Harris Angelakopoulos[3], Shan-Shan Huang[1]
[1]The University of Sheffield, Sheffield, the United Kingdom
[2]University College London, London, the United Kingdom
[3]Zero Waste Works Limited, Sheffield, the United Kingdom
* Corresponding author (yli101@sheffield.ac.uk, Department of Civil and Structural Engineering, the University of Sheffield, Sheffield, UK, S1 4BT)

ABSTRACT

Fire-induced spalling of concrete poses a significant threat to modern concrete structures, given its potential to trigger structural failures and substantial economic losses. To address this concern, and improve the sustainability of concrete structures, this study explores the efficacy of including Recycled Steel Tyre Microfibres (RSTM) and stainless steel rebar into concrete as an approach to mitigate fire spalling. The test programme included different specimen configurations to study the influence of concrete specimen shape, stainless rebar type, cover depth and different steel fibres on fire spalling. The test results indicate that the virgin steel fibres and RSTM are both effective in mitigating the explosive fire spalling. The severity of fire spalling increases as the size of the specimen increases. The type of the stainless steel rebar could also influence fire spalling behaviour whereas a specific configuration of thin cover depth and austenitic stainless steel rebar could mitigate fire spalling. The speculated roles of the adopted concrete configurations in fire spalling of concrete are proposed based on the observation of the tests.

KEYWORDS: Recycled steel tyre microfibre, fire spalling, stainless steel reinforcement, steel fibre reinforced concrete.

4.1 INTRODUCTION

The behaviour of concrete as a structural material has been the focus of extensive research for many decades. Over time, substantial advances have been made in concrete mix design and material properties, mainly aimed at enhancing mechanical performance and durability. Despite such advancements, the behaviour of modern innovative concretes exposed to fire remains a challenging and less understood aspect. It is typically assumed that conventional concrete protects the embedded steel reinforcement during a fire due to its good heat-insulation properties. To achieve greater compressive strength and durability, modern concretes tend to have denser microstructure[1], [2]. However, they have been found to perform less satisfactorily in fire conditions, in particular, more prone to fire spalling, compared to normal strength concrete [3], [4], [5]. Fire spalling, which involves the breakaway of concrete, poses a significant threat to structural stability during fire incidents. It reduces the cross-sectional area of structural elements, exposes steel reinforcement to elevated temperatures and can result in substantial loss of load-carrying capacity, ultimately leading to structural failure. Following a number of fires in concrete structures, and particularly in tunnels (e.g. [6], [7], [8], [9]), there have been increasing concerns within both research and design communities regarding fire-induced spalling in concrete structures, and the associated risk of premature structural failure.

Fire-induced spalling is a complex phenomenon, characterised by a combination of thermo-hydro-chemo-mechanical behaviours. The development of spalling is influenced by a large number of factors, both external and internal. External factors include loading conditions, heating rate, heating temperatures and heat exposure surfaces. Internal factors include specimen geometry, concrete strength, moisture content, aggregate type, reinforcement type, and the presence of fibres [10], [11], [12], [13]. Each of these factors exerts a distinct level of influence on the thermal, chemical and/or mechanical responses of concrete when subjected to fire exposure. A frequently mentioned theory is that the fire-induced spalling is caused by the thermally-induced stress gradient in a concrete section, as well as the build-up of pore pressure inside concrete due to heating [14], [15], [16], [17], [18]. The concept of “moisture clog” assumes a fully saturated layer inside heated concrete due to water accumulation, which stops vapour migration and hence causing a build-up of water vapour pressure and steep thermal gradient [19]. The front of this saturated layer is regarded as a “critical zone” which determines the spalling depth [19], [20]. Nevertheless, the exact mechanisms driving the development and propagation of fire spalling remain not clearly understood, primarily due to the numerous amounts of influencing factors. There is a lack of comprehensive understanding of the impact of these factors on spalling, as well as the interactions between all these factors, posing a big challenge for understanding how and when spalling may develop.

The majority of concrete structures employed in load-bearing applications, such as buildings and tunnels, are reinforced with steel rebars due to concrete's inherent low tensile capacities. The influence of reinforcement on the spalling behaviour of concrete is a vast research area [21], [22], [23], [24], particularly relevant to civil engineering practice. This paper investigates particularly the fire spalling behaviour of stainless steel reinforced concrete. To date, there is no information available on this in the public domain. While stainless steel is conventionally employed for structural sections in its bare form, rather than as a reinforcement for concrete, the shifting trends in construction towards efficiency, extended service life, minimal maintenance, and greater sustainability have sparked increasing interest in employing inherently durable stainless steel for reinforcement. However, stainless steel possesses distinct thermal and mechanical properties compared to carbon steel, potentially leading to differing behaviour when embedded in concrete during a fire event.

Derived from end-of service tyres, Recycled Steel Tyre Microfibers (RSTM) is an environmentally friendly alternative to virgin steel fibres, designed to enhance the structural integrity of concrete, mortar, and grout. RSTM consists of ultra-high strength and flexible steel wires, that form a robust and dense reinforcing network within concrete, which provides superior micro-cracking control, compared to conventional macro fibres or rebar. As a pioneering and cost-effective eco-innovation, RSTM breathes new life into end-of-service reinforcing material from the tyre industry, extending its lifespan as a vital component in concrete construction [25]. The incorporation of RSTM into concrete represents an innovative approach that has, until now, remained largely unexplored with respect to its impact on fire spalling resistance.

By conducting fire spalling tests on concrete with stainless steel reinforcement and RSTM, this study aims to: (1) investigate the influence of stainless steel reinforcement and RSTM on the fire spalling behaviour of concrete; and (2) facilitate the transition towards a circular economy and tackles the mounting issue of problematic waste streams and accelerates sustainable practices.

4.2 BACKGROUND ON MODERN RC STRUCTURES IN FIRE

4.2.1 Stainless steel reinforced concrete

Stainless steel, in comparison to carbon steel, represents a relatively pricier material in terms of initial expenses and carbon emissions. The cost of stainless steel is typically 2 to 4 times higher than that of carbon steel, varying with the specific steel grade [26], [27], [28]. Correspondingly, its carbon emission is approximately 1.5 times that of carbon steel [29]. Nevertheless, owing to its inherent corrosion resistance, stainless steel structures exhibit prolonged durability, leading to reduced maintenance costs and lesser carbon emissions over time. Such advantages are particularly evident in structures like wastewater treatment plant [30], [31] or bridges [32]. It is estimated that, over a service life of 25 to 45 years, the CO_2 emissions from carbon steel structures surpass those from stainless steel structures. By the 80-year mark, carbon steel structures could potentially produce twice the carbon emissions of their stainless steel counterparts [29]. Hence, it has been an increasing interest of using stainless steel in constructions owning its advantages in both environmental and economical perspectives. Accordingly, there has been growing research in this field and much of this has focussed on the ambient performance (e.g. [33], [34], [35]).

As a structural material, stainless steel has excellent characteristics including strength, ductility, stiffness, fatigue resistance, corrosion resistance and toughness [36], [37]. Its stress-strain response is different to that of carbon steel, in that it is highly nonlinear even in the elastic stages, with no distinct yield point, and significant strength enhancement in the plastic stages owing to strain hardening. In terms of the thermal performance, it was shown that stainless steel has very good strength and stiffness retention at elevated temperatures owing to its distinctive constituent elements [38]. Figure 1 presents the reduction factors for (a) the yield stress (or 0.2% proof stress) and (b) the elastic modulus for both hot rolled carbon steel reinforcement and grade 1.4301 stainless steel, as given in Eurocode 2 [39] and Eurocode 3 [40].

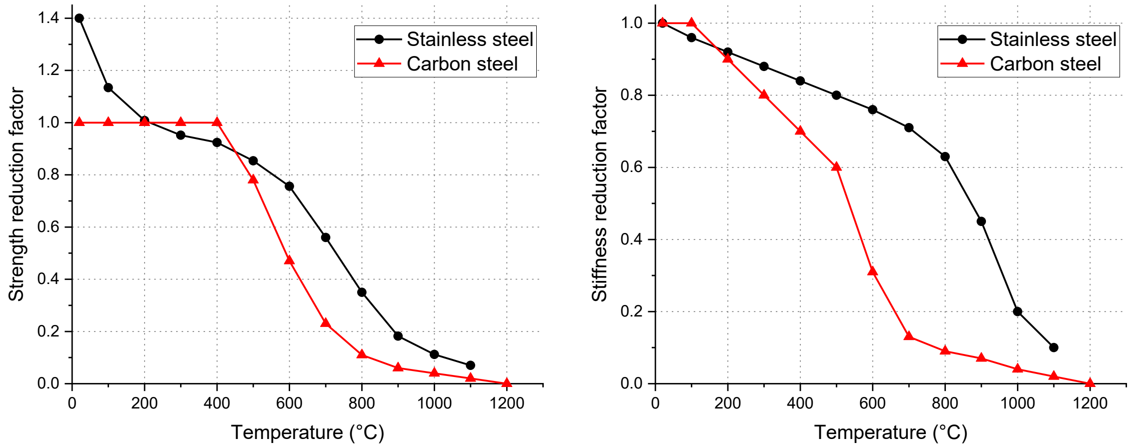

(a) *(b)*

Figure 1 Comparison of the high-temperature mechanical properties of stainless steel and carbon steel, (a) strength and (b) stiffness [39], [40]

To the authors' knowledge, there is no information in the literature on the behaviour of stainless steel reinforced concrete elements under fire conditions, especially on the fire spalling resistance. Hence, the fire spalling behaviour of conventional carbon steel reinforced concrete is introduced as an informative background.

4.2.2 Fire-induced spalling of traditional reinforced and unreinforced concrete

Plenty of fire resistance tests has been conducted on traditional carbon steel reinforced concrete. Morita *et al.* [41] concluded that fire spalling propensity is significantly reduced in concrete without reinforcement. Jansson and Boström [11], [42] also showed that spalling was more severe in reinforced slabs compared with unreinforced specimens. They explained that the steel reinforcement can restrict the development of cracks in concrete, leading to high stresses during heating, which amplified the likelihood of spalling. Another study [43] investigated the pore vapour pressure in concrete with and without reinforcement subject to heating. It was found that steel reinforced specimens experienced less spalling and had higher pore pressure than unreinforced specimens, confirming the restraining effect of the reinforcement during heating. These findings echo the observations from the Mont Blanc Tunnel fire in 1999. There was very limited fire-induced spalling in the unreinforced concrete linings [9] compared to other accidents [6], [7], [8] which observed obvious fire spalling in the reinforced concrete tunnel elements.

There are other parameters influencing the fire spalling behaviour of reinforced concrete. For example, experiments [23] showed that columns under higher compression loading and of larger diameter of steel reinforcement demonstrated a higher propensity of fire spalling. The increase of cover depth can also lead to increase of spalling severity [24].

4.2.3 Steel fibre reinforced concrete

Steel fibres are added to concrete as an effective approach for improving the performance of concrete under both ambient temperature and high temperature conditions [44], [45], [46], [47]. For this reason, steel fibre-reinforced concrete (FRC) is particularly popular in infrastructures such as tunnels and road pavements [48]. However, the effectiveness of steel fibres in preventing the fire-induced explosive spalling is not thoroughly investigated.

An experimental work [49] reported that plain concrete specimens did not experience spalling, whereas those with 60 kg/m^3 of steel fibres spalled at elevated temperatures. Polypropylene (PP) fibres were then added to the same concrete mixes, spalling did not occur under the same test conditions. Similarly, other researcher [50], [51], [52], [53] also reported that the inclusion of steel fibres in concrete could actually trigger explosive spalling, whilst blending steel fibres with polyvinyl alcohol fibres [50] or flax fibres [53] could mitigate fire spalling [50]. Ding *el al.* found that the addition of steel fibres, although not prevent, could reduce the severity of fire spalling [54]. In addition to the influence of fibre dosages and types on fire spalling [49], the effectiveness of a given fibre type and dosage in spalling control may vary as the specimen size alters [55].

Different theories about the mechanisms of steel fibres in fire spalling mitigation reported in the literature are summarised and analysed below:

(1) Some researchers [49], [56] speculated that the high thermal conductivity of steel fibres might decrease the temperature gradient of concrete, hence reducing the thermal stresses and spalling risk. However, there is yet reporting of a large temperature difference between plan concrete and steel FRC in the literature. From the authors' perspective, steel fibres are unlikely to significantly reduce the thermal stress gradient. For a very high dosage of steel fibres, e.g. 80 kg/m^3, it only accounts for 1% of the concrete volume. Such a low volume ratio of steel fibres might not be sufficient to influence the temperature distribution in concrete, as the concrete surrounding steel fibres has very low thermal conductivity (2 W/mK) compared to that of steel (53 W/mK).

(2) It was also speculated that the differential thermal expansions between concrete and steel fibres could induce microcracks, resulting in an increase in permeability of concrete [56] and reduced spalling risk. The scanning electronic microscope (SEM) images obtained by Ding *et al.* [54] and Li *et al.* [57] clearly show the microcracks around the steel fibres in heated concrete. On the other hand, the measured permeability of steel FRC at elevated temperatures was found nearly identical as that of plain concrete, the formation of microcracks seems not to result in an increase in permeability. It was speculated that the microcracks induced by the differential thermal expansion of steel fibres and concrete is not percolated [57]. From the authors' perspective, the testing conditions of SEM and permeability tests might not be representative of a real fire condition due to the slow heating rate (e.g. 1 °C/min) and the drying process required for both experiments. In a real fire, the rapid heating and the moisture condition of the concrete prior to fire could significantly affect the above mentioned behaviour and hence affecting the fire spalling behaviour of concrete.

(3) Researchers also believed that steel fibres might have a crack bridging effect to control the cracking of heated concrete [58], hence reducing the severity of fire spalling [59]. Under moderate temperatures (below 500 °C), the crack bridging effect of steel fibres could be indicated by the crack patterns of heated concrete [44]; flexural strength tests [51]; and the pull-out tests of steel fibres [53]. In addition, Yermak, *et al*. [52] found that steel fibres can effectively restrict the formation of new pores with diameters of 10 μm and larger at 500 °C, which is not observed from plain concrete and PP fibre concrete. However, the crack bridging effect of steel fibres does not necessarily benefit fire spalling resistance. The suppressed cracking could impede the migration of moisture in and out from heated concrete, resulting in larger vapour pressure. In addition, the increased tensile strength of concrete could allow the accumulation of high mechanical potential energy, leading to severe explosive spalling. Both could lead to a higher propensity of fire spalling, which could explains the unfavourable effects of steel fibres on fire spalling observed in fire tests [49], [50], [51], [52], [53].

To sum, Theory (1) might not be the main influencing mechanism of steel fibres in fire spalling. The permeability increase suggested in Theory (2) could potentially mitigate fire spalling but not experimentally verified. The crack bridging effect proposed in Theory (3) is thoroughly verified but this may lead to unfavourable influence on fire spalling. In this study, fire spalling tests are conducted to investigate which of the forementioned theories is more dominant in terms of the influence of steel fibres in fire spalling.

4.2.4 Recycled Steel Tyre Microfibre reinforced concrete

RSTM was first introduced as reinforcement in concrete to improve its ambient-temperature performance, while addressing environmental challenges associated with the huge amount of waste tyres in the world [60]. Every year, there are approximately 1.5 billion waste tyres produced globally, including around 3.5 million tons in the EU alone [61]. The EU banned the landfill of whole waste tyres [60] owing to their detrimental environmental effect [62]. As a result, recycling waste tyres became a necessity, and the construction sector proposed an application for the Recycled Steel Tyre Microfibres, which is to substitute the virgin steel fibres with RSTM as concrete reinforcement. A typical waste tyre contains approximately 15% of steel, and RSTM is estimated to be of about 50% of the cost of virgin steel fibres [25]. In addition to the economic benefit, RSTM was shown to be at least as effective, if not better, than virgin steel fibres in improving the mechanical performance of concrete at ambient temperature [63], [64], [65], [66], [67]. To date, there has been very limited research on the fire-induced spalling of RSTM-reinforced concrete [59], [68], [69]. These studies demonstrate that RSTM could be potentially effective in controlling fire-induced spalling for RSTM concrete. However, the tests were conducted on unloaded small specimens. Hence, further investigation is needed to confirm the effectiveness of RSTM in fire spalling mitigation.

4.3 EXPERIMENTAL PROGRAMME

To understand the fire spalling behaviour of concrete elements reinforced with stainless steel rebars and RSTM, a series of fire spalling tests was designed and conducted. The specimens were cast at the Brunel University London and tested at the University of Sheffield. The aims of the tests were to:

(i) understand the effect of different types of stainless steel rebars on the spalling of the concrete at elevated temperatures;

(ii) assess the effectiveness of RSTM in mitigating the fire induced spalling of concrete;

(iii) study the differences between using virgin steel fibres and RSTM in delaying or preventing concrete spalling; and

(iv) investigate a number of influential factors to the spalling resistance including cover distance, rebar type, structural element type and fibre type.

4.3.1 Test specimens

A total of 24 specimens were cast comprising 14 slabs and 10 short columns. The slabs were of 500 × 500 × 220 mm^3 whilst the dimensions of the short columns were 500 × 200 × 200 mm^3. The details of the test specimens are given in Table 1 and the concrete mix is shown in Table 2. The average compressive strength of the specimens at 28 days are 40 MPa for the plain concrete and 42 MPa for the RSTM and virgin steel fibre concrete. For the specimens with either virgin steel fibres or RSTM, the same dosage (30 kg/m^3) was employed. Since previous tests [70] have shown reasonable repeatability of the spalling behaviour for plain concrete using the same test rig, for each configuration, one plain concrete specimen was cast as the control specimen. Three repeats were cast for specimens with fibres to assess the repeatability of the FRC results.

Table 1 Test specimen details

Specimen type	Name	Fibre Type	Type of reinforcement	Cover depth (mm)	Repeats
Slab	S-PC-Aust-30	-	Austenitic	30	1
	S-Vir-Aust-30	Virgin	Austenitic	30	3
	S-RSTM-Aust-30	RSTM	Austenitic	30	3
	S-PC-Aust-15	-	Austenitic	15	1
	S-RSTM-Aust-15	RSTM	Austenitic	15	3
	S-PC-Dup-30	-	Duplex	30	1
	S-RSTM-Dup-30	RSTM	Duplex	30	1
	S-PC-Dup-15	-	Duplex	15	1
Short column	C-PC-Aust-30	-	Austenitic	30	1
	C-Vir-Aust-30	Virgin	Austenitic	30	2
	C-RSTM-Aust-30	RSTM	Austenitic	30	2
	C-PC-Aust-15	-	Austenitic	15	1
	C-PC-Dup-30	-	Duplex	30	1
	C-RSTM-Dup-30	RSTM	Duplex	30	2
	C-PC-Dup-15	-	Duplex	15	1

Table 2 Concrete mix design

Material	Quantity (kg/m^3)
Aggregate 0-5 mm	1281
Aggregate 5-10 mm	734
Cement (CEM II 52.5)	300
Water	168
PFA	99
Superplasticizer (Twin flow 05)	4
w/c ratio	0.56

As shown in Table 1, grade 1.4401 austenitic stainless steel (also known as grade 316) and grade 1.4462 duplex stainless steel (commonly referred to as grade 2205 stainless steel) were adopted. These are two very common grades of stainless steel and they were procured from local reinforcement stockholders. Their chemical composition, with maximum content values, is given in Table 3.

Table 3 Chemical composition of the stainless steel

	Unit in percentage (%) relative to the total mass								
Grade	*C*[1]	*Cr*	*Mn*	*Ni*	*Si*	*Mo*	*S*	*N*	*P*
1.4401	0.08	16-18	2	10-14	1	2-3	0.03	\	0.03
1.4462	0.03	21-23	2	4.5–6.5	1	2.5 – 3.5	0.015	0.1-0.22	0.035

[1] The symbols in this table are the abbreviations of chemical elements

The nominal properties given in Eurocode BS EN 10088-1:2014 [71] for the different grades of stainless steel adopted in this project are summarised in Table 4 and Table 5. Austenitic stainless steel, the most commonly used stainless steel type for reinforcement, has a mean coefficient of thermal expansion of 16×10^{6}/°C between 20°C and 100°C, whilst the corresponding value for duplex stainless steel is 13×10^{6}/°C. Such a difference in the thermal expansion of these two types of stainless steel is not insignificant and might affect the structural behaviour of concrete structures in fire. The thermal conductivity at 20°C of both austenitic and duplex stainless steels are 15 W/mK, which is much lower than that of carbon steel (51 W/mK).

Table 4 The properties of stainless steel reinforcement at ambient temperature

Stainless steel type	Grade	Density	Coefficient of thermal expansion between 20°C and 100°C	Thermal conductivity	Modulus of Elasticity	Specific thermal capacity
		(kg/m^3)	(10^{-6}/K)	(W/mK)	(Gpa)	(J/KgK)
Austenitic	1.4401	7.9	16.0	15	200	440
Duplex	1.4462	7.8	13	16	200	500

Table 5 The properties of stainless steel reinforcement at elevated temperature

Stainless steel type	Coefficient of thermal expansion (10^{-6} /K)			Modulus of Elasticity (Gpa)			
	100-200°C	200–300 °C	300–400°C	100°C	200°C	300°C	400 °C
Austenitic	16.5	17.0	17.5	194	186	179	172
Duplex	13.5	14.0	NA	194	186	180	NA

The layouts of the steel reinforcement for the slab and short column specimens are shown in Figure 2. All of the specimens were cast in plywood moulds which were built in the structures lab at Brunel University London. All of the reinforcement bars had a diameter of 10 mm and were cut to a specific length, bent as confinement, and then welded together. For the slabs, the bars were 440 mm in length and there was a spacing of 200 mm between adjacent bars. For the short columns, a total of 4 bars were located longitudinally in each corner of the cross-section and three sets of shear links were employed at the centre, 200 mm above and below centre to confine the specimens longitudinally. The design cover depth of the reinforcement was kept using small concrete blocks as spacers in the moulds. The specimens presented in Figure 2 show an example with a cover depth of 30 mm. The cover depth was maintained at all boundaries, as any rebar near the concrete surface could cause localized loading conditions which may lead to cracks and moisture loss during the fire test.

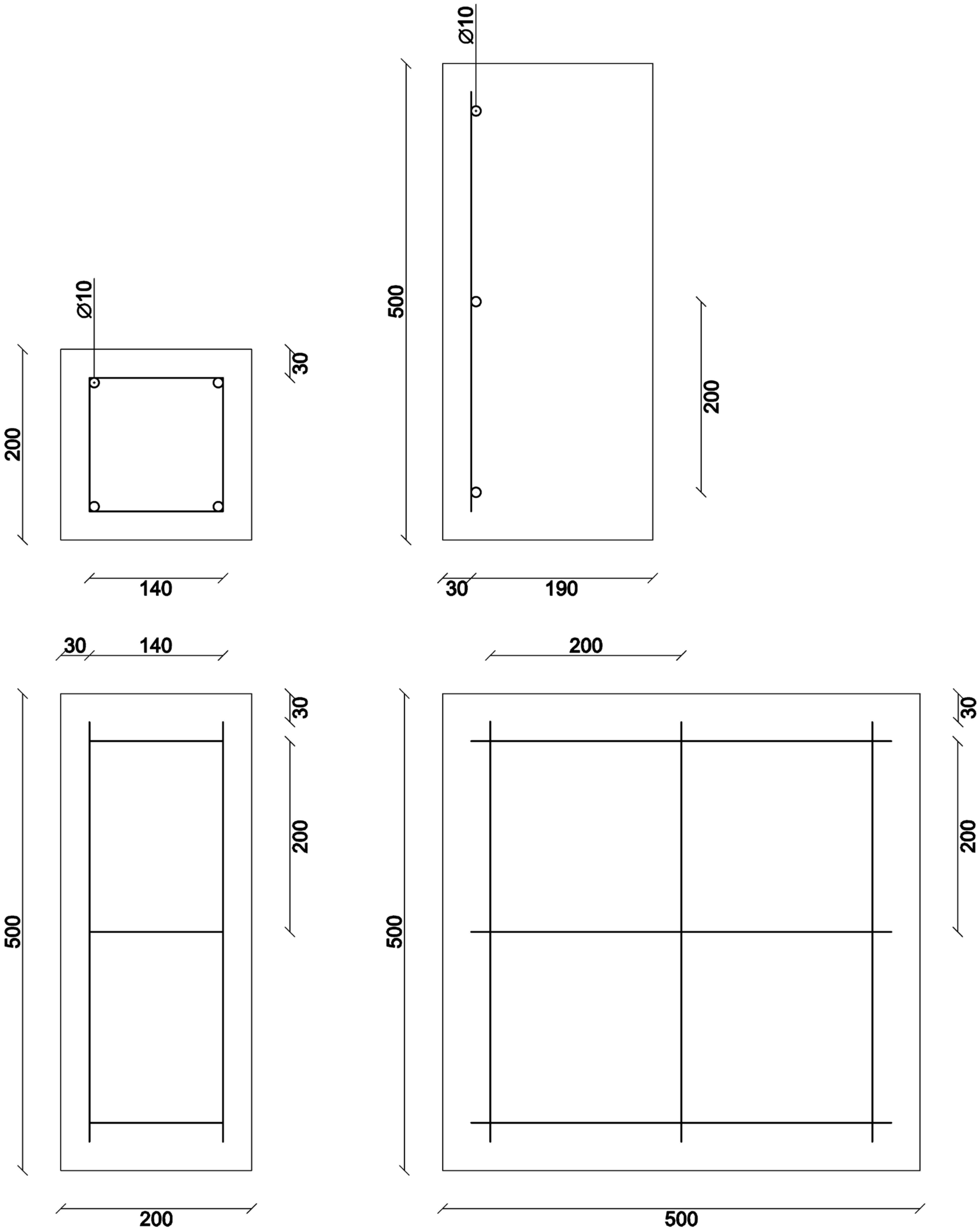

(a) Reinforced short column *(b) Reinforced slab*

Figure 2 Schematics of the reinforcement layout for slab and short column specimens

Figure 3 presents images of the virgin steel fibres as well as the RSTM fibres that were employed in this study. For the virgin steel fibres, hooked end fibres provided by Zero Waste Works which had a length of 60 mm a diameter of 0.75 mm and a tensile strength of 1225 Mpa were used. For the RSTM fibres, the geometry varied due to the wide range of tyre types and the recycling process. The density (7800 kg/m^3) and the elastic modulus (200 Gpa) were similar for both the RSTM and the virgin steel fibres, although the tensile strength of the RSTM was higher with a minimum of 2000 Mpa. Figure 4 shows the length distribution of the RSTM used in the study. The RSTM diameters were ranging between 0.12 – 0.4 mm and the shape was random.

Figure 3 (a) Virgin steel fibres

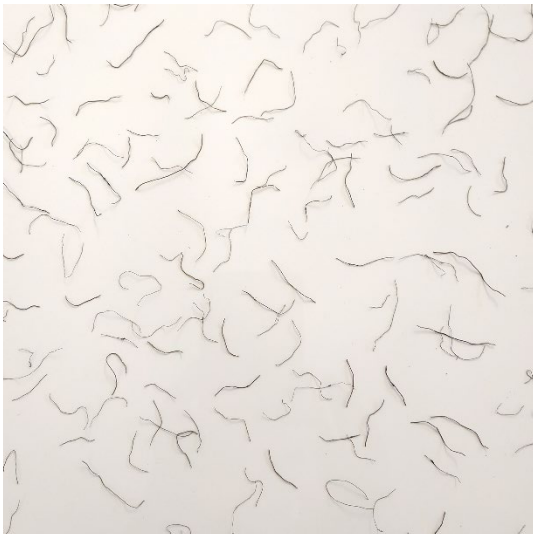

(b) Recycled steel tyre microfibres

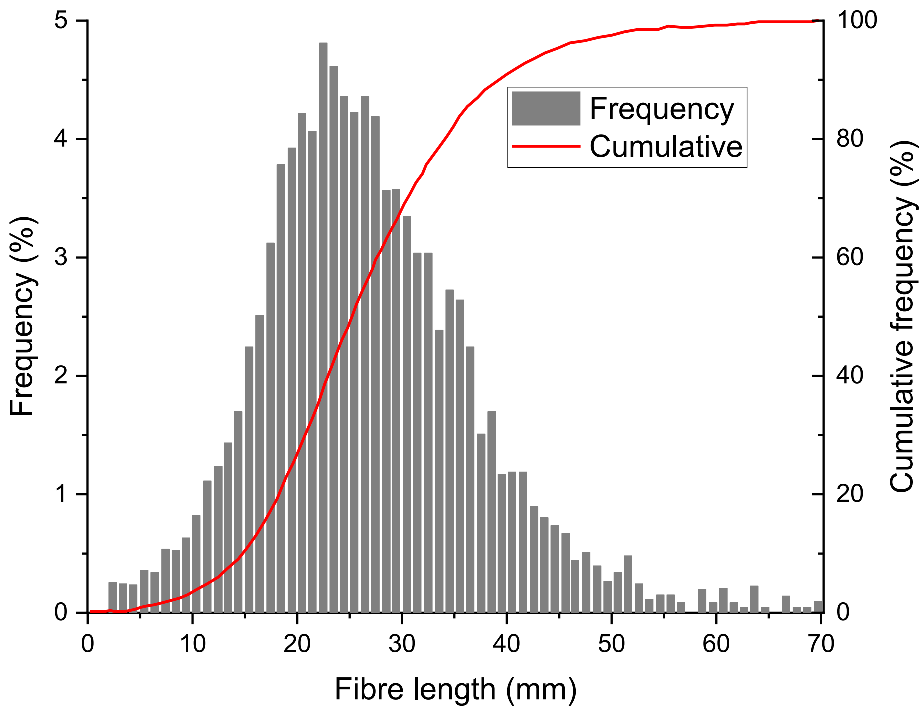

Figure 4 The length distribution of RSTM

To cast the specimens, the dry components, i.e. sand, cement, and aggregates, were first mixed in a drum mixer, followed by wet mixing with water and super-plasticizer. To avoid fibre agglomeration during mixing, the fibres were manually sprinkled into the concrete mixer in small quantities. Cubes were also cast for each concrete mix alongside the slab and short column specimens. These cubes were tested to obtain the water permeable void ratio, moisture content, and compressive strength. Following demoulding, all specimens were cured in a water tank for 28 days. The specimens were subsequently removed from the tank and stored in laboratory conditions at a temperature of 20 ± 2°C and a humidity level of 30% - 50% for three-months before the fire spalling tests. It should be noted that specimens C-PC-Dup-30 and C-PC-Dup-15 experienced an additional 3-month shipment delay before testing. These specimens were stored under the indoor laboratory conditions before the shipment, and so they were dryer than the other specimens when tested.

4.3.2 Spalling test setup

The fire spalling test rig, constructed at the University of Sheffield, consists primarily of a heating system and a loading system. The heating system, illustrated in Figure 5, comprises an electric radiant panel, which can produce 100 kW/m^2 of power onto the test specimens, a temperature controller, and a transformer. The heating system is mounted on a moving track to allow the adjustment of the distance between the heating panel and the concrete specimen.

In this study, the distance between the heating panel and the specimen is fixed at 100 mm. The heating scenario is controlled by adjusting the power output of the radiant panel to follow the ISO 834 standard fire curve [72] and the heating duration of each test is 30 minutes. Before the fire spalling tests, a pre-test calibration is carried out. A plate thermometer is positioned at the centre of the heat exposure surface of a dummy specimen. The power output of the radiant panel is then adjusted to ensure that the temperature-time relationship measures by the plate thermometer followed the standard fire curve. To protect the heating elements from the explosive spalling, one stainless steel mesh is mounted onto the radiant panel, while another is mounted onto the specimen. Moreover, to prevent the spalled concrete from obstructing the heating, the steel mesh on the specimen is left flexible at the bottom, allowing the spalled concrete debris to drop on the floor.

The loading system, as shown in Figure 6, consists of two hydraulic jacks and a self-reacting loading frame that intends to apply a uniformly distributed compression load onto the specimen. The steel plate supporting the bottom surface of the specimen is polished to ensure a continuous contact with the specimen. The top reacting plate is adjusted to ensure it is horizontal. The two hydraulic jacks are connected by a single hydraulic pump, which enables them to maintain the same pressure level throughout a test. The loading system can exert a force of 2500 kN, yielding 22.7 Mpa for the slab specimens and 62.5 Mpa for the short column specimens.

For all tests, the applied load is 30% of the compressive strength of the concrete. Vermiculite fire insulation boards were used to the side of the loading frame which is facing the radiant panel to prevent the heat-induced strength loss and thermal expansion of the loading system. The test conditions are summarized in Table 6 below.

Table 6 Summary of the test condition

Ratio of applied load to compressive strength (%)	Load for slab (kN)	Load for short column (kN)	Load type	Heating scenario	Exposure type	Heating time (min)
30	1250	480	Uniaxial compression	ISO 834 Standard	One-sided exposure	30

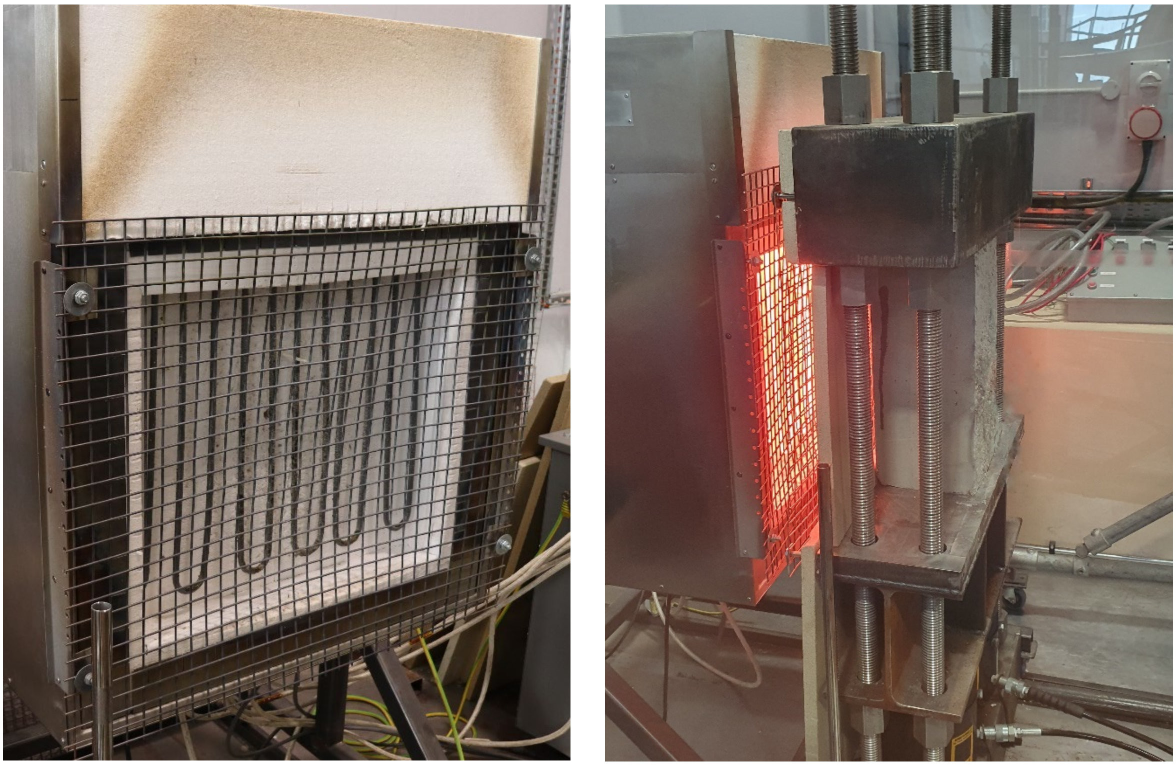

Figure 5 (a) Radiant panel *(b) Radiant panel during heating*

Figure 6 (a) Loading frame facing the radiant panel (b) The back of the loading frame

4.3.3 Spalling profile scanning

To analyse the spalling profile of the spalled specimen, a laser scanner is employed, as shown in Figure 7. The specimen is horizontally levelled, with the spalled surface faced upward. A laser head moving in the horizonal plane can generate the point cloud data of the distance between the spalled surface and the laser head at each measure point. The distance between adjacent measure points adopted for this analysis is 5 mm. To quantify the explosive spalling test results, the maximum depth, spalled volume, and average spalling depth are determined for each specimen. The effective heating area of the slab specimens is 400 mm × 400 mm, whilst it is 400 mm × 200 mm for the short column specimens. To eliminate the boundary effect, 90% of the effective heating area (after disregarding the four edges), is considered for the average spalling depth calculation.

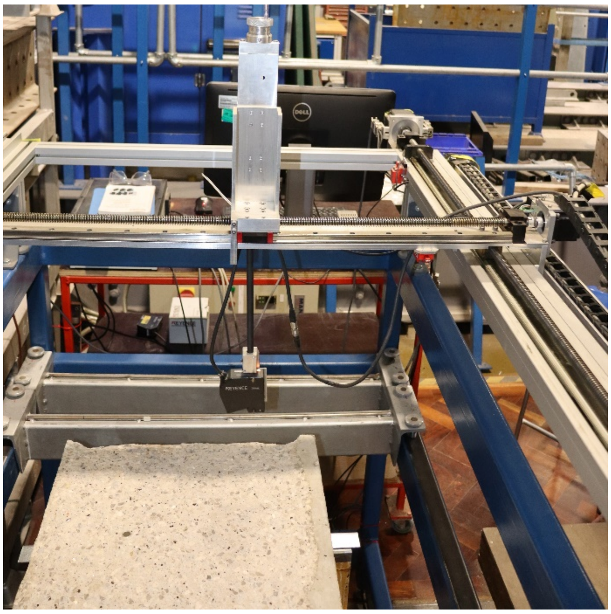

Figure 7 Laser scan to obtain the spalling profile of the spalled specimens

4.3.4 Water permeable void ratio and moisture content tests

To investigate the potential influence of water permeable void ratio and moisture content on spalling behaviour, the water permeable void ratio and moisture content tests are conducted on the cube specimens. As the concrete cubes are cured and stored in the same conditions as the fire spalling test specimens, the moisture content and the water permeable void ratio of the cubes can provide an insight into the moisture conditions and the porosities of the slabs and short columns. Acknowledging the moisture distribution with a specimen should not be uniform, the concrete cubes are split at a depth of 25 mm by dry knocking. The calculations of moisture content are then carried out separately for each section.

The moisture content test is based on Eurocode BS EN 1353:1997 [73] and the water permeable void ratio tests are performed following ASTM C642-21 [74]. Firstly, the dry mass m_d of the concrete cubes are determined by oven-drying the specimens at 105°C until the change in mass within 24 hours is less than 0.5% (otherwise, the heating needs to carry on until this requirement is met). The drying temperature of 105°C is selected to avoid thermal cracks and to minimize any porosity increase due to this pre-heating based on previous experience. The mass of the oven dried specimen in air is measured as m_d. By measuring the initial mass for each section of the cubes before drying m_i, the moisture content $W\%$ of the concrete before the spalling test can be calculated as:

$$W\% = (m_i - m_d)/m_d \times 100 \tag{1}$$

For the water permeable void ratio, the dried cubes are immersed in water until the mass is constant. The mass of the saturated concrete in air after boiling the specimen in water for at least 5 hours is measured as m_s. The mass of the specimen in water after boiling is measured as m_w. Using these measurements, the volume ratio of water permeable voids $V\%$ of the specimen is calculated as follows:

$$V\% = (m_s - m_d)/(m_s - m_w) \times 100 \tag{2}$$

It should be noted that although the water permeable void ratio could offer a simplified indication of the porosity of the concrete specimen, it is not identical to the latter. Some pores of the concrete are fully sealed which makes them impermeable to liquid water. Hence the porosity of the specimens could be larger that indicated by the water permeable void ratio.

4.4 RESULTS AND DISCUSSIONS

4.4.1 Water permeable void ratio and moisture content

On the day of the spalling test, the average moisture content of the 25 mm part of the cubes was found to be 3.2%, while the rest of the cubes had an average moisture content of 3.7%. The water permeable void ratio was measured as 14%, 14.6% and 15.6% for plain concrete, concrete with virgin fibres, and RSTM concrete, respectively. These results suggest that the inclusion of steel fibres in the concrete mixture could increase the porosity of the material, and the RSTM might increase the porosity more than the virgin steel fibres do.

4.4.2 Observations during the fire spalling tests

During the fire spalling tests, observations were made of the emission of water vapour and liquid water from the concrete specimens. As a qualitative analysis, such observations can provide give some insight in to the underlying physics inside the heated concrete. The emitted vapour is a sign for water boiling. The leaking of the liquid water may indicate that the liquid water is pushed out by the pressurized vapour, through the openings of the concrete microstructure.

The times at which the vapour starts to leak from the heated surface are 5 ± 1 minutes for all the slab specimens, regardless of the various concrete mixture used. As heating continues, liquid water leaking starts to be observed from the right and left sides of all specimens. For plain concrete, the water leaking always follows the vapour leaking; specimen S-PC-Aust-30 is shown as an example in Figure 8(a). This phenomenon is commonly observed in other spalling tests [75], [76], which could be due to the low permeability of plain concrete. It is speculated that the vaporised moisture near the moisture clog is trapped, building up pressure, pushing the liquid water out from the sides and back of the specimen, which might explain why the liquid water leaking always occurs after the vapour leaking. For specimens with steel fibres, their vapour leaking from the right and left sides are much less than that of the plain concrete specimens or does not occur. It is speculated that this might be due to the higher permeability of steel FRC than that of plain concrete. The differential thermal expansion between concrete and steel fibres can induce microcracks near the fibres [54]. These microcracks primarily form near the heated surface where temperatures are highest. Consequently, the majority of vaporised moisture could escape from the heated surface of the specimens containing steel fibres, resulting in less vapour leaking from the lateral sides of a specimen compared to the plain concrete specimens.

For plain concrete slabs S-PC-Aust-30, S-PC-Aust-15, S-PC-Dup-30, and S-PC-Dup-15, the times of vapour leaking from the right and left sides of the specimen are 17, 16, 14, and 20 minutes, respectively. The earliest water leaking is observed from specimen S-PC-Aust-30, which is at 8 minutes, and the latest is from S-RSTM-Aust-15 at 25 minutes. Such variation in water/vapour leaking time could be due to the heterogeneity of the concrete and the difference in rebar and fibre types. It should be noted that the flow rate of liquid leaking of specimen S-PC-Aust-15 is significantly greater than that of the other plain concrete slabs, as shown in Figure 8(b). This extra amount of liquid loss may lead to a reduction in the water saturation level inside concrete, delaying the formation of moisture clog and leading to lower pore pressure.

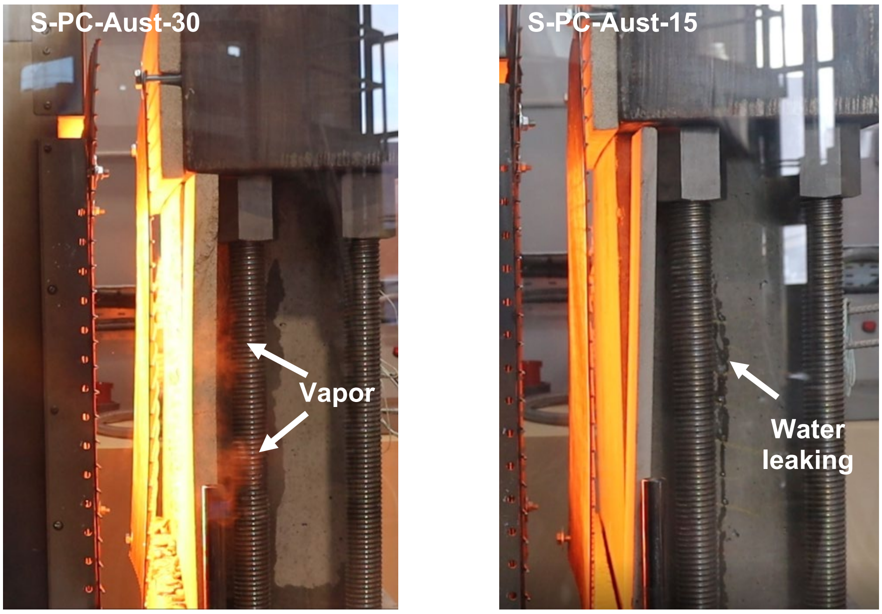

(a) (b)

Figure 8 Photos during heating for (a) specimen S-PC-Aust-30 and (b) specimen S-PC-Aust-15.

As for the short column specimens, neither the plain concrete nor the steel FRC specimens experienced vapour leaking from the right and left sides. Similar to steel fibres, the differential thermal expansion of the steel rebars in concrete can lead to micro cracks, forming paths for the vaporised moisture to migrate and eventually escape. Such moisture migration paths are more easily formed close to the heated surface where the temperature is higher and so the majority of the vapour would escape from the heated surface, leaving less vapour leaking through the right and left sides. The smaller size and additional shear links of the short column specimens make the reinforcement / concrete ratio of the short columns much higher than that of the slab specimens. Therefore, there could be much more cracks formed in the short columns and much less vapour leaking from their right and left sides than the slabs did. The water leaking times for the short columns vary less than those of the slabs, at 10 ± 2 minutes. For specimen C-PC-Aust-15, a large amount of liquid leaking occurs, similar to specimen S-PC-Aust-15, which implies this particular configuration might lead to faster moisture migration during heating compared to the other specimens. For specimen C-PC-Dup-15, there is no liquid leaking at all. This could be due to the 3-month extra drying as described in Section 4.3.1.

4.4.3 Fire spalling test results

Figure 9 shows the heated surfaces of all specimens following the exposure of the ISO 834 fire curve for 30 minutes. The results are grouped based on the fibre type and dosage, as they are expected to be two of the primary influencing factors of explosive spalling. The laser scanned profile of the spalled surface is shown in Figure 10.

The plain concrete specimens demonstrate a considerably higher susceptibility to fire-induced spalling compared to the steel FRC ones. Out of the eight plain concrete specimens, five of them experience explosive spalling, whereas none of the 16 steel FRC specimens exhibit such spalling. Although most of the steel FRC specimens experience aggregate spalling during the test, the severity of spalling is negligible in terms of spalling mass or depth. The potential effectiveness of steel fibre and RSTM in controlling fire spalling is confirmed.

Specimens S-PC-Aust-15 and C-PC-Aust-15 are exposed to the same heating scenario as for the other plain concrete specimens, yet they experience no explosive spalling, which is worth noting. This might be due to the shallower cover depth and the higher thermal expansion coefficient of austenitic stainless steel of these two specimens, compared to the other plain concrete specimens. Subject to heating, the rebars are heated faster as the concrete cover depth decreases, enlarging the differential thermal expansions between the rebars and concrete. The higher thermal expansion of austenitic stainless steel than that of duplex stainless steel further increases the differential thermal expansions between the rebars and concrete. This, in turn, induces more cracking in S-PC-Aust-15 and C-PC-Aust-15, leading to faster moisture migration and vapour/water escape and thereby lower vulnerability to fire spalling than the other specimens. The large amount of water bleeding from the right and left sides of S-PC-Aust-15 and C-PC-Aust-15 as mentioned in Section 4.4.2 serves as additional evidence for this speculation.

(a) Plain concrete specimens:

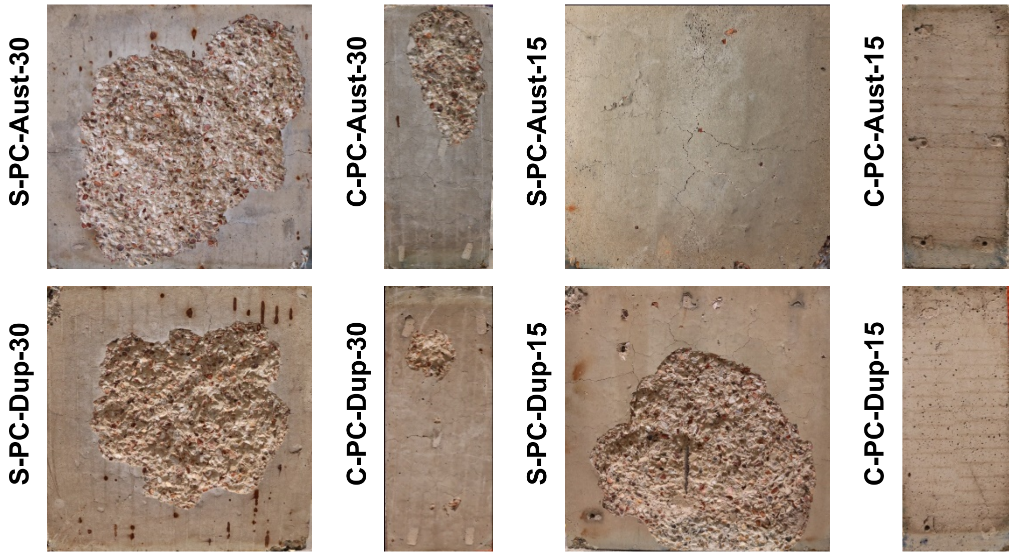

(b) Example virgin steel fibre specimens:

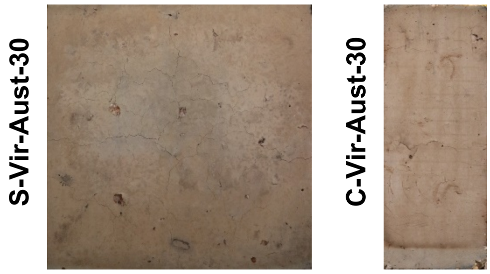

(c) Example RSTM specimens:

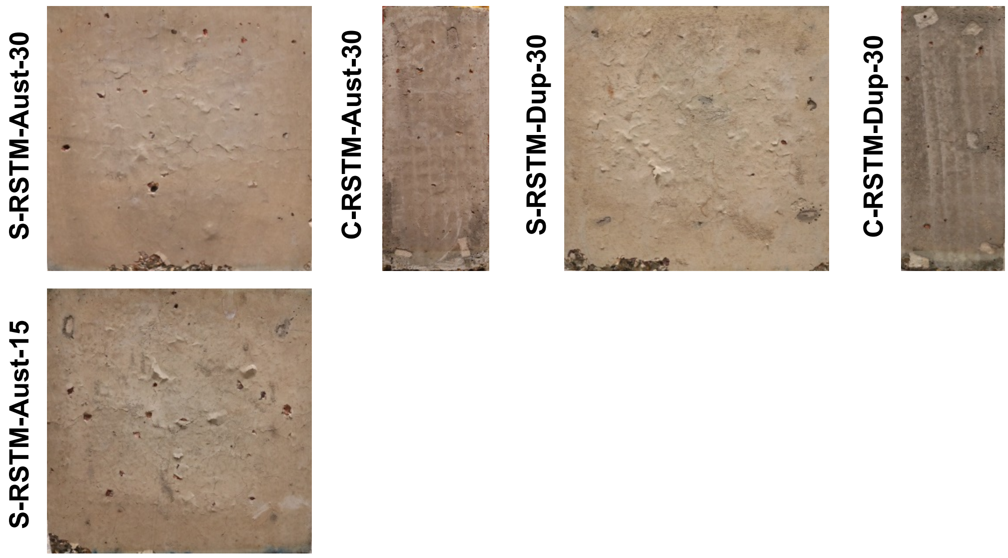

Figure 9 *Heated surface of concrete specimens after the fire spalling tests*

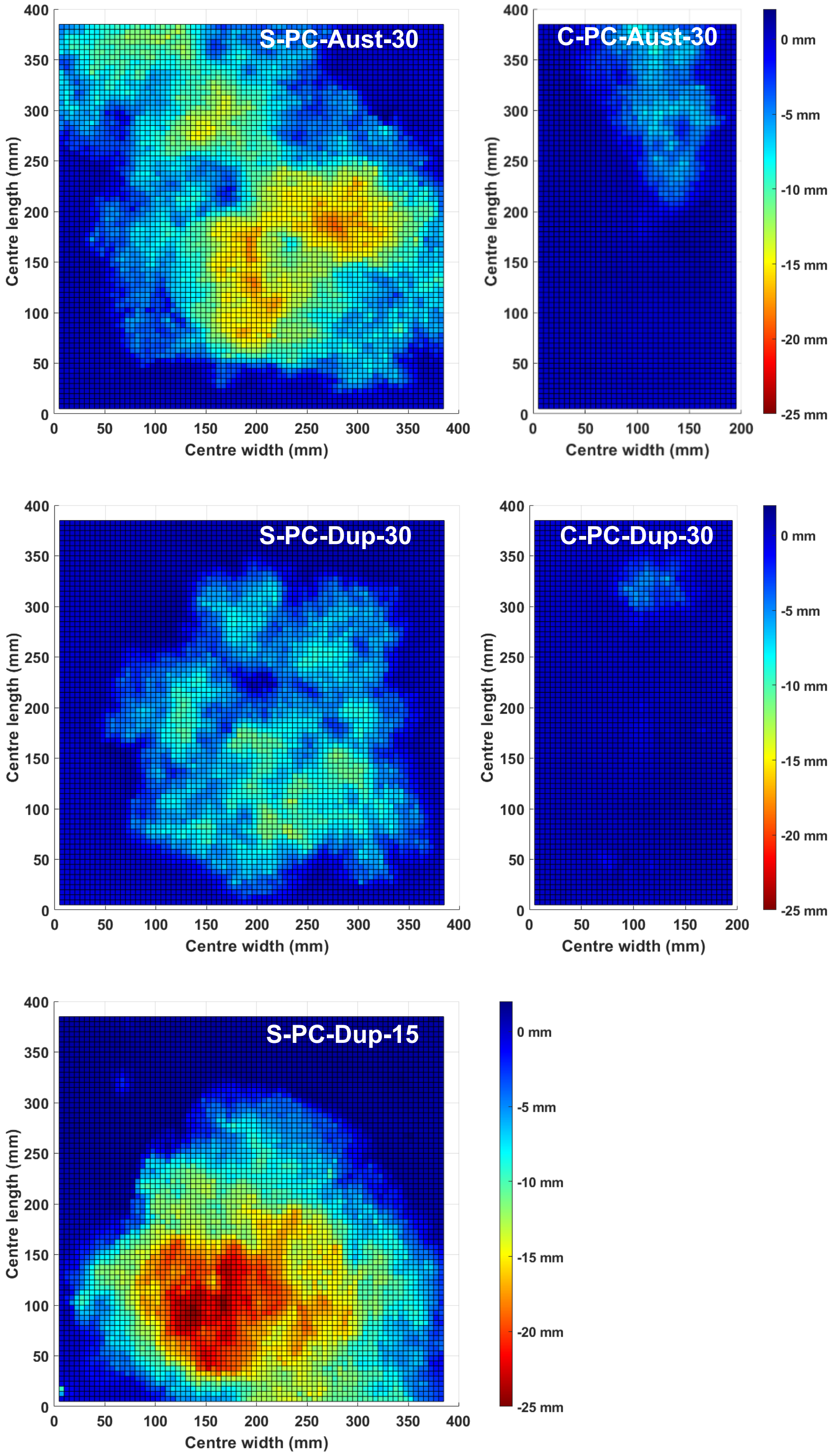

Figure 10 Spalling profile of the effective heated area of spalled specimens

To investigate the effects of the specimen shape and size on fire spalling, the fire spalling behaviour of the slabs are compared with that of the short columns. It is found that for the same concrete composition, the propensity to and/or severity of explosive spalling increase as the specimen size increases. The average explosive spalling depth of the short column specimens C-PC-Aust-30, C-PC-Dup-30, and C-PC-Dup-15 is significantly less than that of their corresponding slabs. This can be attributed to the confinement effect of the shear links within the short columns. Moreover, the smaller width of the short columns compared to the slabs could allow more vapour leakage through the sides of the specimens, hence reducing the severity of fire spalling. Similarly, for the specimens that experienced aggregate spalling, the magnitude of aggregate spalling is less in the short column specimens than in the slabs. In addition, the two C-Vir-Aust-30 specimens experience no aggregate spalling, while the aggregates spalling of S-Vir-Aust-30 is less than that of S-RSTM-Aust-30, S-RSTM-Dup-30, and S-RSTM-Aust-15. These results suggest that virgin steel fibres may be more effective in mitigating aggregate spalling, but more testing is necessary to confirm this conclusion.

For the specimens of the same types of stainless rebars, high repeatability of the first spalling time is observed; S-PC-Aust-30 and C-PC-Aust-30 both spalled at 5 minutes, and S-PC-Dup-30 and C-PC-Dup-30 spalled at 7 minutes. This suggests that duplex stainless rebars may slightly delay the spalling time compared to the austenitic stainless rebars. Specimen S-PC-Dup-15, which had duplex stainless rebars and a 15 mm concrete cover, spalled the latest at 10 minutes, causing the most severe spalling and exposing the rebars to heat. The spalled pieces of S-PC-Dup-15 are the largest compared to the other specimens, as shown in Figure 11. The depth of the concrete cover itself seems not to have a direct impact onto the spalling behaviour of concrete. However, the combination of austenitic stainless steel rebars and shallow concrete cover (15 mm) may have the potential to reduce the risk of fire spalling. The specimens with 30 mm concrete cover (S-PC-Aust-30, C-PC-Aust-30, S-PC-Dup-30, C-PC -Dup-30) all exhibited explosive spalling. However, the specimens with 15 mm concrete cover had either no spalling (S-PC-Aust-15, C-PC-Aust-15, C-PC-Dup-15) or more severe explosive spalling (S-PC-Dup-15) than the specimens of 30 mm concrete cover experienced. To conclude, for this particular project, the influence to the fire spalling behaviour of concrete should be attributed to the combination of rebar type and cover depth. The type of fire spalling for all specimens are summarized in Table 7, the explosive spalling results are summarized in Table 8.

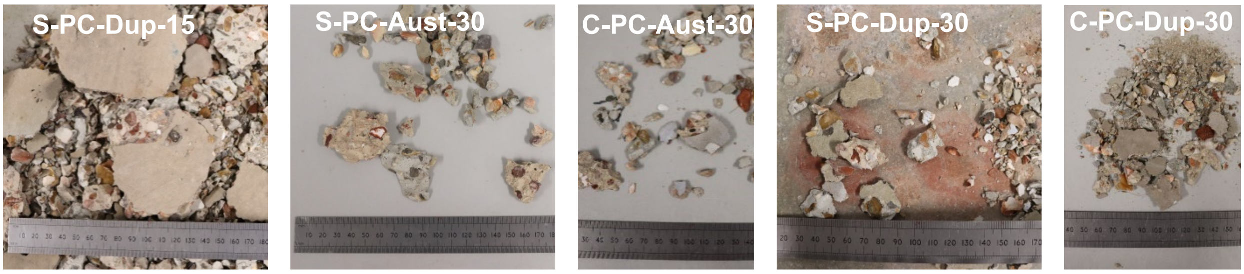

Figure 11 Spalled concrete pieces

Table 7 Summary of fire spalling types

Specimen name	Spalling type
S-PC-Aust-30	Explosive
S-PC-Dup-30	Explosive
S-PC-Dup-15	Explosive
C-PC-Aust-30	Explosive
C-RSTM-Dup-30	Explosive
C-Vir-Aust-30	None
S-Vir-Aust-30	Aggregate
C-Vir-Aust-30	Aggregate
S-RSTM-Aust-30	Aggregate
C-RSTM-Aust-30	Aggregate
S-PC-Aust-15	Aggregate
C-PC-Aust-15	Aggregate
S-RSTM-Aust-15	Aggregate
S-RSTM-Dup-30	Aggregate
C-PC-Dup-15	Aggregate

Table 8 Summary of explosive spalling test results

Specimen name	First spalling time	Number of spalling	Spalling weight loss (kg)	Maximum spalling depth (mm)	Average spalling depth (mm)	Maximum size of spalled pieces (cm)
S-PC-Aust-30	05:25	9	2.17	19.04	6.08	5
S-PC-Dup-30	07:06	5	1.04	12.86	2.83	3
S-PC-Dup-15	10:24	2	2.25	24.76	5.94	10
C-PC-Aust-30	05:39	2	0.22	8.91	0.88	4
C-PC-Dup-30	07:30	1	0.03	5.86	0.04	3

Based on the test results, a schematic illustration of the mechanisms involved in this study is shown in Figure 12. Specimens configurations that could control fire spalling are shown on the left, whereas the configurations that could induce fire spalling are shown on the right. Table 9 summarizes the influence of the adopted test configurations on fire spalling risk.

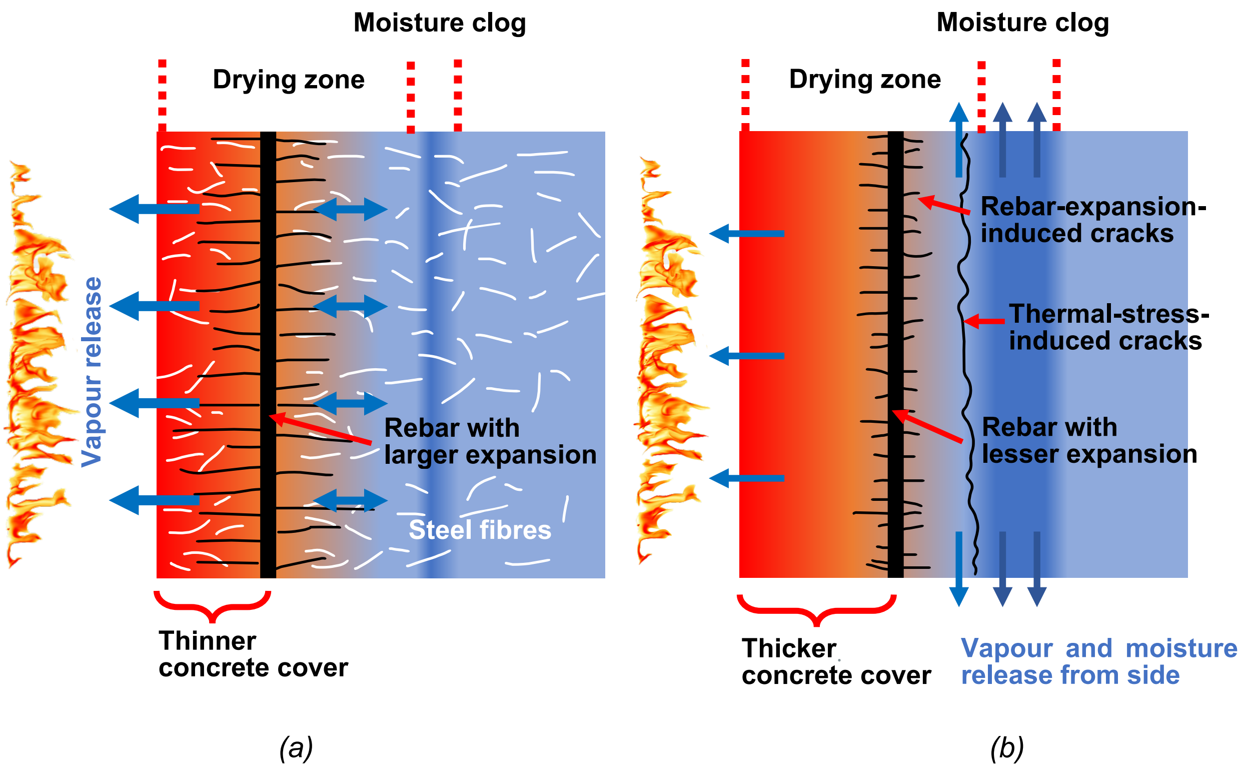

Figure 12 Driving mechanisms of the adopted concrete configurations that could (a) mitigate spalling and (b) induce spalling

Table 9 Influence of the adopted test configurations on fire spalling risk

Configurations that could reduce fire spalling risk:	Configurations that could increase fire spalling risk:
• Inclusion of virgin steel fibres and RSTM	• Plain concrete
• 15 mm concrete cover depth	• 30 mm concrete cover depth
• Austenitic stainless steel rebar	• Duplex stainless steel rebar
• Smaller specimen size (500×200×200 mm^3)	• Larger specimen size (500×500×220 mm^3)

In the configurations as shown in Figure 12 (a), the inclusion of steel fibres shows a positive effect on fire spalling mitigation. The steel fibres increase the concrete permeability due to the microcracks induced by the differential thermal expansion between concrete and steel. The crack bridging effect of steel fibres, which could increase the probability of spalling, seems not to have a significant effect according to the presented test results. The combination of thin concrete cover and long thermal cracks induced by the austenitic stainless steel rebar can create a high permeable layer near the heat exposure surface of the concrete specimen, resulting in a large amount of vapour release. Consequently, the formation of the moisture clog can be delayed, leading to the reduction of vapour pressure accumulated near the moisture clog, hence suppressing fire spalling. In addition, the large amount of vapour release from the heat exposure surface could be the trigger for surface aggregate spalling.

In the configurations as shown in Figure 12 (b), the thick concrete cover can provide thermal insulation to the stainless steel rebar. With a lower thermal expansion coefficient than that of the austenitic stainless steel, the cracks induced by the differential thermal expansion of the duplex stainless steel rebars and concrete can be limited. Without cracks induced by the rebars and steel fibres, the vapour migration towards the heat exposure surface in such configurations can be much less than in Figure 12(a). The large amount of vapour migration towards the inner concrete could from a thick layer of moisture clog and induce high vapour pressure, resulting in high spalling propensity. As shown in Figure 12(b), due to the lack of the crack bridging effect of steel fibres, such configurations are prone to experience thermal stress-induced cracks parallel to the isotherm. Therefore, the moisture accumulated near the moisture clog tends to escape from the sides through the cracks, i.e. the liquid and vapour release from the right and left sides of the fire spalling test specimens. For the short column specimens with less width of the heated surface compared to the slab specimens, this moisture release phenomenon could be further amplified, leading to less fire spalling propensity.

4.5 CONCLUSIONS

This study examines the effects of different parameters on the fire-induced spalling behaviour of stainless steel reinforced concrete specimens under compressive loading. The specimens are subjected to the ISO834 standard fire, while varying the specimen shape, concrete cover depth, steel fibre type and stainless steel rebar type. The spalling behaviour of the test specimens is observed and analysed, with particular attention given to the spalling type, propensity and severity. Based on a comparative analysis of the test results, the following conclusions can be drawn:

• The use of virgin steel fibres and RSTM at 30 kg/m^3 effectively mitigates the fire-induced explosive spalling for the specific test configuration. The spalling mitigation mechanism of steel fibres appears to involve faster relief of heated vapour from the heated surface, as no vapour leaks were observed from the left and right sides of steel FRC concrete compared with plain concrete.
• The virgin steel fibres could be more effective in controlling aggregate spalling.
• For the adopted specimen shapes, the propensity and severity of spalling are found to be higher in larger slab specimens than in smaller short column specimens.
• The use of duplex stainless steel rebars is found to delay concrete spalling compared to austenitic steel rebar. This effect was seen from both the slab and short column specimens.
• All specimens with austenitic stainless steel rebars and 15 mm concrete cover without the addition of fibres do not exhibit any signs of explosive spalling. This could be due to the internal cracking of the concrete caused by the differential thermal expansion between the rebar and concrete, which leads to pore pressure relief.

This study also reveals a positive effect of reducing the concrete cover on lowering the fire spalling risk when austenitic stainless steel rebars are used, enhancing both the long-term durability and fire safety of concrete structures, while potentially reducing the concrete usage to some extent.

AUTHOR CONTRIBUTIONS

Yifan Li: Methodology, Validation, Investigation, Formal analysis, Writing - Original Draft, Project administration. **Katherine A. Cashell:** Conceptualization, Methodology, Resources, Writing - Review & Editing, Funding acquisition. **Harris Angelakopoulos:** Resources, Methodology, Writing - Review & Editing. **Shan-Shan Huang:** Conceptualization, Methodology, Resources, Writing - Review & Editing, Supervision, Project administration, Funding acquisition.

ACKNOWLEDGEMENTS

We would like to acknowledge the support of the Institution of Civil Engineers (ICE), in collaboration with Brunel University London and the University of Sheffield, for their contribution to this work. We are also grateful to Zero Waste Works for supplying the RSTM and Virgin steel fires used in this project.

REFERENCES

[1] S. Patil, H. M. Somasekharaiah, H. S. Rao, and V. G. Ghorpade, "Durability and micro-structure studies on fly ash and silica fume based composite fiber reinforced high-performance concrete," in *Materials Today: Proceedings*, Elsevier Ltd, 2021, pp. 1511–1520. doi: 10.1016/j.matpr.2021.07.247.

[2] M. Jalal, E. Mansouri, M. Sharifipour, and A. R. Pouladkhan, "Mechanical, rheological, durability and microstructural properties of high performance self-compacting concrete containing SiO2 micro and nanoparticles," *Mater Des*, vol. 34, pp. 389–400, Feb. 2012, doi: 10.1016/j.matdes.2011.08.037.

[3] V. K. R. Kodur, "Spalling in High Strength Concrete Exposed to Fire: Concerns, Causes, Critical Parameters and Cures," *Advanced Technology in Structural Engineering*, pp. 1–9, 2000, doi: https://doi.org/10.1061/40492(2000)180.

[4] Y. Li, P. Du, and K. H. Tan, "Fire resistance of ultra-high performance concrete columns subjected to axial and eccentric loading," *Eng Struct*, vol. 248, Dec. 2021, doi: 10.1016/j.engstruct.2021.113158.

[5] J. Yang, G. F. Peng, J. Zhao, and G. S. Shui, "On the explosive spalling behavior of ultra-high performance concrete with and without coarse aggregate exposed to high temperature," *Constr Build Mater*, vol. 226, pp. 932–944, Nov. 2019, doi: 10.1016/j.conbuildmat.2019.07.299.

[6] RAIB, *Technical Investigation Report concerning the Fire on Eurotunnel Freight Shuttle 7412 on 11 September 2008*. Rail Accident Investigation Branch, Department for Transport., 2010. [Online]. Available: http://www.raib.gov.uk

[7] A. Leitner, "The fire catastrophe in the Tauern Tunnel: experience and conclusions for the Austrian guidelines," *Tunnelling and Underground Space Technology*, vol. 16, p. 217223, 2001.

[8] RAIB, *Rail Accident Report: Fire on HGV shuttle in the Channel Tunnel 21 August 2006*. Rail Accident Investigation Branch, Department for Transport., 2007. [Online]. Available: www.raib.gov.uk.

[9] R. M. Faure and M. Karray, "Investigation of the concrete lining after the Mont Blanc tunnel fire," *Structural Engineering International: Journal of the International Association for Bridge and Structural Engineering (IABSE)*, vol. 17, no. 2, pp. 123–132, May 2007, doi: 10.2749/101686607780680763.

[10] M. Khaled al-Bashiti and M. Z. Naser, "What can we learn from over 1000 tests on fire-induced spalling of concrete? A statistical investigation of critical factors and unexplored research space," *Constr Build Mater*, vol. 403, Nov. 2023, doi: 10.1016/j.conbuildmat.2023.133200.

[11] R. Jansson and L. Boström, “Factors influencing fire spalling of self compacting concrete,” *Materials and Structures/Materiaux et Constructions*, vol. 46, no. 10, pp. 1683–1694, Oct. 2013, doi: 10.1617/s11527-012-0007-z.

[12] V. K. R. Kodur and L. Phan, “Critical factors governing the fire performance of high strength concrete systems,” *Fire Saf J*, vol. 42, no. 6–7, pp. 482–488, Sep. 2007, doi: 10.1016/j.firesaf.2006.10.006.

[13] M. Amran, S. S. Huang, A. M. Onaizi, G. Murali, and H. S. Abdelgader, “Fire spalling behavior of high-strength concrete: A critical review,” *Construction and Building Materials*, vol. 341. Elsevier Ltd, Jul. 25, 2022. doi: 10.1016/j.conbuildmat.2022.127902.

[14] P. Kalifa, Ë.-D. Menneteau, and D. Quenard, “Spalling and pore pressure in HPC at high temperatures,” *Cem Concr Res*, pp. 1915–1927, 2000.

[15] S. Dal Pont, H. Colina, A. Dupas, and A. Ehrlacher, “An experimental relationship between complete liquid saturation and violent damage in concrete submitted to high temperature,” *Magazine of Concrete Research*, vol. 57, pp. 455–461, Aug. 2005.

[16] G. Choe, G. Kim, M. Yoon, E. Hwang, J. Nam, and N. Guncunski, “Effect of moisture migration and water vapor pressure build-up with the heating rate on concrete spalling type,” *Cem Concr Res*, vol. 116, pp. 1–10, Feb. 2019, doi: 10.1016/j.cemconres.2018.10.021.

[17] M. Ozawa, S. Uchida, T. Kamada, and H. Morimoto, “Study of mechanisms of explosive spalling in high-strength concrete at high temperatures using acoustic emission,” *Constr Build Mater*, vol. 37, pp. 621–628, Dec. 2012, doi: 10.1016/j.conbuildmat.2012.06.070.

[18] Z. Bazant, “Analysis of Pore Pressure, Thermal Stress and Fracture in Rapidly Heated Concrete,” in *International Workshop on Fire Performance of High-Strength Concrete*, Gaithersburg, 1997. [Online]. Available: https://tsapps.nist.gov/publication/get_pdf.cfm?pub_id=916655

[19] R. Jansson and L. Boström, “The influence of pressure in the pore system on fire spalling of concrete,” *Fire Technol*, vol. 46, no. 1, pp. 217–230, 2010, doi: 10.1007/s10694-009-0093-9.

[20] L. A. Ashton and S. C. C. Bate, “Discussion on the Fire-Resistance of Prestressed Concrete Beams,” in *Proceedings of the Institution of Civil Engineers*, ICE, Oct. 1961, pp. 305–320.

[21] V. Kodur and R. McGrath, “Fire Endurance of High Strength Concrete Columns *,” *Fire Technol*, vol. 39, pp. 73–87, 2003.

[22] A. H. Shah and U. K. Sharma, “Fire resistance and spalling performance of confined concrete columns,” *Constr Build Mater*, vol. 156, pp. 161–174, Dec. 2017, doi: 10.1016/j.conbuildmat.2017.08.167.

[23] A. M. B. Martins and J. P. C. Rodrigues, “Fire behaviour of concrete columns with restrained thermal elongation,” *Journal of Structural Fire Engineering*, vol. 2, no. 4, pp. 319–331, Dec. 2011, doi: 10.1260/2040-2317.2.4.319.

[24] A. M. Gil, B. Fernandes, F. L. Bolina, and B. F. Tutikian, “Experimental analysis of the spalling phenomenon in precast reinforced concrete columns exposed to high temperatures,” *Revista IBRACON de Estruturas e Materiais*, vol. 11, no. 4, pp. 856–875, Aug. 2018, doi: 10.1590/s1983-41952018000400011.

[25] Zero Waste Works, “Recycled Steel Tyre Microfibres.” Accessed: Mar. 18, 2024. [Online]. Available: https://www.zerowasteworks.co.uk/recycled-steel-microfibres

[26] MEPS International, “Europe Stainless Steel Price Forecasts.” Accessed: Oct. 13, 2023. [Online]. Available: https://mepsinternational.com/gb/en/products/europe-stainless-steel-price-forecasts

[27] MEPS International, “Europe Steel Prices.” Accessed: Oct. 13, 2023. [Online]. Available: https://mepsinternational.com/gb/en/products/europe-steel-prices

[28] G. Gedge, “Rationale for using Stainless Steel Reinforcement in the UK Construction Industry.”

[29] World Stainless Association, “World Stainless Org CO2 Emissions Report.” Accessed: Oct. 13, 2023. [Online]. Available: https://www.worldstainless.org/about-stainless/environment/stainless-steels-and-co2-industry-emissions-and-related-data/

[30] A. H. Tuthill and S. Lamb, “GUIDELINES FOR THE USE OF STAINLESS STEEL IN MUNICIPAL WASTE WATER TREATMENT PLANTS.”

[31] M. Nagels, B. Verhoeven, N. Larché, R. Dewil, and B. Rossi, “Comparative life cycle cost assessment of (lean) duplex stainless steel in wastewater treatment environments,” *J Environ Manage*, vol. 306, Mar. 2022, doi: 10.1016/j.jenvman.2021.114375.

[32] B. Karabulut, G. Ferraz, and B. Rossi, “Lifecycle cost assessment of high strength carbon and stainless steel girder bridges,” *J Environ Manage*, vol. 277, Jan. 2021, doi: 10.1016/j.jenvman.2020.111460.

[33] J. T. Pérez-Quiroz, J. Terán, M. J. Herrera, M. Martínez, and J. Genescá, “Assessment of stainless steel reinforcement for concrete structures rehabilitation,” *J Constr Steel Res*, vol. 64, no. 11, pp. 1317–1324, Nov. 2008, doi: 10.1016/j.jcsr.2008.07.024.

[34] M. Rabi, K. A. Cashell, and R. Shamass, “Flexural analysis and design of stainless steel reinforced concrete beams,” *Eng Struct*, vol. 198, Nov. 2019, doi: 10.1016/j.engstruct.2019.109432.

[35] M. Rabi, R. Shamass, and K. A. Cashell, “Structural performance of stainless steel reinforced concrete members: A review,” *Construction and Building Materials*, vol. 325. Elsevier Ltd, Mar. 28, 2022. doi: 10.1016/j.conbuildmat.2022.126673.

[36] P. Boillot and J. Peultier, “Use of stainless steels in the industry: Recent and future developments,” in *Procedia Engineering*, Elsevier Ltd, 2014, pp. 309–321. doi: 10.1016/j.proeng.2014.09.015.

[37] H. Dang, A. Liang, R. Feng, J. Zhang, X. Yu, and Y. Shao, "Experimental study on mechanical properties and low-cycle fatigue behaviour of stainless steels subjected to salt spray and dry/wet cycle," *Int J Fatigue*, vol. 165, Dec. 2022, doi: 10.1016/j.ijfatigue.2022.107187.

[38] L. Gardner, Y. Bu, P. Francis, N. R. Baddoo, K. A. Cashell, and F. McCann, "Elevated temperature material properties of stainless steel reinforcing bar," *Constr Build Mater*, vol. 114, pp. 977–997, Jul. 2016, doi: 10.1016/j.conbuildmat.2016.04.009.

[39] British Standards Institution, "BS EN 1992-1-2:2023, Eurocode 2: Design of concrete structures : Part 1-2: Structural fire design," London, 2023.

[40] British Standards Institution., "BS EN 1993-1-2:2024 Eurocde 3 Design of steel structures Part 1:2 Structural fire design," London, 2024.

[41] T. Morita, A. Nishida, N. Yamazaki, U. Schneider, and U. Diederichs, "An Experimental Study on Spalling of High Strength Concrete Elements under Fire Attack," in *Fire Safety Science-Proceedings of the Sixth International Symposium*, 2000, pp. 855–866. doi: 10.3801/IAFSS.FSS.6-855.

[42] L. Boström and R. Jansson, "Self-Compacting Concrete Exposed to Fire," Borås, 2008.

[43] H. Du and M. Zhang, "Experimental investigation of thermal pore pressure in reinforced C80 high performance concrete slabs at elevated temperatures," *Constr Build Mater*, vol. 260, Nov. 2020, doi: 10.1016/j.conbuildmat.2020.120451.

[44] A. Lau and M. Anson, "Effect of high temperatures on high performance steel fibre reinforced concrete," *Cem Concr Res*, vol. 36, no. 9, pp. 1698–1707, Sep. 2006, doi: 10.1016/j.cemconres.2006.03.024.

[45] R. Serrano, A. Cobo, M. I. Prieto, and M. de las N. González, "Analysis of fire resistance of concrete with polypropylene or steel fibers," *Constr Build Mater*, vol. 122, pp. 302–309, Sep. 2016, doi: 10.1016/j.conbuildmat.2016.06.055.

[46] M. Tayebi and M. Nematzadeh, "Effect of Hot-Compacted waste nylon fine aggregate on compressive Stress-Strain behavior of steel Fiber-Reinforced concrete after exposure to fire: Experiments and optimization," *Constr Build Mater*, vol. 284, May 2021, doi: 10.1016/j.conbuildmat.2021.122742.

[47] J. Kim, G. P. Lee, and D. Y. Moon, "Evaluation of mechanical properties of steel-fibre-reinforced concrete exposed to high temperatures by double-punch test," *Constr Build Mater*, vol. 79, pp. 182–191, Mar. 2015, doi: 10.1016/j.conbuildmat.2015.01.042.

[48] V. K. R. Kodur, ; Fu, P. Cheng, T.-C. Wang, and M. A. Sultan, "Effect of Strength and Fiber Reinforcement on Fire Resistance of High-Strength Concrete Columns," *JOURNAL OF STRUCTURAL ENGINEERING*, vol. 129(2), pp. 253–259, Feb. 2003, doi: 10.1061/ASCE0733-94452003129:2253.

[49] N. Algourdin, P. Pliya, A. L. Beaucour, A. Simon, and A. Noumowé, "Influence of polypropylene and steel fibres on thermal spalling and physical-mechanical properties of

concrete under different heating rates," *Constr Build Mater*, vol. 259, Oct. 2020, doi: 10.1016/j.conbuildmat.2020.119690.

[50] S. Sanchayan and S. J. Foster, "High temperature behaviour of hybrid steel–PVA fibre reinforced reactive powder concrete," *Materials and Structures/Materiaux et Constructions*, vol. 49, no. 3, pp. 769–782, Mar. 2016, doi: 10.1617/s11527-015-0537-2.

[51] O. Czoboly, É. Lublóy, V. Hlavička, G. L. Balázs, O. Kéri, and I. M. Szilágyi, "Fibers and fiber cocktails to improve fire resistance of concrete," *J Therm Anal Calorim*, vol. 128, no. 3, pp. 1453–1461, Jun. 2017, doi: 10.1007/s10973-016-6038-x.

[52] N. Yermak, P. Pliya, A. L. Beaucour, A. Simon, and A. Noumowé, "Influence of steel and/or polypropylene fibres on the behaviour of concrete at high temperature: Spalling, transfer and mechanical properties," *Constr Build Mater*, vol. 132, pp. 240–250, Feb. 2017, doi: 10.1016/j.conbuildmat.2016.11.120.

[53] D. Zhang, G. Y. Tan, and K. H. Tan, "Combined effect of flax fibers and steel fibers on spalling resistance of ultra-high performance concrete at high temperature," *Cem Concr Compos*, vol. 121, Aug. 2021, doi: 10.1016/j.cemconcomp.2021.104067.

[54] Y. Ding, C. Azevedo, J. B. Aguiar, and S. Jalali, "Study on residual behaviour and flexural toughness of fibre cocktail reinforced self compacting high performance concrete after exposure to high temperature," *Constr Build Mater*, vol. 26, no. 1, pp. 21–31, Jan. 2012, doi: 10.1016/j.conbuildmat.2011.04.058.

[55] Y. S. Heo, C. G. Han, and K. M. Kim, "Combined fiber technique for spalling protection of concrete column, slab and beam in fire," *Materials and Structures/Materiaux et Constructions*, vol. 48, no. 10, pp. 3377–3390, Oct. 2015, doi: 10.1617/s11527-014-0406-4.

[56] Y. Ding, C. Zhang, M. Cao, Y. Zhang, and C. Azevedo, "Influence of different fibers on the change of pore pressure of self-consolidating concrete exposed to fire," *Constr Build Mater*, vol. 113, pp. 456–469, Jun. 2016, doi: 10.1016/j.conbuildmat.2016.03.070.

[57] Y. Li, K. H. Tan, and E. H. Yang, "Influence of aggregate size and inclusion of polypropylene and steel fibers on the hot permeability of ultra-high performance concrete (UHPC) at elevated temperature," *Constr Build Mater*, vol. 169, pp. 629–637, Apr. 2018, doi: 10.1016/j.conbuildmat.2018.01.105.

[58] S. L. Suhaendi and T. Horiguchi, "Effect of short fibers on residual permeability and mechanical properties of hybrid fibre reinforced high strength concrete after heat exposition," *Cem Concr Res*, vol. 36, no. 9, pp. 1672–1678, Sep. 2006, doi: 10.1016/j.cemconres.2006.05.006.

[59] R. Y. Ma, J. Yang, and G. F. Peng, "Influence of steel fiber types on residual mechanical properties and explosive spalling of hybrid fiber reinforced ultra-high performance concrete: Optimization and evaluations," *Case Studies in Construction Materials*, vol. 19, Dec. 2023, doi: 10.1016/j.cscm.2023.e02538.

[60] M. Serdar, A. Baričević, S. Lakušić, and D. Bjegović, “Special purpose concrete products from waste tyre recyclates,” *Journal of the Croatian Association of Civil Engineers*, vol. 65, no. Građevinar, pp. 793–801, 2013.

[61] Fazilet Cinaralp and Jean-Pierre Taverne, “End of life tyres: A valuable resource with growing potential,” ETRMA. Accessed: Feb. 08, 2023. [Online]. Available: https://www.etrma.org/wp-content/uploads/2019/09/2010_etrma_elt_management_brochure_final.pdf

[62] B. S. Thomas and R. C. Gupta, “A comprehensive review on the applications of waste tire rubber in cement concrete,” *Renewable and Sustainable Energy Reviews*, vol. 54. Elsevier Ltd, pp. 1323–1333, Feb. 01, 2016. doi: 10.1016/j.rser.2015.10.092.

[63] E. Gholami, H. Afshin, M. Charkhtab Basim, and M. Sharghi, “Ultra-high performance recycled steel fiber reinforced concrete segments under the thrust force of TBM jacks and their environmental potentialities,” *Structures*, vol. 47, pp. 2465–2484, Jan. 2023, doi: 10.1016/j.istruc.2022.12.051.

[64] X. Qin and S. Kaewunruen, “Environment-friendly recycled steel fibre reinforced concrete,” *Construction and Building Materials*, vol. 327. Elsevier Ltd, Apr. 11, 2022. doi: 10.1016/j.conbuildmat.2022.126967.

[65] M. H. Abd-Elrahman, I. S. Agwa, Y. Elsakhawy, and M. S. Rizk, “Effect of utilising ferrosilicon and recycled steel fibres on ultra-high-strength concrete containing recycled granite,” *Case Studies in Construction Materials*, vol. 18, Jul. 2023, doi: 10.1016/j.cscm.2023.e01903.

[66] F. Soltanzadeh, A. Edalat-Behbahani, and E. N. B. Pereira, “Bond behavior of recycled tyre steel fiber reinforced concrete and basalt fiber-reinforced polymer bars under static and fatigue loading conditions,” *Journal of Building Engineering*, p. 106291, Mar. 2023, doi: 10.1016/j.jobe.2023.106291.

[67] H. Zhong, E. W. Poon, K. Chen, and M. Zhang, “Engineering properties of crumb rubber alkali-activated mortar reinforced with recycled steel fibres,” *J Clean Prod*, vol. 238, Nov. 2019, doi: 10.1016/j.jclepro.2019.117950.

[68] F. P. Figueiredo, S. S. Huang, H. Angelakopoulos, K. Pilakoutas, and I. Burgess, “Effects of Recycled Steel and Polymer Fibres on Explosive Fire Spalling of Concrete,” *Fire Technol*, vol. 55, no. 5, pp. 1495–1516, Sep. 2019, doi: 10.1007/s10694-019-00817-9.

[69] J. Yang, G. F. Peng, G. S. Shui, and G. Zhang, “Mechanical properties and anti-spalling behavior of ultra-high performance concrete with recycled and industrial steel fibers,” *Materials*, vol. 12, no. 5, Mar. 2019, doi: 10.3390/ma12050783.

[70] Y. Li, S.-S. Huang, K. Pilakoutas, H. Angelakopoulos, and I. Burgess, “Mitigation of Fire-Induced Spalling of Concrete using Recycled Tyre Polymer Fibre,” in *6th International Workshop on Concrete Spalling due to Fire Exposure*, Sheffield, Sep. 2019, pp. 42–51.

[71] British Standards Institution, “BS EN 10088-1:2014 Stainless steels Part 1: List of stainless steels,” London, 2014.

[72] BSI, “BS EN 1991-1-2:2002, Eurocode 1 : actions on structures. Part 1-2: General actions : actions on structures exposed to fire.,” BSI, Mar. 2009.

[73] British Standards Institution, “BS EN 1353:1997 Determination of moisture content of autoclaved aerated concrete,” British Standards Institution, London, 1997.

[74] ASTM international, “ASTM C642-21 Standard Test Method for Density, Absorption, and Voids in Hardened Concrete,” West Conshohocken, 2022. doi: 10.1520/C0642-21.

[75] Robert Jansson, “Fire Spalling of Concrete：Theoretical and Experimental Studies,” PhD thesis, KTH Architecture and the Built Environment, Stockholm, 2013.

[76] K. D. Hertz, “Limits of spalling of fire-exposed concrete,” *Fire Saf J*, vol. 38, no. 2, pp. 103–116, Mar. 2003, doi: 10.1016/S0379-7112(02)00051-6.

5 Paper III

Study on the fire spalling behaviour of recycled polymer tyre microfibre and virgin polypropylene fibre reinforced concrete

Yifan Li[1*], Kypros Pilakoutas[1], Shan-Shan Huang[1]
[1]The University of Sheffield, Sheffield, the United Kingdom
* Corresponding author (yli101@sheffield.ac.uk, D120, Department of Civil and Structural Engineering, the University of Sheffield, Sheffield, UK, S1 4BT)

ABSTRACT

When concrete is exposed to fire, explosive fire spalling can occur that can lead to severe structural damage. Polypropylene (PP) fibres in concrete are known to be effective in mitigating fire spalling. For environmental benefits, Recycled Polymer Tyre Microfibres (RPTM) are proposed in this study to investigate their effectiveness in fire spalling mitigation. These fibres melt at a higher temperature and have variable length and diameter compared to PP fibres, hence the mechanism of how these fibres will work in heated concrete needs to be understood. This study compares the efficacy of both PP fibres and RSTM in fire spalling mitigation by performing fire spalling tests on high-strength concrete with high moisture content. Scanning Electron Microscopy (SEM), pore pressure, temperature and permeability tests are conducted. The results indicate that RSTM can reduce the risk and the severity of fire spalling. PP fibres exhibit superior performance in spalling mitigation at a dosage of only 1 kg/m^3 in fresh concrete. The influence of RPTM in heated concrete could be different to PP fibres in microstructures.

KEYWORDS: Recycled polymer tyre microfibre, polypropylene fibre, fire spalling of concrete

5.1 INTRODUCTION

Fire spalling of concrete can occur at high temperatures or high heating rates. During fire spalling, concrete pieces are explosively ejected or gradually peeled off from the fire-exposed surface, leading to a reduction in the cross-sectional area and exposing the steel reinforcement to heat. Fire spalling poses a significant threat to modern concrete structures, given its potential to trigger structural damage and failure and substantial economic losses. Previous accidents have shown the destructive nature of fire spalling in concrete structures [1], [2], [3], [4].

A substantial amount of research has demonstrated the effectiveness of PP fibres to mitigate fire-induced spalling [5], [6], [7], [8], [9]. Various test methods, including pore pressure gauges [5], [10], [11], mercury intrusion [7], computed tomography [12], hot permeability [13], [14], and microscopic imaging [15], [16], have been employed to investigate the mechanisms by which fibres act within heated concrete.

Explosive fire spalling, typically occurring in the early stages of heating (as early as 5 minutes) [17], [18], is commonly believed to be caused by thermo-mechanical damage [19], [20] and pore vapour pressure accumulation [21], [22] in the heated concrete. High-strength concrete (HSC) exhibits a higher tendency for fire spalling compared to normal-strength concrete (NSC) owing to its denser microstructure [23], [24], [25]. The moisture content of the concrete is another crucial factor influencing the propensity of fire spalling [17], as it affects both the pour vapour pressure [26] and the mechanical strength of the concrete [27].

Eurocode 1992-1-2 [28] specifically requires the verification of fire spalling in concrete if either of these criteria (high strength or saturated environment) is met, unless polypropylene (PP) fibres are incorporated into the concrete mix. The addition of PP fibres can enhance the high-temperature permeability of concrete by (1) creating microcracks due to the differential thermal expansion between the PP fibres and concrete [16] and (2) forming empty channels through melting at approximately 170 °C [15], [23]. The increased concrete permeability can facilitate moisture leakage and reduce the pore vapour pressure of concrete, thereby reducing the propensity or severity of fire spalling [5].

Recycled Polymer Tyre Microfibres (RPTM), which are normally extracted during the tyre recycling process, have the potential to substitute PP fibres in controlling fire spalling of concrete. In terms of cost-effectiveness, the price of cleaned RPTM in Europe (€600 per ton) is two-thirds of the price of PP microfibres (€900 per ton) [29]. A quote from a UK local supplier indicates that the cost of RSTM is only half of the cost of PP fibres [30]. In terms of environment benefit, there are approximately 1.5 billion waste tyres produced globally every year, including around 3.5 million tons of waste tyres produced in the EU alone [31]. Depending on the grade of the tyres, 5% to 10% of the waste tyres can be recycled as polymer fibres [32]. The vast amount of waste tyres provides a vast amount of RPTM. If appropriately cleaned, these fibres could be used in concrete infrastructures to improve its resistance to drying shrinkage and chlorides penetration [33], hence prolong the life time of concrete structures. For each ton of RPTM recycled, it is estimated that 0.38 tons of CO_2 can be saved by avoiding the use of virgin PP fibres and 1.93 tons of CO_2 by avoiding its incineration [29].

Only few preliminary studies have provided proof of concept for the effectiveness of RPTM in fire spalling control [34], [35]. As the properties of RPTM differ from those of PP fibres, for example, they have variable length and diameter and melt at a higher temperature, their role in fire spalling mitigation still remains unclear. Chen et al. [36] investigated the porous structure of concrete with various dosages of fibres at elevated temperatures. No clear relationship was found between the increase of fibres dosages and the pore size distribution of heated concrete. Besides, the formation of interconnected microcracks near the recycled fibres were observed after heated to 400 °C, which is much higher than the temperature of concrete (10 mm from the heat surface) when spalling occurs [34], [35]. Hence, the current understanding of the role of RPTM in fire spalling is still very limited.

The objective of this study is to compare the effectiveness and mechanisms of RPTM and PP fibres in fire spalling mitigation. Fire spalling tests were performed on concrete specimens containing both RPTM and virgin PP fibres. Parametric studies of concrete age, loading ratio, and fibre dosage were conducted. The vapour pore pressure, permeability, and SEM tests were used to investigate the underlying mechanisms of both fibre types. This work will lead to a better understanding of the fire spalling mechanism and potentially more environmentally friendly solutions to this problem.

5.2 EXPERIMENTAL PROGRAMME

5.2.1 Materials and concrete casting

Two groups of concrete specimens were used for the fire spalling tests according to age, as shown in Table 1. Group 1 contains four slabs that were cast six years prior to the test to investigate the long-term effects of drying and concrete maturity. Group 2 contains eight slabs that were cast four months before the test to maintain a high moisture content. Although the source of concrete aggregates is different between the two groups, the same type of limestone aggregates were used. The concrete mix designs for both groups are presented in Table 2.

Table 1 Test specimen list

Concrete age	Name	RPTM dosage (kg/m^3)	PP fibres dosage (kg/m^3)	Loading ratio (%)	Pressure gauge	Thermocouple Tree	28-day Compressive Strength (MPa)	Test day compressive strength (MPa)
6 years	PC-6y-1	--	--	30	--	yes	48.6	61.4
	PC-6y-2	--	--	30	--	yes		
	R2-6y-1	2	--	30	--	yes	49.4	59.1
	R2-6y-2	2	--	30	--	yes		
4 months	PC-4m-1	--	--	30	yes	yes	58.6	64.2
	PC-4m-2	--	--	10	yes	--		
	PC-4m-3	--	--	10	--	--		
	R1-4m-1	1	--	10	yes	yes	58.8	62.5
	R1-4m-2	1	--	30	yes	--		
	R2-4m-1	2	--	10	yes	yes	51.8	55.1
	PP1-4m-1	--	1	10	yes	yes	51.3	54.6
	PP1-4m-2	--	1	10	yes	--		

Table 2 Concrete mix design

	6 years concrete specimen	4 months concrete specimen
Material	Quantity (kg/m^3)	Quantity (kg/m^3)
Cement (CEM I 52.5 N)	440	440
Water	154	220
Building sand	250 (0 – 2 mm)	170 (0 – 1 mm)
Limestone fines	620 (0 – 4 mm)	700 (0 – 4 mm)
Limestone aggregate	970 (4 - 10 mm)	970 (4 - 10 mm)
Admixture	0.293 (Cemex WRA-CP105)	--
Superplasticiser	0.528 (Cemex - CSP313)	4.9 (Sika ViscoFlow 2000)

The compressive strength of the concrete specimens was measured on 28 days after casting and on the test day. To account for the extra maturity of the concrete of the six-year group, the four-month group was designed to achieve the same strength on the day of testing. The four-month group exhibited slightly higher variations in strength of test day, due to differences in fibre types and dosages. The inclusion of 1 kg/m³ of RPTM fibres exhibited the least detrimental effect on compressive strength.

To examine the impact of the fibre dosage and type, RPTM dosages of 1 kg/m³ and 2 kg/m³, and a PP fibre dosage of 1 kg/m^3 were incorporated into the concrete mix. Plain concrete samples, cast from the same batch, served as the control group. For the second group, the fibre ratio and curing conditions were designed to strongly favour spalling. Thus, the moisture ratio of concrete was maintained at a high level and for half of the concrete specimens, half (i.e. 1 kg/m^3) of the recommended fibre dosage [37] was used.

The PP fibres used in this study are monofilament microfibres with nominal length of 12 mm and diameter of 32 ± 1.6 μm, with density 910 kg/m^3 and melting temperature of around 160°C [15]. The typical composition of RPTM is 60% polyethylene terephthalate (PET), 25% polyamide 66 (PA 66) and 15% polybutylene terephthalate (PBT) [38]. Because of the recycling process, RPTM have more variable properties. The length of RPTM varies from 0.8 – 16 mm and the diameter from 7.5 - 60 μm. The density of RPTM is slightly higher than PP fibres, at around 1320 kg/m^3 [39]. The melting of RPTM starts from 225 °C and continues as temperature increases. The full decomposition of RPTM occurs at 340 °C (decomposition of PBT) and 400 °C (decomposition of PET and PA 66), where 20% of residue can still be found when heated at 500 °C [39]. Figure 1 shows the PP fibre and RPTM used in this study.

Figure 1 Monofilament PP fibre (left) and RPTM (right).

As a recycled material, RPTM's cost-effectiveness and environmental benefit make it a more attractive alternative to PP fibres, but certain drawbacks hinder its current implementation. In comparison to manufactured monofilament PP fibres, RPTM's raw materials are entangled and contaminated with rubber dust. Consequently, incorporating RPTM in concrete requires an additional cleaning process and an integration process to disentangle the fibres, preventing fibre clumping in the concrete.

For the first group of specimens, the fibre untangling process was conducted using a specially developed machine at the University of Sheffield. This consists of several vibrating wire screens to separate the fibres and a vacuum system to pull the fibres and spread them into the concrete mixer. This process would take up to 30 minutes and is carried out during the concrete mixing stage. The time requirement for this process poses challenges for concrete casting. To reduce the time of mixing to below 10 minutes, for the four-month group specimens, small amounts of RPTM were manually added into the concrete mixer. As shown in Figure 2(a), for each layer of RPTM placed on top of the pre-mixed concrete, an additional one minute of mixing was conducted. This step was repeated several times until all fibres were incorporated into the concrete and no visible fibre agglomarations could be seen, as shown in Figure 2(b). The introduction of RPTM in this manner reduced the workability of concrete; hence, an additional amount (0.5% of cement mass) of superplasticizer was added to the 2 kg/m³ RPTM concrete to maintain workability. The PP fibres were added to the concrete all at once due to their monofilament arrangement. A uniform dispersion was relatively easy and individual PP fibres could be physically observed in the concrete, as illustrated in Figure 2(c).

Figure 2 (a) Mixing stage of RPTM (b) RPTM concrete after mixing (c) PP fibre in concrete

The concrete was cast into plywood moulds, as shown in *Figure 3*(a). Pressure gauges and thermocouples were positioned at specific distances from the bottom surface. The design of the pressure gauges was adopted from Kalifa et al [21]. The tip of the pressure gauge is made of a pressure probe, which consists of a porous stainless steel sintered metal disk (diameter of 12.7 mm and thickness of 3.17 mm), connected by a stainless steel pipe (2 mm inner diameter) filled with heat-resistant silicone oil to transmit pressure to the pressure gauge. Type-K thermocouples were placed along side the pressure probes. There tip as located 1 cm away from the pressure probe at the same depth, to minimize the intrusion effect of the pressure probes.

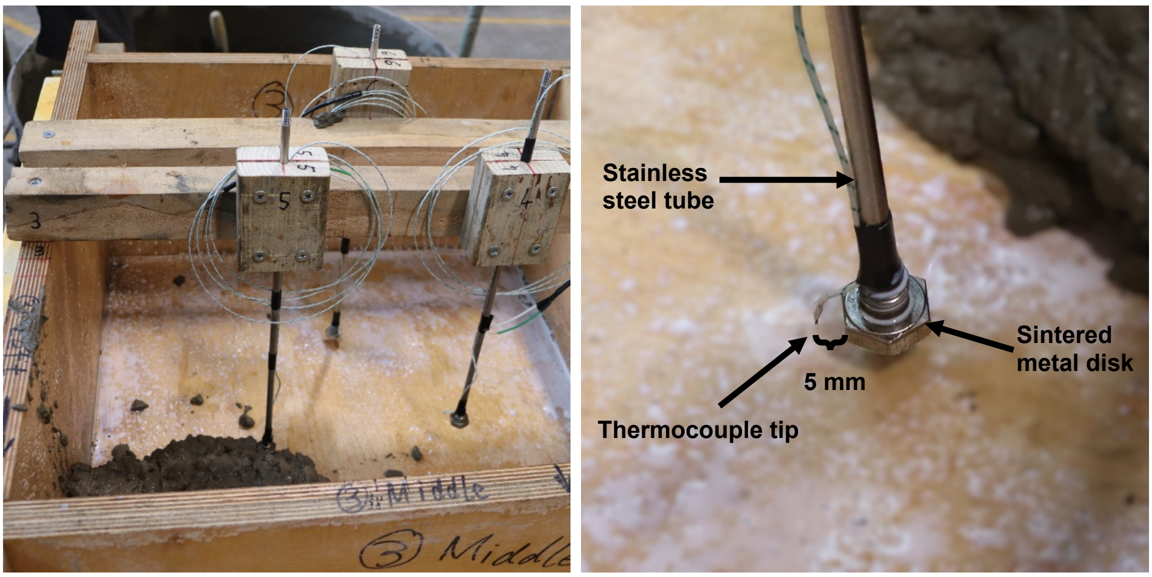

Figure 3 (a) Concrete moulds (b) Mounted pressure probes and thermocouple

The instrumentation layout and embedment depths are illustrated in Figure 4. Three pressure gauges were located at depths of 10 mm, 20 mm, and 50 mm from the heating surface. The triangular arrangement of the pressure probes was designed to maintain an equal distance from the heating centre and minimize the risk of splitting crack development resulting from vertical compressive loading on the specimen. To assess the intrusion effect of the pressure gauges, for one specimen in each fibre dosage, a thermocouple tree was placed at the centre of the specimen at depths of 1 mm, 10 mm, 20 mm, and 50 mm, without pressure gauges.

The specimens were demoulded two days after casting and cured in a water tank for one month. Subsequently, the specimens were removed and dried under indoor laboratory conditions (temperature of 20 ± 3 °C and 30 – 45% relative humidity) for three months. For the six-year test group, the specimens were kept in a water tank for four years and then dried for 14 months until the test day.

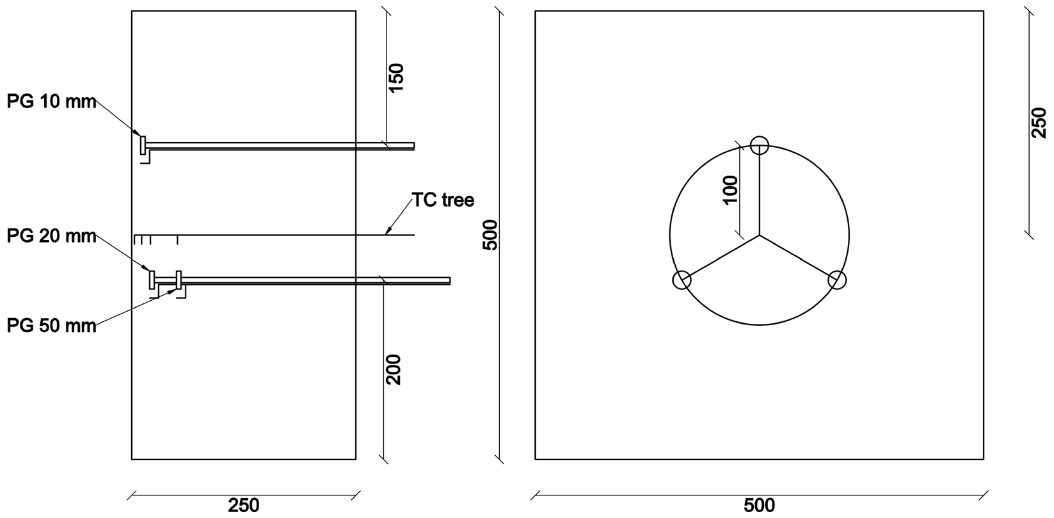

Figure 4 Layout of the concrete specimen and measurement equipment, PG stands for pressure gauge and TC stands for thermocouple

5.2.2 Spalling test setup

The radiation heating panel used for the fire spalling test is shown in Figure 5. The panel consists of six molybdenum elements capable of producing 100 kW/m². The heating panel is mounted on a moving track, to allow adjustment of the distance between the panel and the concrete specimen so as to allow altering the heat flux on the concrete surface if necessary. In this test, the distance during heating was set at 100 mm. The exposure surface temperature was calibrated to the first 30 minutes ISO 834 standard fire curve using plate thermometer following the BS EN 1991-1-2 standard [40]. It should be noted that there is a small gap of about 20 °C between the calibrated surface temperature of concrete and the standard fire curve during the last 5 minutes of heating, due to limitations in the maximum power output.

\

Figure 5 (a) Heating panel for fire spalling test

Loading conditions can increase the propensity of fire spalling in concrete [17]. In this study, a uniaxial compression load was applied to the concrete samples to simulate the working conditions of a tunnel segment. A load ratio of 30% of compressive strength was used as a reasonable working condition [41] in tunnels, while a 10% load ratio was employed to assess the influence of compressive stress level.

The front and back of the loading system are shown in Figure 6. It consists of two paired hydraulic jacks and stiff steel beams to distribute the load uniformly. All surfaces of the loading frame facing the heating panel were covered with vermiculite heat insulation boards (see Figure 6(b)). A heat-resistant stainless steel mesh restrained by two stiffeners were inserted to protect the heating system from exploding pieces of concrete. A gap was left between the bottom fire board and the steel mesh to prevent accumulation of concrete debris after spalling. A summary of the test conditions is shown in Table 3.

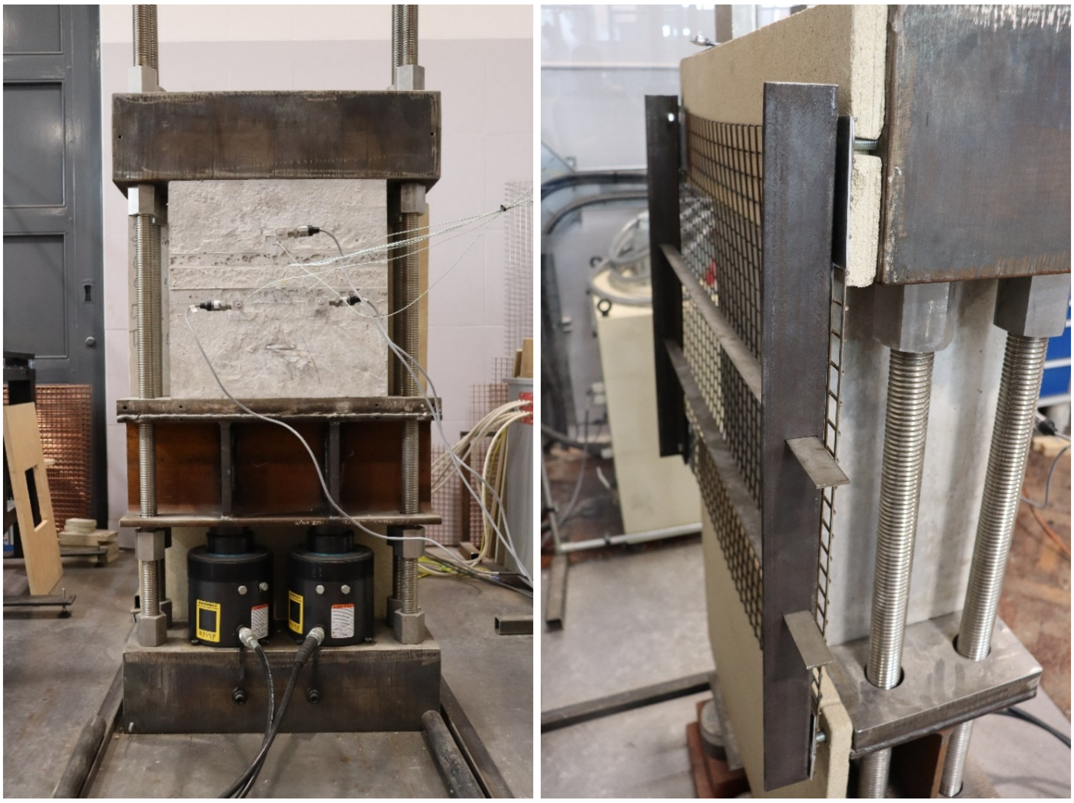

Figure 6 (a) Back of the loading system (b) Front of the loading system

Table 3 Summary of the test condition

Load ratio to compressive strength (%)	Load type	Heat curve	Exposure face	Exposure time (min)	Maximum surface temperature (°C)
30 / 10	Uniaxial compression	ISO 834 Standard fire curve	One-sided exposure	30	830

5.2.3 Moisture content, permeability and SEM test

The moisture content at different depths was monitored using concrete cylinders. Immediately after demoulding, the top section of the cylinder was sliced at depths of 25 mm and 50 mm, as shown in Figure 7. Since the concrete was still very wet at this stage, the wet sawing had minimal influence on moisture content. The side surfaces of the slices were then wrapped with aluminium tape to create unilateral drying conditions, which simulate the drying of the slab (fire spalling test specimen) cores. The gaps between each slice were wrapped again to ensure sealed conditions. Since the moisture test cylinders were cast, cured, and dried under the same conditions as the spalling test slabs, the moisture content of the slices across the depth should indicate the moisture distribution within the cores of the slabs. For each fibre dosage, three cylinders were cast for the moisture content test. One of the cylinders was dried at 105 °C until the change in mass was steady (less than 0.5% per day), allowing for the calculation of the dry mass and the initial moisture content of the cylinder. The moisture content of the other two cylinders were calculated based on the dried cylinder, then the moisture contents were averaged to give an estimation of the moisture content distribution of the slabs.

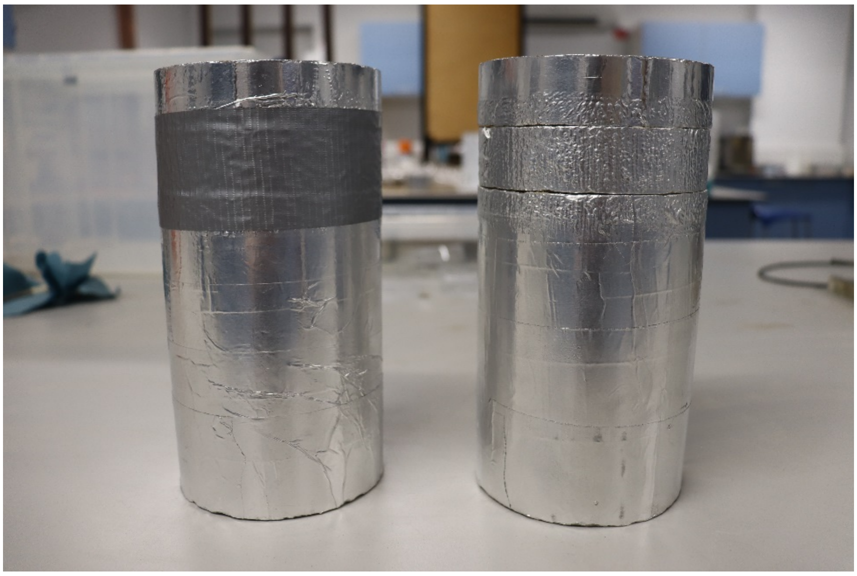

Figure 7 Concrete specimen for moisture content monitoring

For the four-month group, cylindrical concrete specimens (50 mm height and 150 mm diameter) were cast to assess the permeability. To eliminate the boundary effect, the top and bottom surfaces with excess cement were ground off from the cylinders. The test setup and the test procedures were designed based on RILEM TC 116-PCD [42]. Figure 8 shows the test specimen and the setup for the permeability test. For each fibre dosage, three permeability tests were conducted at ambient temperature and after the cylinders were heated to 200 °C. The heating rate was kept at 1 °C per minute to avoid thermal cracking. After heating, the specimens were kept in the oven and were allowed to cool down naturally.

Figure 8 (a) Permeability test specimen (b) Permeability test setup

SEM tests were carried out to assess the distribution of RPTM and their effect on the concrete. Due to the small size requirement for SEM (10 mm x 10 mm) samples, test samples were extracted from different depths within concrete cubes to assess the vertical distribution of fibres in the mix. To avoid using saw cutting that could potentially pull out the fibres, cores extracted from the cubes were fractured via bending to obtain the required size for SEM. The fractured surface is expected to preserve the nature of the concrete microstructure. The test was conducted using an FEI Inspect F microscope to perform field emission gun-scanning electron microscope (FEG-SEM) analysis, providing higher resolution imaging compared to regular SEM.

5.3 RESULTS

5.3.1 Moisture content

On the day of the fire spalling test, the moisture content distribution (0-25 mm, 25-50 mm, and below 50 mm) for the fire spalling test specimens was estimated using the sliced cylinders. The test data are summarised in Table 4. At depth, the moisture content of the six-year group is lower than that of the four-month group, due to the longer drying time. However, the moisture contents in the top two surface layers (0 - 25 mm and 25 – 50 mm) of R2 and R1 specimens are drier than the rest of specimens in both groups, indicating that the inclusion of RPTM has increased the drying speed of concrete. Hence, on the test day, the top surface of the specimens had similar moisture content in both groups, but the inner layer exhibited a much larger difference. The four-month group had almost twice the moisture content compared to the six-year group, which aligns with the objectives of testing in high moisture conditions.

Table 4 Moisture content distribution of the fire spalling test specimen on the test day

Test Group	6 years Group		4 Months Group			
Drying Time	14 Months		3 Months			
Sample Name	PC	R2	PC	R2	R1	PP1
0 - 25 mm	3.6%	3.2%	4.7%	3.3%	3.6%	4.5%
25 - 50 mm	3.8%	3.0%	6.4%	5.9%	5.7%	6.3%
50 - 250 mm	4.5%	4.3%	7.7%	8.6%	8.1%	7.1%

5.3.2 Permeability

The air permeability coefficient is measured before heating at 20°C and after heating to 200°C for the four-month group specimens, as shown in Table 5.

Table 5 Air permeability coefficient of concrete

Air permeability coefficient (m^2)				
Sample name	PC-4m	R2-4m	R1-4m	PP1-4m
Before heating	8.26E-17	6.34E-17	6.76E-17	6.80E-17
After heating	2.45E-16	1.66E-16	2.01E-16	5.98E-16

At ambient temperature, plain concrete specimens exhibit slightly higher permeability than those with added fibres. This could be attributed to the shrinkage cracking control provided by both PP fibres [43] and RPTM fibres [44]. After heating at 200 °C, the melting of PP fibres increases the permeability of sample PP1 to the highest level among all samples. The plain concrete specimen has the second highest permeability, whereas specimens R1-4m and R2-4m exhibit the lowest permeability as the RPTM dosage increases. This suggests that the higher melting temperature of RPTM may still contribute to concrete bonding at 200 °C, resulting in fewer microcracks and lower permeability compared to plain concrete. Therefore, it is plausible that RPTM may function differently in controlling concrete spalling compared to virgin PP fibres. In heated concrete, RPTM could mitigate thermo-mechanical damage to reduce the risk of spalling, while PP fibres could increase concrete permeability, thereby reducing thermo-hydraulic pore pressure and mitigating fire spalling.

5.3.3 SEM of PP fibre and RPTM

The detailed microstructure and the effects of RPTM and virgin PP fibres on concrete can be observed in the SEM images obtained from the four-month group specimens, as shown in Figure 9.

Since all the specimens were fractured by bending to obtain the cracking surface with fibres, there are initial cracks formed due to the fracturing process in RPTM specimens, as shown in Figure 9(a). Upon closer examination of the area surrounding a single strand of RPTM, an example is shown in Figure 9(b), no cracks are formed near the fibre, indicating the bonding effect of RPTM at ambient temperature. After heating to 200 °C, the RPTM in concrete does not melt but undergoes some deformation due to heat, as shown in Figure 9(c). Microcracks resulting from the differential thermal expansion coefficient between the cement matrix and RPTM are observed around the interface of RPTM and cement, as shown in Figure 9(d).

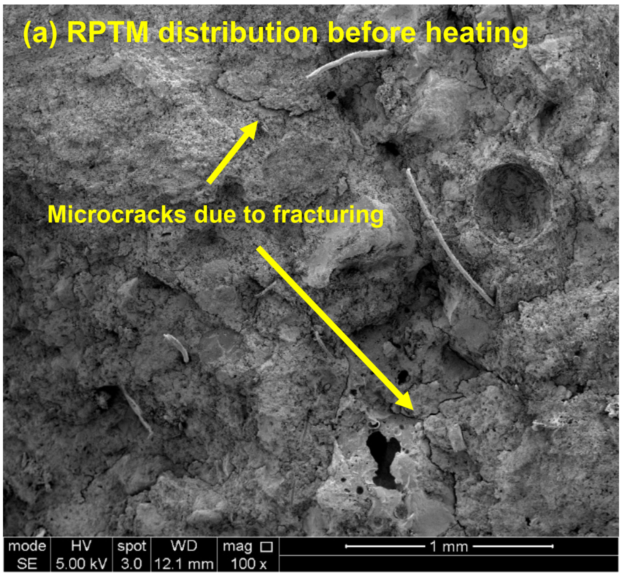

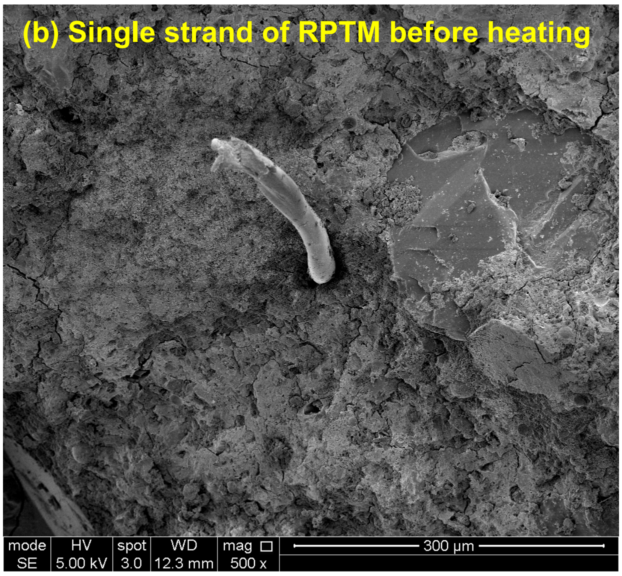

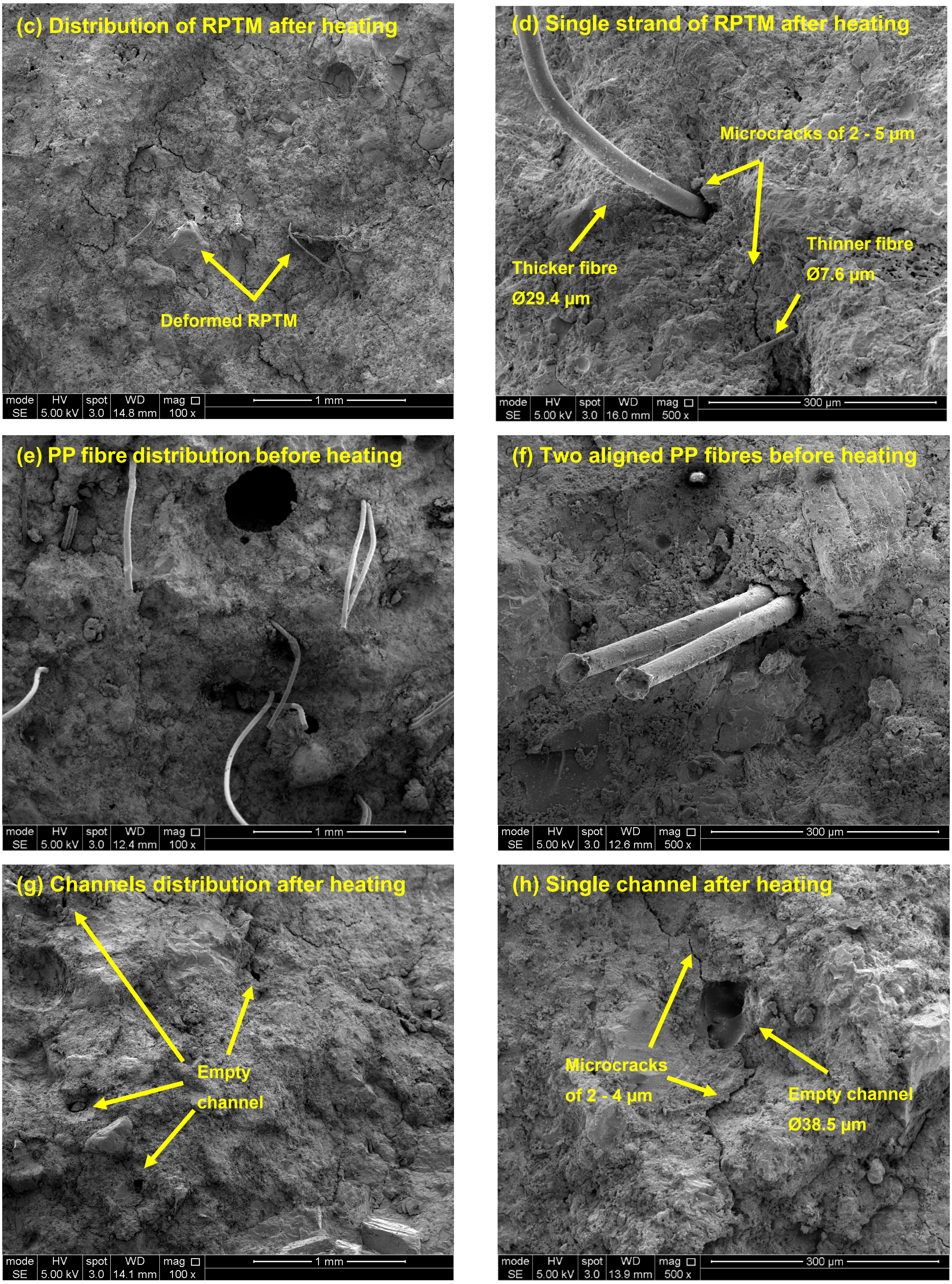

Figure 7 SEM image of RPTM and PP fibre concrete specimens before and after heating

The ambient temperature fibre distribution in concrete for RTPM and PP fibres was examined within the area of interest (3 × 3 mm^2) in SEM, as shown in Figure 9(a) and Figure 9(e). Despite RPTM are tangled before adding to the concrete, both PP fibres and RPTM demonstrated relatively even distribution within the concrete, thus confirming the suitability of the manual dispersion method adopted in the four-month group. Unlike RPTM, which appeared as single strands, the monofilament PP fibres could be observed in strands of two or more fibres within the concrete, as shown in Figure 9(f). After heating, all the PP fibres disappeared from the SEM image, leaving empty channels in the cement matrix, as shown in Figure 9(g). Similarly to RPTM, the differential thermal expansion between the cement and PP could induce microcracks, which were observed surrounding the empty channels left by the melted PP fibres, as shown in Figure 9(h).

Based on the permeability measurements of concrete with different fibres in Section 5.3.2, although microcracks were found in both types of fibres, the higher permeability of the PP1 specimen compared to R1 could be attributed to (1) empty channels left by melted fibres and (2) percolation between the microcracks and empty channels.

5.3.4 Temperature

To measure the temperature distribution on the fire exposure surface of the specimens at the location of the pressure probes, thermocouples were embedded at 1 mm from the heating surface of specimen PC-4m-3, as shown in Figure 10(a).

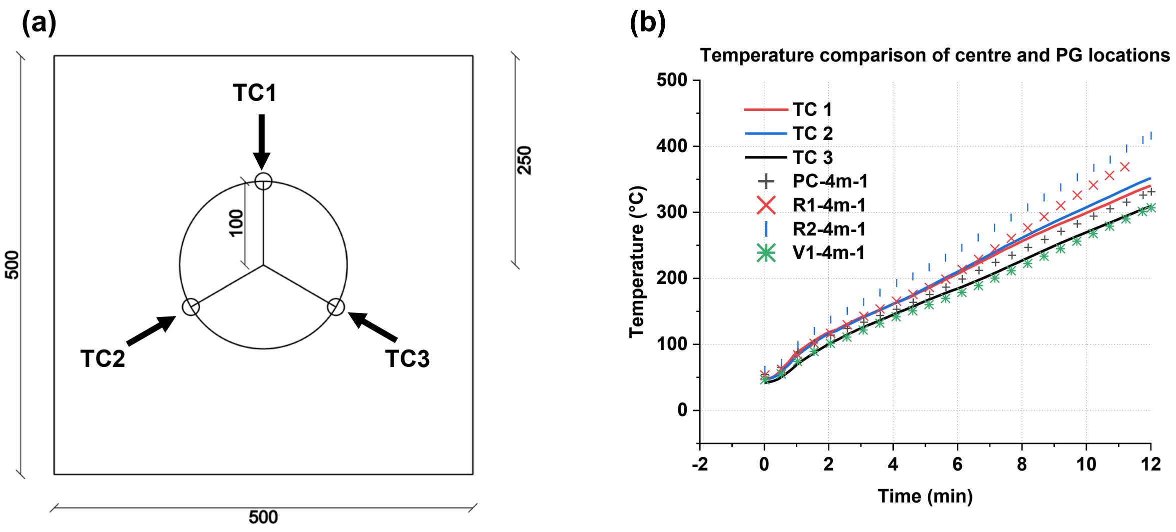

Figure 10 (a) Thermocouples at the location of pressure probes for specimen PC-4m-3 (b) Temperature distribution at 1mm depth in pressure gauge locations of specimen PC-4m-3 and in centre locations of other specimens

The comparison of temperatures between the pressure probe locations and the central location of other specimens is shown in Figure 10(b). The time range is shortened from 30 minutes to 12 minutes because explosive spalling occurred hence influencing the temperature data after. To simulate the beginning of the standard fire curve, a pre-heat process (one minute) was performed, leading to higher initial temperature than room temperature. The results show a fairly constant range for the temperature distribution on the heat exposure surface across different locations and different specimens. The temperature variations between curves could be due to the change in thermocouple depths during the concrete pouring and vibration process.

The temperature profiles of all the test samples are shown in Figure 11, in which “PG” stands for thermocouple readings near the probes of pressure gauges and “TC” stands for readings from the thermocouple trees inserted in the centre of the specimen.

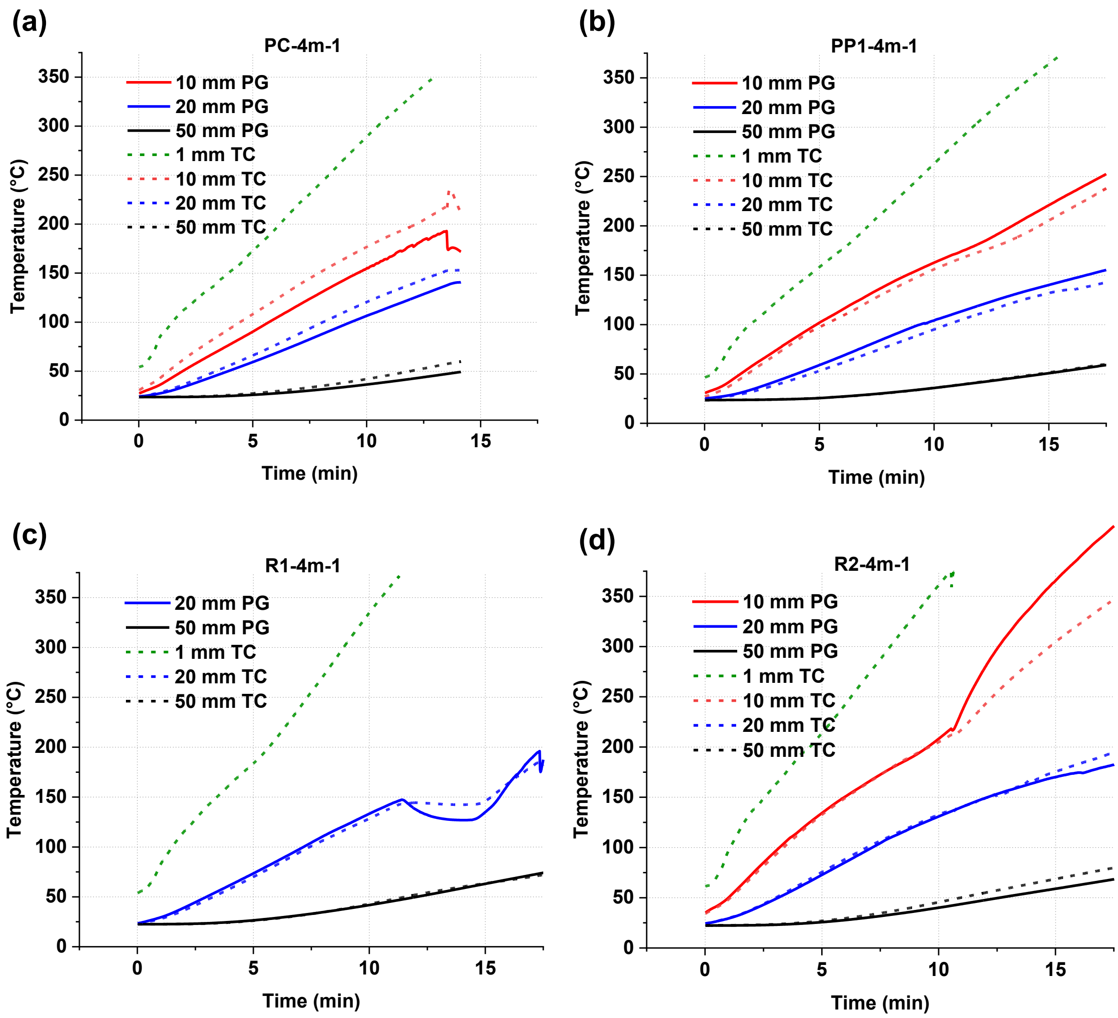

Figure 11 Temperature distribution of concrete (a) PC-4m-1 and (b) PP1-4m-1 (c) R1-4m-1 and (d) R2-4m-1 in fire spalling test

Figure 11 reveals difference between PG temperature curves and TC temperature curves in plain concrete specimen PC-4m-1. Smaller difference were found in Specimen PP1-4m-1, and there was nearly no disparity in specimens R1-4m-1 and R2-4m-1. This temperature variation between thermocouple readings and pressure gauge measurements could indirectly indicate alterations in the inherent porous structure of the concrete due to the presence of pressure gauges. The presence of microcracks and air voids near the pressure gauge can accelerate the drying rate of the concrete, thereby altering the surrounding thermal properties and causing fluctuations in temperature. Depending on the magnitude of the disparity, it can be inferred that the impact of pressure gauges is most pronounced in plain concrete and least pronounced in RPTM concrete. This could be attributed to the crack-bridging effect of RPTM, which hinder the formation of cracks near the pressure gauge heads and hence reducing the influence on temperature.

5.3.5 Fire spalling test result

During the fire spalling test, the damage caused by the explosive spalling of concrete could also be a rough indication of the fire spalling intensity. At high moisture content in the four-month group, the damages induced by the explosive concrete pieces from plain concrete specimens were the most severe ones. The protective steel mesh and the heat-resistant stiffeners were severely bent and damaged by the spalling of plain concrete, as shown in Figure 12. On the contrary, the spalling of the RPTM concrete, induced nearly no damage to the protective mesh. This observation could be an indication that, although RPTM cannot prevent spalling, they could somewhat control the severity of explosive fire spalling.

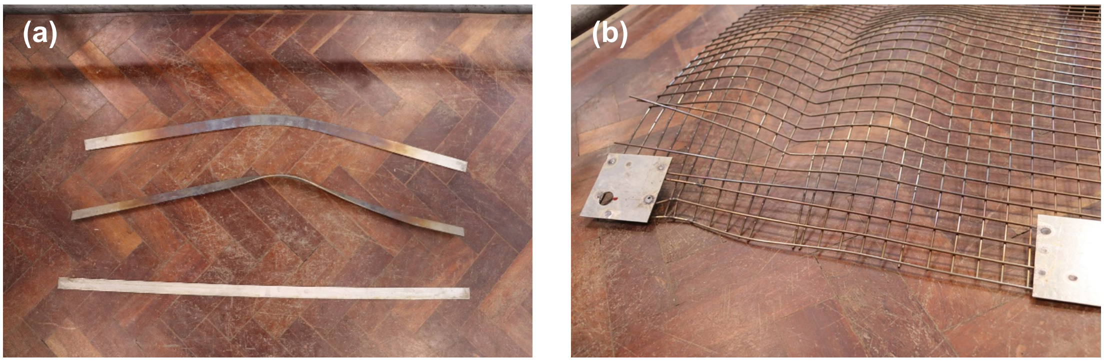

Figure 12 Fire spalling damaged (a) stiffeners and (b) protective mesh in plain concrete specimen tests

After the fire spalling test, the images of the heat exposure surfaces of 12 specimens are shown in Figure 13. In the six-year group, explosive fire spalling was observed in plain concrete specimens PC-6y-1 and PC-6y-2, whereas the RPTM-added specimens R2-6y-1 and R2-6y-2 did not experience spalling. This demonstrate the effectiveness of RPTM in controlling fire spalling in aged concrete, or in concrete with lower moisture content. For the four-month group, explosive fire spalling occurred in all specimens except PP1-4m-1 and PP1-4m-2. RPTM dosages of 1 kg/m³ and 2 kg/m³ specimens have explosive spalling, indicating that virgin PP fibres could be more effective in fire spalling mitigation than RPTM in concrete with high moisture content. The average surface moisture content of R2-6y-1 and R2-6y-2 is 3.1%, and the average surface moisture content of R2-4m-1 is 4.6%, indicating that the surface moisture content range of 3.1% - 4.6% could be one of the decisive factors for the propensity of fire spalling in RPTM concrete.

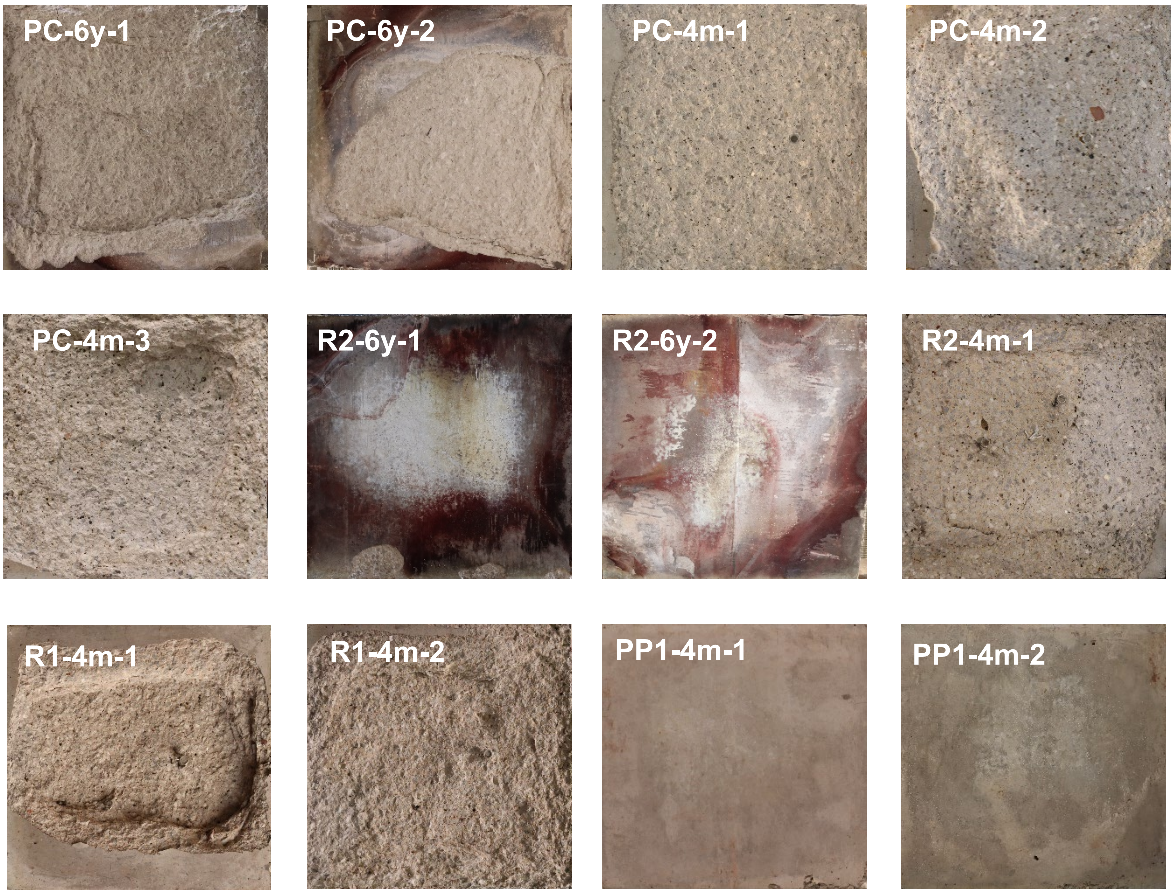

Figure 13 Heated surface of concrete specimens after the fire spalling test

To quantify the severity of fire spalling, a laser scanner was used to obtain the 3-D point cloud for the surface of the spalled specimen, as shown in Figure 14. A colour map is applied to the surface data, with the scale of the colour bar shown on the right of the figures.

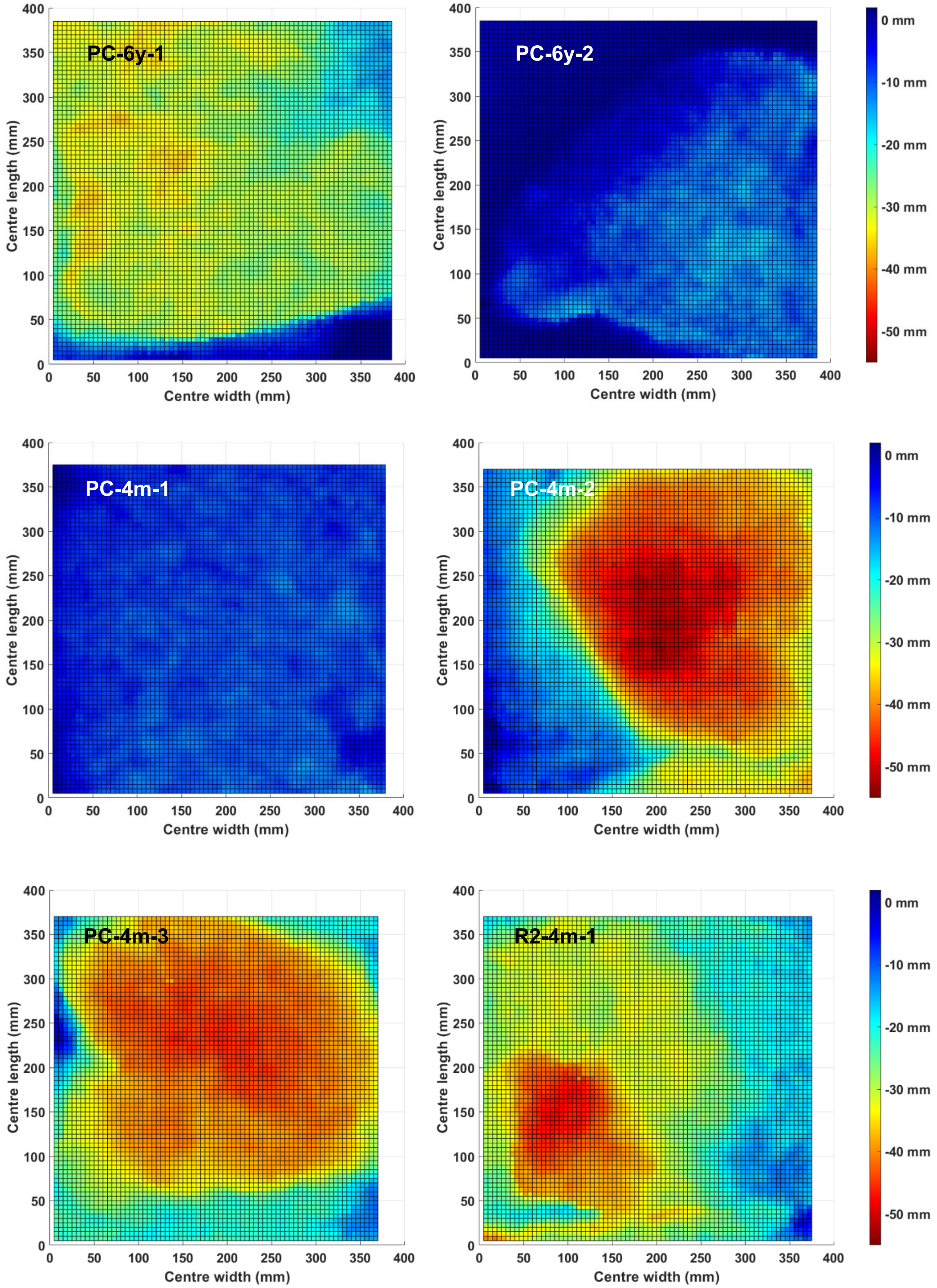

PC-6y-1
PC-6y-2
PC-4m-1
PC-4m-2
PC-4m-3
R2-4m-1
Centre length (mm)
Centre width (mm)
0 mm
-10 mm
-20 mm
-30 mm
-40 mm
-50 mm

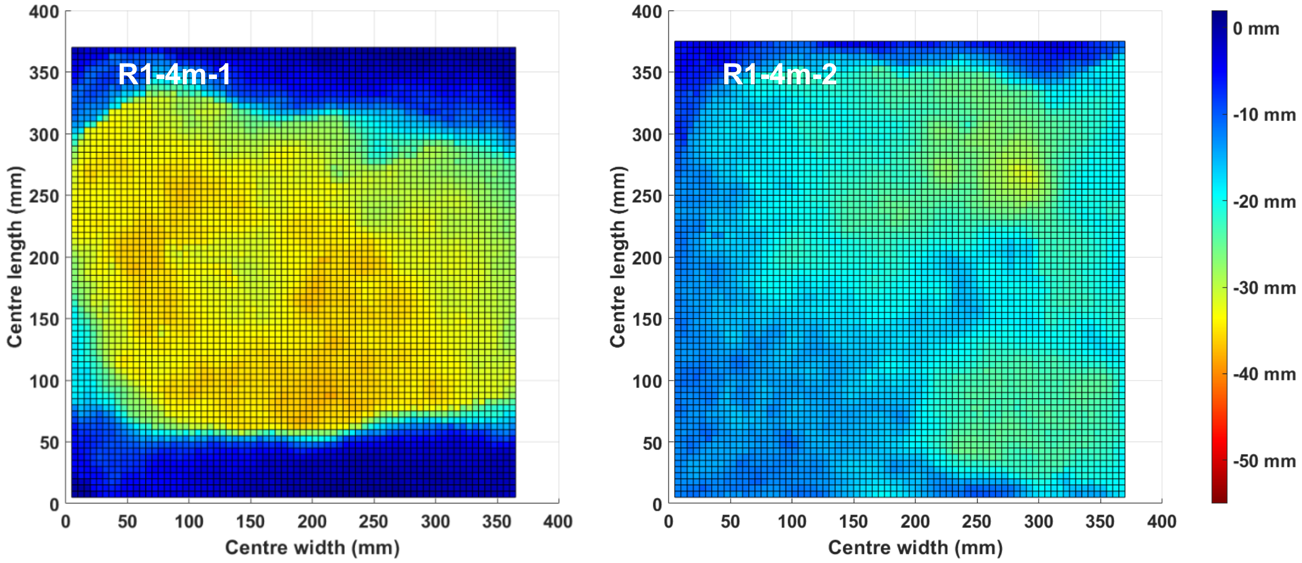

Figure 14 Spalling surface profile of the effective heating area of spalled specimens

The data analysis of the spalling profile was conducted on the effective heating area of the specimen, which is 400 mm × 400 mm in this test. For partially spalled concrete, the analysis area was adopted to be 10% less than the heating area in this test. The maximum spalling depth, average spalling depth, and mass of spalling were calculated according to the analysis area, which is summarised in the total spalling information, shown in Table 6 at last.

5.3.6 Pore pressure

The pore pressure was measured simultaneously with the temperature measurement. Figure 15 illustrates the result for all test specimens that embedded with pressure gauges.

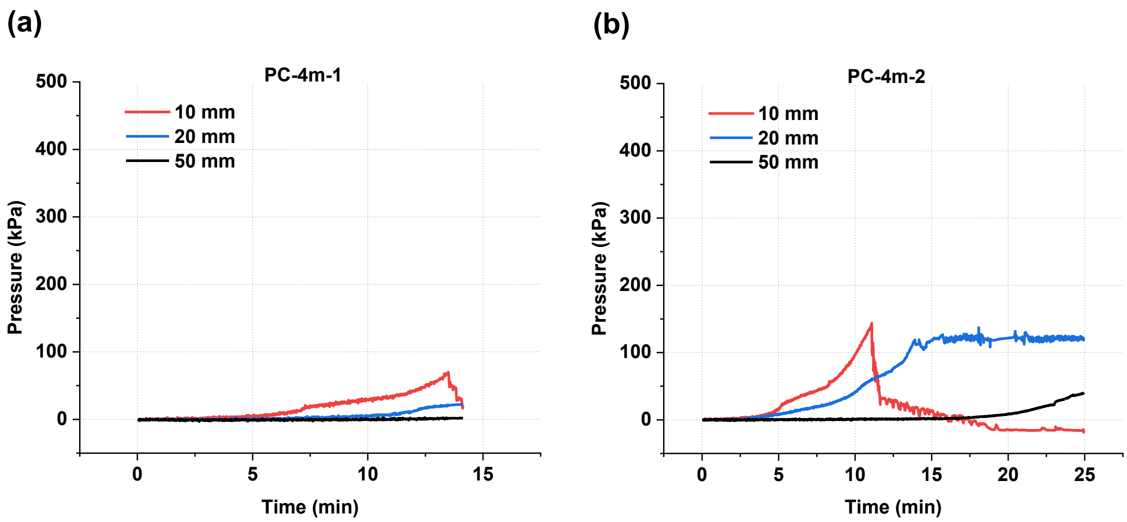

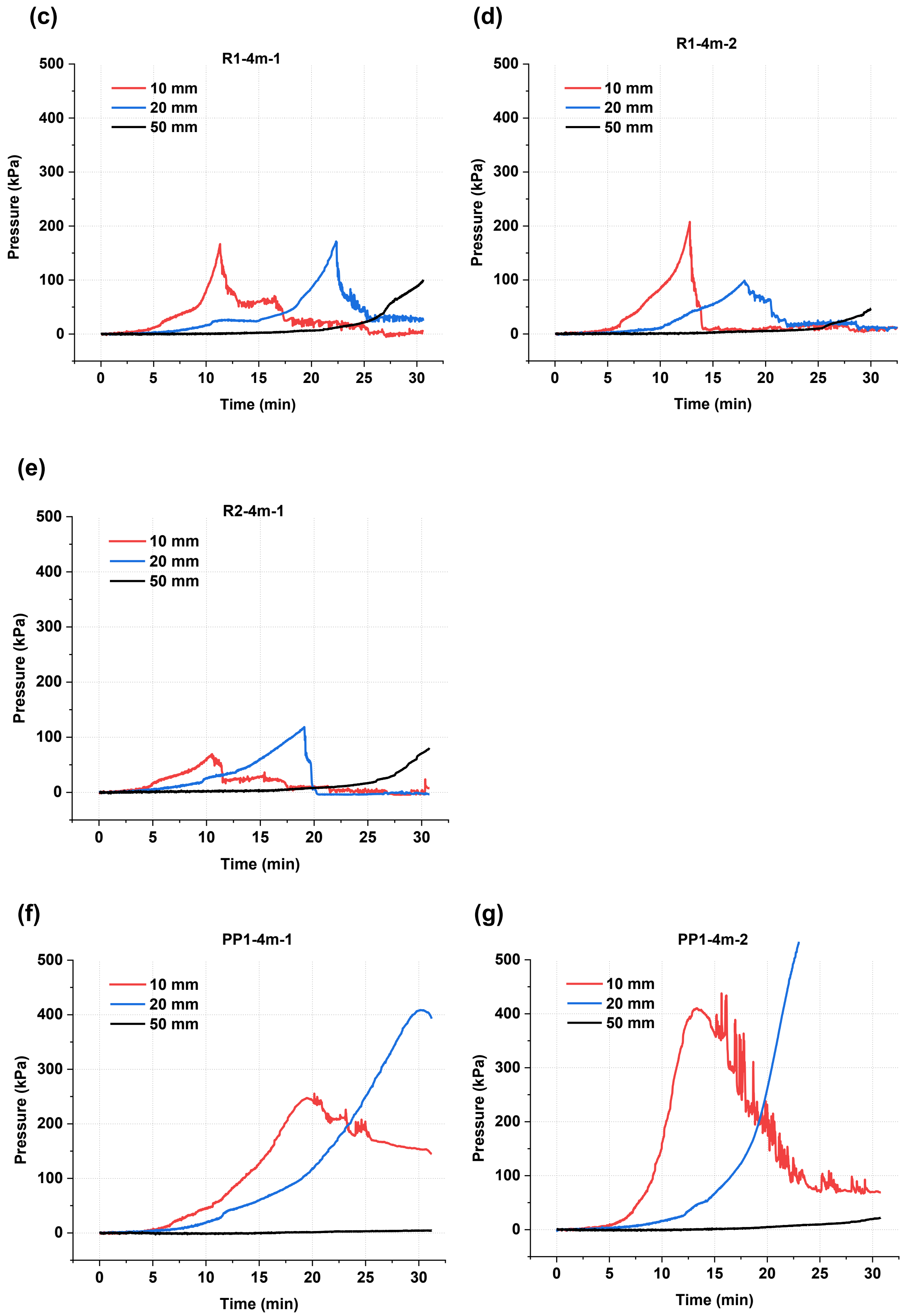

Figure 15 Pore pressure distribution of heated concrete specimens

The pore pressure data in the same concrete mix specimens do not have good repeatability, which is probably due to multiple influencing factors such as concrete heterogeneity, localized cracking, pressure gauge intrusion and the explosive spalling of concrete. Nevertheless, there are some findings in the results that could give insights on the fire spalling behaviour of the specimens:

- Among all specimens, there is no pore pressure building up before 5 minutes, as the concrete temperature is not high enough to vaporise moisture that time.
- The data for specimen PC-4m-1 only lasted 13 minutes because the spalling of that specimen was too strong, the exploded concrete pieces cracked the heating elements and stopped the test.
- The peak pore pressure of spalled plain concrete specimen is at 0.14 MPa on PC-4m-2, which is lower than that of R1-4m-1 (0.17 MPa) and R1-4m-2 (0.21 MPa), but higher than that of R2-4m-1 (0.12 MPa). To explain why different dosages of RPTM can induced opposite effect on pore pressure development in heated concrete, a speculated scenario is proposed. There might be a critical dosage of RPTM that the thermal microcracking of RPTM (due to differential thermal expansion) and the crack control behaviour of RPTM (due to cement bonding) are balancing in heated concrete. Below this critical dosage, the crack control ability of RPTM is dominant since the thermal-induced microcracks are not connected due to the limited number of fibres. Hence, the vapour pressure is higher in the specimen as less vapour can transport through the cracks. For RPTM above this critical dosage, the large number of microcracks can result in a connected network for vapour transport, leading to a decrease of peak vapour pressure.
- Virgin PP fibre specimens exhibited the highest level of pore pressure among all specimens. This is mainly attributed by the release of pore vapour pressure in the spalling events of other specimens. In the study conducted by Jansson and Boström [10], the vapour pressure was also observed to be higher in PP concrete compared to the plain concrete that spalled.

The relationship of pore pressure and temperature, as well as the saturation vapour pressure (SVP), is investigated for PP fibre concrete. The data of specimen PP1-4m-2 is illustrated in Figure 16 as an example. For the melting temperature of PP at 160 – 170 °C, there is an obvious drop of the pore pressure in 10 mm of the concrete. Simultaneously, the pore pressure at 20 mm increases dramatically. This phenomenon can be an indication of the movement of the moisture clog, where the pore pressure peaks in front of it. The saturation vapour pressure is the maximum pore pressure that can be achieved at the corresponding temperature. If the pore pressure level is higher than that, the excessive vapour is going to condense into liquid, which did not happen in all specimens.

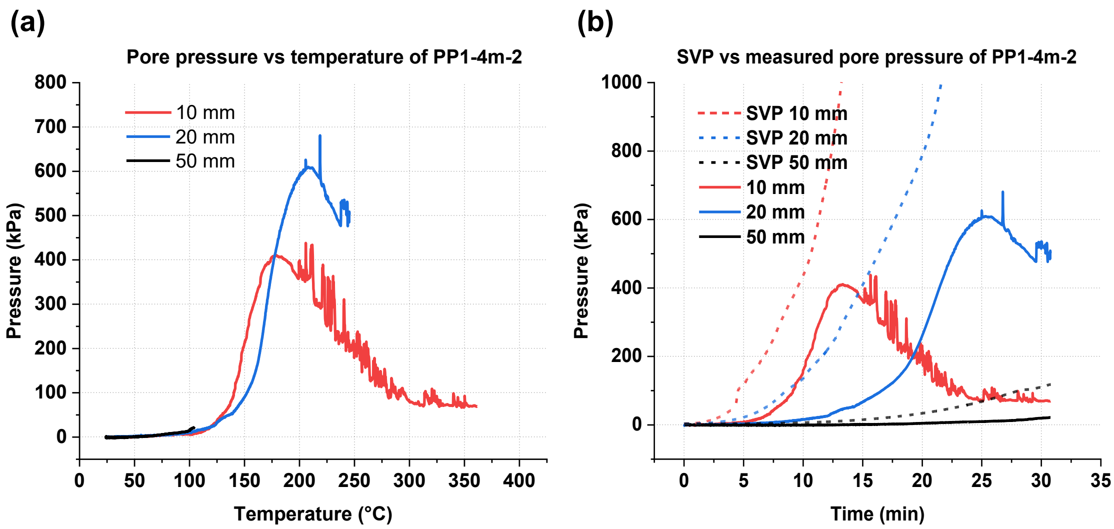

Figure 16 (a) Pore pressure distribution against temperature of PP1-4m-2 (b) Saturation vapor pressure compared with the pore pressure of PP1-4m-2

Among all test specimens, the highest pore pressure measurement is in PP1-4m-2, at 0.6 MPa, which is much less than the tensile strength of concrete. The pore pressure of the spalled concrete is even lower, in which the highest pore pressure is in R1-4m-2, at only 0.2 MPa. These measurements again confirm the conclusion drawn by Felicetti et al. [45], who indicate that the occurrence of fire spalling is not solely caused by pore pressure, it also requires the thermos-mechanical mechanisms. To summary, the peak pore pressure data, as well as the fire spalling data obtained from previous sections, are presented in Table 6.

Table 6 Summarize of the fire spalling result

Sample name	Surface moisture content (%)	Deep Moisture content (%)	Peak pore pressure (kPa)	First spalling time (min)	Number of Spalling	Spalling Weight loss (kg)	Maximum spalling depth (mm)	Average spalling depth (mm)
PC-6y-1	3.7	4.5	--	08:40	5	9.46	37.1	26.6
PC-6y-2			--	06:40	2	2.25	16.9	6.3
R2-6y-1	3.1	4.4	--	--	--	--	--	--
R2-6y-2			--	--	--	--	--	--
PC-4m-1	5.6	7.7	70	13:30	1	3.02	14.9	8.8
PC-4m-2			140	11:10	50	10.6	53	31.9
PC-4m-3			--	14:10	72	11.15	46.5	33.9
R1-4m-1	4.6	8.1	170	11:20	12	7.6	38.2	23.4
R1-4m-2			210	13:00	6	6.1	31.7	18.3
R2-4m-1	4.6	8.6	120	10:30	12	9.27	48	27.8
PP1-4m-1	5.4	7.1	410	--	--	--	--	--
PP1-4m-2			610	--	--	--	--	--

In Table 6, except for the emergency stop caused by PC-4m-1, the spalling data for PC-4m-2 and PC-4m-3 are also underestimated. During the test, as the spalled volume was too much, a layer of concrete covered the heating elements and caused localized heating. To prevent the overheating of the heating elements, the spalling test was manually terminated at 25 minutes. Based on the spalling frequency near the end of the test, the actual spalling depth and spalled volume should be about 30% more than the measured data. Due to the lack of full-time test data, there is insufficient evidence to conclude the influence of the load ratio on spalling severity for this study. In addition, the spalling severity of plain concrete is undoubtedly the highest among all samples if the full time test is conducted. The RPTM dosage of 2 kg/m³ is only capable of mitigating spalling in the six-year group with lower moisture content. For the four-month concrete, RPTM can only control the severity of spalling but cannot completely suppress it. The increased RPTM dosage does not show a clear contribution to the spalling mitigation ability. The PP fibre hence emerges as the most effective fire type for spalling mitigation in this study.

5.4 CONCLUSION

To conclude, this study aims to investigate the spalling behaviour of concrete with the inclusion of PP fibres and RPTM, specifically examining their effectiveness in high moisture ratio concrete. The pore pressure and temperature of concrete specimens were monitored during the spalling test, and the underlying mechanisms of both fibres were investigated. Based on the specified test conditions, test results reveal the following key findings:

- Inclusion of 1 kg/m^3 Virgin PP fibres in concrete is an effective method for mitigating fire spalling. The increases in the permeability of the PP fibre concrete at high temperatures could be the main reason for its influence in fire spalling control.

- The inclusion of RPTM is relatively less effective in mitigating fire spalling compared to PP fibres but still offers some benefits. RPTM may primarily act to control the microcracks in the concrete at 200 °C.

- The manual integration process of RPTM in concrete casting could result in a fairly uniform fibre distribution condition in the tested specimen.

- The level of pore pressure in heated concrete may not be directly linked to the propensity of fire spalling, as the measured pore pressure in spalled specimens could be lower than that of unspalled concrete.

- The non-melting of RPTM and the internal connectivity of the microcracks due to RPTM expansion at high temperatures could be key factors in explaining the differential performance of RPTM and PP fibres in fire spalling.

Further research is recommended to quantify the optimal fibre dosages of RPTM in concrete for enhanced fire spalling resistance. Investigating the underlying mechanisms responsible for the differing performances of RPTM and PP fibres in fire spalling mitigation can be carried out, especially through microstructural analysis.

AUTHOR CONTRIBUTIONS

Yifan Li: Conceptualization, Methodology, Validation, Formal analysis, Investigation, Resources, Writing - Original Draft, Project administration. **Kypros Pilakoutas:** Methodology, Writing - Review & Editing, Supervision. **Shan-Shan Huang:** Conceptualization, Methodology, Resources, Writing - Review & Editing, Supervision, Project administration, Funding acquisition.

REFERENCES

[1] RAIB, *Technical Investigation Report concerning the Fire on Eurotunnel Freight Shuttle 7412 on 11 September 2008*. Rail Accident Investigation Branch, Department for Transport., 2010. [Online]. Available: http://www.raib.gov.uk

[2] RAIB, *Rail Accident Report: Fire on HGV shuttle in the Channel Tunnel 21 August 2006*. Rail Accident Investigation Branch, Department for Transport., 2007. [Online]. Available: www.raib.gov.uk.

[3] A. Leitner, "The fire catastrophe in the Tauern Tunnel: experience and conclusions for the Austrian guidelines," *Tunnelling and Underground Space Technology*, vol. 16, p. 217223, 2001.

[4] R. Jansson and K. Ödeen, "Fire in Storehouse 6 in the Free Port of Stockholm," in *2nd International RILEM Workshop on Concrete Spalling due to Fire Exposure*, Delft, 2011, pp. 205–210. [Online]. Available: https://www.researchgate.net/publication/281107891

[5] P. Kalifa, G. Chéné, and C. Gallé, "High-temperature behaviour of HPC with polypropylene fibres From spalling to microstructure," *Cem Concr Res*, pp. 1487–1499, 2001.

[6] A. Bilodeau, V. K. R. Kodur, and G. C. Hoff, "Optimization of the type and amount of polypropylene fibres for preventing the spalling of lightweight concrete subjected to hydrocarbon fire," *Cem Concr Compos*, vol. 26, no. 2, pp. 163–174, Feb. 2004, doi: 10.1016/S0958-9465(03)00085-4.

[7] N. Yermak, P. Pliya, A. L. Beaucour, A. Simon, and A. Noumowé, "Influence of steel and/or polypropylene fibres on the behaviour of concrete at high temperature: Spalling, transfer and mechanical properties," *Constr Build Mater*, vol. 132, pp. 240–250, Feb. 2017, doi: 10.1016/j.conbuildmat.2016.11.120.

[8] M. Ozawa, T. Tanibe, R. Kamata, Y. Uchida, K. Rokugo, and S. S. Parajuli, "Behavior of ring-restrained high-performance concrete under extreme heating and development of screening test," *Constr Build Mater*, vol. 162, pp. 215–228, Feb. 2018, doi: 10.1016/j.conbuildmat.2017.11.144.

[9] H. Dang, A. Liang, R. Feng, J. Zhang, X. Yu, and Y. Shao, "Experimental study on mechanical properties and low-cycle fatigue behaviour of stainless steels subjected to salt spray and dry/wet cycle," *Int J Fatigue*, vol. 165, Dec. 2022, doi: 10.1016/j.ijfatigue.2022.107187.

[10] R. Jansson and L. Boström, "The influence of pressure in the pore system on fire spalling of concrete," *Fire Technol*, vol. 46, no. 1, pp. 217–230, 2010, doi: 10.1007/s10694-009-0093-9.

[11] M. R. Bangi and T. Horiguchi, "Effect of fibre type and geometry on maximum pore pressures in fibre-reinforced high strength concrete at elevated temperatures," *Cem Concr Res*, vol. 42, no. 2, pp. 459–466, Feb. 2012, doi: 10.1016/j.cemconres.2011.11.014.

[12] J. D. Ríos, J. Mínguez, A. Martínez-De La Concha, M. Á. Vicente, and H. Cifuentes, "Microstructural analyses of the addition of PP fibres on the fracture properties of high-strength self-compacting concrete by X-ray computed tomography," *Constr Build Mater*, vol. 261, Nov. 2020, doi: 10.1016/j.conbuildmat.2020.120499.

[13] M. Ozawa and H. Morimoto, "Effects of various fibres on high-temperature spalling in high-performance concrete," *Constr Build Mater*, vol. 71, pp. 83–92, Nov. 2014, doi: 10.1016/j.conbuildmat.2014.07.068.

[14] Y. Li, Y. Zhang, E. H. Yang, and K. H. Tan, "Effects of geometry and fraction of polypropylene fibers on permeability of ultra-high performance concrete after heat exposure," *Cem Concr Res*, vol. 116, pp. 168–178, Feb. 2019, doi: 10.1016/j.cemconres.2018.11.009.

[15] Y. Li, K. H. Tan, and E. H. Yang, "Influence of aggregate size and inclusion of polypropylene and steel fibers on the hot permeability of ultra-high performance concrete (UHPC) at elevated temperature," *Constr Build Mater*, vol. 169, pp. 629–637, Apr. 2018, doi: 10.1016/j.conbuildmat.2018.01.105.

[16] D. Zhang, A. Dasari, and K. H. Tan, "On the mechanism of prevention of explosive spalling in ultra-high performance concrete with polymer fibers," *Cem Concr Res*, vol. 113, pp. 169–177, Nov. 2018, doi: 10.1016/j.cemconres.2018.08.012.

[17] R. Jansson and L. Boström, "Factors influencing fire spalling of self compacting concrete," *Materials and Structures/Materiaux et Constructions*, vol. 46, no. 10, pp. 1683–1694, Oct. 2013, doi: 10.1617/s11527-012-0007-z.

[18] C. H. M. Zedán, "Development and Application of a Novel Test Method for Studying the Fire Behaviour of CFRP Prestressed Concrete Structural Elements," 2014.

[19] K. D. Hertz, "Limits of spalling of fire-exposed concrete," *Fire Saf J*, vol. 38, no. 2, pp. 103–116, Mar. 2003, doi: 10.1016/S0379-7112(02)00051-6.

[20] W. H. Johnson and W. H. Parsons, "Thermal Expansion of Concrete Aggregate Materials," *Part of Journal of Research of the National Bureau of Standards*, vol. 32, Mar. 1944.

[21] P. Kalifa, Ë.-D. Menneteau, and D. Quenard, "Spalling and pore pressure in HPC at high temperatures," *Cem Concr Res*, pp. 1915–1927, 2000.

[22] G. Choe, G. Kim, M. Yoon, E. Hwang, J. Nam, and N. Guncunski, "Effect of moisture migration and water vapor pressure build-up with the heating rate on concrete spalling type," *Cem Concr Res*, vol. 116, pp. 1–10, Feb. 2019, doi: 10.1016/j.cemconres.2018.10.021.

[23] V. K. R. Kodur, "Spalling in High Strength Concrete Exposed to Fire: Concerns, Causes, Critical Parameters and Cures," *Advanced Technology in Structural Engineering*, pp. 1–9, 2000, doi: https://doi.org/10.1061/40492(2000)180.

[24] Y. Li, P. Du, and K. H. Tan, "Fire resistance of ultra-high performance concrete columns subjected to axial and eccentric loading," *Eng Struct*, vol. 248, Dec. 2021, doi: 10.1016/j.engstruct.2021.113158.

[25] J. Yang, G. F. Peng, J. Zhao, and G. S. Shui, “On the explosive spalling behavior of ultra-high performance concrete with and without coarse aggregate exposed to high temperature,” *Constr Build Mater*, vol. 226, pp. 932–944, Nov. 2019, doi: 10.1016/j.conbuildmat.2019.07.299.

[26] Y. Li, E. H. Yang, A. Zhou, and T. Liu, “Pore pressure build-up and explosive spalling in concrete at elevated temperature: A review,” *Constr Build Mater*, vol. 284, May 2021, doi: 10.1016/j.conbuildmat.2021.122818.

[27] J. S. Guo and P. Waldron{, “An elastic model to quantify the effect of moisture on the mechanical properties of concrete at the time of test,” *Magazine of Concrete Research*, vol. 53, no. 3, pp. 151–162, Jun. 2001.

[28] British Standards Institution, “BS EN 1992-1-2:2023, Eurocode 2: Design of concrete structures : Part 1-2: Structural fire design,” London, 2023.

[29] S. Gigli, D. Landi, and M. Germani, “Cost-benefit analysis of a circular economy project: a study on a recycling system for end-of-life tyres,” *J Clean Prod*, vol. 229, pp. 680–694, Aug. 2019, doi: 10.1016/j.jclepro.2019.03.223.

[30] Zero Waste Works, “Recycled Polymer Tyre Microfibres.” Accessed: Apr. 20, 2024. [Online]. Available: https://www.zerowasteworks.co.uk/recycled-polymer-tyre-microfibres

[31] Fazilet Cinaralp and Jean-Pierre Taverne, “End of life tyres: A valuable resource with growing potential,” ETRMA. Accessed: Feb. 08, 2023. [Online]. Available: https://www.etrma.org/wp-content/uploads/2019/09/2010_etrma_elt_management_brochure_final.pdf

[32] Anne and E. Russ, “The Composition of a Tyre: Typical Components Creating markets for recycled resources,” May 2006. Accessed: Apr. 06, 2024. [Online]. Available: https://docplayer.net/20736072-The-composition-of-a-tyre-typical-components.html

[33] M. Serdar, A. Baričević, S. Lakušić, and D. Bjegović, “Special purpose concrete products from waste tyre recyclates,” *Journal of the Croatian Association of Civil Engineers*, vol. 65, no. Građevinar, pp. 793–801, 2013.

[34] F. P. Figueiredo, S. S. Huang, H. Angelakopoulos, K. Pilakoutas, and I. Burgess, “Effects of Recycled Steel and Polymer Fibres on Explosive Fire Spalling of Concrete,” *Fire Technol*, vol. 55, no. 5, pp. 1495–1516, Sep. 2019, doi: 10.1007/s10694-019-00817-9.

[35] Y. Li, S.-S. Huang, K. Pilakoutas, H. Angelakopoulos, and I. Burgess, “Mitigation of Fire-Induced Spalling of Concrete using Recycled Tyre Polymer Fibre,” in *6th International Workshop on Concrete Spalling due to Fire Exposure*, Sheffield, Sep. 2019, pp. 42–51.

[36] M. Chen, Z. Sun, W. Tu, X. Yan, and M. Zhang, “Behaviour of recycled tyre polymer fibre reinforced concrete at elevated temperatures,” *Cem Concr Compos*, vol. 124, Nov. 2021, doi: 10.1016/j.cemconcomp.2021.104257.

[37] British Standards Institution., “BS EN 1992-1-2:2004, Eurocode 2: Design of concrete structures : Part 1-2: General rules — Structural fire design,” BSi, London, 2010.

[38] A. Baricevic, M. Pezer, M. Jelcic Rukavina, M. Serdar, and N. Stirmer, “Effect of polymer fibers recycled from waste tires on properties of wet-sprayed concrete,” *Constr Build Mater*, vol. 176, pp. 135–144, Jul. 2018, doi: 10.1016/j.conbuildmat.2018.04.229.

[39] M. Jelcic Rukavina, A. Baricevic, M. Serdar, and M. Grubor, “Study on the post-fire properties of concrete with recycled tyre polymer fibres,” *Cem Concr Compos*, vol. 123, Oct. 2021, doi: 10.1016/j.cemconcomp.2021.104184.

[40] BSI, “BS EN 1991-1-2:2002, Eurocode 1 : actions on structures. Part 1-2: General actions : actions on structures exposed to fire.,” BSI, Mar. 2009.

[41] I. Jack and C. Rickard, “Explosive Spalling of Concrete in Fire: Novel Experiments under Controlled Thermal and Mechanical Conditions,” 2020.

[42] RILEM Technical Committees, “RILEM TC 116-PCD Permeability of Concrete as a Criterion of its Durability,” *Material and Structures*, vol. 32, pp. 174–179, 1999.

[43] K. M. Arslan and M. E. Karagüler, “Shrinkage cracking and mechanical properties of cementitious composites produced with multiwall carbon nano tubes and different types of polypropylene fibres,” *Constr Build Mater*, vol. 420, Mar. 2024, doi: 10.1016/j.conbuildmat.2024.135599.

[44] M. Serdar, A. Baričević, M. Jelčić Rukavina, M. Pezer, D. Bjegović, and N. Štirmer, “Shrinkage Behaviour of Fibre Reinforced Concrete with Recycled Tyre Polymer Fibres,” *Int J Polym Sci*, vol. 2015, 2015, doi: 10.1155/2015/145918.

[45] R. Felicetti, F. Lo Monte, and P. Pimienta, “A new test method to study the influence of pore pressure on fracture behaviour of concrete during heating,” *Cem Concr Res*, vol. 94, pp. 13–23, Apr. 2017, doi: 10.1016/j.cemconres.2017.01.002.

6 Paper IV

Fire Spalling Mechanisms and effect of Recycled Polymer Tyre Microfibres in Concrete at Elevated Temperatures through Neutron and X-Ray Tomographies

Yifan Li[1*], Stefano Dal Pont[2], Alessandro Tengattini[2], Kypros Pilakoutas[1], Shan-Shan Huang[1]
[1] University of Sheffield, Sheffield, United Kingdom
[2] Université Grenoble Alpes, Grenoble, France
* Corresponding author (yli101@sheffield.ac.uk, Department of Civil and Structural Engineering, University of Sheffield, Sheffield, UK, S1 4BT)

ABSTRACT

Fire-induced spalling of concrete could lead to severe structural damages and significant economic and life losses. An eco-friendly substitute for polypropylene fibres (used to control fire spalling), named Recycled Polymer Tyre Microfibres (RPTM) have been created at the University of Sheffield and found to be effective in mitigating fire spalling. However, the mechanisms of fire spalling and the role of RPTM in controlling spalling lack general agreement and experimental validation.

For the first time, combined neutron and X-ray tomographies are performed on concrete with RPTM at elevated temperatures. This in-situ, non-intrusive imaging technique reveals the evolution of 3D moisture profile and porous structure within heated concrete. The inclusion of RPTM is found to increase the concrete porosity and accelerate the moisture migration, which explains its effectiveness in fire spalling control. The tests confirm the presence of moisture clog and reveal a significant influence of thermocouples on the moisture drying process.

KEYWORD: Fire Spalling, Moisture Clog, Neutron Tomography, X-Ray Tomography, Recycled Polymer Tyre Microfibres.

6.1 INTRODUCTION

Traditionally, concrete is considered to possess good fire resistance due to its low heat conductivity [1] and high heat capacity [2]. As a result, in structural fire design, a sufficient layer of concrete can serve as fire insulation for the steel reinforcement [3]. However, the use of high-performance concretes with denser micro-structures could negatively impact the heat-resistant properties of concrete in fire due to explosive fire spalling. Previous accidents have demonstrated the destructive nature of explosive fire spalling [4], [5], [6], [7]. For example, during the 2008 Channel tunnel fire, the most damaged concrete section spanned over 16 meters, with spalling depths exceeding 400 mm in certain areas, penetrating the entire depth of the concrete lining [8]. The extensive damage led to a repair cost exceeding 50 million euros at the time [9].

Explosive fire spalling is a deterioration process that causes the surface of concrete elements to explosively break off, exposing the steel reinforcement to heat, thereby reducing the load-carrying capacity of the structure. Two primary mechanisms are typically accepted as the causes of fire spalling: (1) the high-temperature gradient near the heated surface generates differential thermal expansion, which is restrained by the inner cold concrete and external load, resulting in inhomogeneous stress distribution, leading to concrete cracks and delamination parallel to the heated surface [10], [11]; (2) the compact microstructure of high-performance concrete inhibits the escape of heat-vaporized water, leading to an increase in pore vapour pressure until it reaches the maximum tensile strength of concrete, resulting in a "boiling liquid expanding vapour explosion" (BLEVE) [12], [13].

The inclusion of synthetic fibres, such as polypropylene (PP) fibres, in concrete is a widely recognized method of preventing fire-induced spalling [14], [15], [16]. According to the new Eurocode 2 [17], specific spalling assessment has to be conducted on concrete with higher risk (high moisture content, high strength, etc) unless there is inclusion of PP fibres. Compared to the previous version [3], the new Eurocode mentions various spalling related factors and re-emphasis the effectiveness of PP fibres. In pursuit of sustainable alternative materials, Recycled Polymer Tyre Microfibres (RPTM) have been explored and found to have similar effectiveness in mitigating fire-induced spalling [18], [19], [20]. In Europe alone, over 3.5 million tonnes of waste tyres are discarded each year [21]. The use of RPTM can be beneficial to both construction and waste management industries [22].

The compressive strength and modulus of elasticity of concrete with and without micro PP fibre are very similar at both ambient temperature and 200 °C [23]. The flexural strength of micro PP fibre concrete is higher than that of the plain concrete at ambient temperature due to the bridging effect of the fibres [24]. However, this flexural strength enhancement brought by the PP fibres decreases as temperature increases due to the softening and subsequent melting of PP fibres [23], [25]. It is believed that the addition of PP fibres can enhance high-temperature permeability of concrete by creating empty capillaries and thermal microcracks due to melting and thermal expansion of the fibres, respectively [26]. As vapour can escape through these tunnels and microcracks, the peak pore pressure within concrete with PP fibres is reduced, leading to the suppression of explosive fire spalling. To verify this theory, Kalifa et al. [14] firstly investigated the role of PP fibres using the PTM (pressure, temperature, mass) tests, which concluded that increasing the dosage of PP fibres can decrease the peak pore pressure in heated concrete. However, some later PTM tests show that the peak pore pressure has no direct relationship with the spalling behaviour of concrete. For instance, Choe et al. [12] and Mindeguia et al. [27] found that some concrete samples spalled at pore pressures below 0.5 MPa, which was much lower than the maximum tensile strength of the concrete sample. Jansson and Boström [28] even found the vapour pressure was higher in PP fibre-added concrete than that of spalled plain concrete, as the spalling released the vapour near the heated surface. Felicetti et al. [29] designed an in-situ heating split test which verified that pore pressure is only one of the reasons behind explosive fire spalling. Further research is, therefore, of utmost importance to fully understand the complex mechanisms of polymer fibres in fire spalling mitigation.

Another explanation for spalling is the "moisture clog" theory that has gained popularity since Shorter and Harmathy [30] first proposed it in 1961. It explains that the cause of explosive spalling is an accumulated layer of condensed moisture that travels some distance from the heated surface, with a sharply defined interface separating the dry and saturated concrete, named the "drying front." This drying front is deemed the critical zone for explosive spalling. Drawing from the "moisture clog" theory [28], [30], the authors propose a series of hypotheses for the cause of fire spalling and the spalling mitigation mechanism of polymer fibres for experimental validation. The schematic drawing of the proposed hypotheses is presented in Figure 1, in which the top figure represents the thermal behaviour of plain concrete and the bottom figure represents the thermal behaviour of concrete with polymer fibres.

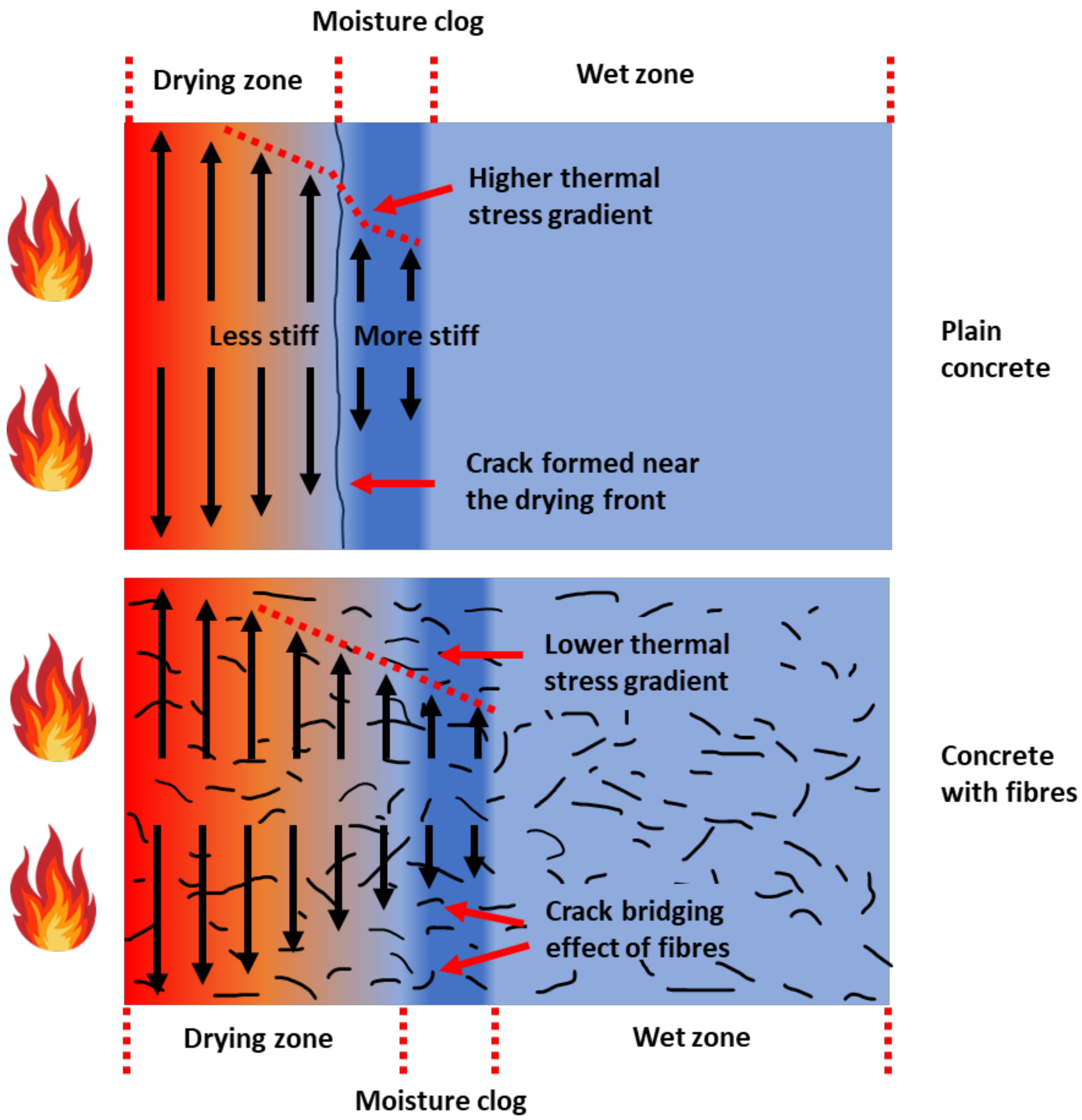

Figure 1 Mechanism for explaining the role of polymer fibres in heated concrete.

Hypothesis 1: The low permeability of more saturated concrete impedes the migration of moisture towards colder regions, leading to moisture accumulation and the formation of a moisture clog near the drying front [31]. Depending on the heating temperature near the moisture clog, the trapped moisture exerts pore vapour pressure on the concrete voids. The inclusion of polymer fibres in concrete can facilitate the migration of moisture, leading to the formation of the drying front in deeper and colder regions of concrete, hence lowering the pore vapour pressure.

Hypothesis 2: The heat transfer coefficients between gas and liquid differ significantly, resulting in a sudden temperature step near the drying front [32], which in turn leads to a dramatic thermal stress gradient. The inclusion of polymer fibres can reduce the temperature gradient as the drying front progresses faster towards the colder concrete region.

Hypothesis 3: Concrete with a higher saturation level has a higher Young's modulus, but lower compressive strength, compared with dry concrete because liquid water is nearly incompressible in nature [33], [34]. For heated concrete, thermal-induced vapour pressure drives moisture transfer from the gel pores to capillary pores and macropores, stiffening the cement matrix near the moisture clog. The stiffness difference between the low stiffness drying zone and the high stiffness moisture clog, as well as the thermal stress gradient introduced in Hypothesis 2, could trigger cracking at the drying front parallel to the fire-exposed surface [28]. The inclusion of polymer fibres could suppress the thermal cracks by decreasing the thermal gradient at the drying front and the crack bridging effect [24], [25].

To verify Hypothesis 1, which is also the premise of the Hypotheses 2 and 3, it is necessary to observe the moisture profile, particularly the drying front within heated concrete. Jansson and Boström [35] used a simple method to physically observe the existence of a "moisture clog" by splitting a concrete specimen during heating. Due to the intrusive nature of the test method, it is difficult to quantify the saturation level and the moisture migration process in concrete using the splitting method or the previously mentioned PTM test.

Recently, non-intrusive tests have been conducted to avoid altering the concrete's microstructure. Nuclear magnetic resonance (NMR) [36] was used to successfully observe the existence of moisture, but it was limited by one-directional analysis. X-ray tomography was used to help with detecting the density variations in concrete pores [37], however, this is an indirect method of detecting moisture since the change in concrete density is also influenced by thermal cracks. A combined, non-simultaneous, X-ray and NMR technique was also introduced to investigate the effect of PP fibres on heated concrete [38] which concluded that the inclusion of PP fibres can lead to a faster and deeper migration of the drying front. Dauti et al. [39] conducted neutron tomography on heated concrete to investigate the effect of aggregate size on the moisture migration process, using the Neutron and X-ray Tomography (NeXT) facility developed by Tengattini et al. [40] at Institut Laue Langevin (ILL). The high attenuation coefficient of hydrogen atoms in water molecules makes the neutron beam ideal for detecting the presence of moisture. Moreira et al. [41] further improved the sealing condition of the concrete specimens and confirmed the presence of moisture clog in heated concrete. Later on, Cheikh Sleiman et al. [42] conducted simultaneous neutron and X-ray tomographies on concrete at moderate temperatures (140 °C) for more than 12 hours, where the interactions between the drying process and crack propagation inside the concrete specimens were analysed. It should be noted that among all these neutron tomography investigations [39], [41], [42], the concrete specimens contained no fibres. So far, due to the limited number of non-intrusive tests on concrete with polymer fibres and the variability of concrete properties, further exploration is necessary in the effectiveness of detecting methods as well as specially designed tests to reveal the mechanism of heat-induced spalling and the spalling mitigation mechanism of polymer fibres.

In this study, for the first time, the full potential of simultaneous neutron and X-ray topographies developed at NeXT is applied on heated concrete specimens with RPTM. The X-ray beam is sensitive to density due to its interaction with electrons. This feature makes X-ray tomography ideal for detecting the porous system of concrete, as the pores have a lower density than the surrounding cement matrix. On the other hand, Neutron tomography is good at detecting moisture movement. Taking advantage of the high complementarity of neutron and X-ray beams, the understanding of the role of RPTM in mitigating fire-induced spalling could be improved via investigating the interlocking relationship between moisture migration and the evolution of the porous structure of heated concrete during heating.

To address the three proposed hypotheses, the experiments aim to achieve the following objectives: (1) to identify moisture evolution and the presence of moisture clog; (2) to reveal the temperature gradient near the drying front; and (3) to track the change in porous structure and possible parallel cracks that form near the drying front due to differential thermal stresses and differential stiffnesses between the drying zone and moisture clog. By comparing samples with and without RPTM, the effect of RPTM on both moisture migration and the porous structure of concrete can be investigated. Ultimately, this study aims to enhance the understanding of fire spalling, elucidate the actual mechanism of fibre inclusion, promote sustainability through the use of recycled materials, and generate data on various parameters for numerical modelling of fire spalling.

6.2 SPECIMEN PREPARATION AND TEST SETUP

6.2.1 Test specimens

Ultra-High-Performance Concrete (UHPC) was used due to its high susceptibility to fire-induced spalling. Table 1 shows the adopted mixture proportions that are based on those used by Dauti et al. [39] for comparison purposes, with a slight variation in aggregate size to accommodate material availability. To overcome the reduced workability caused by the inclusion of RPTM, 2% of superplasticizer by cement mass was added. 12 specimens were tested in three test series, as summarized in Table 2. All specimens were Ø 34 mm × 60 mm cylinders, which are ideal for tomography analysis as it requires rotation of the scanning object. The maximum thickness (34 mm) of the sample was adopted to allow sufficient penetration of neutron particles. Two specimens were fitted with type-K thermocouples at three depths (3 mm, 10 mm, and 20 mm) from the heated surface along the longitudinal axis of the cylinder, as shown in Figure 2. To minimize intrusion into the concrete porous structure, the cover of the thermocouples was peeled off to reduce their diameter to 0.3 mm. The concrete was cast into the moulds in two layers with vibration for 1 minute each time to eliminate air voids. The specimens were cured in a mist room at 90% relative humidity and 20°C for 28 days. The specimens were then wrapped in cling film to prevent drying and shipped to the test site at ILL. The specimens were kept wrapped in indoor lab conditions until the test day. Test Series 1 was conducted one month after casting. Due to beam time availability, Series 2 was conducted 9 months after casting. Series 3 specimens were cast in a different batch at a later stage using slightly different gradation of aggregates of the same type of limestone due to material availability. The Series 3 specimens aged one month and only two tests were allowed due to beam time limitation.

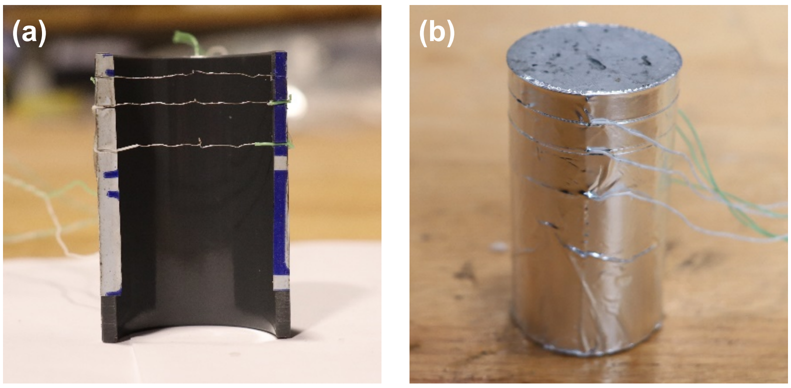

Figure 2 (a) Thermocouples installation in concrete moulds (b) concrete specimen with thermocouples.

Table 1 Concrete mixture for plain concrete and RPTM concrete

Material	Dosage (kg/m^3)
Cement OPC CEM1	488
Silica Fume	122
Building sand[1] 0 - 1 mm	632
Limestone Coarse Aggregate[2] 1 - 4 mm	949
Superplasticizer SIKA 30HE (2.0%)	9.76
Water	189.10
RPTM (for fibre added concrete only)	2
w/b ratio	0.31

[1] The gradation of the sand used for Series 3 specimens is 0 – 1.18mm.

[2] The gradation of the limestone coarse aggregate for Series 3 specimens is 1.18 – 4.75 mm.

Table 2 Specimen list

Cast batch	Test series	Label	RPTM dosage (kg/m^3)	RPTM/specimen ratio (volume in %)	Neutron scan	X-ray scan	28-days Strength (MPa)	Age (month)
1	1	RPTM1[1]-1[2]	1	0.2	In-situ[3]	None	130	1
		RPTM2-1	2	0.4	In-situ	In-situ	140	
	2	RPTM1-2	1	0.2	In-situ	None	130	9
		RPTM1-3	1	0.2	In-situ	None	130	
		RPTM2-2	2	0.4	In-situ	None	140	
		RPTM2-3	2	0.4	In-situ	None	140	
		RPTM2-TC[4]	2	0.4	In-situ	Ex-situ[5]	140	
		PC[6]-1	0	--	In-situ	None	125	
		PC-2	0	--	In-situ	None	125	
		PC-TC	0	--	In-situ	Ex-situ	125	
2	3	RPTM2-4	2	0.4	In-situ	None	110	1
		PC-3	0	--	In-situ	None	100	

[1] RPTM dosage.

[2] Repeat ID number.

[3] In-situ = simultaneous scanning and heating.

[4] TC means implementation of thermocouples.

[5] Ex-situ = pre-heat and post-heat X-ray scanning of the specimen.

[6] PC = plain concrete.

Plain concrete without fibres and specimens with various dosages 1 kg/m^3 and 2 kg/m^3 (volume ratios 0.2% and 0.4%) of RPTM were tested to investigate the influence of RPTM and fibre dosage. The volume ratios were approximated based on a mean density (500 kg/m^3) of RPTM. It should be noted that the bulk density of RPTM usually ranges from 400 to 600 kg/m^3, depending on the source of waste tyres and the fibre cleaning process. Uncleaned waste tyre fluff is contaminated with rubber particles and dust. Specially designed devices at the University of Sheffield were employed to purify the fibres and disperse them into concrete during the mixing process. RPTM before and after the cleaning process are shown in Figure 3. The length of RPTM ranges from 0.8 mm to 16 mm, with diameter ranging from 7.5 μm to 60 μm. The RPTM has a melting temperature ranging from 210° to 260 °C [43], [44], which is generally higher than those of PP fibres (170°C).

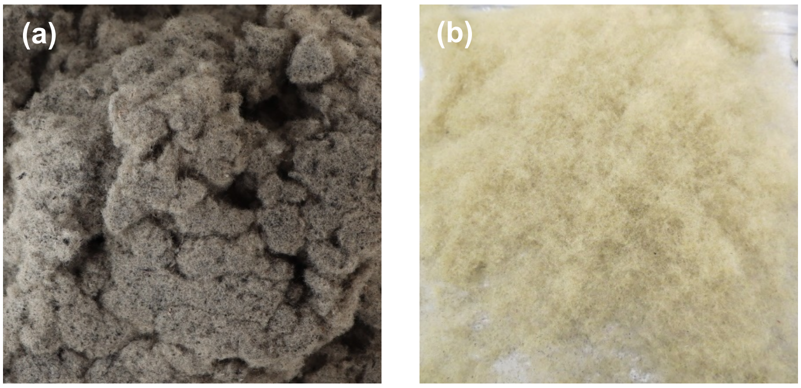

Figure 3 (a) Waste tyre fluff (b) Cleaned and untangled RPTM.

6.2.2 Test setup

The neutron and X-ray tomography setup is shown in Figure 4. The neutron tomography used cold neutrons produced from a heavy-water cooled nuclear reactor at ILL, which is currently the most intense neutron source in the world. A neutron detector was positioned behind the test samples at a distance of 10 cm to minimize neutron scattering. The neutron detector consisted of a scintillator and a CMOS camera. The X-ray system was constructed using a commercial X-ray source and detector. To prevent interference, the neutron and X-ray sources were placed orthogonally. Boron and lead shielding materials were used to protect electronic components from radiation damage in both tomography systems. A specially designed heating chamber was placed on a scissor lift for height adjustment. The concrete specimen was placed on rotation capable of rotating the specimen 180° per minute, synchronised with both neutron and X-ray tomographies. A flexible extraction pipe was inserted into the heating chamber to vacuum out the radioactive steam and dust from the heated concrete.

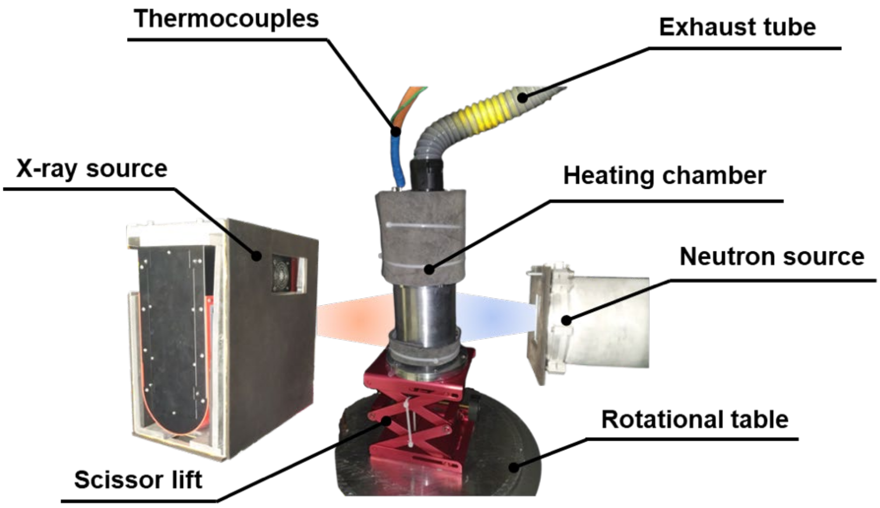

Figure 4 The test setup of simultaneous neutron and X-ray tomographies, NeXT-Grenoble, ILL.

During the tomography scanning, unidirectional heating was applied 6 mm away from the concrete top surface using a 6 × 6 cm ceramic radiant panel, as shown in Figure 5. The small gap left between the radiant panel and the heated surface was there to allow the escape of steam and dust in case of spalling. As fire spalling of concrete can change drastically the heating and moisture condition of the sample, the heating rate was controlled to prevent spalling. The radiant panel reached 500 °C within the first 3 minutes and then remained constant throughout the test. The side surface of the specimen was wrapped with aluminium foil to reduce moisture leakage through the side boundary (see Figure 5(b)). The specimens were then placed in an aluminium chamber and surrounded by an alumina insulation blanket. These materials were specifically chosen due to their low attenuation coefficient to neutrons.

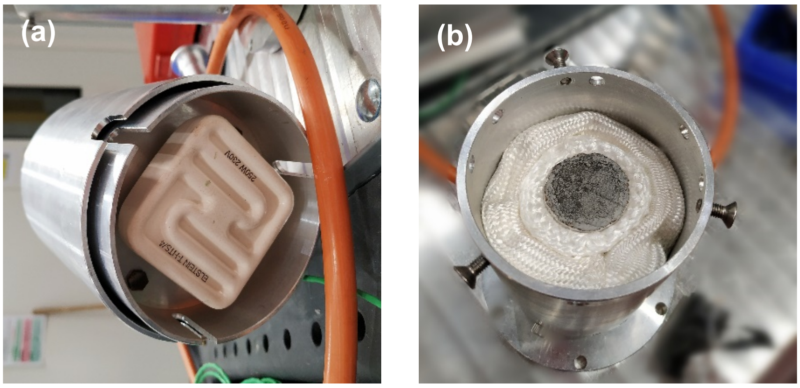

Figure 5 (a) Radiant heating panel; (b) Specimen in the heating chamber.

The field of view of the Neutron detecting camera was calibrated to 100 ×100 mm with 2048 × 2048 pixels, resulting in a pixel size of 50 μm. However, achieving high image resolution requires a longer exposure time, taking around 20 minutes for a single tomography, which is too slow to capture the moisture migration within the heated concrete specimen. To avoid this issue, the pixel binning 4x4 method was employed to reduce the projection time to only 1 minute for a single tomography, which increased the pixel size to ~200 μm. For the X-ray tomography that took place simultaneously with the Neutron tomography, a relatively low resolution and large pixel size (100 μm) was required to track the fast change of the concrete pore structure during heating. However, this resolution was not sufficient to detect the finer pores. Therefore, slower (30 minutes) ex-situ pre-heating and post-heating X-ray scans with high resolution and small pixel size (45 μm) were also performed to determine changes in the porous structure including the finer pores. It is not recommended to further increase the resolution of these ex-situ X-ray scans and elongate the scan duration, since the post heating scans should ideally take place immediately after heating to eliminate the effect of cooling.

6.3 DATA ANALYSIS AND RESULTS

6.3.1 Temperature measurements

The location of the thermocouples can be identified from the X-ray tomography, as the metal wire has a distinctive density compared to concrete, as shown in Figure 6. The actual depth of the thermocouple head can be determined by counting the pixel length from the concrete top surface. The calibrated depth of thermocouples TC1, TC2 and TC3 in RPTM2-TC and PC-TC are 1.6 mm, 9.5 mm, 17.8 mm and 2.5 mm, 9.3 mm, 17.7 mm, respectively.

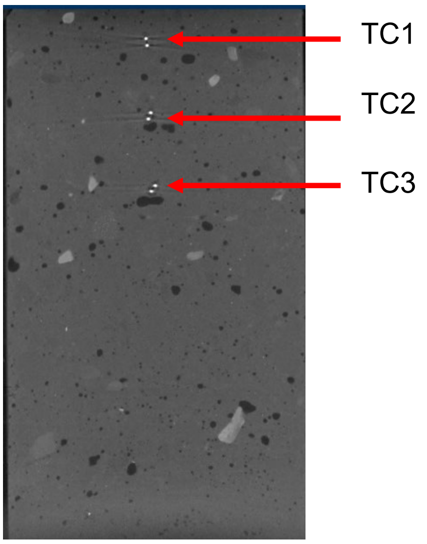

Figure 6 Location of thermocouples as detected by X-ray tomography.

The temperature distributions across the depth of PC-TC and RPTM2-TC at different heating times are shown in Figure 7(a) and Figure 7(b). The data points are connected using a second order polynomial fitting curve. As expected, the surface of the samples heats up much faster than the inner layers due to the low conductivity of concrete. The temperature in plain concrete is slightly higher than that of RPTM2 specimens and the biggest difference (8 °C) occurs after 20 min of heating at 6 mm depth. At that time and depth, the temperature measurement of PC-TC is 130 °C and that of RPTM2-TC is 138 °C. Assuming completely sealed pores with water, the difference in water saturation pressure between these two specimens at 6 mm depth is estimated to be only 0.06 MPa. Such a difference in pore vapor pressure is negligible in the event of fire spalling, compared to the tensile strength of concrete. This contradicts Hypothesis 2, which assumes that the polymer fibres can reduce the temperature gradient, hence reduce the corresponding water vapour pressure.

The temperature evolution profiles of the specimens PC-TC and RPTM2-TC are shown in Figure 8. No sudden changes in temperature or flattening of the temperature gradient are observed in the RPTM2 specimen. Similar temperature profiles were also obtained in previous research on concrete with and without fibres[14], [45], with neither significant temperature difference nor any flattening of the temperature gradient between the plain and fibre specimens.

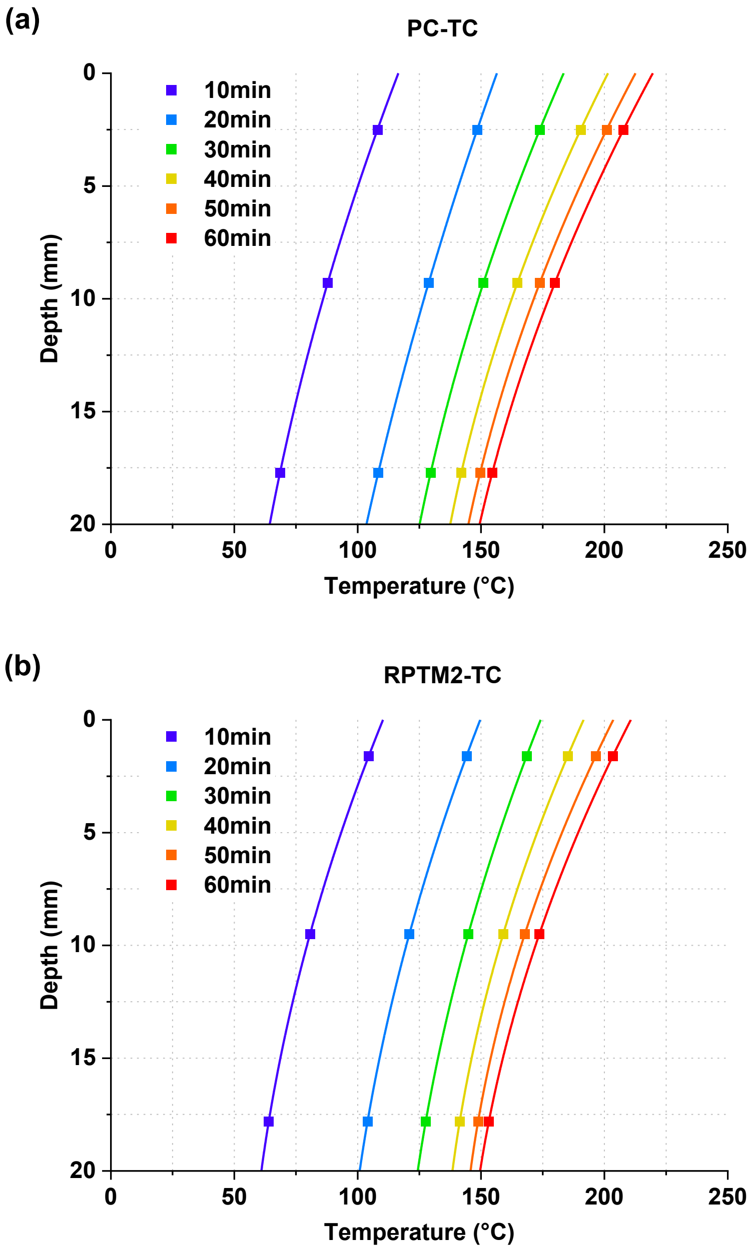

Figure 7 Temperature distribution across the depth of PC-TC and RPTM-TC at different heating times.

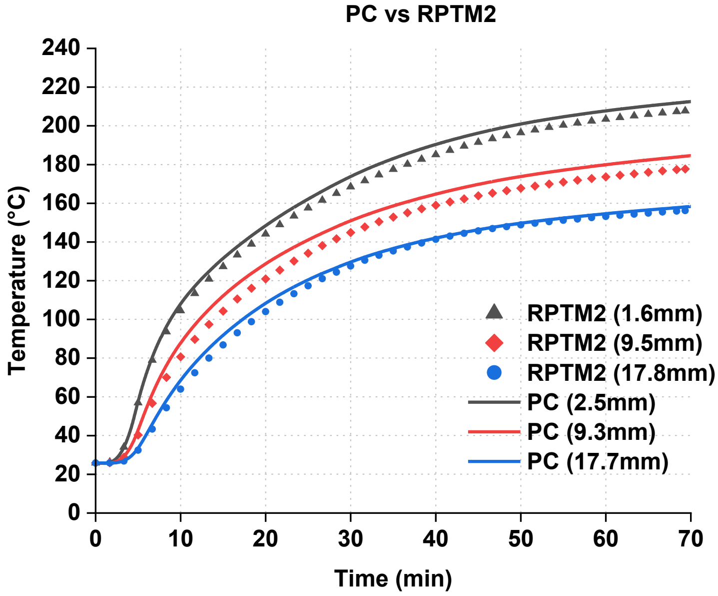

Figure 8 Temperature profiles as a function of time of PC-TC and RPTM2-TC.

However, the neutron and X-ray tomographies reveal that the above-mentioned low impact of RPTM on temperature gradients is questionable, owing to the intrusive nature of the thermocouples. The air voids induced by the insertion of the thermocouples [46], the interfacial transition zone between the thermocouples and the concrete matrix, as well as the differential thermal expansion of the thermocouples compared to that of concrete can significantly alter the concrete porous structure near the thermocouples. These highly permeable areas around the thermocouples accelerate moisture evaporation, regardless of fibre inclusion or not. Figure 9(a) shows the X-ray image of a slice of the concrete specimen near an embedded thermocouple. In this figure, the two slightly darker lines along the thermocouple (one above, one below) indicate the empty channel around the thermocouple. The measured outer diameter of the ring-shaped empty channel is 1.2 mm, which is three times larger than the diameter (0.3 mm) of the thermocouple after peeling of the cover. Figure 9(b) shows the neutron image of the same slice of the specimen. The level of saturation of concrete after heating is indicated by the colormap. A clear zone of additional drying in close proximity to the thermocouples can be observed in this figure, which confirms the negative impact of the thermocouple on the drying process of heated concrete.

In Hypothesis 2, a clear drying front is essential for a steep thermal gradient to be developed. However, the drying process is very much affected by the thermocouples, and so the measured relationship between the drying and temperature may not represent that of a specimen without thermocouple. Hence, for heated concrete with or without fibres, although similar temperature results are found in this study compared to previous investigations [14],

[45], there is still insufficient evidence to either substantiate or oppose Hypothesis 2. So far, identifying differences in temperature gradients due to the dry-wet interface proves challenging due to the intrusive presence of thermocouples. A non-intrusive method or extremely fine thermocouples to measure the temperatures within heated concrete would be preferable.

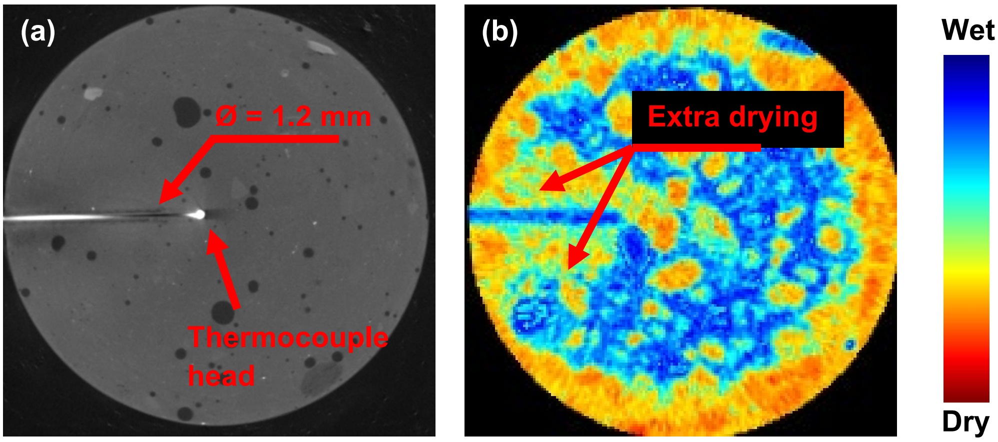

Figure 9 (a) X-ray image showing the crack opening induced by thermocouple (b) Neutron image showing the extra drying induced by the thermocouple.

6.3.2 Neutron tomography

6.3.2.1 Image processing and visual inspection of water drying

To assess Hypothesis 1, which posits that the inclusion of RPTM facilitates the migration of the "moisture clog" into colder areas, the neutron tomography results were analysed. The tomography adopted in this work is based on the Beer-Lambert law. The transmitted neutron beam intensity is related to the incident beam intensity, the neutron attenuation coefficient of the scanned material, and the length of the neutron path. For simplicity, these are considered constant for the concrete solid skeleton, and the length of the moisture path is considered to be the only distinct variable during heating. Hence, changes in the incident beam intensity, observed in the scale images during heating of the concrete, are considered to be directly related to moisture content. For example, brighter pixels with higher grey values indicate higher water content in that specific pixel area.

Image processing techniques were employed to illustrate the drying process of the heated specimens. As shown in Figure 10, the reconstructed neutron tomography image can be seen as a stack of slices. Each slice represents a disc of the specimen at a specific depth along the heating direction. These slices constitute a 3D array representing the whole volume of the specimen. 3D rendering as well as vertical cross-sectional cuts of the specimen are shown in Fig17 (the latter with a "CV2_Jet" colormap in Python).

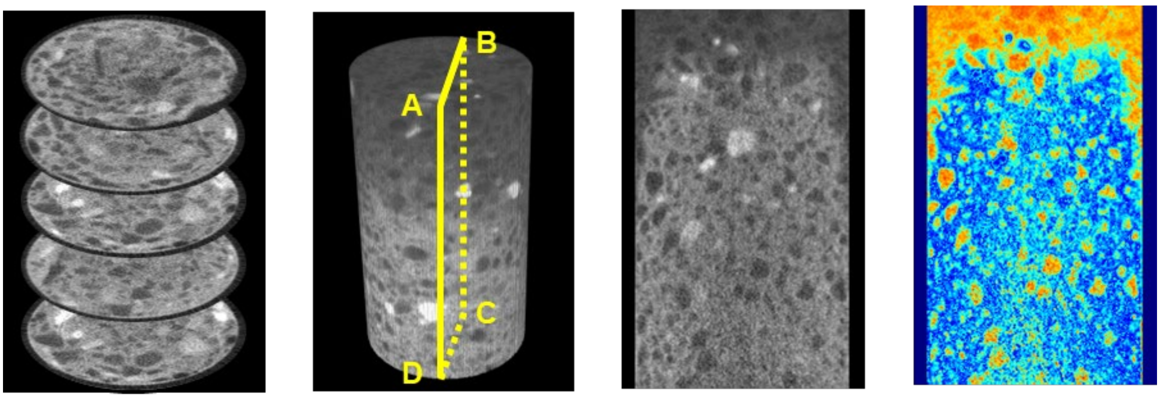

(a) Stack of 2D slices

(b) 3D rendering of concrete sample

(c) Cross-section ABCD in (b)

(d) After applying the colour map

Figure 10 Processing of the neutron tomography images

From the processed images, the global dehydration rates of the specimens can be compared. Figure 11 shows selected cross-sectional slices for specimens PC-2, RPTM1-2, and RPTM2-2 that contain various RPTM dosages to investigate their impact on moisture transport.

The first neutron scan (at 0 = min) was conducted during the first minute of heating and can be regarded as the initial state of the specimen, since the drying process had not yet started. As shown in Figure 11, all specimens exhibit similar moisture distribution without any visible drying front at this initial stage. This is expected as all specimen were cured in the same way and kept in plastic wrapping until the day of testing. As aggregates in concrete are typically dry and practically impermeable to water, dry areas in the images can be considered to represent aggregates. Another notable aspect of the image is the cupping effect that can lead to an underestimation of water content near the specimen's central axis. This is observed in all specimens as the inner voxels appear to be drier than the outer voxels. This effect results from the forward scattering of the specimen. This is most pronounced near the central axis of the cylindrical specimen, where the influence of cupping is at its greatest. An estimation of this effect has been conducted in a previous study [47], which featured a specimen size similar to the current investigation. It is important to note that this effect primarily influences the assessment of the exact moisture content, with minimal impact on the drying front position evaluation.

At 20 minutes of heating, a distinct drying front begins to develop from the top, illustrated as a red-orange layer. At this stage, no significant difference in the depth of the drying front is observed among the specimens. Starting from about 35 to 40 minutes of heating, the top section of the concrete reaches approximately 170°C and the drying front of all specimens moves further down. The drying front location of RPTM2-2 is the deepest among all specimens, whereas the difference in drying front depth between RPTM1-2 and PC-2 remains subtle. As heating continues, both RPTM1-2 and RPTM2-2 experience faster moisture movement compared to PC-2. By the end of the test, the difference in drying front depth between the specimens with various fibre dosages is pronounced. The black dotted lines in the final row images of Figure 11 indicate the final location of the drying front at the end of each test. It can be seen that the final depth of the drying front increases with RPTM dosage However, due to variability in concrete properties and the faster drying at the boundaries, variabilities are observed between different specimens. To achieve this, a more quantifiable analysis is needed to evaluate the influence of the RPTM inclusion in concrete; an initial attempt is presented below.

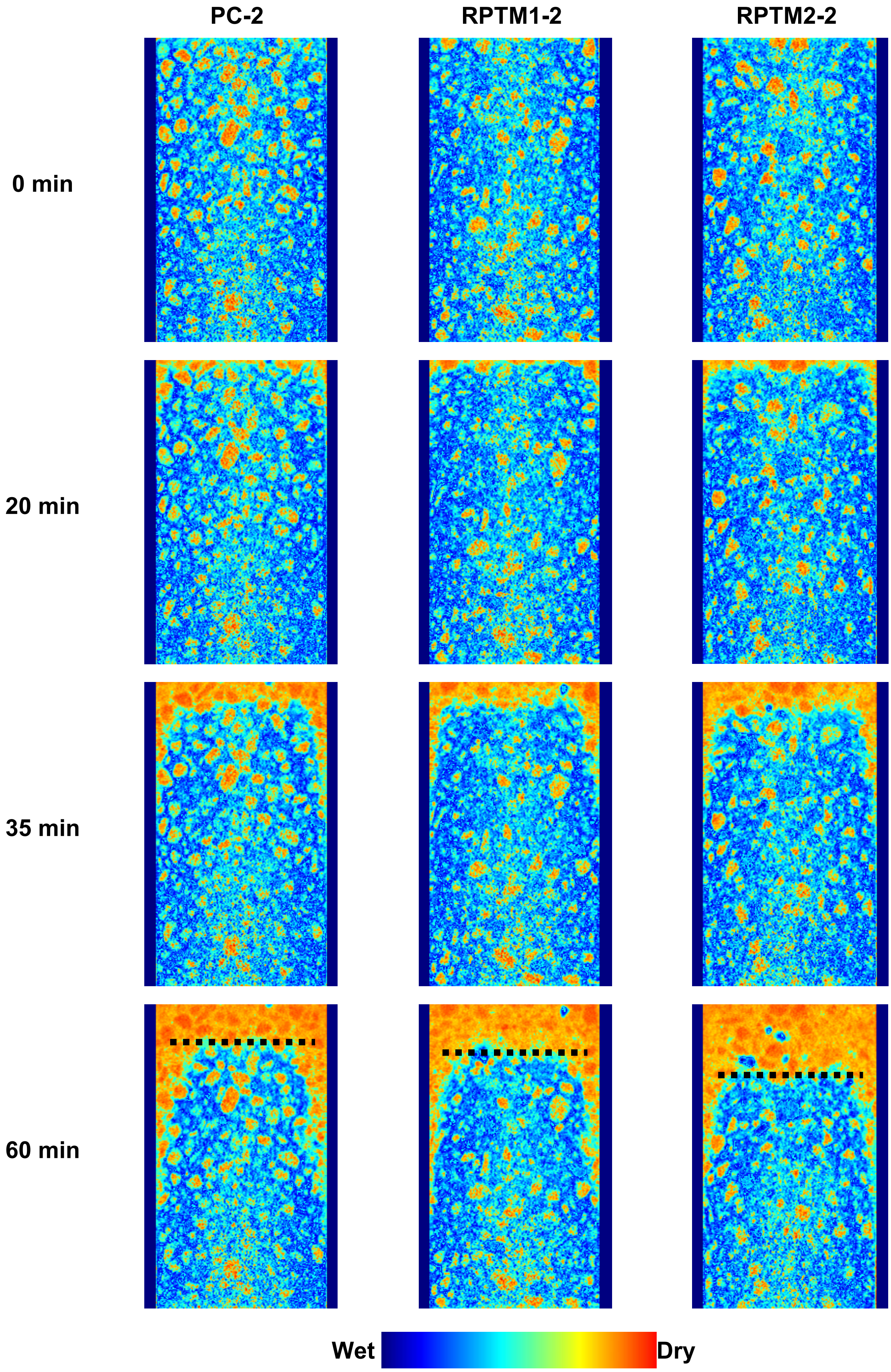

Figure 11 Drying process of specimen PC-2, RPTM1-2 and RPTM2-2 at different times of heating.

6.3.2.2 Quantification of drying

After visually inspecting the drying process of different concrete specimens from the vertical slices, a quantification of the influence of RPTM on concrete drying is attempted. The first step involves removing the boundary effect. Although the specimens were wrapped with aluminium tape and insulated around the side surface, drying near the boundary was inevitable as the tape cannot prevent moisture loss under pressure. New casing materials were found to effectively reduce the boundary drying effect [41], however, this technique was not available when this test was performed. To analyse the uniaxial drying of concrete, the boundary effect was removed by disregarding the part of the specimen close to the perimeter. As shown in Figure 12, instead of analysing the original specimen which is of 34 mm (170 pixels) diameter, a core of 24 mm (120 pixels) diameter is considered.

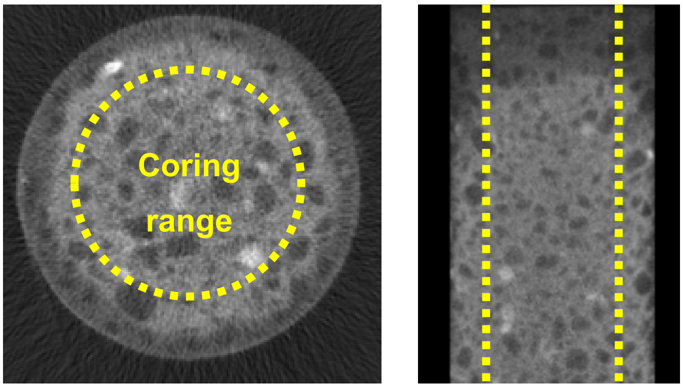

Figure 12 Coring range of the neutron image to remove the boundary effect.

To distinguish between dry and wet volumes within an image, histogram-based thresholding is employed as an image segmentation technique. This technique involves separating images into two groups, whose pixels share similar attenuation. The values of the voxel for a representative specimen throughout the duration of the test are plotted into multiple histograms (Figure 13). The threshold is defined as the intersection point of the histogram curves at different times. As drying evolves, the number of dark (dry) voxels increases on the left-hand side of the threshold, while the number of bright (wet) voxels decreases correspondingly. Figure 13 provides an example of the threshold determination process from the PC-TC specimen.

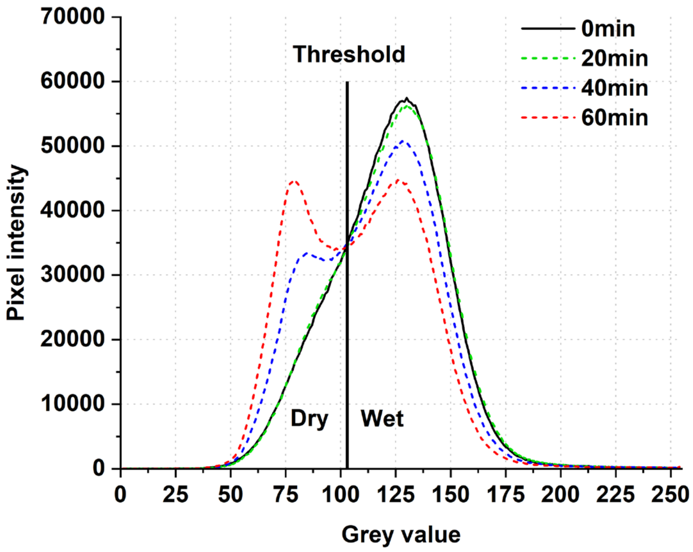

Figure 13 Determination of threshold between dry and wet volumes in specimen PC-TC.

Once the unique threshold for the entirety of the specimens has been determined, the drying process can be quantified as the drying volume ratio (the number of voxels below by the drying threshold divided by the total number of voxels). The drying volume ratios for all specimens is plotted against heating time in Figure 14. To exclude the influence of dry aggregates, which do not participate in the moisture migration process, the volume of dry aggregates is removed so that the initial dry volume ratio is zero.

Test Series 1 aimed to examine the influence of varying RPTM dosages. The drying volume ratios for both specimens (RPTM1-1, RPTM1-2) are nearly identical until after 40 minutes, suggesting that, subject to the reported test condition, 2 kg/m³ of RPTM offer limited additional benefits in terms of facilitating drying compared to the 1 kg/m³ of RPTM.

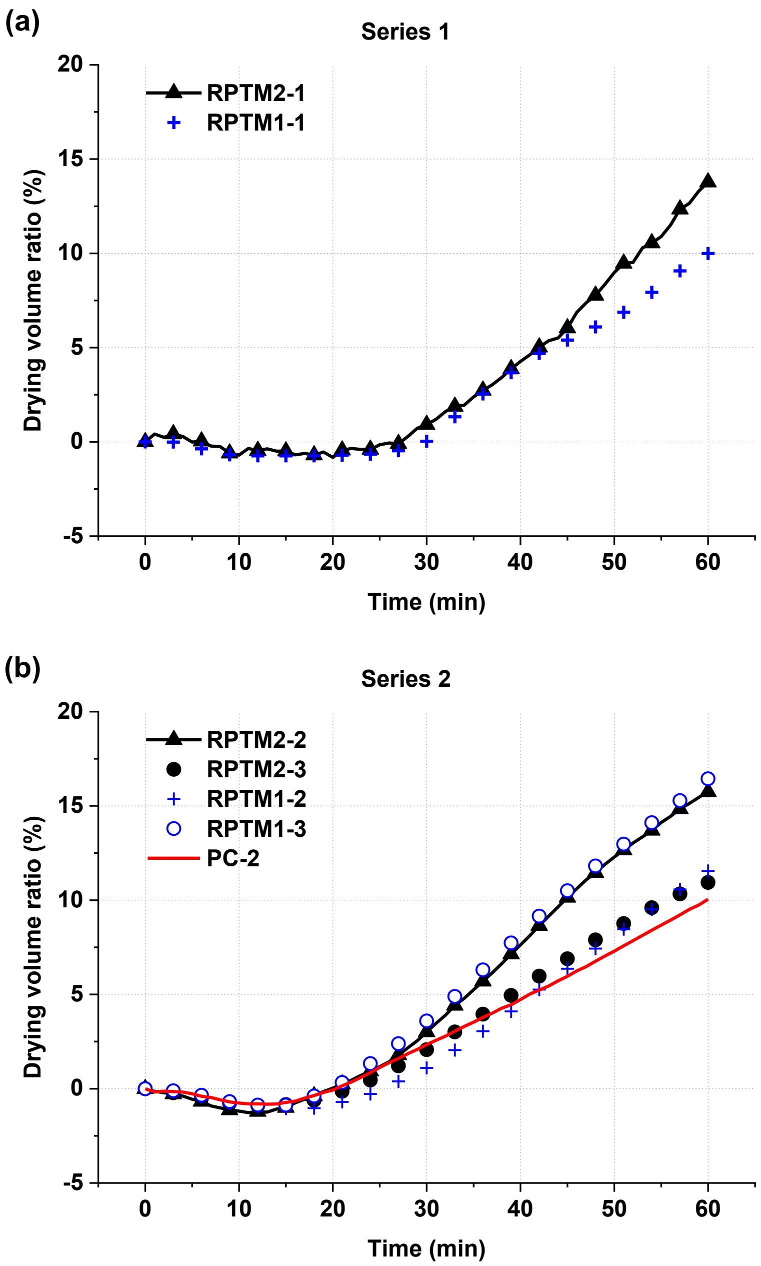
(a)
Series 1
RPTM2-1
RPTM1-1
Drying volume ratio (%)
Time (min)
(b)
Series 2
RPTM2-2
RPTM2-3
RPTM1-2
RPTM1-3
PC-2
Drying volume ratio (%)
Time (min)

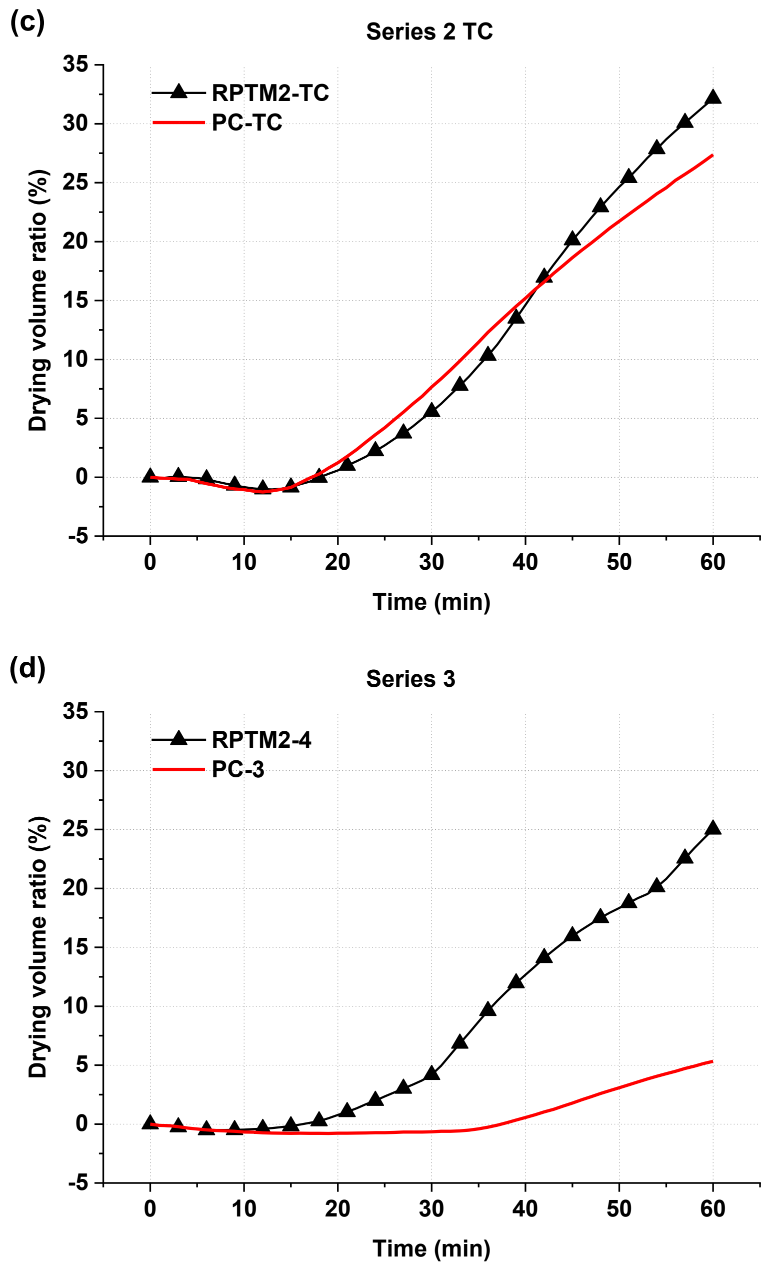

Figure 14 The development of drying volume ratios over heating time for specimens with 0, 1 kg/m³ and 2 kg/m³ of RPTM in all three series.

Test Series 2 is divided into two groups: Group 1 (RPTM1-2, RPTM1-3, RPTM2-2, RPTM2-3, PC-1, PC-2) with no thermocouples, and Group 2 (RPTM2-TC, PC-TC) with thermocouples. For Group 1, up to approximately 30 minutes of heating, the initial drying volume ratio of plain concrete specimen PC-2 is not the lowest. This suggests that the initial drying speed of concrete is not dependent on fibre dosage. Instead, it is more influenced by the specimen's heterogeneity and intrinsic permeability. For the same reasons, the initial drying volume ratios within the first ~30 minutes of heating of the two repeats of the same fibre dosage (RPTM1-

2 vs RPTM1-3 and RPTM2-2 vs RPTM2-3) are different. After around 30 minutes, the concrete temperature ranges from ~200 °C at the heated surface to ~130 °C at 20 mm depth and the drying speed of the specimens with RPTM begins to increase. The end-of-heating drying volume ratios of all RPTM specimens surpass that of the plain concrete. Due to the intrusion effect of the thermocouples, the drying volume ratios of both specimens with thermocouples (RTPM-TC and PC-TC) are higher than those of the rest of the specimens in Series 2. The influence of RPTM remains evident regardless of the influence of thermocouples after 30 minutes of heating.

For Series 3, the maximum drying volume ratios and drying rates of the specimens differ from those of the previous series. This is because these specimens were cast in a different batch with aggregates from different suppliers, as detailed in Section 6.2.1. Nevertheless, the accelerating effect of RPTM on drying is further confirmed, as the increase in drying speed between 30 and 40 minutes is conspicuous.

The drying speed is determined from the slope gradient of the drying volume ratio-time relationships, as shown in Figure 15. For plain concrete specimens PC-2, PC-TC, and PC-3, the drying speed remains relatively consistent throughout the test period. For all RPTM specimens, the drying speed starts to peak at approximately 25 to 30 minutes, corresponding to concrete temperature of around 160 - 170 °C at the heated surface and 110 - 125 °C at 20 mm depth from the heated surface. The drying speed peaks between 35 and 50 minutes, while the temperature ranges from around 180 - 210 °C at the heated surface and 125 - 135 °C at the 20 mm depth. Some specimens exhibit fluctuations in drying speed, but the overall drying rate is higher in RPTM than plain concrete specimens. This provides evidence to support Hypothesis 1. The difference between 1 kg/m³ and 2 kg/m³ of RPTM does not have a significant impact on the speed of the drying process, possibly due to the heterogeneity and variability in the intrinsic properties of the specimens. It may also indicate that 1 kg of RPTM is enough to alter the porous structure of concrete and the second 1 kg fibre does not contribute further help. It is anticipated that the effect of higher fibre dosage will be more evident at higher heating rates.

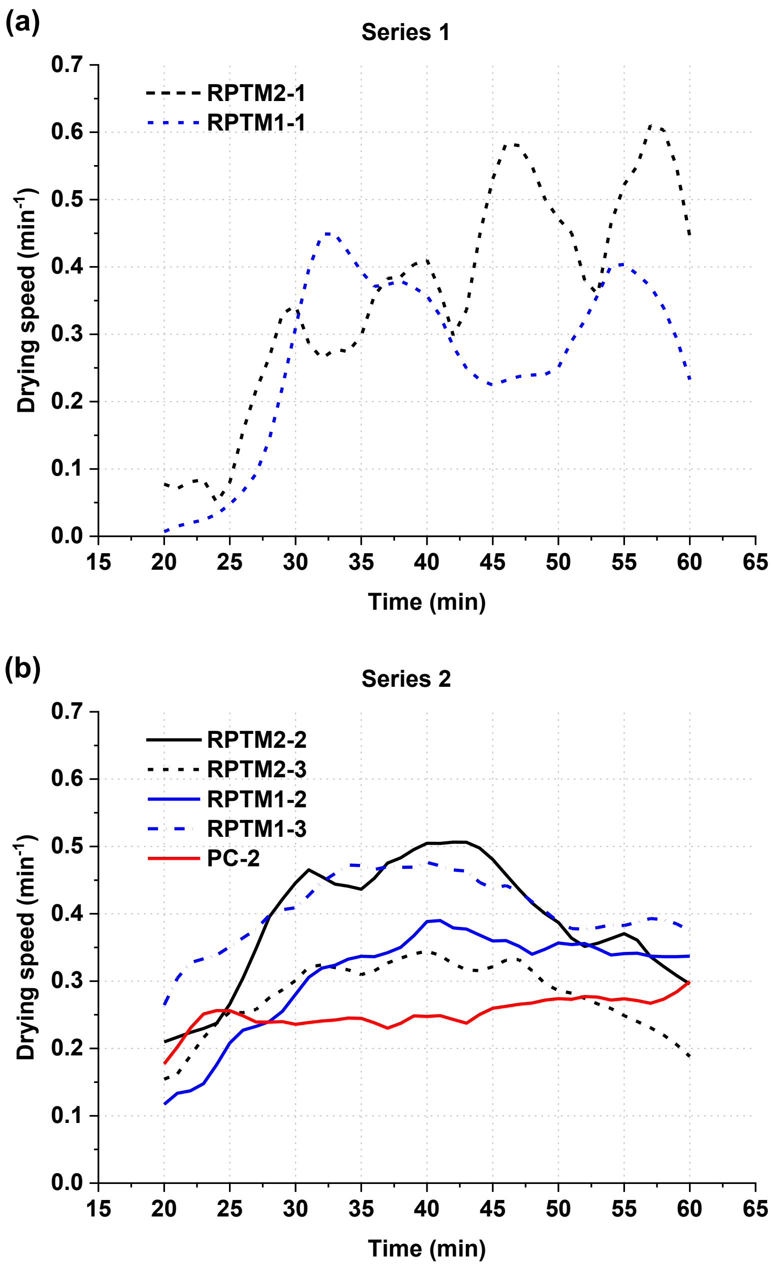
(a)
Series 1
RPTM2-1
RPTM1-1
Drying speed (min-1)
Time (min)
(b)
Series 2
RPTM2-2
RPTM2-3
RPTM1-2
RPTM1-3
PC-2
Drying speed (min-1)
Time (min)

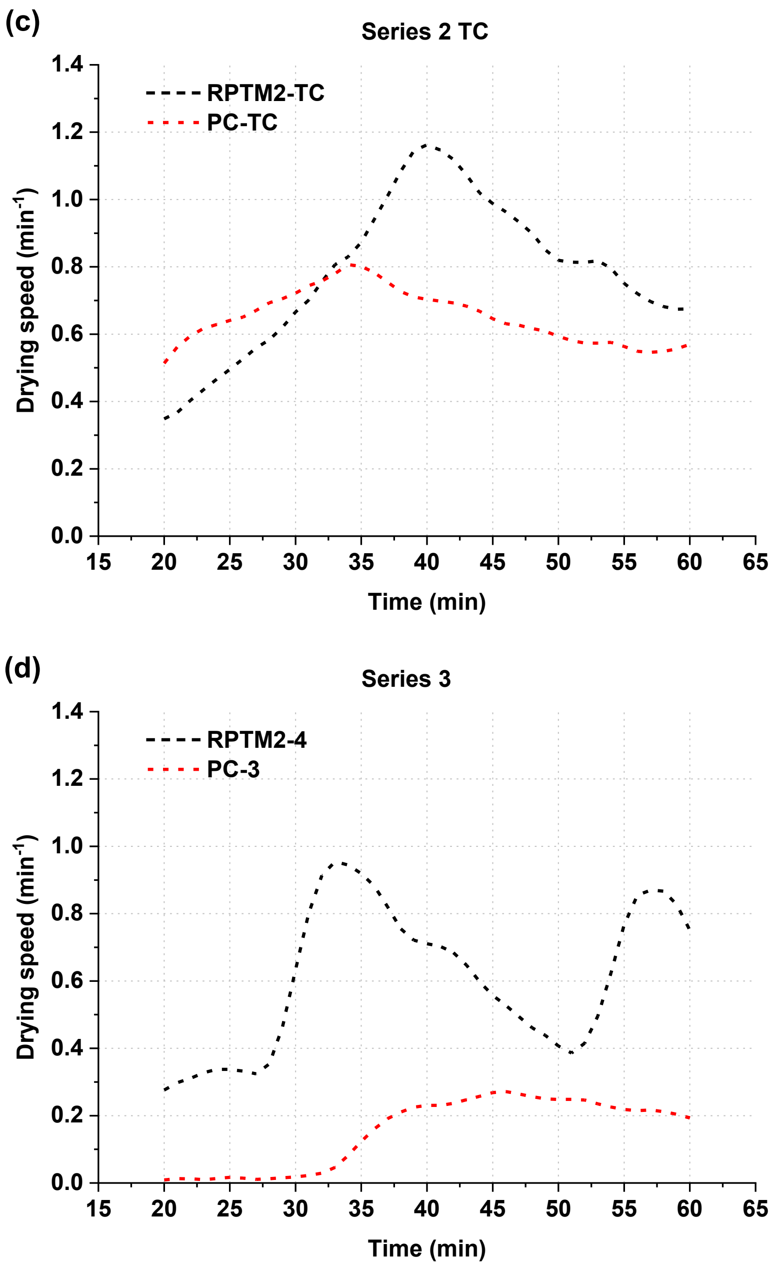

Figure 85 Drying speed of the drying volume ratio curves of all specimens.

It should be noted that in Figure 14, the drying volume ratios of all samples initially shows slightly negative values at the beginning of the tests, indicating an increase in wet concrete volume. Previous studies [39], [41] also observed this response at the beginning of the heating with a primitive hypothesis.

This initial phase, observed in all tests, may be attributed to relocation and redistribution of moisture within the concrete. Specifically, after 10 to 20 minutes of heating, the concrete temperature near the heated surface increases beyond 100°C. Though moisture will vaporise it may initially remain trapped within the concrete microstructure. As the pore pressure builds up [13], [48], [49], liquid moisture from saturated gel pores will be pushed into drier capillaries and unsaturated macropores. Although the overall moisture content in the specimen remains relatively constant or is slightly decreasing, the volume ratio of the wet concrete in the colder regions increases due to moisture accumulation in the detectable macropores, leading to apparent decrease in the drying volume ratio.

To better illustrate by example the wetting phase of the heated concrete, specimen RPTM2-2 is divided into three 20 mm layers to track moisture behaviour at various depths. The drying volume ratio of each layer is shown in Figure 16, and the speculated corresponding moisture behaviour for each layer is shown in Figure 17.

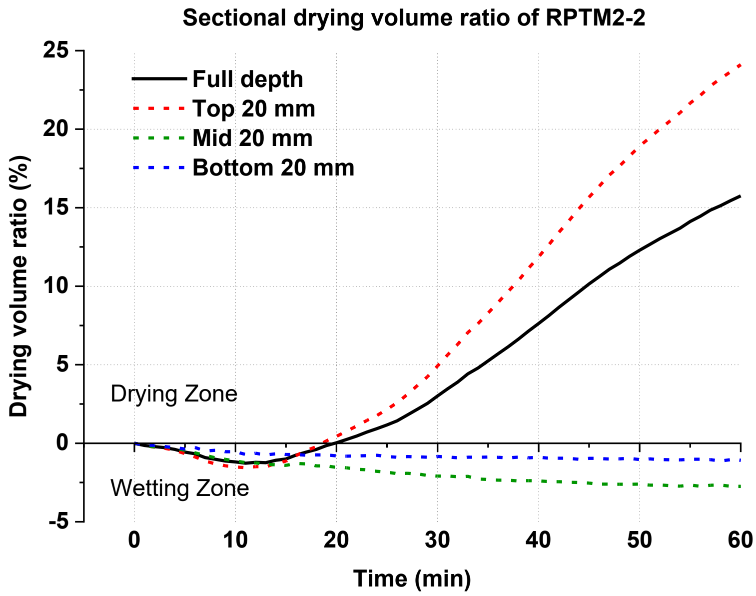

Figure 16 Sectional drying volume ratios of specimen RPTM2-2 comparing to the full depth drying volume ratio.

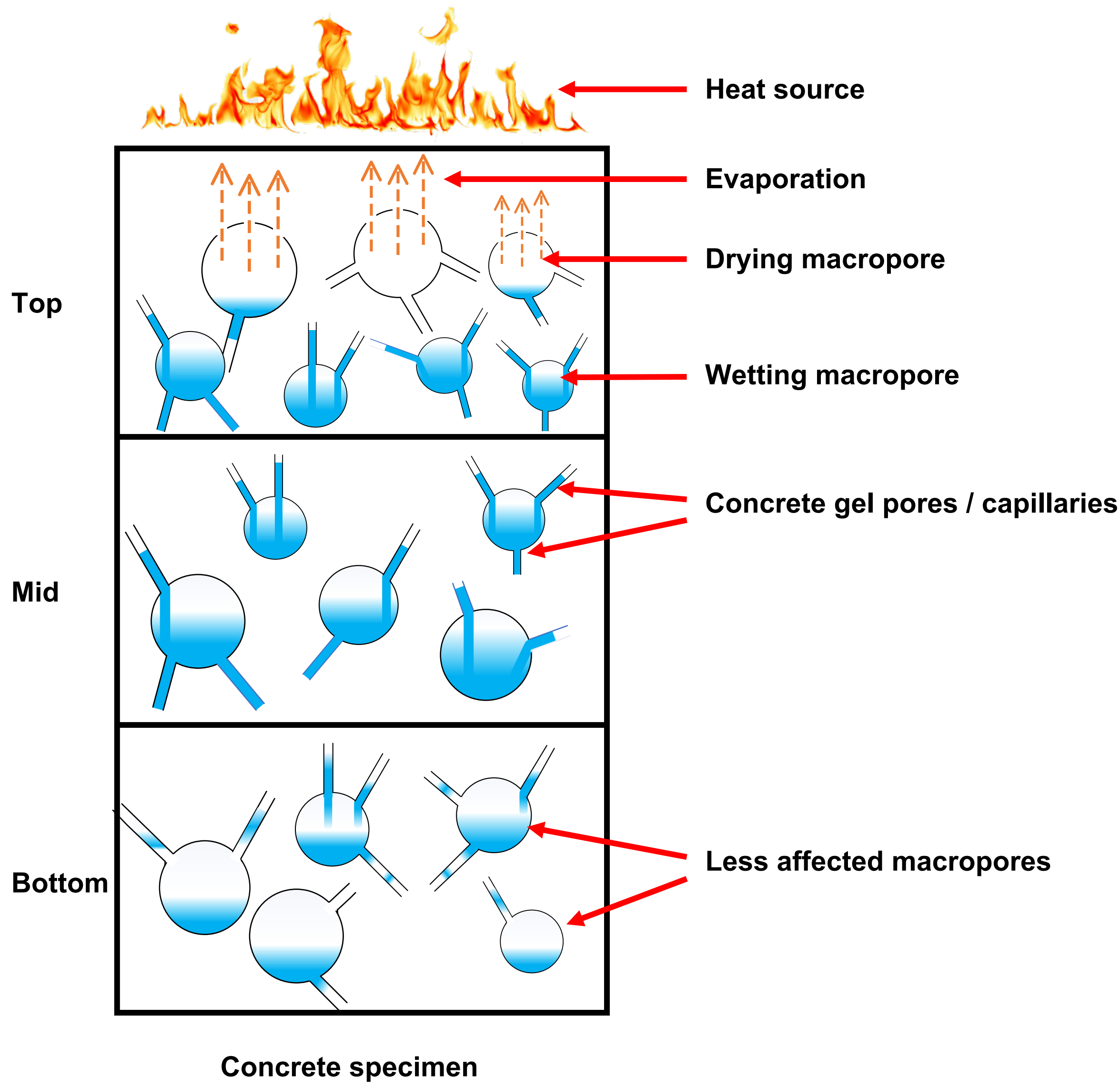

Figure 17 The proposed explanation for the observed moisture migration within each layer of concrete.

When heating starts, moisture stored near the top surface of the specimen tends to evaporate and exert vapour pressure in the concrete porous network. Part of the vapour escapes through the top surface whereas the other part of the vapour drives the moisture towards the inner layer of the concrete specimen. At this resolution, when the moisture migrates from the gel pores, below the observability limit, and capillaries to the detectable macropores, the neutron tomography will show an increase in the amount of voxels above the drying limit which is interpreted as the "wetting" of macropores resulting in a decrease in the drying volume ratio. Since the specimen is heated from the top, the top layer experiences the fastest decrease in the drying volume ratio, indicated by the "Top 20 mm" curve in Figure 16. When heating continues, more and more moisture escapes from the top surface, the drying of the top layer concrete gradually becomes dominant, causing the drying ratio of the top 20 mm to turn positive and continue to increase until the end of the test. Unlike the top layer, moisture in the mid layer cannot easily escape through the specimen boundaries. Hence, the migrated moisture driven by the vapour pressure stays in the mid layer and starts filling the porous network, corresponding to a steady decrease in the drying volume ratio in the “Mid 20 mm” curve in Figure 16. The bottom layer, which is the least affected by the moisture migration and heating, experiences minimal variations in drying volume ratio throughout the test duration (the “Bottom 20 mm” curve in Figure 16).

To summarize, the wetting phase shown in the neutron tomography of heated concrete provides indirect evidence that the moisture can migrate from saturated gel pores and capillaries to fill macropores. This lends further credibility to Hypothesis 3 as an explanation for the stiffening of the cement matrix. To investigate the evolution of the moisture profile within the heated concrete, the average grey value of each slice throughout the depth of the specimen is plotted against heating time in Figure 18. The initial average grey value of the specimen at beginning of the test is used as the benchmark; after heating higher values indicate water accumulation, whilst lower values indicate drying. The difference in grey value is represented in percentage and marked as a colormap. The interface between the mostly dry (red) concrete and saturated (blue) concrete is considered to be the "drying front", as marked by the green-yellow colour. For all specimens, clear moisture accumulation can be observed just below the drying front. The contour lines 0, 2 and 4 indicate the areas of the specimen with 0%, 2% and 4% increases of grey values, respectively, highlighting moisture accumulation areas, or the so called “moisture clog”. The moisture clog is always located just below the drying front, which validates Hypothesis 1. From these three test series, it can be concluded that the moisture clog develops in heated concrete irrespective of RPTM inclusion, concrete age or thermocouple intrusions.

It should be noted that all specimens were kept in sealed saturated conditions, which means that on the testing day the concrete pores were highly saturated, leaving less space for water accumulation. Compared to Series 1, the additional 8 months of curing of Series 2 specimens allowed for a higher degree of cement hydration, resulting in lower water content in the pores and an increased potential for water accumulation. Hence, some of the Series 2 specimens show 4% increase in grey value, whereas the Series 1 specimens experience around 2% increase. On the other hand, the potential for concrete drying is much larger than that of moisture accumulation. The closer proximity to the heated surface, the drier the concrete becomes, with the maximum grey value difference being about 30% for Series 1, 35% for

Series 2, and 50% for Series 3. The higher grey value difference in Series 3 maybe attributed to the differences in aggregate gradation.

A reference zone of temperature 160 – 170 °C is drawn on the average grey value map to compare with the moisture profile. The temperature distribution is estimated based on the surface temperature of specimens after 25 – 30 minutes of heating, when the drying speed of most specimens starts peaking, as mentioned in Section 6.3.2.2.

In Series 1, both specimens exhibit slow initial drying before 20 minutes; however, once the temperature reaches the reference zone, a clear acceleration in the drying slope can be observed. The drying acceleration in the specimen of 2 kg/m³ RPTM is more pronounced than that of 1 kg/m³ RPTM, shown as the drying slope of RPTM2-1 followed the 170°C line more closely than that of RPTM1-1.

In Series 2, there is no discernible difference in the moisture profile between the two RPTM RPTM dosages (1 and 2 kg/m³). This might be due to the variability in concrete properties and concrete age or, alternatively, could indicate that after a certain amount of additive there is no more variation in response. Since the longer hydration time leads to lower saturation level of Series 2 concrete, more dried pores can act as moisture reservoirs which negate the influence of higher fibre dosages. Similar to Series 1, most of the corresponding RPTM specimens in Series 2 show faster drying up to the reference zone and the drying continues within the zone. One exception can be seen in the last 10 minutes of RPTM2-3, which might be due to non-uniform distribution of fibres in that specimen. The most significant difference in the moisture migration behaviour is between PC-2 and the RPTM specimens. The reference zone has a minimal effect on the drying behaviour of PC-2, as the slope of drying is rather gentle, and most of the drying front is above the top 170 °C line.

For Series 2 TC specimens, the inclusion of thermocouples has clearly an impact on the water accumulation process, with "saw-tooth" shaped moisture clogs appearing at locations below the thermocouples. With extra voids and cracks alongside the thermocouples, the accelerated moisture migration causes the moisture clogs to form deeper in concrete. For instance, in Series 2 the moisture clog at 30 minutes is usually located at 10 mm depth, whereas for that specimen it is located at about 20 mm depth.

In Series 3, the effect of RPTM is much more significant compared to Series 1 and 2. The drying speed of RPTM2-4 is initially faster than that of PC-3, then there is a clear increase of the slope after 30 minutes. On the other hand, the drying of PC-3 is very slow and the reference temperature zone has virtually no effect on the drying speed of plain concrete. Consequently, the moisture clog is formed at a much hotter region in PC-3 compared to RPTM2-4. For 30 minutes of heating in perfectly sealed pore in the moisture clog, the pore pressure is expected to be around 0.6 MPa in PC-3 and 0.2 MPa in RPTM2-4, resulting in a lower stress gradient in the latter.

To summarize, the moisture clog theory of Hypothesis 1 appears confirmed and quantified through the neutron tomography tests. RPTM are found to clearly facilitate moisture movement and push to water clogging deeper, providing evidence to support Hypothesis 2 and Hypothesis 3.

Series 1

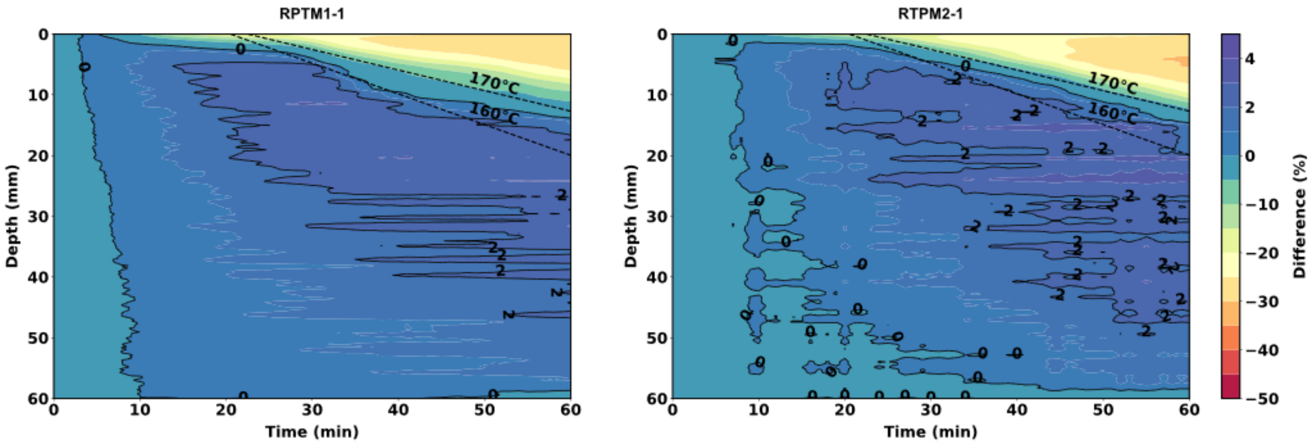

Series 2

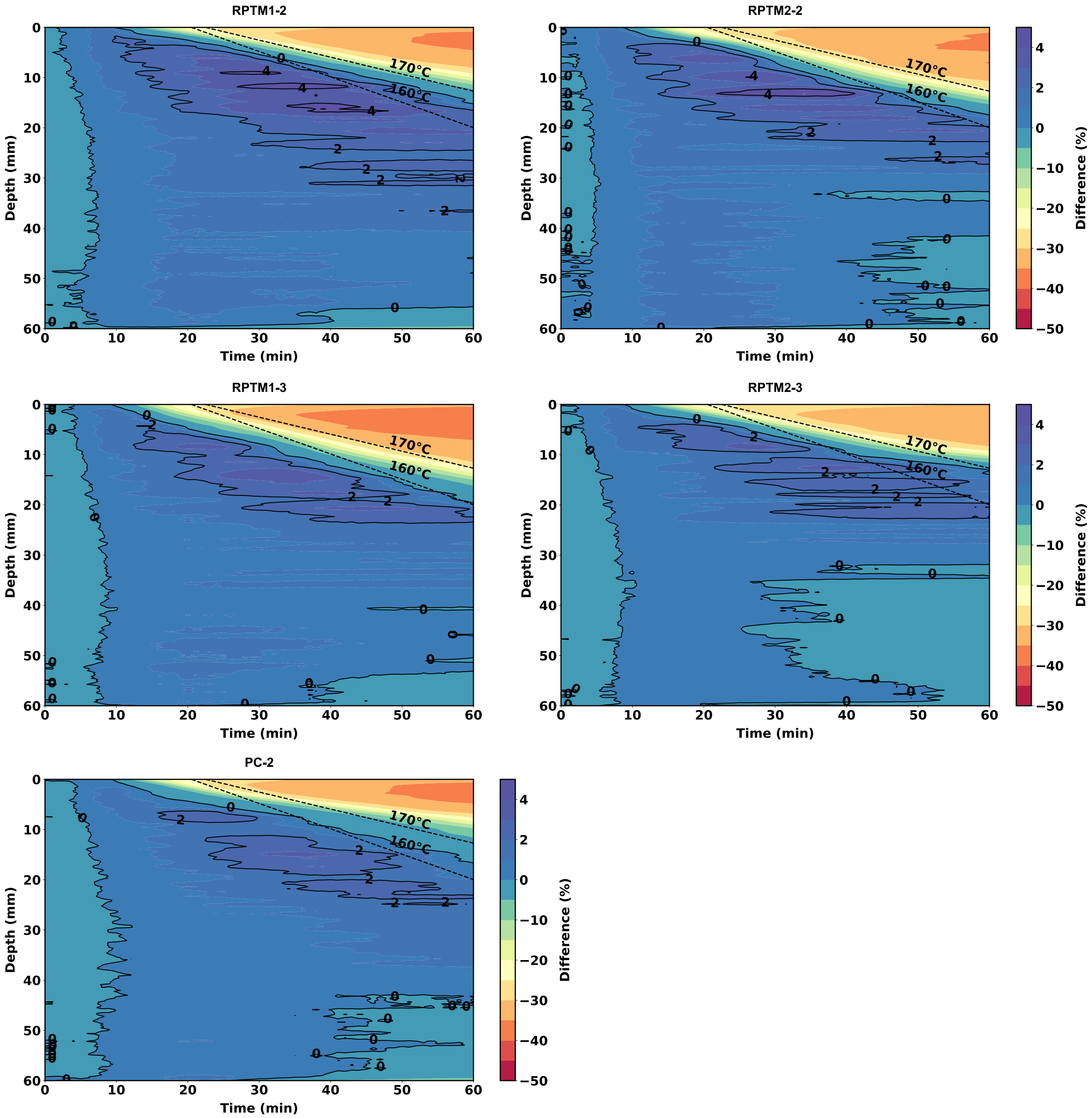
RPTM1-2
RPTM2-2
RPTM1-3
RPTM2-3
PC-2
170°C
160°C
Depth (mm)
Time (min)
Difference (%)

Series 2 TC

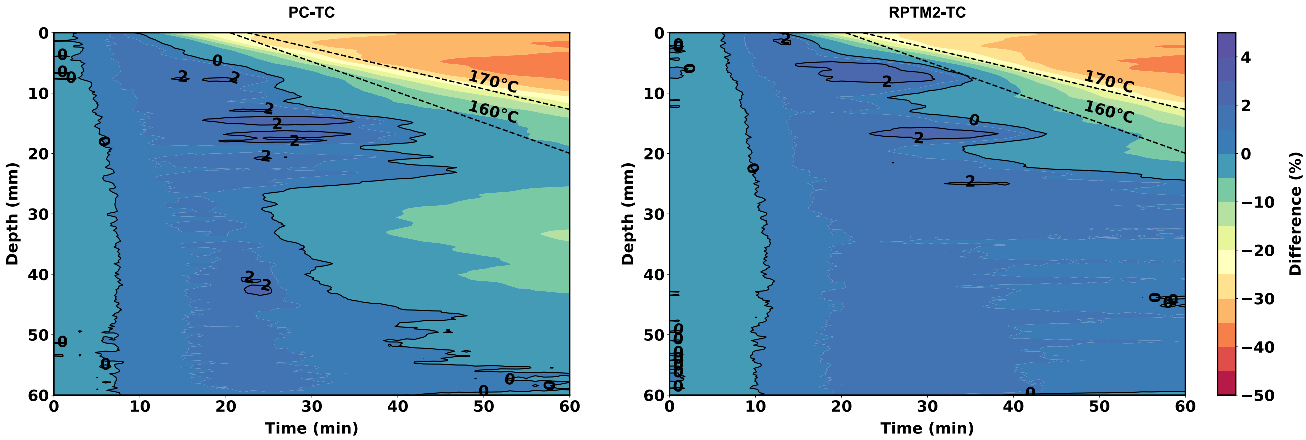

Series 3

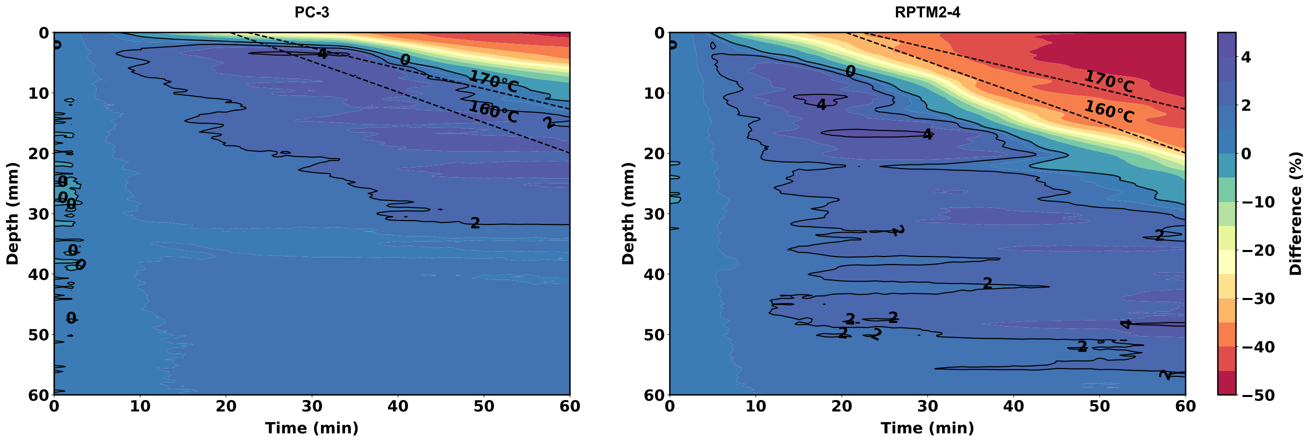

Figure 18 Average grey value map indicating the moisture profile of all test specimens

6.3.3 X-ray tomography

X-ray tomography tests were conducted before and after heating on specimens PC-TC and RPTM2-TC to further understand the effect of RPTM on the drying mechanism. The adopted voxel size is 0.046 mm (width) x 0.046 mm (length) x 0.0465 mm (height). The porous structure of concrete is primarily detected by the density difference between empty pores and the solid volume. The higher the density, the brighter the voxel appears in the image.

6.3.3.1 X-ray image processing

A threshold-based segmentation was adopted to detect pores. The threshold was determined with the commonly-adopted Otsu's method. This method separates pixels using a single value that minimises the intra-class intensity variance. Otsu's method is here effective in determining the threshold between low-density pores and high-density cement and aggregates. However, due to the presence of high-density aggregates, as shown in Figure 19(a), the image comprises three classes instead of two, which makes this thresholding approach challenging. To address this issue, all high-density aggregates are set to the mean pixel value of the image, as shown in Figure 19(b). Subsequently, a 4-pixel median filter is applied to reduce noise. Finally, Otsu's threshold is applied, successfully extracting the pores of the specimen, as shown in Figure 19(c).

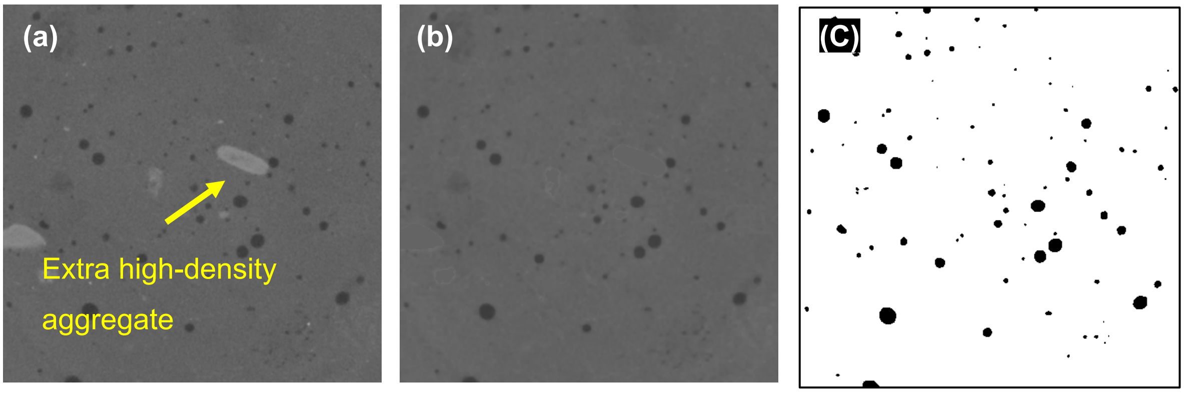

Figure 19 (a) Initial image (b) High-density aggregate moved (c) Binary image of pores.

The porous structure of concrete is composed of micropores (1 to 100 nm), mesopores (100 nm to 10 μm), and macropores (100 μm and above). Due to the limitation on the voxel size, the smallest detectable pores have a diameter of 57 μm. The largest pores detected are around 2.2 – 2.4 mm in diameter. The porous structure detected by X-ray tomography can primarily be regarded as the macropore structure. To quantify the influence of RPTM on the macropore structure of concrete at elevated temperature, the top 20 mm sections of specimen

RPTM2-TC and PC-TC are examined in detail. Figure 20 shows the 3-D rendered image of specimen PC-TC with the considered sections and the excluded volume for the analysis. In the considered sections, the thermocouple affected areas, which span 1.8 – 3 mm in depth depending on the orientation of the thermocouples, are disregarded. As detailed in Section 6.3.1, thermocouples in fact locally disturb the pore structure of the concrete. Furthermore, the volume below 20 mm does not get hot enough for the softening and thermal expansion of the fibres to occur. The large crack seen in specimen PC-TC may have resulted from the small mould size and inadequate vibration during casting. This large crack has no impact on the analysis, as it is outside the sections of interest.

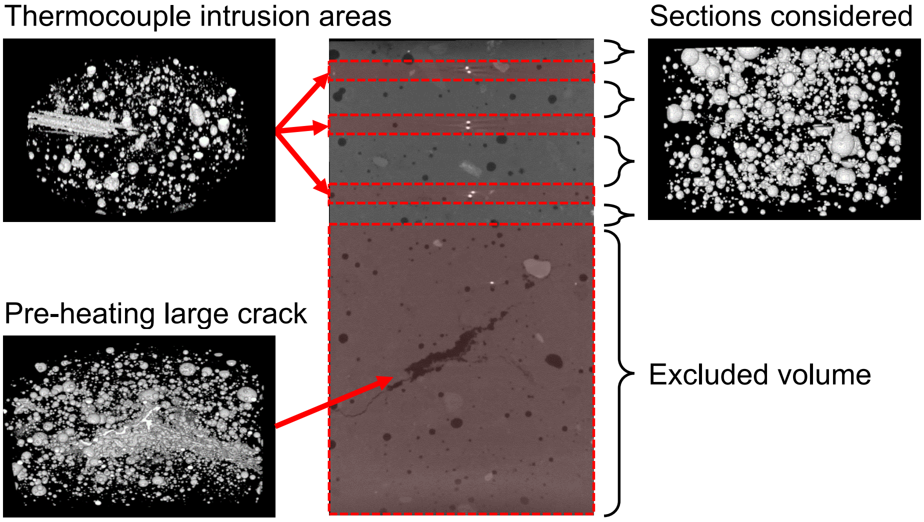

Figure 20 3D rendering of the thermocouple intrusion areas, pre-heating large crack and the analysed and excluded sections of the porous structure analysis of specimen PC-TC.

6.3.3.2 Porous structure of concrete

The initial states and the post- heating states of the porous structures of the analysed sections of specimens PC-TC and RPTM2-TC are shown in Figure 21(a). The frequency of occurrence of the pores is plotted as a function of the logarithm of the volume distribution. The pore count of the specimen with RPTM is significantly higher than that of plain concrete before heating, with the maximum difference being in the range of 0.001 mm3 to 0.03 mm3, corresponding to pore diameters of 120 μm to 380 μm. This increase in pore volume can be attributed to the inclusion of RPTM fibres. As with the thermocouples, air voids can be formed around RPTM during the casting stage, creating additional pores compared to plain concrete. The SEM scanning images of RPTM concrete also support this hypothesis, as many pores are found to nucleate around fibres. The diameter of these pores is around 300 μm, as shown in Figure 22. By comparing the pore volume distribution before and after heating, there is only a marginal increase in pore counts for both specimens. This may be due to the voxel size, which means that the X-ray tomography employed cannot capture the micro cracks created by RPTM thermal expansion. Hence, the main change in the detected porous network is caused by the thermal-mechanical actions of macropores.

To verify Hypothesis 3, the sphericity of the porous structure of both specimens is calculated. As mentioned in Hypothesis 3, for heated concrete, a primary cause of mechanical strength degradation is due to the thermal stress gradient and the stiffening of the saturated cement matrix near the drying front. These could induce damage in the concrete leading to cracks parallel to the heating surface and flat or slender empty channels in the porous structure. Since the sphericity of the pore measures how closely the shape of the pore matches that of a perfect sphere, a decrease in the pore sphericity could indicate the development of such cracks parallel to the heating surface. However, as shown in Figure 21(b), no obvious decrease in pore sphericity is observed in the post heating curve for both specimens, providing insufficient evidence for crack formation. The following might help explain this lack of crack formation: firstly, the heating intensity of the tests was relatively low to prevent fire spalling and avoid damaging the test rig. Hence, the heating rate might not be sufficient to induce significant thermal-mechanical damage to the concrete skeletons; secondly, the size of thermally induced cracks could be below the detectable range of the X-ray tomography.

(a)

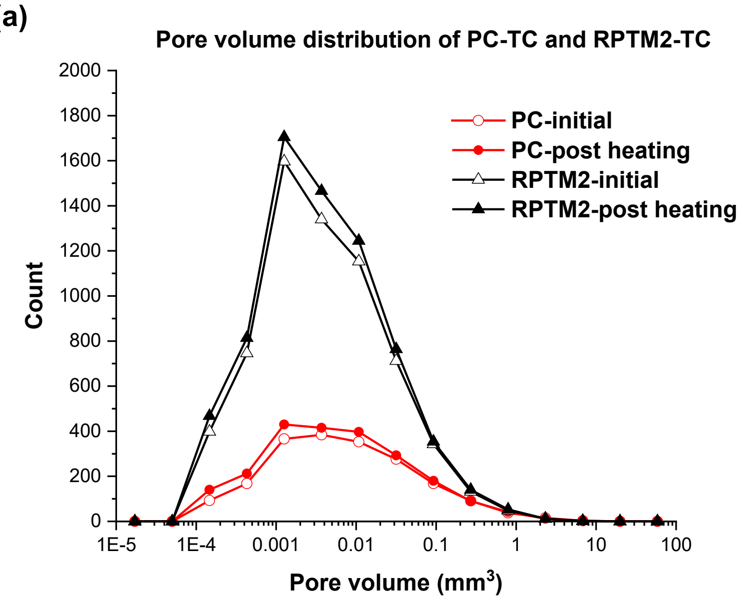

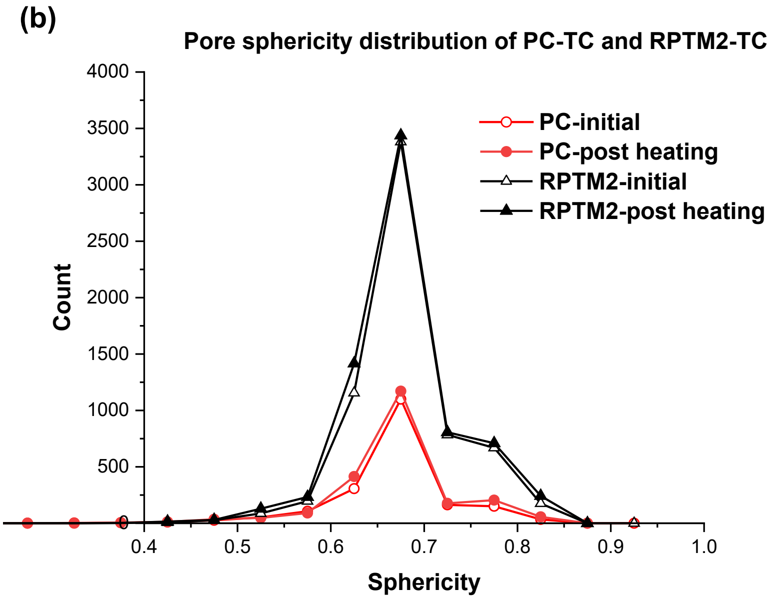

Figure 21 (a) Pore volume distribution of specimens (b) Pore sphericity distribution of specimens

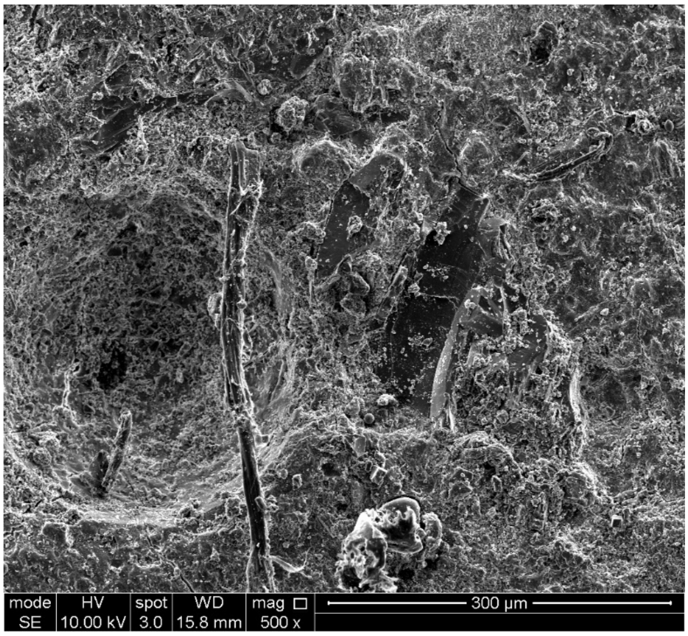

Figure 22 SEM image of a pore and RPTM fibres in a specimen

The results of the global pore analysis are summarized in Table 3. The macropore volume ratios of specimens PC-TC and RPTM2-TC before and after heating are obtained from the X-ray tomographies. The global porosity is obtained from the water-permeable pore ratio test based on ASTM C642-21 [50]. The difference between the macropore volume ratio and the global porosity can give an indication of the number of pores that are undetected by the adopted X-ray tomography. The last three rows of Table 3 show the differences in macropore volume ratio, global porosity and undetected pore ratio between PC-TC and RPTM2-TC.

In the X-ray tomography, the macropore volume ratio of the plain concrete specimen PC-TC is 2.31%, which exhibits nearly no change before and after heating. As shown in Figure 21(a), although there is a slight increase in the pore counts of specimen PC-TC after heating, the volume of the newly formed pores is minimal to affect the total macropore volume. Compared to PC-TC, specimen RPTM2-TC has a significantly higher number of pores, while its actual porosity is only 0.76% higher (33% in relative change) than that of PC-TC. This is also attributed to the fact that the majority of the pores are constituting only a small volume of the total pore volume. For specimen RPTM2-TC, the pore volume above 0.05 mm³ accounts for 78% of the total macropore porosity. On the other side, for specimen PC-TC, pores with a volume above 0.05 mm³ account for 90% of the total macropore volume. The increase (from 3.07% to 3.18%) in porosity due to heating is more noticeable in RPTM2-TC than that of PC-TC. Although the RPTM are too small to be directly detected by the X-ray tomography, the difference in thermal expansion between concrete and RPTM may also increase the macropore size, contributing to the increase in porosity.

To provide an impression of the amount of undetected micropores and mesopores, the macropore volume ratio obtained in X-ray tomography are compared to the global porosity, which is obtained from the specimens cast at the same time as the tomography specimens. The intrinsic global porosities for PC-TC and RPTM2-TC are 5.71% and 6.82%, respectively. The difference in global porosity between PC-TC and RPTM2-TC is 1.11%, while the difference in macropore volume ratio between these two specimens is 0.76%. Therefore, it can be estimated that the RPTM specimen has 0.35% more undetected pores than plain concrete, which is close to the 0.4% volume ratio for 2kg/m^3 RPTM dosage in the concrete specimen. This demonstrates that apart from the macropores, the inclusion of RPTM can also directly contribute to the increase in concrete mesopores/micropores before heating.

Table 3 Pore volume ratios from X-ray tomography and water permeable porosity test

Condition	**Initial**		**Post heating**	
Sample	PC-TC	RPTM2-TC	PC-TC	RPTM2-TC
Macropore volume ratio (%)	2.31	3.07	2.31	3.18
Global porosity (%)	5.71	6.82	--	--
Undetected porosity (%)	3.4	3.75	--	--
Difference in macropore volume ratio (%)	0.76		--	
Difference in global porosity (%)	1.11		--	
Difference in undetected pore ratio (%)	0.35		--	

In the future, if the mesopores could be detected thanks to higher resolution X-ray images, that would be useful in terms of investigating the empty channels created by melted RPTM, with voxel sizes below the average diameter of RPTM, at 15 μm or lower. In that way, the examination of pore volume changes in heated concrete would further reveal the mechanism of RPTM at the mesopore level, providing further insight into the behaviour and performance of concrete under elevated temperatures.

6.4 CONCLUSIONS

To experimentally validate three hypotheses proposed for the mechanisms of RPTM fibres in controlling the fire spalling of concrete, neutron and X-ray tomographies were acquired. Three series of specimens were tested with different parameters, including concrete age, fibre dosage, and aggregate gradation. The main conclusions are:

1. The formation of moisture clog and its location were observed through neutron tomography. The inclusion of RPTM facilitates moisture migration and leads to a lower temperature at the drying front compared with plain concrete. The X-ray results indicate that the inclusion of RPTM can increase both the intrinsic porosity and thermal porosity of concrete via fibre addition and thermal expansion. All test specimens provide some evidence to support the moisture clog theory of Hypothesis 1.
2. The presence of thermocouples can alter the intrinsic porous structure and the moisture migration process in heated concrete, even when the diameter of the thermocouple is minimised. Hence, although there is a lack of observations of the thermal gradient due to the existence of the dry-wet interface, there was no evidence to oppose Hypothesis 2. Until the development of a non-intrusive method for temperature measurements within concrete, the validation of Hypothesis 2 remains difficult.
3. The observed wetting phase in the drying volume ratios analysis of heated concrete provides indirect evidence to indicate the transport of moisture from gel pores and capillaries to macropores. This supports Hypothesis 3, which suggests a stiffened layer of concrete due to moisture accumulation near the drying front. However, no obvious crack opening was observed near the drying front in the X-ray tomography results, as the sphericity of the pores remained constant after heating. This may be due to the low heating intensity or the relatively low resolution of the X-ray tomography.

Other findings from the test results are summarized below:

1. The 2 kg/m^3 RPTM dosage does not have a significant advantage in drying acceleration compared to 1 kg/m^3.
2. The drying rate of plain concrete specimens is relatively constant under uniform heating.
3. There is no significant change in the macropore volume ratio for both plain and RPTM concrete after heating.

Please note all above conclusions are based on the reported test specimens subject to the particular test conditions. To draw more generalised conclusions, more investigations are required. X-ray tomography with higher resolution is recommended to further investigate the influence of the melting of RPTM on the mesopores of concrete at elevated temperatures. A non-intrusive temperature measurement method to determine the inner temperature distribution within a solid specimen would also be highly beneficial to the thermo-hydro-mechanical mechanism of heated concrete.

AUTHOR CONTRIBUTIONS

Yifan Li: Conceptualization, Methodology, Software, Investigation, Formal analysis, Writing - Original Draft, Project administration. **Stefano Dal Pont:** Methodology, Resources, Writing - Review & Editing**. Alessandro Tengattini:** Methodology, Software, Resources, Data Curation, Writing - Review & Editing. **Kypros Pilakoutas:** Writing - Review & Editing, Supervision**. Shan-Shan Huang:** Conceptualization, Methodology, Resources, Writing - Review & Editing, Supervision, Project administration, Funding acquisition.

ACKNOWLEDGEMENTS

This work has been supported by Institut Laue-Langevin at test instrument D50 T. Data collection is available for ILL user club members at https://doi.ill.fr/10.5291/ILL-DATA.UGA-67, https://dx.doi.org/10.5291/ILL-DATA.UGA-104, https://doi.ill.fr/10.5291/ILL-DATA.NIM-4.

REFERENCES

[1] T. T. Lie and J. L. Woollerton, *Fire resistance of reinforced concrete columns: test results*. National Research Council Canada, Institute for Research in Construction, 1988.

[2] M. Achenbach, T. Lahmer, and G. Morgenthal, "Identification of the thermal properties of concrete for the temperature calculation of concrete slabs and columns subjected to a standard fire—Methodology and proposal for simplified formulations," *Fire Saf J*, vol. 87, pp. 80–86, Jan. 2017, doi: 10.1016/j.firesaf.2016.12.003.

[3] British Standards Institution, "BS EN 1992-1-2:2004, Eurocode 2: Design of concrete structures : Part 1-2: General rules — Structural fire design," BSi, London, 2010.

[4] RAIB, *Rail Accident Report: Fire on HGV shuttle in the Channel Tunnel 21 August 2006*. Rail Accident Investigation Branch, Department for Transport., 2007. [Online]. Available: www.raib.gov.uk.

[5] J. Albrektsson, M. Flansbjer, J. E. Lindqvist, and R. Jansson, *Assessment of concrete structures after fire*. SP Technical Research Institute of Sweden, 2011.

[6] A. Leitner, "The fire catastrophe in the Tauern Tunnel: experience and conclusions for the Austrian guidelines," *Tunnelling and Underground Space Technology*, vol. 16, p. 217223, 2001.

[7] R. Jansson and K. Ödeen, "Fire in Storehouse 6 in the Free Port of Stockholm," in *2nd International RILEM Workshop on Concrete Spalling due to Fire Exposure*, Delft, 2011, pp. 205–210. [Online]. Available: https://www.researchgate.net/publication/281107891

[8] RAIB, *Technical Investigation Report concerning the Fire on Eurotunnel Freight Shuttle 7412 on 11 September 2008*. Rail Accident Investigation Branch, Department for Transport., 2010. [Online]. Available: http://www.raib.gov.uk

[9] Freyssinet Limited, "Rail - Concrete Repair & Tunnel Strengthening - Channel Tunnel Fire Damage Repair - FreyssinetUK." Accessed: Feb. 06, 2023. [Online]. Available: https://freyssinet.co.uk/rail-concrete-repair-tunnel-strengthening-channel-tunnel-fire-damage-repair/

[10] K. D. Hertz, "Limits of spalling of fire-exposed concrete," *Fire Saf J*, vol. 38, no. 2, pp. 103–116, Mar. 2003, doi: 10.1016/S0379-7112(02)00051-6.

[11] Z. Bazant, "Analysis of Pore Pressure, Thermal Stress and Fracture in Rapidly Heated Concrete," in *International Workshop on Fire Performance of High-Strength Concrete*, Gaithersburg, 1997. [Online]. Available: https://tsapps.nist.gov/publication/get_pdf.cfm?pub_id=916655

[12] G. Choe, G. Kim, M. Yoon, E. Hwang, J. Nam, and N. Guncunski, "Effect of moisture migration and water vapor pressure build-up with the heating rate on concrete spalling type," *Cem Concr Res*, vol. 116, pp. 1–10, Feb. 2019, doi: 10.1016/j.cemconres.2018.10.021.

[13] S. Dal Pont, H. Colina, A. Dupas, and A. Ehrlacher, “An experimental relationship between complete liquid saturation and violent damage in concrete submitted to high temperature,” *Magazine of Concrete Research*, vol. 57, no. 8, pp. 455–461, Oct. 2005.

[14] P. Kalifa, G. Chéné, and C. Gallé, “High-temperature behaviour of HPC with polypropylene fibres From spalling to microstructure,” *Cem Concr Res*, pp. 1487–1499, 2001.

[15] A. Bilodeau, V. K. R. Kodur, and G. C. Hoff, “Optimization of the type and amount of polypropylene fibres for preventing the spalling of lightweight concrete subjected to hydrocarbon fire,” *Cem Concr Compos*, vol. 26, no. 2, pp. 163–174, Feb. 2004, doi: 10.1016/S0958-9465(03)00085-4.

[16] N. Yermak, P. Pliya, A. L. Beaucour, A. Simon, and A. Noumowé, “Influence of steel and/or polypropylene fibres on the behaviour of concrete at high temperature: Spalling, transfer and mechanical properties,” *Constr Build Mater*, vol. 132, pp. 240–250, Feb. 2017, doi: 10.1016/j.conbuildmat.2016.11.120.

[17] British Standards Institution, “BS EN 1992-1-2:2023, Eurocode 2: Design of concrete structures : Part 1-2: Structural fire design,” London, 2023.

[18] S. S. Huang, H. Angelakopoulos, K. Pilakoutas, and I. Burgess, “Reused tyre polymer fibre for fire-spalling mitigation,” in *Applications of Structural Fire Engineering 2015*, Prague, Oct. 2015. doi: 10.14311/asfe.2015.056.

[19] Y. Li, S.-S. Huang, K. Pilakoutas, H. Angelakopoulos, and I. Burgess, “Mitigation of Fire-Induced Spalling of Concrete using Recycled Tyre Polymer Fibre,” in *6th International Workshop on Concrete Spalling due to Fire Exposure*, Sheffield, Sep. 2019, pp. 42–51.

[20] F. P. Figueiredo, S. S. Huang, H. Angelakopoulos, K. Pilakoutas, and I. Burgess, “Effects of Recycled Steel and Polymer Fibres on Explosive Fire Spalling of Concrete,” *Fire Technol*, vol. 55, no. 5, pp. 1495–1516, Sep. 2019, doi: 10.1007/s10694-019-00817-9.

[21] Fazilet Cinaralp and Jean-Pierre Taverne, “End of life tyres: A valuable resource with growing potential,” ETRMA. Accessed: Feb. 08, 2023. [Online]. Available: https://www.etrma.org/wp-content/uploads/2019/09/2010_etrma_elt_management_brochure_final.pdf

[22] M. Serdar, A. Baričević, S. Lakušić, and D. Bjegović, “Special purpose concrete products from waste tyre recyclates,” *Journal of the Croatian Association of Civil Engineers*, vol. 65, no. Građevinar, pp. 793–801, 2013.

[23] A. Noumowe, “Mechanical properties and microstructure of high strength concrete containing polypropylene fibres exposed to temperatures up to 200 °c,” *Cem Concr Res*, vol. 35, no. 11, pp. 2192–2198, Nov. 2005, doi: 10.1016/j.cemconres.2005.03.007.

[24] A. Bentur, S. Mindessf, and G. Vondran4, “Bonding in polypropylene fibre reinforced concretes,” *The International Journal of Cement Composites and Lightweight Concrete*, vol. 11, pp. 153–158, 1989.

[25] S. P. Yap, Y. Goh, W. X. Goh, K. H. Mo, M. Y. J. Liu, and H. A. Ibrahim, "Relationship between microstructure and performance of polypropylene fibre reinforced cement composites subjected to elevated temperature," *European Journal of Environmental and Civil Engineering*, vol. 26, no. 5, pp. 1792–1806, 2022, doi: 10.1080/19648189.2020.1734489.

[26] Y. Li, K. H. Tan, and E. H. Yang, "Influence of aggregate size and inclusion of polypropylene and steel fibers on the hot permeability of ultra-high performance concrete (UHPC) at elevated temperature," *Constr Build Mater*, vol. 169, pp. 629–637, Apr. 2018, doi: 10.1016/j.conbuildmat.2018.01.105.

[27] J. C. Mindeguia, P. Pimienta, A. Noumowé, and M. Kanema, "Temperature, pore pressure and mass variation of concrete subjected to high temperature - Experimental and numerical discussion on spalling risk," *Cem Concr Res*, vol. 40, no. 3, pp. 477–487, Mar. 2010, doi: 10.1016/j.cemconres.2009.10.011.

[28] R. Jansson and L. Boström, "The influence of pressure in the pore system on fire spalling of concrete," *Fire Technol*, vol. 46, no. 1, pp. 217–230, 2010, doi: 10.1007/s10694-009-0093-9.

[29] R. Felicetti, F. Lo Monte, and P. Pimienta, "A new test method to study the influence of pore pressure on fracture behaviour of concrete during heating," *Cem Concr Res*, vol. 94, pp. 13–23, Apr. 2017, doi: 10.1016/j.cemconres.2017.01.002.

[30] L. A. Ashton and S. C. C. Bate, "Discussion on the Fire-Resistance of Prestressed Concrete Beams," in *Proceedings of the Institution of Civil Engineers*, ICE, Oct. 1961, pp. 305–320.

[31] Z. A. Kameche, F. Ghomari, M. Choinska, and A. Khelidj, "Assessment of liquid water and gas permeabilities of partially saturated ordinary concrete," *Constr Build Mater*, vol. 65, pp. 551–565, Aug. 2014, doi: 10.1016/j.conbuildmat.2014.04.137.

[32] Harmathy T. Z., "Effect of moisture on the fire endurance of building elements," *ASTM Special Technical Publications no.385*, no. Ottawa, pp. 74–95, 1965, [Online]. Available: https://publications-cnrc.canada.ca/fra/voir/objet/?id=fcaa348d-5a0c-4341-92d4-ab6defae1340

[33] J. S. Guo and P. Waldron{, "An elastic model to quantify the effect of moisture on the mechanical properties of concrete at the time of test," *Magazine of Concrete Research*, vol. 53, no. 3, pp. 151–162, Jun. 2001.

[34] G. E. Bessey and S. Dilnot, "The relation between strength and free water content of aerated concretes*," *Magazine of Concrete Research*, vol. 1, no. 3, pp. 119–122, 1949.

[35] R. Jansson and L. Boström, "Fire Spalling-The Moisture Effect," in *1st International Workshop on Concrete Spalling due to Fire Exposure*, Leipzig: MFPA Institute, Sep. 2009, pp. 120–129. [Online]. Available: https://www.researchgate.net/publication/281113999

[36] G. H. A. Van Der Heijden, H. P. Huinink, L. Pel, and K. Kopinga, "One-dimensional scanning of moisture in heated porous building materials with NMR," *Journal of Magnetic Resonance*, vol. 208, no. 2, pp. 235–242, Feb. 2011, doi: 10.1016/j.jmr.2010.11.010.

[37] J. D. Ríos, J. Mínguez, A. Martínez-De La Concha, M. Á. Vicente, and H. Cifuentes, "Microstructural analyses of the addition of PP fibres on the fracture properties of high-strength self-compacting concrete by X-ray computed tomography," *Constr Build Mater*, vol. 261, Nov. 2020, doi: 10.1016/j.conbuildmat.2020.120499.

[38] L. Stelzner, B. Powierza, T. Oesch, R. Dlugosch, and F. Weise, "Thermally-induced moisture transport in high-performance concrete studied by X-ray-CT and 1H-NMR," *Constr Build Mater*, vol. 224, pp. 600–609, Nov. 2019, doi: 10.1016/j.conbuildmat.2019.07.065.

[39] D. Dauti, A. Tengattini, S. Dal Pont, N. Toropovs, M. Briffaut, and B. Weber, "Analysis of moisture migration in concrete at high temperature through in-situ neutron tomography," *Cem Concr Res*, vol. 111, pp. 41–55, Sep. 2018, doi: 10.1016/j.cemconres.2018.06.010.

[40] A. Tengattini *et al.*, "NeXT-Grenoble, the Neutron and X-ray tomograph in Grenoble," *Nucl Instrum Methods Phys Res A*, vol. 968, Jul. 2020, doi: 10.1016/j.nima.2020.163939.

[41] M. H. Moreira, S. Dal Pont, A. Tengattini, A. P. Luz, and V. C. Pandolfelli, "Experimental proof of moisture clog through neutron tomography in a porous medium under truly one-directional drying," *Journal of American Ceramic Society*, vol. 105, no. 5, pp. 3534–3543, May 2022.

[42] H. Cheikh Sleiman, A. Tengattini, M. Briffaut, B. Huet, and S. Dal Pont, "Simultaneous x-ray and neutron 4D tomographic study of drying-driven hydro-mechanical behavior of cement-based materials at moderate temperatures," *Cem Concr Res*, vol. 147, Sep. 2021, doi: 10.1016/j.cemconres.2021.106503.

[43] M. Chen, Z. Sun, W. Tu, X. Yan, and M. Zhang, "Behaviour of recycled tyre polymer fibre reinforced concrete at elevated temperatures," *Cem Concr Compos*, vol. 124, Nov. 2021, doi: 10.1016/j.cemconcomp.2021.104257.

[44] M. Serdar, A. Baričević, M. Jelčić Rukavina, M. Pezer, D. Bjegović, and N. Štirmer, "Shrinkage Behaviour of Fibre Reinforced Concrete with Recycled Tyre Polymer Fibres," *Int J Polym Sci*, vol. 2015, 2015, doi: 10.1155/2015/145918.

[45] M. Ozawa, S. Subedi Parajuli, Y. Uchida, and B. Zhou, "Preventive effects of polypropylene and jute fibers on spalling of UHPC at high temperatures in combination with waste porous ceramic fine aggregate as an internal curing material," *Constr Build Mater*, vol. 206, pp. 219–225, May 2019, doi: 10.1016/j.conbuildmat.2019.02.056.

[46] D. Dauti, A. Tengattini, S. D. Pont, N. Toropovs, M. Briffaut, and B. Weber, "Some Observations on Testing Conditions of High-Temperature Experiments on Concrete: An Insight from Neutron Tomography," *Transp Porous Media*, vol. 132, no. 2, pp. 299–310, Mar. 2020, doi: 10.1007/s11242-020-01392-2.

[47] D. Dauti, A. Tengattini, S. Dal Pont, N. Toropovs, M. Briffaut, and B. Weber, "Analysis of moisture migration in concrete at high temperature through in-situ neutron tomography," *Cem Concr Res*, vol. 111, pp. 41–55, Sep. 2018, doi: 10.1016/j.cemconres.2018.06.010.

[48] M. R. Bangi and T. Horiguchi, “Effect of fibre type and geometry on maximum pore pressures in fibre-reinforced high strength concrete at elevated temperatures,” *Cem Concr Res*, vol. 42, no. 2, pp. 459–466, Feb. 2012, doi: 10.1016/j.cemconres.2011.11.014.

[49] L. T. Phan, “Pore pressure and explosive spalling in concrete,” *Materials and Structures/Materiaux et Constructions*, vol. 41, no. 10, pp. 1623–1632, Dec. 2008, doi: 10.1617/s11527-008-9353-2.

[50] ASTM international, “ASTM C642-21 Standard Test Method for Density, Absorption, and Voids in Hardened Concrete,” West Conshohocken, 2022. doi: 10.1520/C0642-21.